Geological Survey of Finland

Bulletin 321

Characteristics and results of an airborne electromagnetic method of geophysical surveying

by Markku Peltoniemi

Geologinen tutkimuslaitos
Espoo 1982

Geological Survey of Finland, Bulletin 321

CHARACTERISTICS AND RESULTS OF AN AIRBORNE ELECTROMAGNETIC METHOD OF GEOPHYSICAL SURVEYING

by
MARKKU PELTONIEMI

with 117 figures and 20 tables in the text

GEOLOGINEN TUTKIMUSLAITOS
ESPOO 1982

Peltoniemi, Markku 1982. Characteristics and results of an airborne electromagnetic method of geophysical surveying. *Geological Survey of Finland, Bulletin 321.* 229 pages, 117 figures and 20 tables.

The development and application of airborne electromagnetic (AEM) methods are described and the underlying principles outlined. The AEM measurements and methods applied in Finland are reviewed. The vertical coaxial fixed-coil AEM system fitted in a DC-3 aircraft is described with special reference to technical performance, measurements and data processing. In 1973–1979 the Geological Survey of Finland applied the system to aerogeophysical studies over a total of 295 000 line kilometres.

The physical properties of the Finnish rocks and soils as well as the methods used in the interpretation of the AEM results are discussed. Characteristic diagrams were deduced by numerical modelling for a conductive and/or susceptive layered earth, and a conductive sphere in a resistive medium. Results for a conductive halfplane were elaborated by means of scale modelling. The conductivity, conductance and susceptibility apertures as well as the penetration of the system were established on the basis of the modelling results. Computer programs were developed that permit the anomaly data to be transformed into apparent conductivity, conductance and depth values.

The examples include 8 case histories. AEM anomalies due to conductive overburden and sheet-like and local conductors in the bedrock are compared with results obtained by other electrical methods. Similarly, susceptibility and remanence effects were studied with the aid of AEM and aeromagnetic survey data. The penetration of the DC-3 AEM system was found to be equal to or better than the normal slingram method but the resolution and discrimination lower. The examples demonstrate that the transformed AEM values could be used to guide follow-up studies and to establish targets even in explorationally difficult areas.

Key words: airborne methods, geophysical surveys, geological surveys, instruments, data processing, models, interpretation, case histories, conductive materials, Finland.

Markku Peltoniemi, Geological Survey of Finland,
Geophysics Department, SF-02150 Espoo 15

ISBN 951-690-162-X
ISSN 0367-522X

Vammala 1982 Vammalan Kirjapaino Oy Offset


KAR-AIR

CONTENTS

LIST OF SYMBOLS

a [m]	radius of a spherical conductor
$\bar{A}$ [mV]	average of original AEM anomaly data
A_i [mV]	original AEM anomaly value at observation point i
A_i' [ppm]	corrected AEM anomaly value at point i
A_i'' [ppm]	filtered AEM anomaly value at point i
A_T [m^2]	area of transmitter coil
b_o, b_1, b_2	coefficients of a recursive filter
B [Hz]	amplifier bandwidth
B_T [nT]	absolute value of magnetic total field 1965.0
c_o, c_1 [mV]	coefficients of a drift correcting equation
d [m]	thickness of a conductor
da_1, da_2, da_3, da_4 [m]	apparent depth of burial to a conductive half-space, a horizontal layer, a half-plane or a sphere, respectively
d_i [m]	thickness of layer i
d_{lim} [m]	limiting thickness of an electrically thin sheet-like conductor
D_i [mV]	AEM anomaly value with a local zero level
e_o, e_D [m]	coefficients of equation for Doppler along-track error calculation
f [Hz]	frequency of an alternating EM field
f_N [Hz]	Nyquist frequency of a sampled signal
h [m]	flight elevation
$\bar{h}$ [m]	average of flight elevation data
H_a [Am^{-1}]	EM noise field originating from aircraft
H_p, H_s, H_t [Am^{-1}]	primary, secondary or total EM field, respectively
H_t (Im), H_t (Re) [Am^{-1}]	quadrature or in-phase component of total EM field, respectively
i	index counter
I, I_o [A]	transmitter current of harmonic time variation or constant value, respectively
$I(\lambda)_{i+\frac{1}{2}}$, $I'(\lambda)_{i+\frac{1}{2}}$	modified Bessel function of fractional order $i+\frac{1}{2}$ and its derivative
Im [ppm]	quadrature anomaly
$\bar{Im}$ [ppm]	average of quadrature anomaly data
Im_{min} [ppm]	minimum of quadrature anomaly values accepted in the transformation
j	imaginary unit $\sqrt{-1}$
k	magnetic susceptibility, in SI units

k_a	apparent magnetic susceptibility, in SI units
k_B [VA/°K]	Boltzmann's constant, $1.38 \cdot 10^{-23}$
l [m]	coil separation of a two-coil EM device
l_1, l_2 [m]	significant linear dimensions of a conductor and an EM device
L [km]	length of a flight line
m [Am^2]	dipole moment of EM transmitter coil
n	number of turns in a coil
n_p	number of measurement points per line
n_{ADC}	number of bits converted in the ADC circuit
N [V or ppm]	noise of an AEM system
N_a, N_b [ppm]	motion-induced noise anomalies of systems a and b, respectively
N_{ADC} [ppm]	noise due to the finite accuracy in ADC conversion
N_T [$V/\sqrt{Hz}$]	thermal noise in coil
p_i	number of multipoles
q_1, q_2	constants of drift correction
q_3 [ppm/mV]	conversion constant from AEM signal into anomaly values
Q	Koenigsberger ratio
Q_t	tuning ratio of a receiver coil
r [m]	distance from the centre of a transmitter coil
$\mathbf{r}_o$, $\mathbf{r}_A$	unit vectors
r_T [m]	radius of transmitter coil
R [Ω]	resistance of receiver coil
Re [ppm]	in-phase anomaly
Re [ppm]	average of in-phase anomaly
Re_{max} [ppm]	inductive limit of in-phase anomaly values
Re_{min} [ppm]	minimum of in-phase anomaly values accepted in the transformation
Rx	receiver coil
RF	response function
s [S]	electrical conductance
s_a [S]	apparent electrical conductance
S [V or ppm]	signal of an AEM system
S_d [ppm]	detection limit of signal
S/N	signal/noise ratio of an AEM system
t_i [s]	recording time of data value i
T [°K]	absolute temperature
Tx	transmitter coil
v [ms^{-1}]	velocity of aircraft
v_s [ms^{-1}]	velocity of acoustic waves in ground
v_D, v_{FP} [ms^{-1}]	estimated velocity of aircraft, based on Doppler or fixpoint data, respectively
$\mathbf{w}_{1/2}$ [m]	anomaly half-width

x, y, z [m or km]	Cartesian coordinates
za_1, za_2 [m]	apparent depth to a conductive half-space or a horizontal layer, respectively
z_1, z_2 [m]	depth to the top and bottom of a magnetised plate, respectively
α [degr]	dip angle
β_1, β_2, β_3 [degr]	inclination angle of a transmitter coil, a towing cable or a receiver coil, respectively
δ [m]	skin depth value of a conductor
$\triangle e$ [m]	total along-track error of Doppler positioning data
$\overline{\triangle g_z}$ [ms^{-2} or mV]	average of vertical acceleration change data
$\triangle l$ [m]	change in coil separation
$\triangle p_1$ [m]	navigation accuracy
$\triangle p_2$, $\triangle p_3$ [m]	positioning accuracy on a navigation map or a topographic map, respectively
$\triangle t$ [s]	time interval between successive digital recordings
$\triangle x$, $\triangle y$ [m]	observation point spacing in x or y direction, respectively
$\triangle B_z$ [nT]	vertical component anomaly of magnetic total field
$\triangle B_T$ [nT]	magnetic total field anomaly
$\triangle H$ [Am^{-1}]	change in magnetic field
ε [Fm^{-1}]	dielectric permittivity
ε_r	relative dielectric permittivity
ε_o [Fm^{-1}]	dielectric permittivity of free space
θ	response parameter of a conductor
$\boldsymbol{\theta}_1$, $\boldsymbol{\theta}_2$, $\boldsymbol{\theta}_3$, $\boldsymbol{\theta}_4$	response parameter for a conductive half-space, a horizontal layer, a half-plane and a sphere, respectively
λ	formal parameter of modified Bessel functions
μ [Hm^{-1}]	magnetic permeability
μ_r	relative magnetic permeability
μ_o [Hm^{-1}]	magnetic permeability of free space
ϱ_a [Ωm]	apparent resistivity
σ [Sm^{-1}]	electrical conductivity
σ_a [Sm^{-1}]	apparent electrical conductivity
σ_h [m]	standard deviation of flight elevation data
σ_A [mV]	standard deviation of original AEM data
$\sigma_{\triangle gz}$ [ms^{-2} or mV]	standard deviation of vertical acceleration change data
σ_{Im} [ppm]	standard deviation of quadrature anomaly data
$\overline{\sigma_{Im}}$ [ppm]	average standard deviation of quadrature anomaly data
σ_{Re} [ppm]	standard deviation of in-phase anomaly data
$\overline{\sigma_{Re}}$ [ppm]	average standard deviation of in-phase anomaly data
τ [s]	detector time constant
τ_{max} [s]	maximum acceptable value of detector time constant
$\boldsymbol{\phi}$ [degr]	phase angle of harmonic EM field
ω [s^{-1}]	angular frequency

PREFACE

The aim of the present study is to promote the use of airborne electromagnetic (AEM) survey data, particularly in Finland. AEM measurements have been conducted throughout practically the whole country, and the survey data are voluminous and continuously increasing. The present study deals exclusively with the AEM data of the Geological Survey of Finland, which has been engaged in the development and use of AEM methods since the early 1950's and has carried out the majority of the measurements. Several AEM methods have been applied during that time, and hence they reflect the development in AEM methods in general. A discussion of all these methods is beyond the scope of the present paper. Attention is focused on the vertical coaxial rigid-coil system installed in a DC-3 aircraft and used for low-elevation surveys in 1973–1979. Judging by its results, it is a representative example of an up-to-date AEM system and of the applicability of the data produced by such a system.

On account of the mutual correlation of the survey data and of the costs involved, aeromagnetic, AEM and airborne gamma-ray surveys should be undertaken simultaneously. This is the procedure the Geological Survey of Finland has invariably followed in its systematic surveys. Difficulties arise, however, when the geophysical instruments constitute complicated units that place great demands on the space and payload of the aircraft. In these respects, the DC-3 is a highly suitable platform.

The application of the results of the combined surveys to exploration and geological mapping requires that the survey data of various methods be presented systematically and with sufficient uniformity. Consequently, from the outset, the Geological Survey has stressed the importance of presenting the original AEM data as anomaly maps, and thus of increasing the usefulness of the results. This is particularly important for the results of the low-elevation AEM surveys, since these surveys are conducted in detail in an attempt to replace electromagnetic (EM) ground surveys over extensive areas.

There are four major parts to the present study. The first part is an introduction to the principles underlying the method and reviews the various AEM measurements undertaken in Finland. The second part describes the DC-3 low-elevation survey system in terms of AEM and auxiliary functions. The computer processing of the data and the concepts underlying the application of the results are also discussed. In the third part the theoretical responses of the DC-3 AEM system are examined with the aid of numerical and scale modelling methods; the important properties of the system are analysed by means of modelling results, and an inversion method based on computer processing of the AEM anomaly data is presented. The last part of the study shows how the theoretical results can be applied to actual field survey data. Finally, the limits of the applicability of the results produced by the system are summarised.

INTRODUCTION

Development of airborne electromagnetic (AEM) methods

Aerogeophysical surveys were started after the Second World War, although some test measurements had been conducted before that. The surveys began with aeromagnetics; the results obtained were of such undisputable benefit to geological studies that the method soon came into general use. At the end of the 1940's the development of airborne electromagnetic methods got underway in Canada, Finland and Sweden. As early as 1947 Hans Lundberg undertook experiments in Canada with helicopter-borne AEM equipment. Systematic AEM measurements, however, did not begin until 1950 when the AEM method developed by the McPhar Engineering Co. of Canada Ltd. and the International Nickel Company of Canada Ltd. went into use. The method was long used with success in exploration by the latter company.

In Finland the Geological Survey initiated aeromagnetic surveys in 1951. The first test flights were undertaken in 1953 with an AEM method developed by Maunu Puranen, Aarno Kahma and Väinö Rönkä. In 1954 the Geological Survey started systematic AEM surveys. In Sweden the company Boliden Ab commenced AEM measurements in the same year by a method developed at that company.

In 1955 Aeromagnetic Surveys Ltd. of Toronto introduced in Canada a dual-frequency method (later known also as the Canadian or Hunting Canso method) that became very popular and was applied successfully over large areas. This method, too, was developed by Puranen, Kahma and Rönkä. In the same year at least two other AEM methods went into use, namely, the rotary-field method developed by the Swedish company AB Elektrisk Malmletning and the helicopter-borne rigid-coil method of the American Metals Company.

In 1957 at least ten different types of AEM units were in use in various parts of the world. All of them were based on the transmitting of an audio-frequency, continuous wave by means of an induction coil. At the same time a new AFMAG method, based on the use of the natural electromagnetic field, was also tested as an airborne version. The next new AEM method was the pulse transient method, which was developed in Canada by the Selco Explorations Company and went into use in 1959. Towards the end of the 1950's a line-source method, i.e. a semi-ground, semi-airborne method, was also tested in Canada. Finally, the very low frequency (VLF) plane wave method was adopted for airborne use at the beginning of the 1970's.

In the USSR a rotary-field method was first put to use at the end of the 1950's; the line-source method was introduced in the early 1960's and since 1968 a pulse transient AEM method has been developed and employed as a helicopter-borne application.

To improve the resolution, accuracy and sensitivity of the AEM data the Nordic countries switched in the 1970's from towed-coil methods with a large coil separation to rigid-coil methods with a shorter coil separation. In North America emphasis shifted in the latter half of the 1960's to the pulse transient method. So far, the airborne applications of the VLF method have been to supplement rather than replace other methods (the Geological Survey of Sweden being a notable exception), whereas the AFMAG method is still at an experimental stage.

In the 1970's a common trend in development was towards the introduction of digital techniques for measuring and recording devices. Although the basic output of the AEM detector is the analog voltage signal, the digitisation of the signal markedly enlarges its dynamic range and thus improves the accuracy of the measurement. The digital storage of the survey data allows the production of various types of anomaly, derivative and interpretation maps by means of computer techniques.

The development of AEM methods has been treated in more detail by several authors, e.g. Puranen (1959), Mizyuk (1960), Pemberton (1962), Ward (1967b), Grip (1978) and Becker (1979).

Classification of AEM methods

As the previous chapter shows, numerous AEM methods have been developed. With some exaggeration, one could claim that no two AEM units are exactly alike in technical details. AEM methods differ from other aerogeophysical methods in that the structure of the aircraft largely determines the type of AEM system that the aircraft can house. This results from the noise generated by the mechanical (structural deformation) and electrical (conductive metal structure and electric circuitry) properties of the aircraft.

The large number of methods means that they can be classified on the basis of many diverse properties, the most common being the nature of the signal (harmonic continuous wave or pulse wave), the geometry of the source field (dipole, line or plane wave source) and the coil configuration (moving towed-coil or rigid fixed-coil system). The majority of the AEM systems are included in the harmonic dipole source methods; only the line source and the VLF and AFMAG methods belong to the less frequently used groups of line and plane source methods. In terms of data recording, the AEM systems, excluding the pulse transient methods, usually feature one or two channels. In the 1970's, however, the harmonic dipole source methods also experienced a certain shift towards the multichannel AEM systems with several frequencies or coil pairs.

Fields of application of AEM methods

AEM methods have been applied to exploration, geological mapping and special studies. Depending on the problem, the surveys are conducted as regional, local, detailed or special measurements.

The most important field of application of the AEM methods has been and still is exploration. The aim of the survey may be either directly to locate conductive formations, such as sulphide ores, or to apply it indirectly, e.g. to locate and trace ore-potential rock types. The mapping of ore-

ence signal also allows for the time variation of the total field, i.e. the signal measured can be divided into an in-phase component and a quadrature component 90° out of phase.

The intensity of the primary field for an arbitrary coil configuration can be deduced from the general formula of an oscillating magnetic dipole,

$$(2)\quad \mathbf{H}_p = -\frac{\mathbf{m}}{4\pi r^3} + \frac{3(\mathbf{m}\cdot\mathbf{r})\mathbf{r}}{4\pi r^5}\ (\mathrm{Am}^{-1}),$$

where $\mathbf{m} = nIA_T\mathbf{r}_A$ = magnetic dipole moment of the transmitter coil (Am^2), n = number of turns in the coil, I = output current (A), A_T = surface area of the coil (m^2), $\mathbf{r} = r\mathbf{r}_o$ = distance from the centre of the coil to the measuring point (m) and $\mathbf{r}_A, \mathbf{r}_o$ = unit vectors. A harmonic time variation $I = I_o e^{j\omega t}$ is assumed where I_o = a complex constant, $j = \sqrt{-1}$ = imaginary unit, $\omega = 2\pi f$ = angular frequency of the harmonic alternating field (s^{-1}), f = frequency (Hz) and t = time (s).

The formula (2) is valid when $r \geq 10 \cdot r_T$ where r_T = radius of the transmitter coil. It is also assumed that the displacement currents are negligible, or that the condition (Ward 1967a, p. 46)

$$(3)\quad \frac{\sigma}{\omega\varepsilon} >> 1$$

is met, where σ = electrical conductivity (hereafter abbreviated as conductivity) of the medium (Sm^{-1}) and ε = dielectric permittivity of the medium (Fm^{-1}).

From the formula (2) we obtain for the two AEM rigid-coil systems in general use:

$$(4)\quad H_p = -\frac{m}{4\pi r^3},$$

for a vertical coplanar coil configuration, and

$$(5)\quad H_p = \frac{m}{2\pi r^3},$$

for a vertical coaxial configuration. The coil configurations of towed-coil systems have not been standardised to such an extent as have those of the rigid-coil systems. Hence, once the dimensions of the coil configuration are known, the intensities for the primary field of the towed-coil systems must be deduced from the general formula (2).

AEM survey data are commonly given as relative changes, i.e. as anomaly values divided into in-phase and quadrature components Re and Im

$$(6)\quad \mathrm{Re} = \left(\frac{H_t\,(\mathrm{Re})}{H_p} - 1\right)10^6\ (\mathrm{ppm})$$

$$(7)\quad \mathrm{Im} = \frac{H_t\,(\mathrm{Im})}{H_p}\,10^6\ (\mathrm{ppm}),$$

where H_t (Re) and H_t (Im) are the in-phase and quadrature components of the total field, and the abbreviation ppm stands for parts per million.

The formula of the primary field (2) shows that the field strength of the dipole source is attenuated proportional to the inverse third power of the distance r from the source. In addition to this *geometric attenuation*, an *electrical attenuation* also takes place in a conductive medium. Its magnitude is defined as a *skin depth* distance δ, over which the intensity of the plane wave is reduced by 1/e, i.e. the field strength is 37 % of the primary one. The formula of the skin depth distance can be deduced from the expression of the field strength of a plane wave (Ward 1967a, pp. 41–46) by assuming the effect of the displacement currents to be negligible

$$(8)\quad \delta = \sqrt{\frac{2}{\sigma\mu\omega}}\ (\mathrm{m}),$$

where μ = magnetic permeability of the medium; in the international (SI) system of units

potential structural conductors (joint and fracture zones) may also be included in this group.

In geological mapping, AEM data supplement the results obtained by aeromagnetics. Provided that the surveys have been undertaken systematically and that the results are displayed appropriately, AEM data allow weakly magnetised but conductive formations to be traced effectively in areas of poor outcrop. Even so, AEM data do not seem to have been used very often in this way except in the Nordic countries and in the USSR. Lately, however, their use has shown a distinct increase, and good results have been reported, even from tropical areas with strongly weathered bedrock (Palacky 1981).

The application of AEM methods to overburden studies, although at its initial stage, shows some promise for the future. Its task may be to indicate soils that are either distinctly better (clay) or poorer (gravel) conductors than the surrounding ones (Fraser 1978, Becker 1979). Special applications include studies on the degree of fracturing in bedrock, investigations related to civil engineering projects or areas producing geothermal energy (Barringer 1971, Sellman, Arcone & Delaney 1976) and permafrost studies in arctic regions (Hoekstra, Sellman & Delaney 1975).

Principles and definitions

The present study deals in detail with a harmonic, continuous wave type of AEM method with a dipolar source and a rigid coil configuration. Consequently, unless otherwise stated, the following discussion refers to this type of AEM method.

The principle underlying the AEM method is the electromagnetic induction produced in the conductive medium (Fig. 1). The transmitter oscillator feeds alternating current into the transmitter coil. This gives rise to a primary field $\mathbf{H}_p$ that is dependent on the dimensions and self inductance of the coil. The primary field generates an electromotive force in the subsurface conductor, which produces an eddy current that is dependent on the properties of the conductor. The eddy current produces the secondary field $\mathbf{H}_s$. The primary field also induces eddy currents into the metal components of the aircraft, which generate their own secondary field $\mathbf{H}_a$. An electromotive force, which is proportional to the sum of all the above field components, i.e. to total field vector $\mathbf{H}_t$,

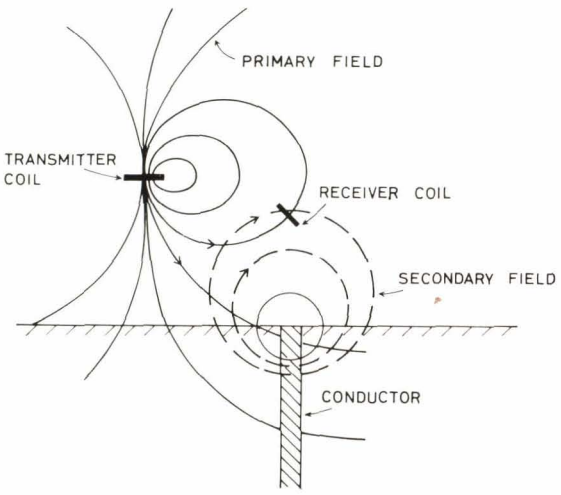

Fig. 1. Principle of the AEM method.

$$(1) \quad \mathbf{H}_t = \mathbf{H}_p + \mathbf{H}_s + \mathbf{H}_a,$$

is induced in the receiver coil.

The difficulty of the AEM measurements arises from the fact that, whereas $\mathbf{H}_s$ is the only part of the signal that carries geological information, both $\mathbf{H}_p$ and $\mathbf{H}_a$ are several orders of magnitude bigger than $\mathbf{H}_s$. Attempts are made to eliminate the influence of $\mathbf{H}_p$ and $\mathbf{H}_a$ by means of a reference signal and an electric compensation circuit. The refer-

ence signal also allows for the time variation of the total field, i.e. the signal measured can be divided into an in-phase component and a quadrature component 90° out of phase.

The intensity of the primary field for an arbitrary coil configuration can be deduced from the general formula of an oscillating magnetic dipole,

$$(2)\quad \mathbf{H}_p = -\frac{\mathbf{m}}{4\pi r^3} + \frac{3(\mathbf{m}\cdot\mathbf{r})\mathbf{r}}{4\pi r^5}\ (\mathrm{Am}^{-1}),$$

where $\mathbf{m} = nIA_T\mathbf{r}_A$ = magnetic dipole moment of the transmitter coil (Am^2), n = number of turns in the coil, I = output current (A), A_T = surface area of the coil (m^2), $\mathbf{r} = r\mathbf{r}_o$ = distance from the centre of the coil to the measuring point (m) and $\mathbf{r}_A, \mathbf{r}_o$ = unit vectors. A harmonic time variation $I = I_o e^{j\omega t}$ is assumed where I_o = a complex constant, $j = \sqrt{-1}$ = imaginary unit, $\omega = 2\pi f$ = angular frequency of the harmonic alternating field (s^{-1}), f = frequency (Hz) and t = time (s).

The formula (2) is valid when $r \geq 10 \cdot r_T$ where r_T = radius of the transmitter coil. It is also assumed that the displacement currents are negligible, or that the condition (Ward 1967a, p. 46)

$$(3)\quad \frac{\sigma}{\omega\varepsilon} >> 1$$

is met, where σ = electrical conductivity (hereafter abbreviated as conductivity) of the medium (Sm^{-1}) and ε = dielectric permittivity of the medium (Fm^{-1}).

From the formula (2) we obtain for the two AEM rigid-coil systems in general use:

$$(4)\quad H_p = -\frac{m}{4\pi r^3},$$

for a vertical coplanar coil configuration, and

$$(5)\quad H_p = \frac{m}{2\pi r^3},$$

for a vertical coaxial configuration. The coil configurations of towed-coil systems have not been standardised to such an extent as have those of the rigid-coil systems. Hence, once the dimensions of the coil configuration are known, the intensities for the primary field of the towed-coil systems must be deduced from the general formula (2).

AEM survey data are commonly given as relative changes, i.e. as anomaly values divided into in-phase and quadrature components Re and Im

$$(6)\quad \mathrm{Re} = \left(\frac{H_t\,(\mathrm{Re})}{H_p} - 1\right)10^6\ (\mathrm{ppm})$$

$$(7)\quad \mathrm{Im} = \frac{H_t\,(\mathrm{Im})}{H_p}\,10^6\ (\mathrm{ppm}),$$

where H_t (Re) and H_t (Im) are the in-phase and quadrature components of the total field, and the abbreviation ppm stands for parts per million.

The formula of the primary field (2) shows that the field strength of the dipole source is attenuated proportional to the inverse third power of the distance r from the source. In addition to this *geometric attenuation*, an *electrical attenuation* also takes place in a conductive medium. Its magnitude is defined as a *skin depth* distance δ, over which the intensity of the plane wave is reduced by 1/e, i.e. the field strength is 37 % of the primary one. The formula of the skin depth distance can be deduced from the expression of the field strength of a plane wave (Ward 1967a, pp. 41–46) by assuming the effect of the displacement currents to be negligible

$$(8)\quad \delta = \sqrt{\frac{2}{\sigma\mu\omega}}\ (\mathrm{m}),$$

where μ = magnetic permeability of the medium; in the international (SI) system of units

(9) $\mu = (1 + k)4\pi 10^{-7}$ (Hm^{-1})
$= \mu_r\mu_o$

where k = magnetic susceptibility and μ_r = 1 + k = relative permeability of the medium.

The skin depth parameter plays a significant role in the application of EM methods. Practical experience shows that the interpretability of EM data depends on the δ value of the conductor (e.g. Frischknecht 1967, p. 15). At high δ values the conductor is electrically thin and it is not possible, within the limits of measuring accuracy, to interpret separately its conductivity σ and thickness d from the survey data but merely the conductance s

(10) $s = \sigma d$ (S).

Within the limits allowed by the method, however, the σ and d values can be determined separately for an electrically thick conductor, i.e. when $d \geq \delta$.

The *sensitivity* of an AEM system is the ratio of the signal S produced by the conductive formation to the noise N of the system. Hence the sensitivity of an AEM system can be enhanced either by increasing the signal or by reducing the noise level, or both. Problems related to the design of the AEM instrumentation affecting the sensitivity have been discussed in detail by Ward and Hood (1969). Note that the sensitivity refers to the S/N ratio when the normal operational specifications of the AEM system have been met and that the properties of the conductor must be unambiguously defined (Paterson 1971). The signal S can then be determined by means of modelling and the noise level N from the data of field measurements.

If the depth to the upper surface of the conductor measured from the AEM unit increases while the other parameters remain constant, the anomaly and sensitivity, or the S/N ratio, decrease. The *penetration* of the AEM method is defined as the maximum depth of the conductor from which its effect is still detected in the survey data. The detection limit of an anomaly, S_d, is given in terms of S/N ratio and is generally set up at

(11) $S_d = 4N$.

As with sensitivity, the unambiguous determination of penetration requires definition of the parameters for the conductor and the AEM system, particularly if various systems are compared with each other.

The *resolution* of the AEM system means the possibility of recognising in the survey data the influence of the adjacent conductors. The property depends in declining order of importance on coil separation, flight elevation and coil configuration.

The *discrimination* of the AEM system refers to the possibility of deriving from survey data information relevant to the shape, location and physical properties of the conductor. Discrimination depends on the same factors as resolution, but in the reverse order of importance.

The *lateral coverage* of the method describes how well the strips between the flight traverses are surveyed when the line spacing is given. The factors primarily affecting the lateral coverage are flight elevation and coil separation.

The *response function* of the AEM system defines the behaviour of the in-phase and quadrature components as a function of the properties of the conductor and the system. On the basis of the theory of electromagnetism, it can be shown (Grant & West 1965, pp. 485–492, and Ward 1970, pp. 86–88) that the Re, Im anomaly values remain constant within certain limits at the constant values of the *response parameter* when the latter is combined from the variables of the conductor and the AEM system in a certain

manner. The general form for the response function RF is

(12) $RF = Re(\theta) + jIm(\theta)$,

and the response parameter θ is a dimensionless quantity of the form

(13) $\theta = \sigma\mu\omega l_1 l_2$.

In expression (13), l_1 and l_2 are the two linear dimensions of the measuring system and the conductor that have the greatest effect on the eddy current distribution in the conductor. It follows from the definition that the response function changes when the geometry of the conductor or the AEM system changes. The response function, however, retains its general form in spite of the changes and is thus very useful when the results of different conductors and AEM systems are compared, as is also shown by the examples in the present study. The problems entailed in selecting response parameters have been discussed by Ward (1970, pp. 86–88).

Fig. 2 is an example of the graph of a response function. It shows that the behaviour of the in-phase and quadrature components as a function of the response parameter is different. With $\mu_r = 1.0$ and at low θ values the in-phase component becomes zero, and at high θ values it reaches the saturation value Re_{max}, from which the in-phase anomaly will not change even if some of the factors in the response parameter, such as conductivity σ, increase. In contrast, the quadrature component equals zero at both low and high θ values and attains its maximum between these limit values. Only in an area where the values of the response function change is it possible to interpret the properties of the anomaly source in any detail. The area is called either a σ or a σd *aperture*, because the conductivity or the conductance are the parameters that alter the θ value within a given measuring system.

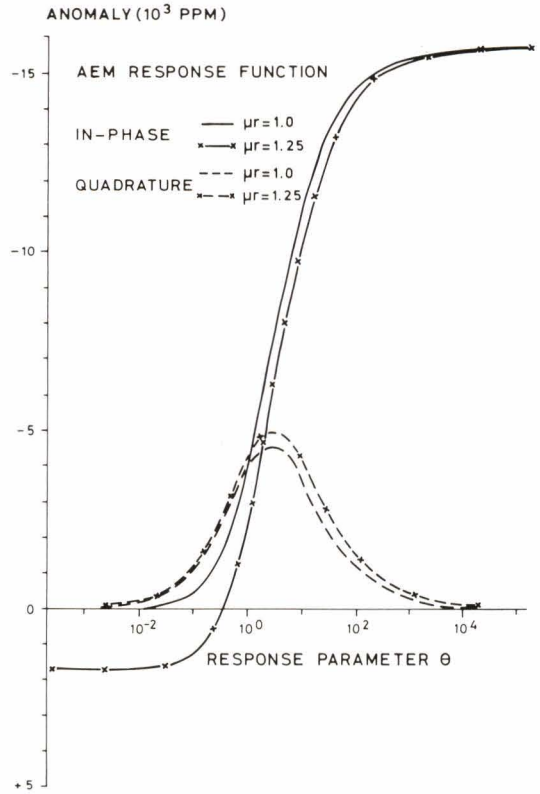

Fig. 2. Response function of the conductive, susceptive half-space in the DC-3 AEM system: the in-phase and quadrature anomalies as a function of the response parameter θ as defined by equations (13) and (26). The flight elevation h = 30 m is constant.

The lower (resistive) limit of the aperture defines the minimum value of σ or σd that is needed to make an anomaly recognisable within the sensitivity of the system. The upper (inductive) limit of the aperture may be either closed or open. In methods based solely on the measurement of the quadrature component or pulse transients the aperture is closed, which means that at high conductivities no anomalies are obtained. In methods measuring the in-phase component the aperture is open; thus, even if the discrimination range is truncated at the saturation limit Re_{max}, good conductors will always produce an anomaly. Since the response parameter is also a function of the frequency, it is

possible to affect the location of the aperture on the conductivity scale by appropriate choice of the frequency of the AEM system.

When $\mu_r > 1.0$ and the response parameter is on the resistive limit, the in-phase component of the response function receives values that are reversed to those of the normal responses due to conductivity. The response remains nearly constant up to a limit value; it then grades within a narrow range of response parameter values towards a normal conductivity response. The quadrature component is less affected, but the response values are systematically higher than those obtained with $\mu_r = 1.0$.

Coil separation plays a complicated role in AEM methods. When the coil separation increases while the other parameters remain constant the anomaly increases (H_p, which intersects the receiver coil, is reduced more than H_s), as does the lateral coverage of the method. On the other hand, the noise level also increases, and resolution and possibly discrimination are reduced. Even though the anomaly amplitude is enhanced the increase in coil separation does not necessarily imply an increase in sensitivity and penetration, the type of change being determined by the accompanying change in noise level. As the first approximation, let us assume that the noise level of the system is controlled by the motion-induced noise resulting from the small changes in the distance $\triangle l$ between the transmitter and the receiver coils. The effect of the change in the distance on the in-phase noise signal is (cf. formula (2))

$$(14) \quad N = \left| \frac{\triangle H_p}{H_p} \right| \approx 3 \left| \frac{\triangle l}{l} \right| 10^6 \text{ (ppm)}.$$

Thus, for example, with a coil separation of $l = 25$ m, the effect of $\triangle l = 1$ mm on the noise signal is N = 120 ppm. For two different systems with coil separations of l_a and l_b, respectively, to be equal in terms of this noise factor, the noise levels N_a and N_b must change in proportion to the change in the primary field, or

$$(15) \quad \frac{N_a}{N_b} = \left(\frac{l_a}{l_b}\right)^3$$

Hence, for example, the following systems are equal in terms of motion-induced noise: $l_a = 25$ m, $N_a = 25$ ppm and $l_b = 10$ m, $N_b = 1.6$ ppm. In practice, however, the situation is more complicated because the changes in $\triangle l$ and $\triangle H_p$ also give rise to a change in the field H_a produced by the aircraft, which in turn results in a noise signal on both the in-phase and quadrature channels.

The list of principles and definitions given also reflects the requirements the AEM method has to meet. Some of the requirements are contradictory. Hence, compromises must be made at the design stage by taking into consideration the properties of the aircraft, the purpose of application of the AEM results and the general geological setup of the survey area. Thus, there is no such thing as an AEM system ideal in all circumstances. The discussion also demonstrates that the design, constructing and installation of a high-quality AEM system is a complex process that requires expertise in various fields and is partly »more art than science».

AEM SURVEYS IN FINLAND

Since only a few of the AEM surveys carried out in Finland have been discussed in the literature, a brief summary of the subject is given.

Systematic measurements by the Geological Survey

Most aerogeophysical measurements in Finland have been undertaken by the Geological Survey. As stated on page 00, the Survey was among the first organisations to develop AEM methods. Development of and preparations for the measurements took several years (Puranen & Kahma 1947, 1949; the Geological Survey of Finland Annual Report 1951), and the decision reached in 1950 to start systematic aerogeophysical mapping to cover the whole country was a bold and far-reaching one. Mapping started in 1951 with aeromagnetics using a flux-gate magnetometer acquired from Canada. In 1954, measurements by a towed-coil AEM system constructed at the Survey were started, and in 1956 the equipment was supplemented by a gamma-ray scintillometer acquired from the USA (The Geological Survey of Finland Annual Report 1952, 1955, 1957). These high-elevation surveys were undertaken at a flight elevation of 150 m, with a line spacing of 400 m and an average survey speed of 260 km/h. The whole equipment was installed in a Lockheed Lodestar aircraft, owned and operated by Veljekset Karhumäki, later Kar-Air Oy. Field work for the high-elevation airborne surveys was completed in 1972 when general aeromagnetic mapping covered the whole country. In the same year more detailed low-elevation surveys were started with a nominal flight elevation of 30 m, a line spacing of 125–200 m and a survey speed of 170–200 km/h. In 1973–1979 the equipment, which included the AEM rigid-coil system, was fitted in a Douglas DC-3 aircraft owned and operated by Kar-Air Oy, and in 1972 and since 1980 again in a DHC-6 Twin Otter aircraft belonging to the same company.

Since 1954 the Geological Survey has used four different AEM dipole systems in its systematic surveys. In addition, various modifications of the main systems have been employed, but with less conspicuous differences in the survey data. The coil configurations of the AEM systems are shown in Fig. 3 and their main specifications in Table 1.

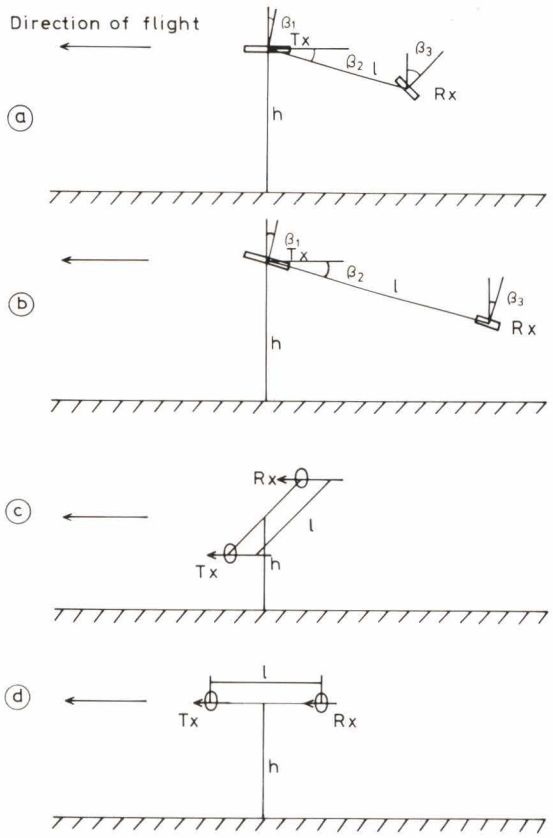

Fig. 3. Coil configurations used by the Geological Survey of Finland in systematic AEM surveys. Tx = transmitter coil, Rx = receiver coil, h = flight elevation, l = coil separation, β_1, β_3 = inclination angles of the transmitter and receiver coils, respectively, β_2 = towing angle of the receiver coil. (a) Towed-coil system I of the high-elevation surveys (Lockheed Lodestar, 1954–1959). (b) Towed-coil system II of the high-elevation surveys (Lockheed Lodestar, 1960–1971). (c) Rigid-coil system III of the low-elevation surveys (De Havilland Twin Otter, 1972, 1980–). (d) Rigid-coil system IV of the low-elevation surveys (Douglas DC-3, 1973–1979).

Two different towed-coil methods were used in the high-elevation flights. These are referred to as system I and system II. System I, which utilised only the quadrature component, was in service as two modifications in 1954–1959, the only visible difference

Table 1

Specifications of the systematic AEM survey systems used by the Geological Survey of Finland. Years of application for different versions are given in brackets.

	Towed-coil systems		Rigid-coil systems	
	I Lockheed Lodestar (1954–59)	II Lockheed Lodestar (1960–71)	III DHC-6 Twin Otter (1972, 1980–)	IV Douglas DC-3 (1973–79)
Survey specifications				
Line spacing (m)	400	400	200	200
Velocity (km/h)	260	260	180	200
Flight elevation (m)	150	150	30	30
Instrumentation specifications				
Coil separation (m)	150	150 (1960) 190 (1961) 250 (1962–71)	21.0 (1972) 21.44 (1980–)	26.5 (1973–74) 25.8 (1975–77) 25.0 (1978–79)
Frequency (Hz)	390 (1954–55) 410 (1956–59)	390 (1960) 410 (1961–66, 1968–71) 820 (1967)	3220	3220
Transmitter coil inclination angle β_1 (degr.)	0	15	90	90
Receiver coil inclination angle β_3 (degr.)	45	15	90	90
Towing angle β_2 (degr.)	15	15	–	–
Recorder type	analog	analog	digital	digital
Recording rate (times/s)	continuous	continuous	2 (1972) 4 (1980–)	2
Detector time constant (s)	1	1	0.3	0.3
Components recorded	quadrature (in-phase)	in-phase, quadrature } (1960) amplitude, phase angle } (1961–71)	in-phase quadrature	in-phase quadrature
Recorder resolution	0.1 %	0.2 % 0.1 degr.	5 ppm (1972) 1 ppm (1980–)	5 ppm
Noise level (under normal flight conditions)	0.1–0.2 %	0.5–1.0 % 0.1–0.2 degr.	40 ppm	25 ppm

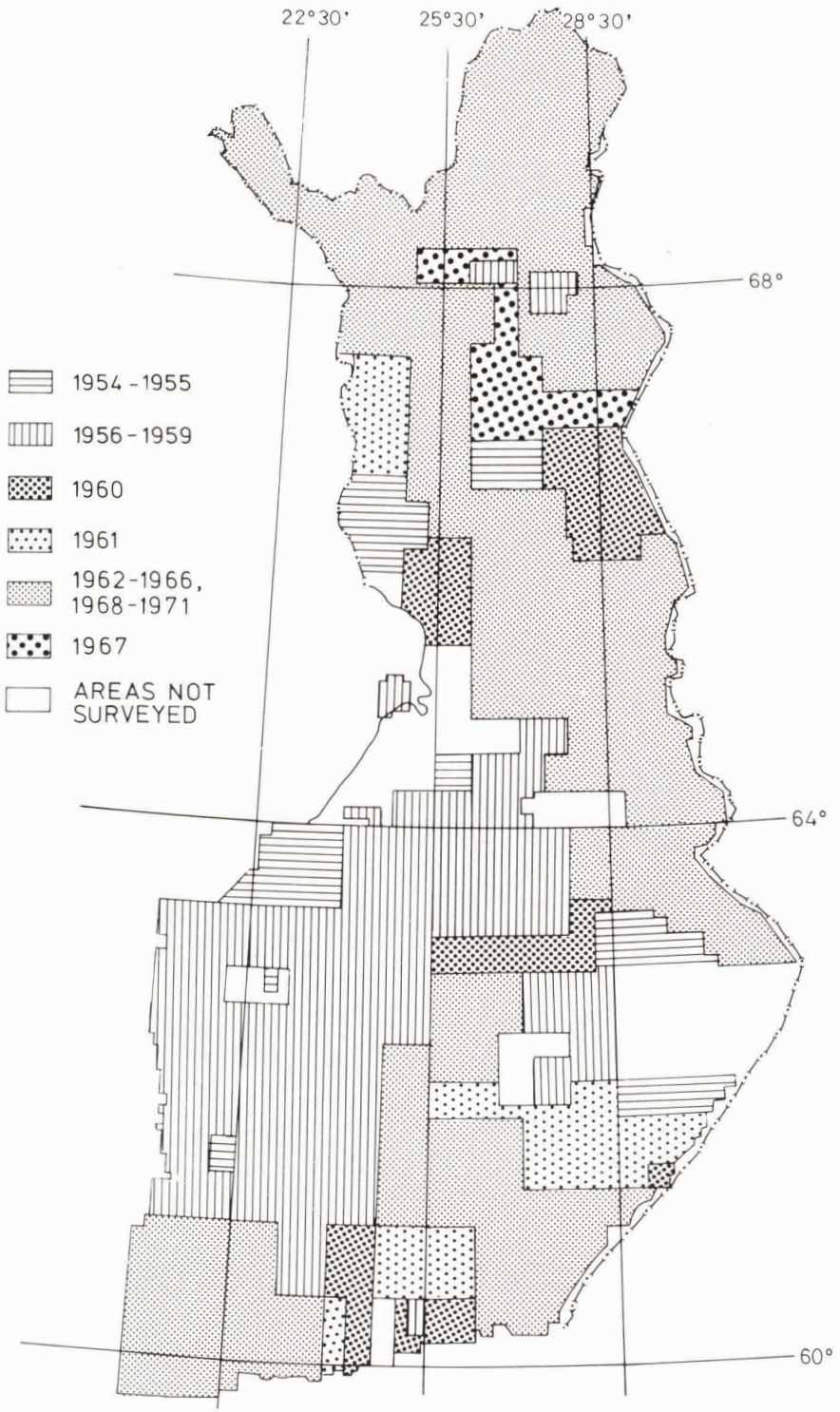

Fig. 4. Areal distribution of the systematic AEM surveys undertaken in Finland by the Geological Survey using the high-elevation towed-coil airborne systems.

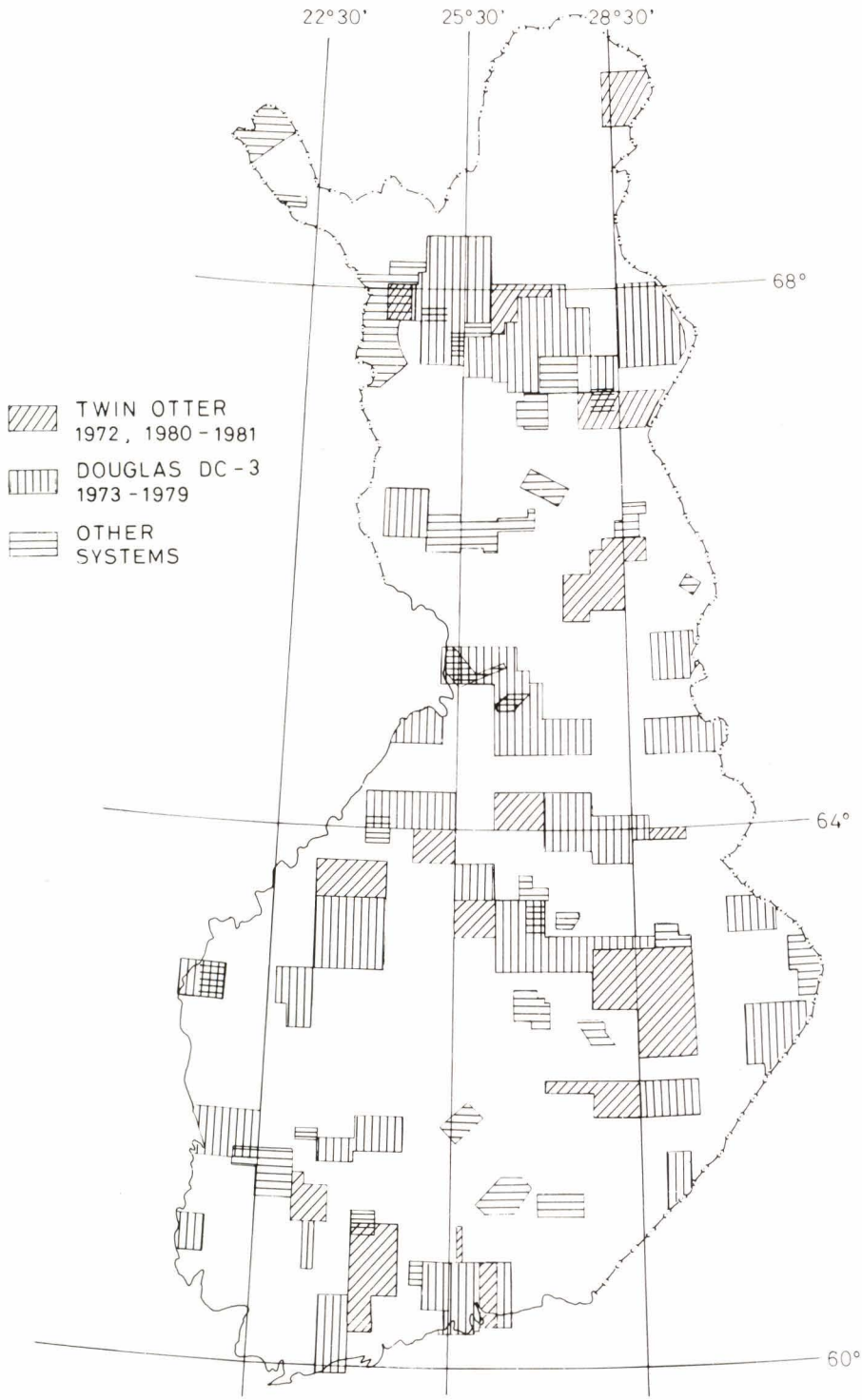

Fig. 5. Low-elevation AEM survey areas in Finland in 1972–1981.

being in the operating frequency. Since the lack of in-phase component data in the towed-coil methods restricts the usability of the results, the equipment was improved by slightly changing the coil configuration and increasing the tow resistance of the receiver coil unit. As a result, the variation in the coil separation became so small that it warranted the utilisation of in-phase component data as well. This improvement, which greatly enhanced the usefulness of the towed-coil method, seems to have been a rare achievement in routine use at that time. Thus renewed, system II went into operation in 1960. In the following year, the coil separation was increased to 190 m and the recording of new parameters (amplitude and phase angle) was started. The principal version of system II was developed in 1962, when the coil separation was further lengthened to 250 m, and was in service as such until 1971.

Towed-coil methods like those of systems I and II as used by the Geological Survey of Finland do not seem to have been in service elsewhere; at least they have not been reported in the literature. Probably the closest counterpart is the dual-frequency (Hunting Canso or Canadian) method developed by the same investigators (Puranen & Kahma 1956, Rönkä 1958), but which differs from the towed-coil systems of the Geological Survey in both coil configuration and principle of operation. The dual-frequency method has been described in detail by Puranen (1959) and Paterson (1961).

The data of the towed-coil systems were recorded in analog form on a chart recorder and then processed manually into profile maps on a scale of 1: 20 000. After photographic reduction and compilation, maps on a scale of 1: 100 000 were also released.

The low-elevation surveys in 1972 and 1980– were conducted with the vertical coplanar rigid-coil system III. In 1973–1979 the surveys were undertaken with the vertical coaxial rigid-coil system IV. The data of rigid-coil systems III and IV were recorded in digital form and processed by computer methods into profile and contour maps on a scale of 1: 20 000.

Fig. 4 illustrates the areal distribution of the surveys undertaken with the various high-elevation AEM systems. The areas surveyed in 1954–1971 cover a total of 316 000 km² (about 800 000 line kilometres), or about 94 % of the surface area of the Finnish mainland. With the exception of the Turku Archipelago, no AEM surveys were conducted over sea areas. In 1972–1981 the Geological Survey undertook low-elevation AEM surveys with a total coverage of 86 000 km² (430 000 line kilometres) in the areas shown by the index map in Fig. 5. Of them 58 100 km² were covered by the DC-3 AEM system IV (295 000 line kilometres).

Mention should be made of the publications relevant to systematic AEM surveys. Especially noteworthy is the pioneering but little known work by Puranen (1959) that describes in detail the development, measuring technique and interpretation of the results of the high-elevation system I. The application of AEM data to prospecting and geological mapping has been discussed by Puranen (1963), Marmo (1964), Marmo and Puranen (1966) and Lanne (1980a, 1980b). The data given in the preceding pages on the later AEM systems of the Geological Survey are based on a paper by Peltoniemi (1977), which also describes modelling results for various systems. AEM instrumentation and data processing of low-elevation systems have been described by Peltoniemi (1975, 1978a). Liljestrand (1972) has carried out scale model studies to interpret the results of system II. Hämäläinen (1977) has performed similar studies for systems III and IV. Ovaskainen and Peltoniemi (1979) have reported what is so far the largest set of results for scale model studies on systems I–IV of the

Geological Survey. Peltoniemi (1978b, 1980a, 1980b) has given numerical modelling results for layered earth and a conductive sphere on most of the AEM methods used in Finland.

Supplementary studies by the Geological Survey

Apart from the above systems in routine use, the Survey has applied several other AEM methods either in supplementary or experimental studies. In 1959 detailed measurements were carried out with a towed-coil system attached to a Cessna 195 aircraft; the coil configuration was similar to that of the Lockheed system I in use in those days. The flight elevation was 50–70 m, the coil separation 120 m or 150 m and the line spacing 400 m. The frequency of the transmitter was 1 620 Hz, and the data were recorded as in-phase and quadrature components. In 1960–1963 the same system was installed in an Aero Commander aircraft. The coil separation was 200 m, the flight elevation 100 m and the line spacing 200 m. A total of 5 000 km² was covered with this system over prospecting targets in various parts of Finland.

An experiment was undertaken in 1964 with a vertical coaxial rigid-coil system mounted in a helicopter-towed boom. The experiment had to be suspended for lack of a helicopter with a bigger payload than the Bell 47J then available. In 1966 tests were run with the same equipment as a vertical coplanar coil system fitted to Aero Commander 500 and Pilatus Porter aircraft.

In 1972, experimental measurements were performed with the VLF method in association with systematic low-elevation surveys. In these measurements use was made of the primary field of a transmitter station in the Omega navigation chain in Norway. Both magnetic and electric field components were recorded in the measurements. In 1978 airborne VLF measurements were performed over an area of 1 530 km² in NW Lapland with a VLF receiver fitted in a Sikorsky 55B helicopter and by using the GBR (Rugby, England) transmitter station. Savolainen (1979) has reported in detail on the measurements and the results obtained. In the same year, a 4 345-line-km AEM survey was flown for the Geological Survey with Suomen Malmi Oy as contractor. The equipment is described in the next chapter.

Other measurements undertaken in Finland

The national aerogeophysical mapping programme of the Geological Survey of Finland was not alone able to meet all the survey requirements of Finnish exploration organisations. Moreover, it was often necessary to perform more accurate measurements for exploration purposes over smaller targets with a shorter line spacing and lower flight elevation than was possible with the national mapping programme. As a consequence, bigger exploration organisations have performed quite extensive AEM surveys either with their own systems or with those of contractors.

Outokumpu Oy started aerogeophysical surveying in 1957 with aeromagnetics. In 1959 the company started with AEM test measurements and in 1960 it began systematic surveying with its own equipment. Until 1970 surveys were undertaken with a rotary-

field method. In 1973–1979 a vertical coplanar rigid-coil method was in use. A total of 173 000 line kilometres was covered with the rotary-field system and 58 330 line kilometres (7 250 km²) with the rigid-coil system.

Törnqvist (1958) has described the concept of the rotary-field method. Ketola, Laurila and Suokonaukio (1971) and Ketola (1972) have reported on the system as it was used by Outokumpu Oy. The company applied the system as a two-aircraft modification, the distance between the aircraft, i.e. the coil separation, being 220–260 m, the frequency 880 Hz, the flight elevation 60–100 m and the line spacing 250 m. Until 1968 the data were recorded in analog form and profile maps were drawn manually. The results of the rigid-coil method used later have been reported by Ketola (1979) and Laurila (personal communication). The system, operated first with Finnprospecting Ky and then with Suomen Malmi Oy as contractors, was installed in a Pilatus Turbo Porter aircraft. The coil separation was 16.4 m and the frequency 3 600 Hz. The surveying was undertaken from a nominal flight elevation of 30 m with a line spacing of 125 m. The unit was provided with digital data recording, and the results were drawn as contour maps by computer processing methods.

Rautaruukki Oy (formerly Otanmäki Oy) started aerogeophysical surveying with aeromagnetics in 1955. From 1966 onwards the company undertook AEM measurements with its own rigid-coil unit installed in a Cessna 185 aircraft. The coil separation of the vertical coplanar system was 11 m and the frequency 1 920 Hz. The surveys were performed at a nominal flight elevation of 30 m and with a line spacing of 200 m. The data were recorded in analog form and the profile maps were compiled manually. In 1973–1979 Rautaruukki Oy conducted AEM surveys with the same contractors as Outokumpu Oy. From 1966 to 1979 the company undertook AEM measurements over an area totalling 33 190 km². Paarma (1969, 1971) and Nuutilainen (personal communication) have summarised the aerogeophysical methods employed by Rautaruukki Oy.

The survey and data processing methods used by the various organisations in their systematic low-elevation AEM studies have all been fairly similar. Hence, the target areas of the AEM surveys conducted by Outokumpu Oy and Rautaruukki Oy in 1973–1979 are also marked on the index map of low-elevation surveys in Fig. 5.

Finally, as a speciality of AEM surveying, it is worth mentioning the airborne measurements of the field intensity of Finnish broadcasting stations undertaken by Oy Yleisradio Ab. The results have been compiled by Laiho (1975) as a ground conductivity map on a scale of 1 : 2 million covering the whole country. The map is, however, of a rather generalised nature on account of the measuring and data processing techniques.

Finland has been fairly self-sufficient in its AEM surveying, only some test flights being undertaken with foreign equipment. Rotary-field test surveys from AB Elektrisk Malmletning, Sweden, were ordered by Outokumpu Oy in 1959 before the company acquired its own instrumentation. In 1964 Otanmäki Oy performed a test survey with a fixed-coil wingtip system developed by Boliden Ab, Sweden. In 1961 the same system had been applied in a test survey at the Pyhäsalmi ore deposit (Bärlund 1966). In 1965 Barringer Research Ltd. of Canada collaborated with Otanmäki Oy in experiments with the pulse transient method off the town of Raahe (Boniwell 1967) and in the following year with both Otanmäki Oy and Outokumpu Oy on various prospects in NW Finland.

THE DC-3 AEM SYSTEM OF THE GEOLOGICAL SURVEY OF FINLAND

The present study deals with the characteristics and results of the vertical coaxial coil system installed in a DC-3 aircraft. Therefore, only the instrumentation of this AEM system is treated here in more detail. The main specifications of the equipment are listed in Table 1.

Instrumentation

The concept and main components of the AEM device are shown in Fig. 6. The transmitter unit consists of a stabilised power source, a crystal-controlled oscillator, a current transformer for reference output and a tuned transmitter coil. The receiver unit features a tuned receiver coil, a compensating circuit and two tuned, phase-locked amplifiers. Except for the amplifiers, the equipment was designed and constructed in 1971–1972 by Maunu Puranen, Uljas Hämäläinen, Simo Lehtinen, Kalevi Sulkanen and Keijo Westerlund at the Geophysics Department of the Geological Survey. Some smaller alterations and improvements have been made every year. The main technical and operational specifications of the equipment were as follows.

The output power on the terminals of the air-cored transmitter coil was 50 W. The moment of the magnetic dipole produced by the transmitter coil was originally $m = 27$ Am² (the diameter of the transmitter coil 0.28 m) and, since 1975, owing to the new and larger coil (diameter 1.01 m), $m = 120$ Am². The increase in the dipole moment substantially improved the S/N ratio of the system. The transmitter fed a square wave into the coil at a frequency of $f = 3\,220$ Hz. The mass of the transmitter coil was 5 kg and that of the crossbeam support 36 kg.

The air-cored, tuned receiver coil had 680 turns and a tuning ratio of $Q_t = 85$ without load. The coil diameter was 0.28 m and the mass 5 kg. As an original crossbeam structure, the mass of the support was 37 kg and since 1978, as a shell structure, 38 kg. The coil installations with the supports are illustrated in Fig. 7a (transmitter coil) and Fig. 7b (receiver coil).

The coil separation of the system was originally $l = 26.5$ m; after the changes in the transmitter coil and receiver support it was $l = 25.0$ m. Structurally, the vertical coaxial coil system used was well suited to the DC-3 aircraft, because, in spite of the fairly large coil separation, the fuselage was subject to only very slight bending and vibration during flight.

According to the manufacturer's specifications, the phase-locked amplifiers (type Brookdeal 401A) have an accuracy of 3 %, an output stability of < 0.1 %/°C and < 0.03 %/24 h, and a non-linearity value of < 0.01 %. The specified noise of the amplifier is < 10 nV/$\sqrt{\text{Hz}}$ with an optimum load. The time constant of the low-pass filter in the amplifier output was set at $\tau = 0.3$ s, which should be kept in mind when judging the noise value N of the system. Such an exceptionally low time constant is essential in low-elevation airborne surveying with fixed-wing aircraft so that the sharp anomalies caused by small conductors can be recognised in the recorded data. The noise value, the importance of the time constant and the noise filtering of the data are discussed in greater detail on pages 32–41.

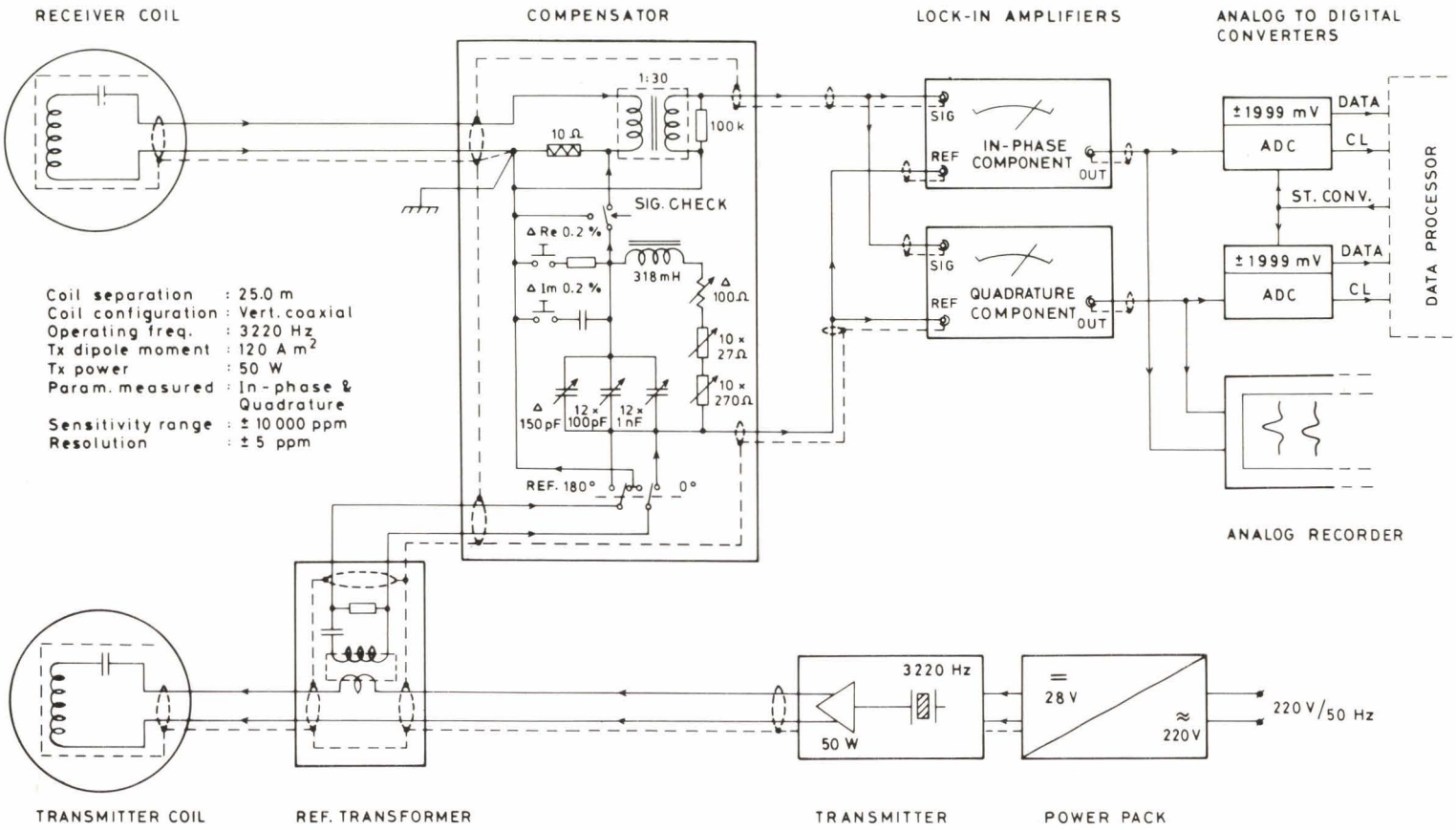

Fig. 6. Main components and schematic circuitry of the DC-3 AEM device.

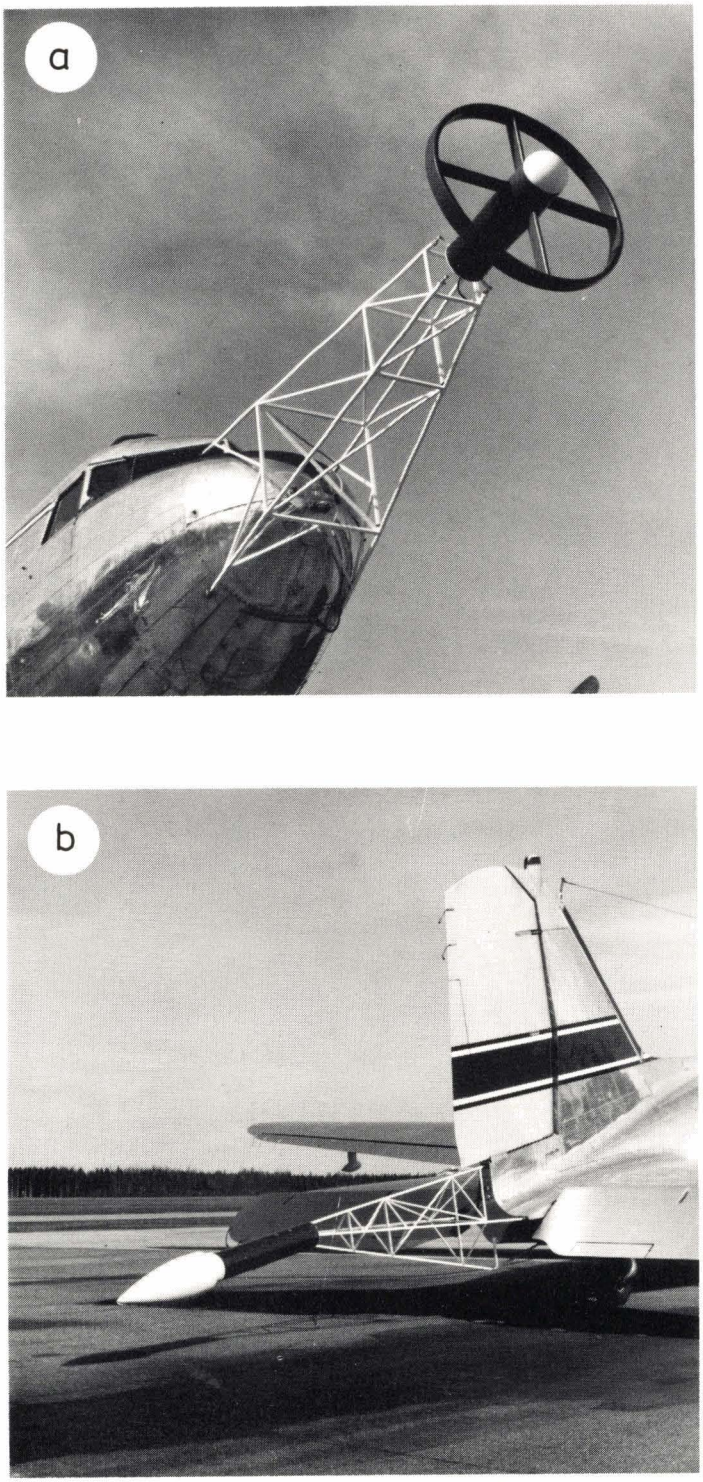

Fig. 7. Coils and supports of the AEM device fitted in a DC-3 aircraft (Photo E. Halme). (a) Transmitter coil. (b) Receiver coil.

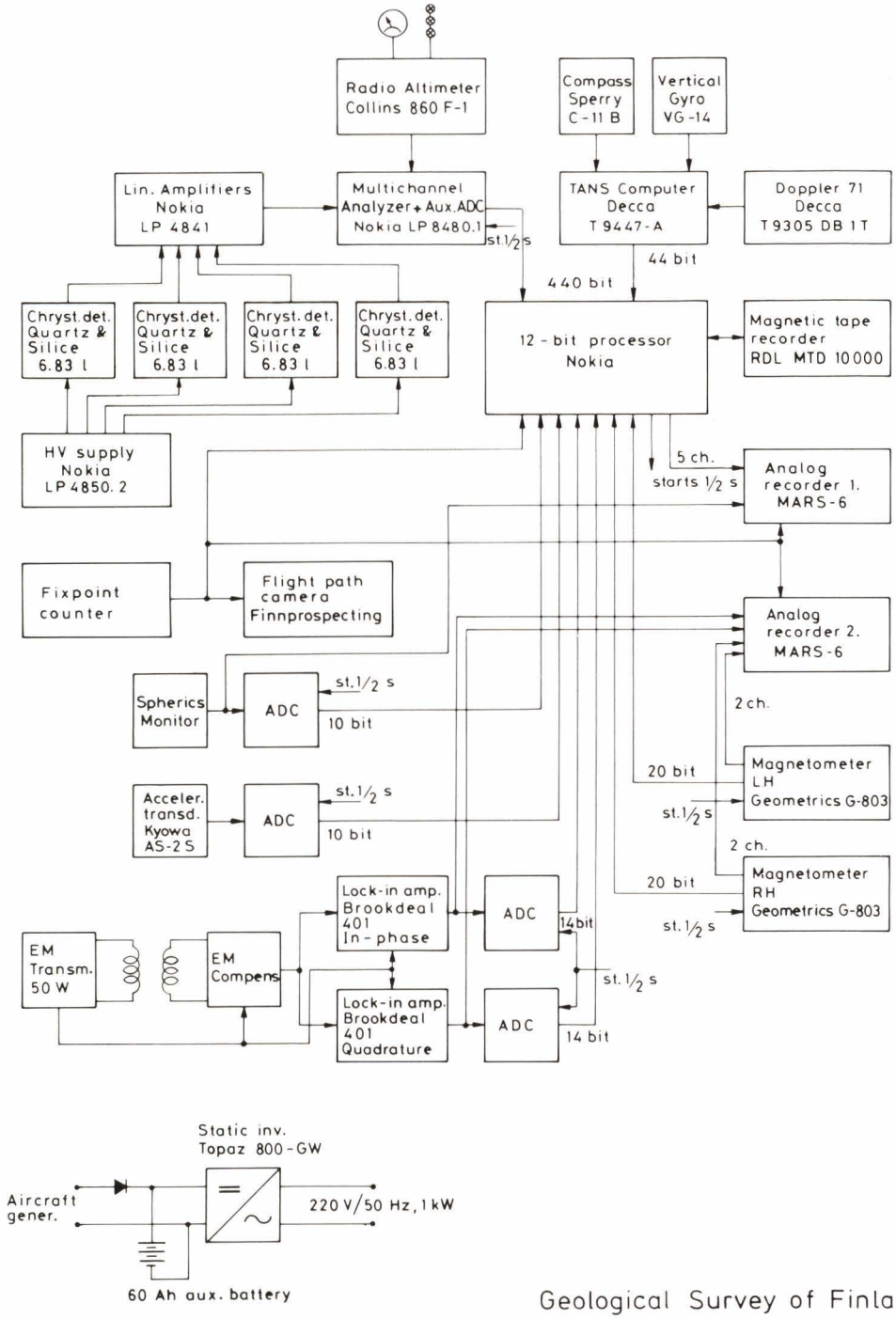

Fig. 8. Signal flow diagram of the DC-3 aerogeophysical system.

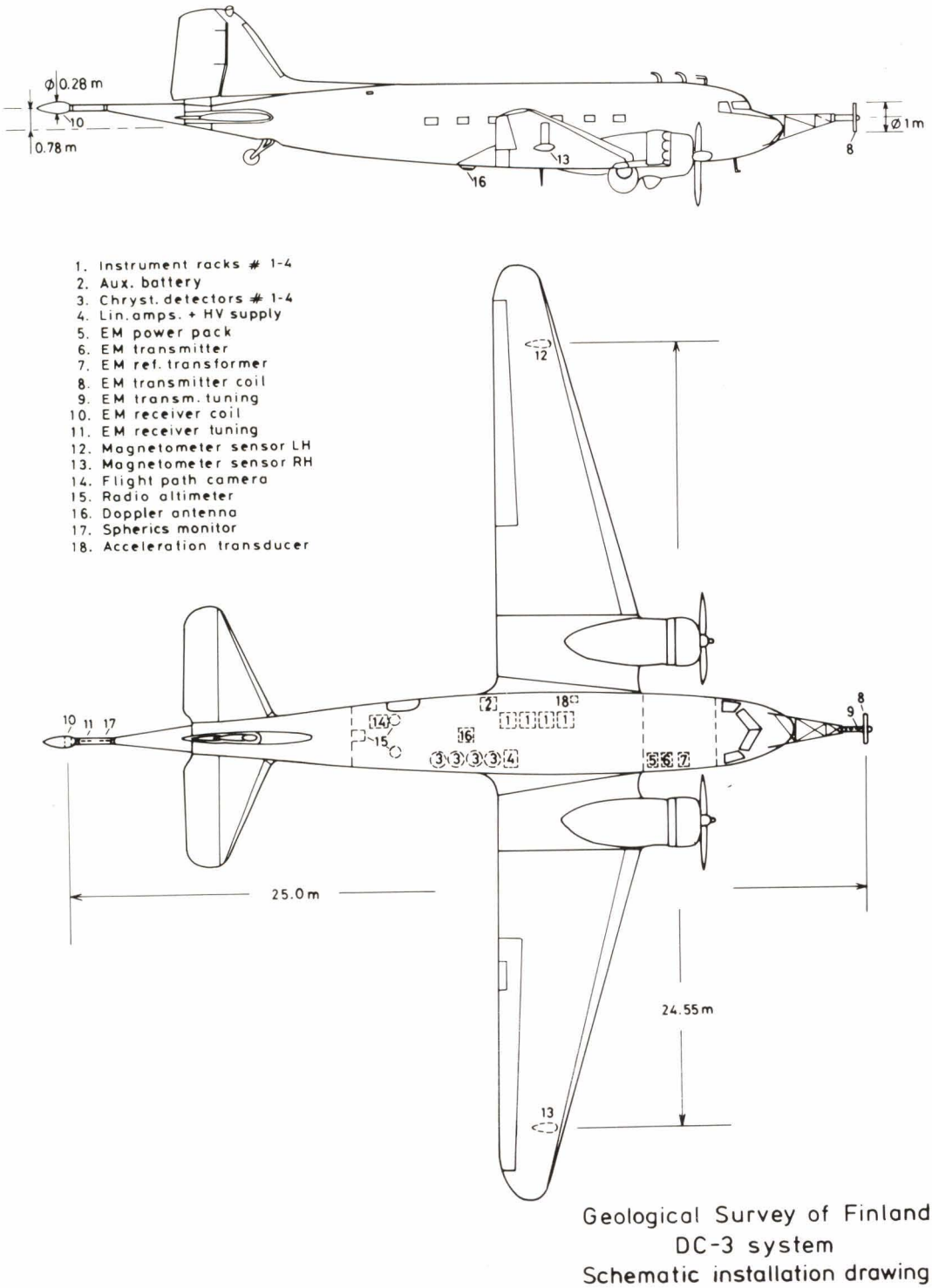

Fig. 9. Schematic installation drawing of the DC-3 aerogeophysical survey system.

The AEM analog voltage signals of the in-phase and quadrature components were converted into digital form in 14-bit analog-to-digital conversion (ADC) circuits (Datel Systems Inc. type E12D) with a conversion time of 5 ms/sample. The digital data were recorded at 0.5 s intervals with 3 significant digits and with an electrical resolution of ± 1 mV (± 5 ppm). The sign and the ADC overflow bits were stored into a fourth digit. For monitoring purposes during the flight, the analog signals were displayed by a chart recorder on two channels, initially with a sensitivity of 40 ppm/mm and later 200 ppm/mm.

Important peripherals and auxiliary devices in the DC-3 AEM system included:

- A digital incremental magnetic tape recorder, originally with a recording

Table 2

Contents and format of the 1-second digital record of data in the DC-3 aerogeophysical system.

Variable	Identifier	Number of digits	Resolution	Remarks
Day	T	3		update cycle 1 s
Time		6	1 s	
Doppler x-coordinate	X	5	10 m	
Doppler y-coordinate	Y	5	10 m	
Flight elevation	A	3	1 m	update cycle 0.5 s, first period
Fixpoint	P	3		
AEM in-phase component	E	4	5 ppm	
AEM quadrature component		4	5 ppm	
Magnetic total field (left-wing sensor)	M	5	1 nT	
Magnetic total field (right-wing sensor)	N	5	1 nT	
Doppler time	C	1	0.1 s	
Vertical acceleration change		3	0.05 ms^{-2}	
Fixpoint time		1	0.1 s	
Spherics monitor channel		3	1 mV	
Gamma-ray spectrometer channel 1	R	2		
2		2		
⋮		⋮		
54		2		
Synchronisation character	S			
Flight elevation	A	3	1 m	update cycle 0.5 s, second period
Fixpoint	P	3		
AEM in-phase component	E	4	5 ppm	
AEM quadrature component		4	5 ppm	
Magnetic total field (left-wing sensor)	M	5	1 nT	
Magnetic total field (right-wing sensor)	N	5	1 nT	
Doppler time	C	1	0.1 s	
Vertical acceleration change		3	0.05 ms^{2}	
Fixpoint time		1	0.1 s	
Spherics monitor channel		3	1 mV	
Gamma-ray spectrometer channel 1	R	2		
2		2		
⋮		⋮		
54		2		
Synchronisation character	S			
Total number of variables/s 132				
Total number of characters/s		318		

density of 200 bytes per inch (BPI), in 1974 of 556 BPI and finally since 1975 of 800 BPI.

- A digital data acquisition device with a processor unit having a reprogram mable read-only-memory capacity of 2 k 12-bit words and a direct-access memory capacity of 256 words. From 1975 onwards the basic 1-second digital record included 299 digits of geophysical data and 19 control digits, that is, a total of 318 ASCII characters as listed in Table 2. The data acquisition device was modified by Eero Hiltunen from a processor originally produced by Nokia Oy for the »Mikko 1» microcomputer. He was also responsible for the assembler programming of the processor unit.
- A spherics monitor to recognise spurious anomalies (noise transients from atmospheric electricity) originated outside the AEM instrumentation. The device featured a small auxiliary coil and a bandpass (1–10 kHz) amplifier. The output voltage of the amplifier was digitised and recorded at 0.5 s intervals.
- A strain-gauge transducer to measure the changes in the vertical acceleration of the aircraft. These data, which give an indirect measure on the motion-induced AEM noise, were also digitally recorded at 0.5 s intervals.
- A flight-path camera.
- A Dopper positioning system.
- A radio altimeter.

The total mass of the instrumentation was about 1 100 kg and the power consumed about 1 700 W. The signal flow diagram of the whole aerogeophysical system is shown in Fig. 8 and the schematic installation drawing in Fig. 9. The instrumentation inside the

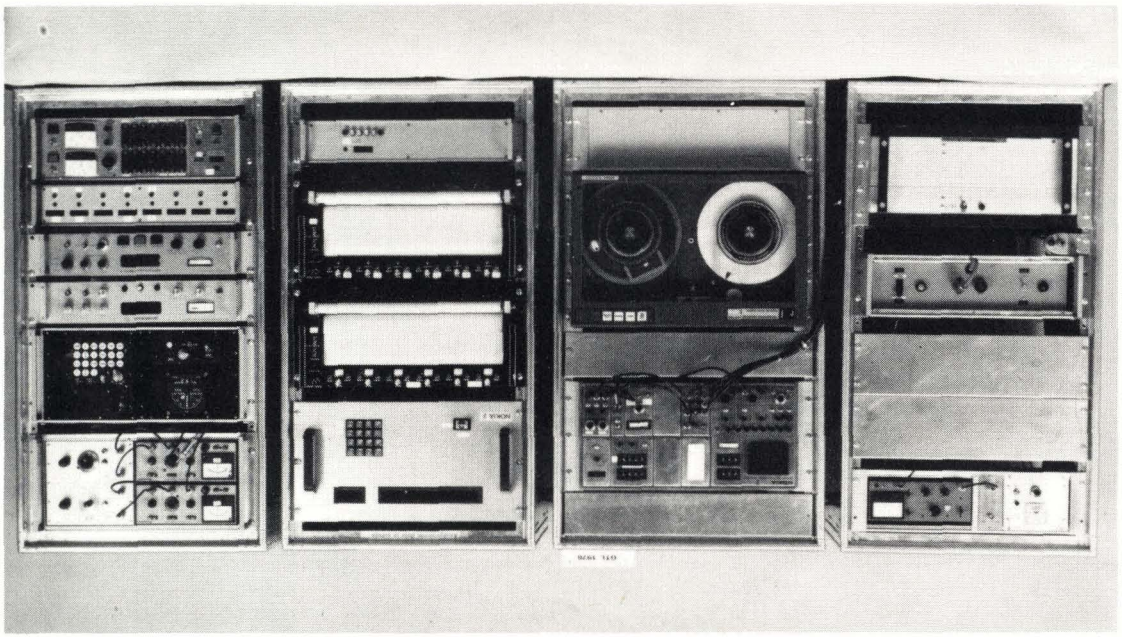

Fig. 10. DC-3 aerogeophysical survey instrumentation. From left to right: strain gauge transducer and spherics monitor amplifiers, DC/AC converter and power pack (rack I), gamma-ray spectrometer and magnetic tape recorder (rack II), digital data logger and two multichannel analog recorders (rack III), AEM compensator and lock-in amplifiers, Doppler navigation unit, two proton free-precession magnetometers, ADC converter, switch and fuse board (rack IV) (Photo E. Halme).

aircraft was fitted in four racks as illustrated in Fig. 10.

Aeromagnetic surveying with the DC-3 aerogeophysical system has been described by Korhonen (1979), and gamma-ray spectrometer studies by Peltoniemi (1975, 1979b) and Peltoniemi and Kuittinen (1978).

Noise level of the system

Sources of noise

The noise in the AEM data is due to:

- Noise generated within the measuring system.
- Noise from external sources.
- Noise due to geology.

The noise that is generated within the measuring system derives from the aircraft or from the AEM instrumentation. The noise produced by the aircraft is due to the ignition circuitry of the engines and to the eddy currents that are induced in the metallic components (e.g. propellers, ailerons) as they move in relation to the AEM coil configuration. Noise due to movements of the rudder, elevator and the ailerons can be reduced by cutting off the eddy current loops. Temporary changes in the compensation of the anomaly produced by the aircraft (H_a in equation (1)) manifest themselves in the data as noise that generally has a low rate of drift.

It would be highly advantageous for the AEM installation, if all the instruments, including the aircraft's electrical systems, were wired using two-lead cables (floating) and the whole circuitry had only one earthing point. Since, however, the two-lead design is not used in the aircraft's electric circuitry, the minimising of the electrical noise produced by the earthing currents and by the current loops of its instruments is a very important phase in the final installation of the AEM equipment. If this is successfully achieved, the biggest source of electronic noise is the compensator, as all distortions in the reference waveform are transferred as spurious signal voltages from the compensator into the amplifiers.

Noise in the AEM installation is also produced by changes in the separation and attitude of the coils (motion-induced noise, equation (14)), by the thermal drift of the mechanical structures and the components of the electric circuitry, and by the thermal agitation (Johnson) noise caused in the receiver coil, compensator and amplifiers. The magnitude N_T of the Johnson noise in the terminals of the receiver coil can be calculated from the equation (Ward & Hood 1969 p. 65)

$$(16) \quad N_T = \sqrt{4k_B BTR}\ (V/\sqrt{Hz})$$

where k_B = Boltzmann's constant, $1.38 \cdot 10^{-23}$ (VA/°K), B = bandwidth of the tuned receiver coil circuitry (Hz), T = temperature (°K), and R = resistance of the receiver coil (Ω). In the DC-3 AEM system the equation gives N_T = 6.9 nV (0.4 ppm)/$\sqrt{Hz}$, when T = 300 °K, R = 24 Ω and B = 119 Hz.

The maximum noise N_{ADC} due to the finite accuracy in the digitisation of the analog voltage signal can be calculated from the formula (Hartimo 1981)

$$(17) \quad \frac{S}{N_{ADC}} = 6n_{ADC} - 1.24\ (dB),$$

where n_{ADC} is the number of bits in the ADC conversion circuit. When S = 1000 mV and n_{ADC} = 12, the formula gives for the DC-3 system N_{ADC} = 1.5 ppm as the maximum noise value.

Natural and man-made electromagnetic fields are the predominant sources of external noise. The natural EM field creates both a background noise that fluctuates rather slowly and rapid noise transients due to thunderstorms and other atmospheric electricity discharges. The man-made noise derives from transmission lines, railways and telegraph lines. As individual sources of noise, their effect is felt only within a narrow area around the source, and the linear anomaly produced is usually readily recognisable on the AEM profile map. In the vicinity of towns and industrial developments the effects are summed up and the signal/noise ratio is so reduced that the AEM data do not have much value.

The concept of geological noise can be clearly defined only when the AEM system is applied to exploration. The geological noise is then due to variations in the conductivity and thickness of the overburden and to changes in the anomalies caused by weakly conductive and/or susceptive country rocks. The amount of geological noise can be affected by the dimensioning of the AEM system, as was demonstrated in connection with the response parameter (p. 16). If, however, the AEM data are used in other applications than direct exploration, the geological noise signal may not exist at all. The success of the geological assessment of the data then depends on the interpretation employed by the user and on the follow-up studies.

As was stated on page 15, the signal to noise ratio S/N, which affects decisively the usefulness of the data, can be improved by increasing the signal S and/or reducing the noise N. The changes in coil separation and coil attitude introduce noise that is directly proportional to the primary field H_p, equation (14), and hence their effect on the noise level cannot be eliminated by increasing the signal. Thus, motion-induced noise remains the predominant one in continuous-wave, rigid-coil systems, even if all the other sources of noise could be minimised.

Estimation of noise level

In the DC-3 AEM system the voltage signal induced by the primary field in the receiver

Table 3

Noise in the DC-3 AEM data: the averages of the in-phase and quadrature data $\overline{Re}$, $\overline{Im}$ and the standard deviations σ_{Re}, σ_{Im} calculated from the profiles marked in Fig. 11. The averages of the flight elevation (Fig. 19) h, the average changes in vertical acceleration (Fig. 21) Δg_z, and the standard deviations σ_h and $\sigma_{\Delta gz}$ are also given for the same profiles.

Survey profile number	Flight conditions	Number of points	AEM				Flight elevation		Vert. acceleration	
			$\overline{Re}$ (ppm)	σ_{Re} (ppm)	$\overline{Im}$ (ppm)	σ_{Im} Pppm	$\bar{h}$ (m)	$\sigma_{\bar{h}}$ (m)	$\overline{\Delta g}_z$ (mV)	$\sigma_{\Delta gz}$ (mV)
108	good	73	18.5	20.3	−77.2	11.5	44.0	7.2	14.1	13.6
109	good	59	38.4	26.0	3.1	15.0	43.5	5.1	14.6	18.3
113	good	54	− 9.7	14.0	14.9	11.4	46.2	6.7	14.1	11.9
118	good	113	−17.5	14.2	12.7	20.9	45.6	6.4	13.8	15.7
144	good	63	2.5	17.6	− 9.8	18.5	41.5	6.8	2.1	9.2
101	fair	68	− 5.6	37.2	18.1	37.1	38.0	4.7	16.6	15.1
107	fair	53	−25.0	21.1	68.6	14.9	39.9	4.8	17.1	17.2
127	poor	58	1.6	12.9	37.7	14.7	50.6	6.2	3.1	19.5
135	poor	81	−21.0	15.7	29.5	23.3	40.9	4.5	4.3	13.7
139	poor	62	−34.2	28.3	− 9.5	18.7	37.8	3.9	3.3	17.4
141	poor	63	23.4	26.7	30.9	37.7	38.1	6.4	2.6	11.7

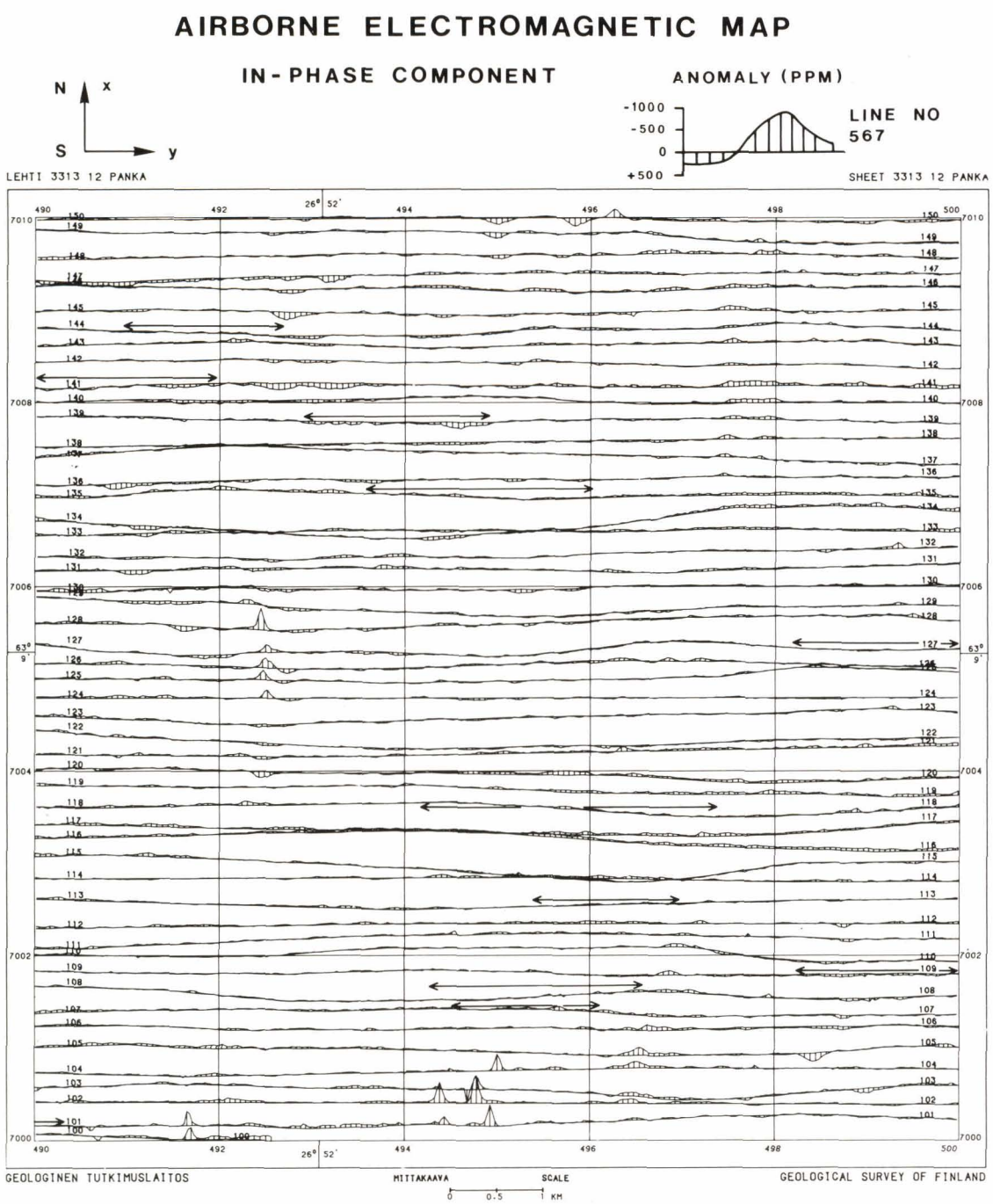

Fig. 11. Anomaly maps drawn from DC-3 AEM data, map sheet 3313 12 from the Tervo area. The portions of the profiles used in calculating the noise level are marked on the figure. (a) In-phase component. (b) Quadrature component (see page 35).

AIRBORNE ELECTROMAGNETIC MAP

QUADRATURE COMPONENT

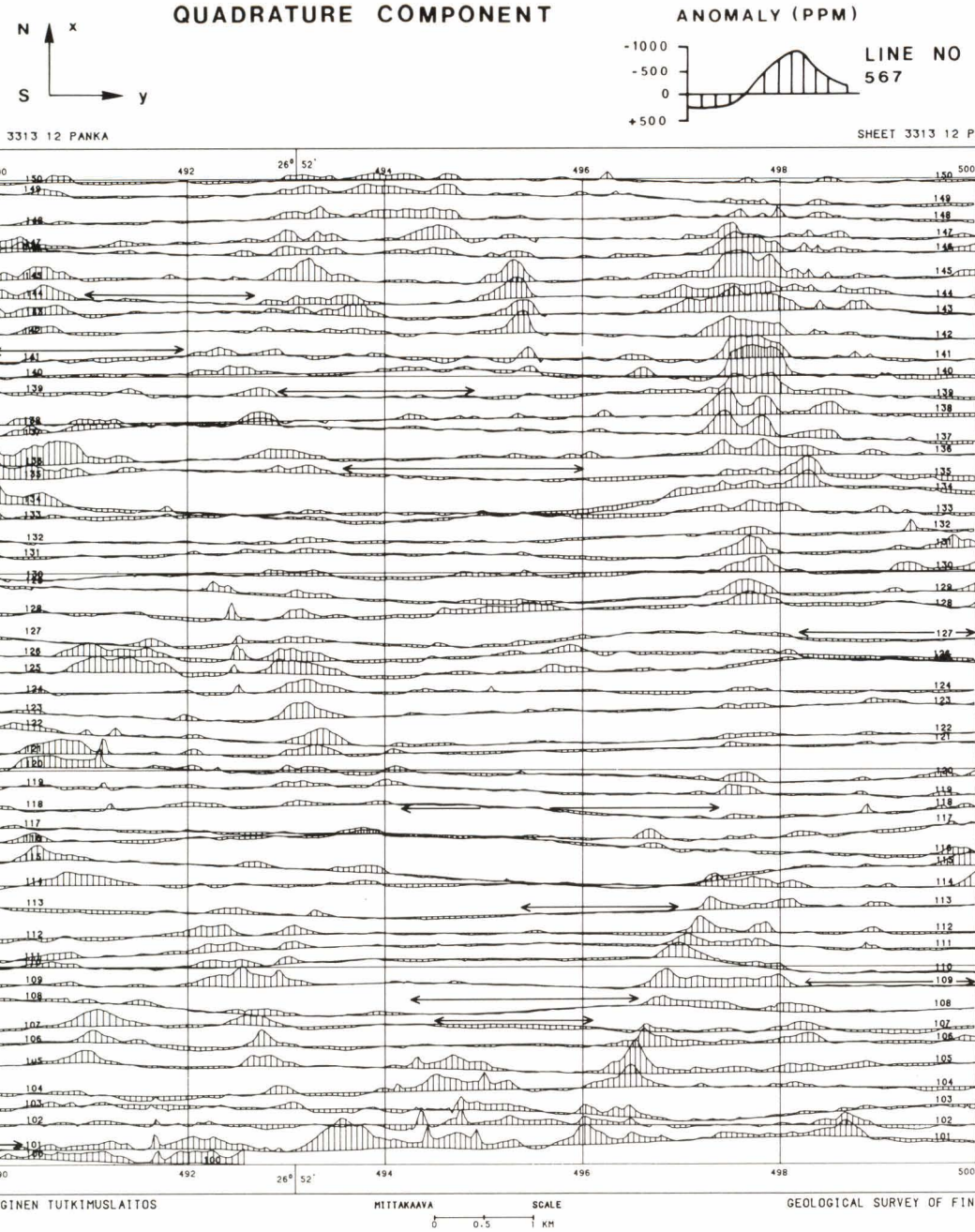

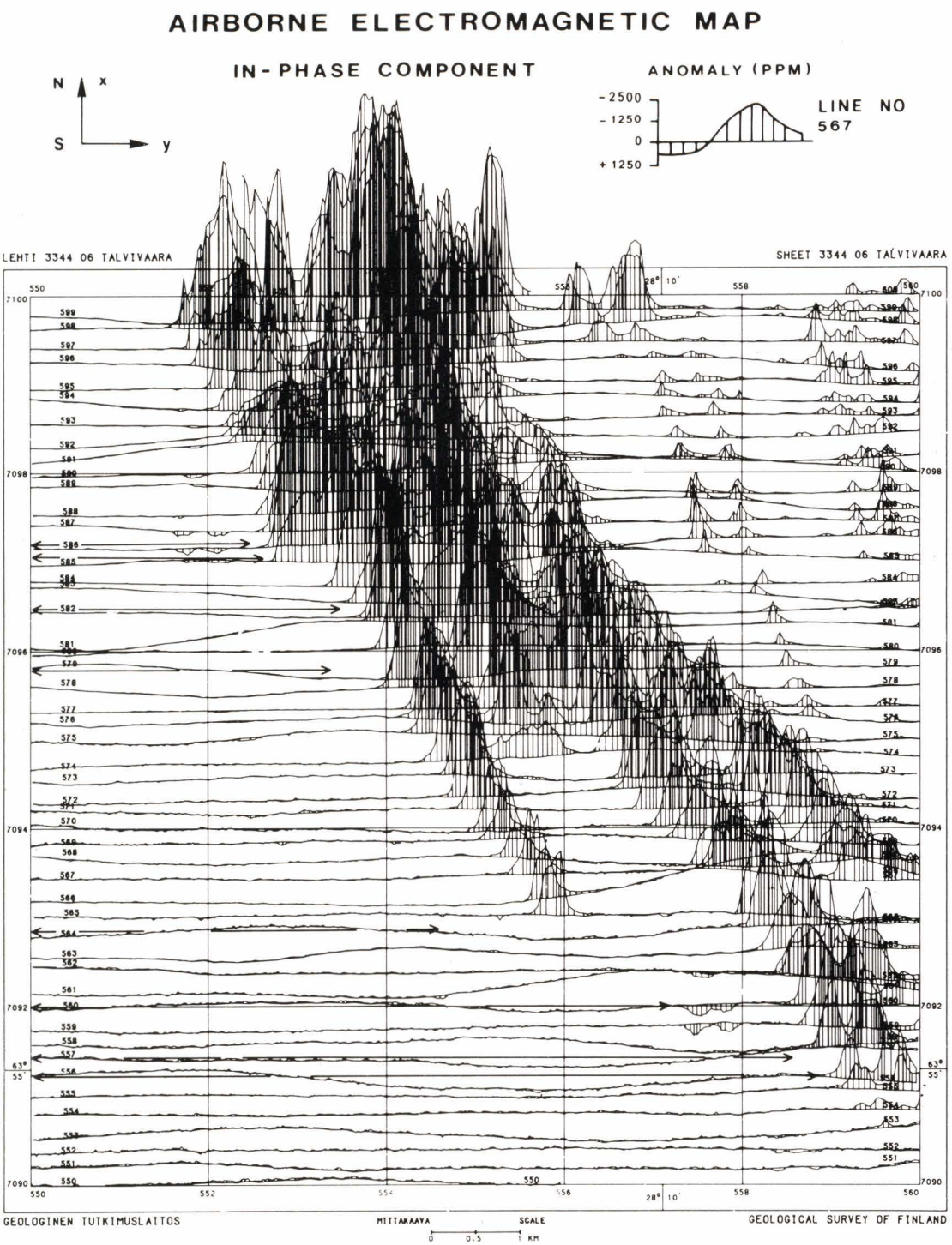

Fig. 12. DC-3 AEM anomaly maps of the Sotkamo area, map sheet 3344 06. The portions of the profiles used in calculating the noise level are marked on the figure. (a) In-phase component. (b) Quadrature component (with exceptionally high noise level) (see page 37).

AIRBORNE ELECTROMAGNETIC MAP

QUADRATURE COMPONENT

ANOMALY (PPM)

LEHTI 3344 06 TALVIVAARA

SHEET 3344 06 TALVIVAARA

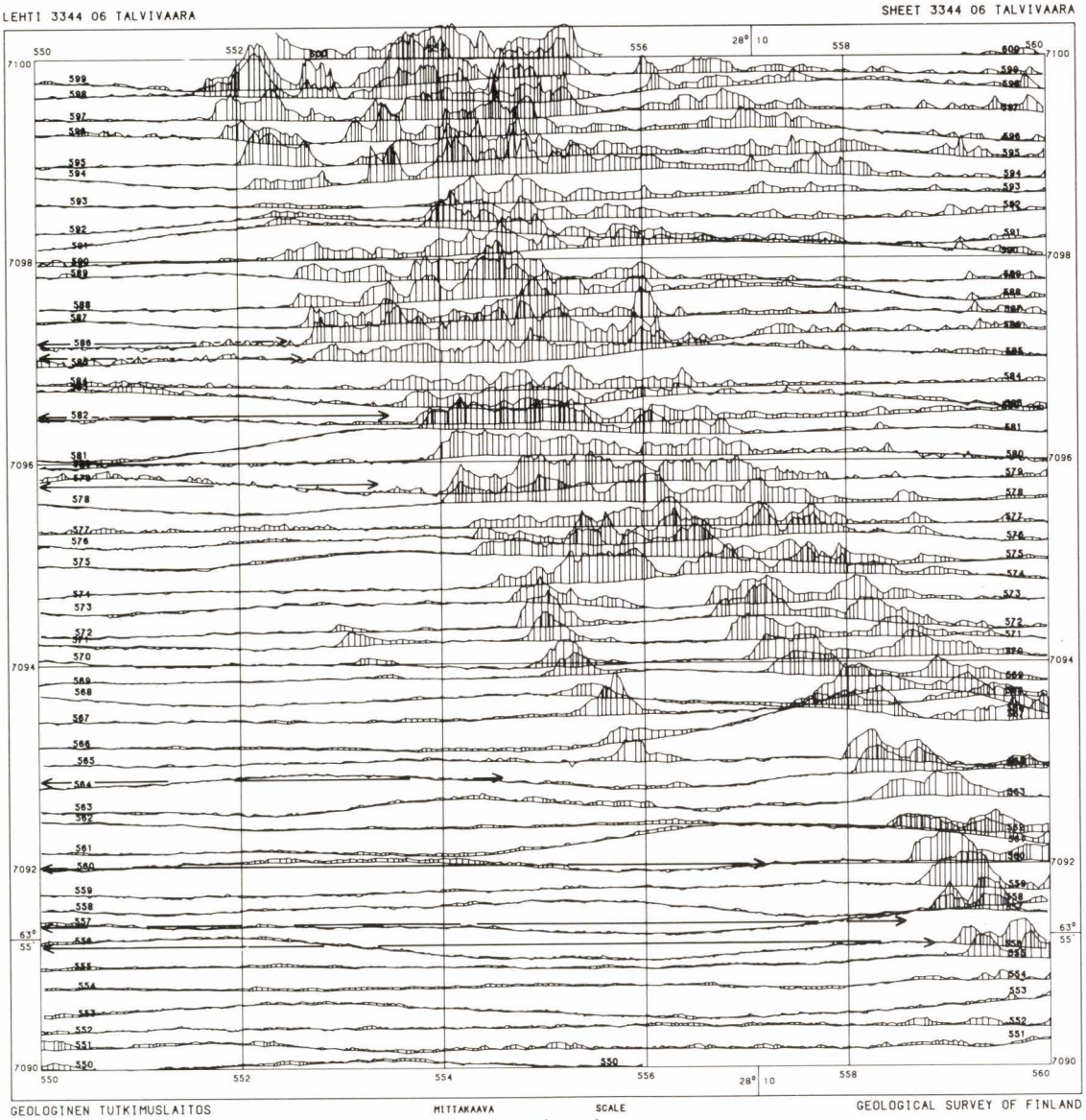

GEOLOGINEN TUTKIMUSLAITOS

MITTAKAAVA SCALE

0 0.5 1 KM

GEOLOGICAL SURVEY OF FINLAND

coil was 20 mV. After compensation and owing to the combined effect of the slow-varying noise factors listed, the noise voltage on the input of phase-lock amplifiers was 0.1–1μV at τ = 0.3 s time constant. The noise voltage equals 5–50 ppm of anomaly values and was generally distinctly less than the upper limit.

The true noise level of an AEM system can be determined more accurately from the field survey data. Fig. 11 illustrates the in-phase and quadrature component maps for map sheet 3313 12 of the Tervo area surveyed with the DC-3 AEM system in 1978. In terms of noise level, the data represent a normal outcome. The data shown in the figure were subjected to basic computer processing in the manner described in the following chapter. No smoothing procedures were applied. The spherics transients were eliminated in the basic computer data processing, but this in no way alters the normal values. The figure displays portions of profiles that do not contain any observable geological signals (true anomalies). The standard deviations of the anomaly values σ_{Re}, σ_{Im} have been calculated for these portions and are listed in Table 3. The average standard deviations of the anomaly values are $\sigma_{Re} = 21$ ppm and $\sigma_{Im} = 20$ ppm.

An abnormally high noise level is exemplified in Fig. 12 in data from the Sotkamo 1977 survey area, map sheet 3344 06. The average standard deviations of the anomaly values calculated from the profiles marked on the figure are $\sigma_{Re} = 45$ ppm for the in-phase component and $\sigma_{Im} = 85$ ppm for the quadrature component. As the survey maps released demonstrate, however, such results are rare. On the basis of the entire data the present author has made a conservative estimation that, after the removal of the spherics transients, the average noise level of the DC-3 AEM system is

$$(18) \quad N = 25 \text{ ppm},$$

for both in-phase and quadrature components.

The time stability of the system was so good that it was not necessary to make any zero level adjustments during a normal survey flight of 3 to 4 hours, the average drift being about 100–500 ppm/h. Excluding some data in 1978–1979, the drift was linear and easily removed during the basic data processing.

Noise filtering

The study of the field survey data indicates that the problem of noise level in the DC-3 AEM system is not of such magnitude as to warrant systematic noise filtering of all data. If desired, however, an auxiliary program can be used for this purpose, and this was done for the primary data in Fig. 12. The filtered Im anomaly values are shown in Fig. 13. As a consequence, the average standard deviations of the filtered data were reduced to $\sigma_{Re} = 35$ ppm, $\sigma_{Im} = 69$ ppm.

The filtering was accomplished by a 3-point recursive filter, which, although simple in terms of computational technique, is an efficient procedure (Tammenmaa, Grasty & Peltoniemi 1976),

$$(19) \quad A''_i = b_o A'_i + b_1 A''_{i-1} + b_2 A''_{i-2} \qquad (i = 1 \ldots n_p),$$

where A'_i are the primary values, A''_i the filtered anomaly values and b_o, b_1 and b_2 coefficients. Since the AEM data are recorded at $\Delta t = 0.5$ s intervals, the sampling frequency is 2 Hz and the Nyquist frequency f_N

$$(20) \quad f_N = \frac{1}{2\Delta t} = 1 \text{ Hz}.$$

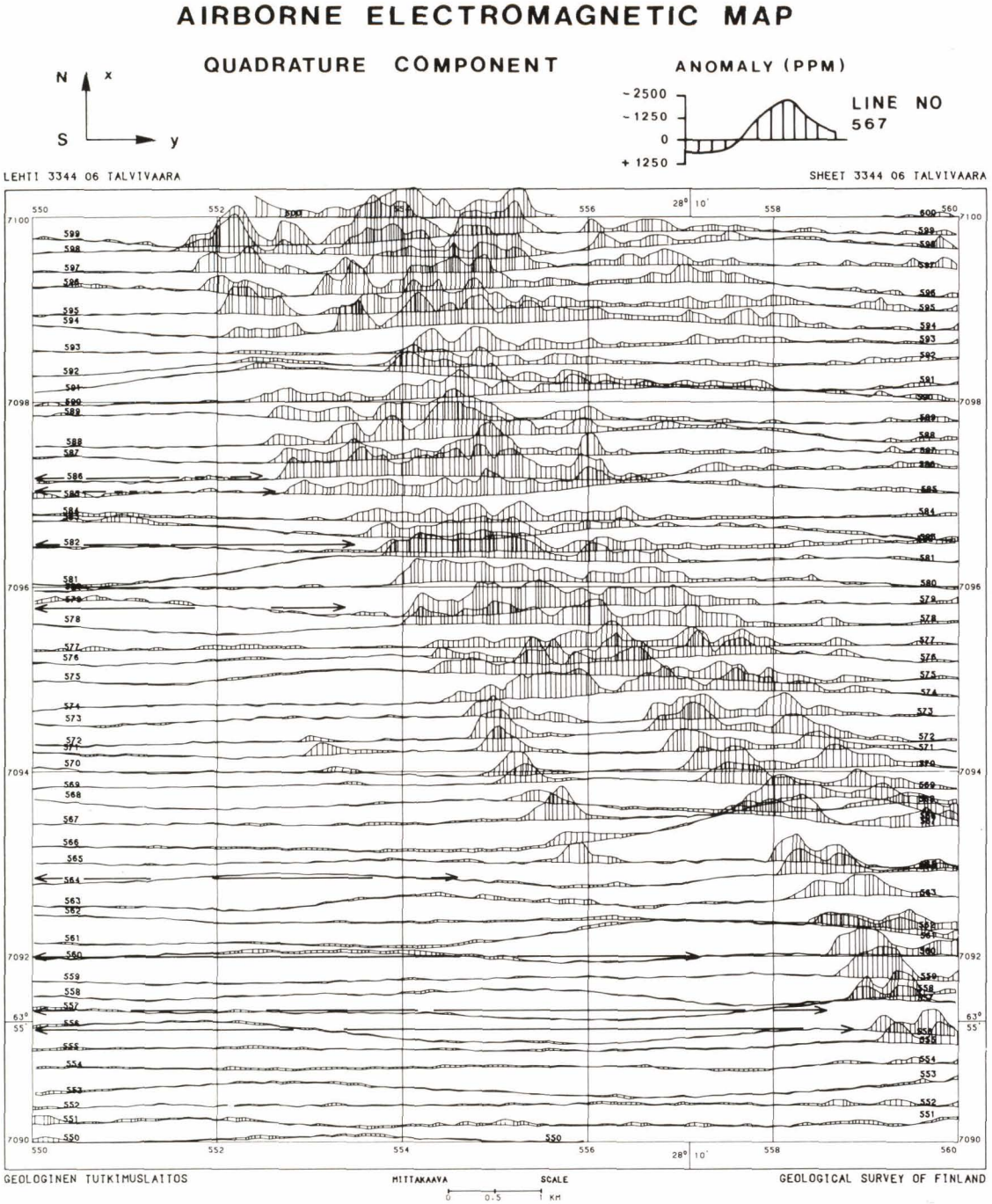

Fig. 13. AEM quadrature anomaly data of map sheet 3344 06 (cf. Fig. 12 b) filtered by the recursive filter of equation (19).

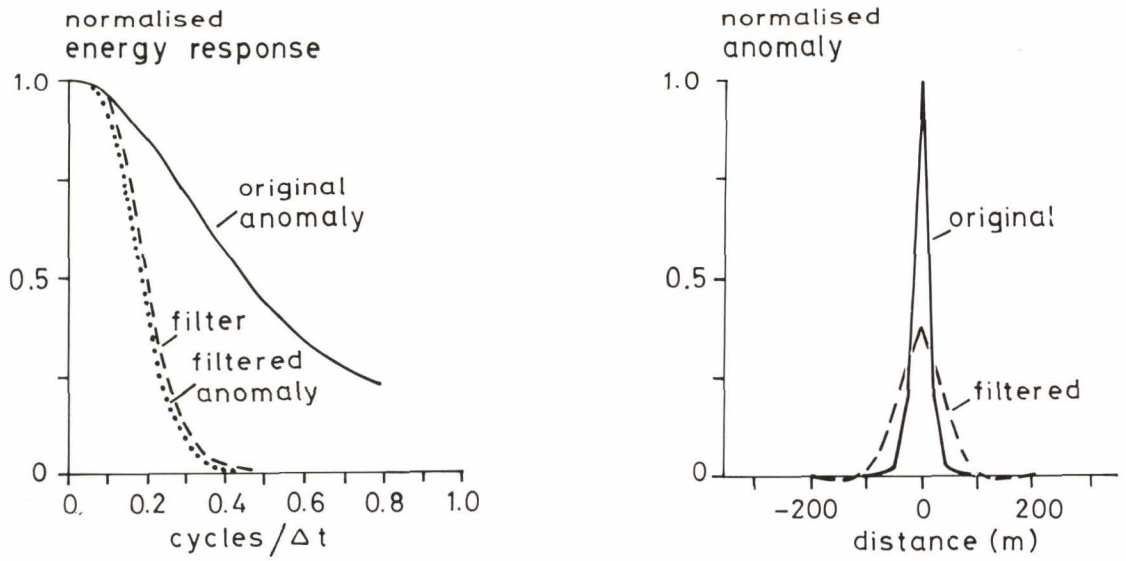

Fig. 14. Effect of filtering on the AEM anomaly of a thin, perfectly conductive vertical half-plane in the DC-3 system, with a flight elevation of h = 30 m. Energy spectra of the original anomaly, the filter and the filtered anomaly as a function of the signal frequency (left). The original anomaly and its filtered version (right).

According to the sampling theory, only signal frequencies lower than f_N can be correctly recovered from the sampled data. Hence, the true anomalies should only contain signal frequencies lower than f_N. An anomaly produced by a vertical thin half-plane conductor and measured from the nominal flight elevation is a reasonable approximation in practice of a true anomaly with the highest signal frequencies. The energy spectrum of such an anomaly as a function of signal frequency has been calculated with the Fourier transform method (Ruotoistenmäki 1979). The spectrum is shown in Fig. 14. The energy spectrum of the recursive filter (19) with coefficients $b_0 = 0.339$, $b_1 = 0.992$, $b_2 = -0.331$ and cut-off frequency = $0.2f_N$ is also shown in the same figure as is the energy spectrum of the anomaly after filtering. It is seen that the spectrum of the anomaly changes markedly as does the anomaly itself. The problem is that, as the aim is to reduce the noise alone, the cut-off frequency of the filter cannot be decreased significantly. Hence, the coefficients of the filter are a compromise between efficiency of noise filtering and distortion of true anomalies.

The simplest way to reduce short-wavelength noise would be to increase the time constant of the low-pass filter of the amplifier. The influence of the detector time constant on the field survey data has been treated in general terms by Ghosh (1972) and Palacky (1976) and in more detail by Jensen and Becker (1979). The time constant makes it possible to apply phase-locking techniques in amplifier design and reduces the aliasing of the high signal frequencies in the digital sampling of the data. On the other hand, the time constant reduces the amplitude of the anomaly and causes a phase shift. The values of the time constant settings reported in the literature vary between 1 and 5 s. Although a high τ value reduces the noise value N, the signal to noise ratio will be materially im-

proved only for large anomalies in which the wavelength of the signal is much greater than that of the noise. In contrast, the anomaly wavelength of narrow conductors is shorter and the high time constant reduces the signal as well, with the consequence that the S/N ratio does not necessarily improve. Hence, the maximum τ value allowed is determined by the wavelength of the true anomalies, that is, in practice, by the survey flight elevation h and the speed v. Jensen and Becker (1979) have given a condition for the maximum value τ_{max}

$$(21) \quad \tau_{max}\, v \leq h$$

to keep the distortion of true anomalies so low that it does not seriously affect the interpretation of the results. In the DC-3 AEM system with h = 30 m, v = 58 m/s the equation (21) gives $\tau_{max} \leq 0.5$ s, i.e. the applied value of τ was quite conservative. However, as the results on page 40 show, even a time constant as short as $\tau = 0.3$ s cannot be held insignificant. Hence, the constraint expressed by equation (21) must be considered as too wide.

On account of the small difference between the maximum signal and the Nyquist frequencies of the DC-3 AEM system, inverse filtering to eliminate the effects of the time constant (Jensen & Becker 1979) would lead to severe distortions in the short-wavelength anomaly data. This was not considered appropriate. Therefore, the theoretical modelling results (pages 82–87 and 90–96) were prepared so that the effect of the time constant is taken into account when necessary.

Auxiliary instrumentation and results

The auxiliary procedures that directly affect the quality of the AEM survey results are the recording and processing of the position data. Indirectly and mainly for monitoring, use can be made of the data relevant to flight elevation, vertical acceleration of the aircraft and the spherics monitor.

Positioning

The reduced elevation of low-elevation surveying, nominally 30 m, introduces difficulties in both flight-time navigation and subsequent flight-path recovery and positioning of the survey data. The narrow line spacing, 200 m, however, requires highly accurate navigation and positioning in order to keep errors in the location of the survey points within reasonable limits. Large errors would hamper the production of contour maps from the aerogeophysical survey data and increase the amount and cost of follow-up studies. Taking into consideration the characteristics of the DC-3 aircraft and the quality of the navigation maps, the aim in the accuracy of across-track navigation has been set at $\triangle p_1 = \pm 50$ m. Correspondingly, the positioning accuracy of the survey points on the navigation map should be $\triangle p_2 = \pm 30$ m and on the topographic map $\triangle p_3 = \pm 50$ m.

Navigation is accomplished with the aid of aerial maps or aerial mosaics on a scale of 1: 10 000 on which the desired survey lines are drawn in advance. The most accurate navigation map is obtained with aerial maps but these are not available for the whole country. The accuracy of an aerial map on a scale of 1: 10 000 corrected with a dry glue method is generally 3–5 m in flat or undulating terrain (Noukka 1979). If the variation in topographic elevation is large the errors may be significantly higher. The aerial mosaics are compiled with uncorrected

aerial photos enlarged from originals on a scale of 1: 31 000 or 1: 60 000. Thus, as is demonstrated on page 45, aerial mosaics may differ markedly from the corresponding topographic maps.

The flight line is photographed for the positioning with a continuous-strip film camera provided with a wide-angle 1:2.8/7.5 mm lens and a 35 mm/120 m film cassette. The scale of the exposed film is about 1: 7 000 in along-track and about 1: 4 000 in across-track direction. The location code and the fixpoint number are also recorded in the margin of the film. To meet the positioning requirements, the spacing between the fixpoints must be short, 1–2 km, when the navigation is done visually and the x,y coordinates of the intervening points are linearly interpolated. Hence, changes in flight velocity and across-track deviations are unable to make the errors at the intervening points too large.

Navigation requirements can only be met when the flight weather is practically free from turbulence, and the across-track wind component is less than 5 m/s. Under such conditions the average across-track deviation was $\Delta p_1 = 22$ m, when 477 fixpoints of the Porvoo 1975 and Savukoski 1977 survey lines were compared with the nominal line positions.

Before the introduction of a Doppler positioning system the above accuracy requirements entailed considerable manual work: about 30 000 fixpoints had to be processed annually. In addition to the high costs involved, there was also a marked time lag in the computer data processing of the survey data.

In 1975, Doppler navigation equipment was added to the DC-3 instrumentation to facilitate and speed up the positioning. When tested, the equipment was found to be very good as regards short-term accuracy. However, the drift of the whole equipment as specified by the manufacturer, 1 % of the total distance travelled, was so high that the long-term accuracy is not good enough for flight-time navigation in this application. Nevertheless, since the adoption of the Doppler equipment, it has been possible to increase the distance between the fixpoints to 5–10 km. As a result, there has been a marked reduction in the processing of the fixpoints, the annual number of points having been reduced to 5 000–10 000. The introduction of the Doppler equipment has also made positioning somewhat easier, because the most readily recognisable landmarks can be selected as fixpoints and because all the x,y coordinates of the intervening points are recorded.

The Doppler equipment is composed of three main units: the Doppler radar, a gyroscope and a calculator. The Doppler radar measures the ground-speed vector of the aircraft, and the gyroscope determines the angle between the longitudinal axis of the aircraft and the reference axis, e.g. North. The calculator integrates the ground-speed vector and transforms the along-track, across-track data into the coordinate system desired, e.g. a rectangular x,y coordinate system. The calculator updates the x,y coordinates of the survey point with a ± 10 m resolution at an average time interval of 1.6 s. An example of the flight path recovery based on original, uncorrected Doppler data is shown in Fig. 15.

The drift in the Doppler data is removed in the computer data processing with the aid of the fixpoint coordinates checked from the navigation map and the flight-path film. At first, the accuracy of the fixpoint coordinates collected manually is tested by comparing the flight speed estimates v_{FP} and v_D calculated between each pair of fixpoints from the respective manual and Doppler coordinates. The drift of the Doppler equipment is so small over the distance between two successive fixpoints 2–10 km apart that the calcu-

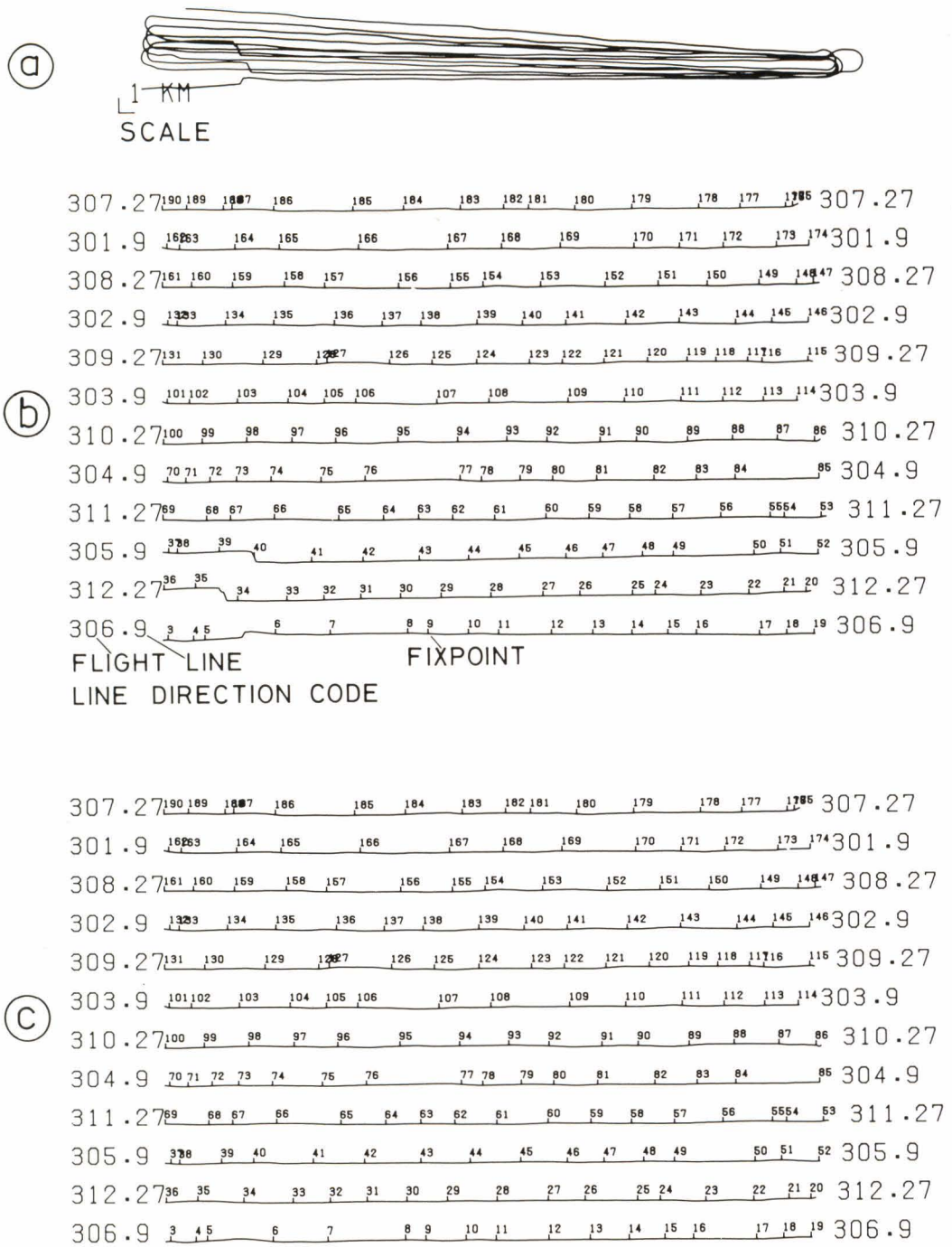

Fig. 15. Example of a survey flight route map based on Doppler data. (a) Uncorrected data, total flight time 3.37 h and distance travelled 610 km. Closure error Δx = 6 080 m, Δy = 2 550 m. (b) Position estimates of survey lines after a least squares fit to the original data. Note the errors between fixpoints 5–6, 34–35 and 39–41. (c) Position estimates of survey lines after the correction of Doppler errors. The correction is based on the extrapolation of the last correct recordings of heading, drift angle and ground speed data.

lated estimate of flight speed v_D is a useful parameter for comparison. If the difference between the estimates v_{FP} and $\overline{v_D}$ exceeds a given limit, the values of the manual fixpoints are checked. Once the coordinates of the manual fixpoints are approved, they are assumed to be exactly correct and the Doppler data are linearly adjusted to match them.

The theory, instrumentation and accuracy of the Doppler navigation method has been described comprehensively by Boie (1970). By elaborating the method that Boie proposed, Peltoniemi and Vironmäki (1977) studied the accuracy of the Doppler equipment of the Geological Survey. They reached the following conclusions: the average drift calculated from the closure errors of the survey flights in 1976, 99 in all, was 0.46 % of the total distance flown. The results of the four survey flights made in the Porvoo area in southern Finland were analysed in more detail. The test material included data on 24 flight lines, each 70 km long, with a total of 852 fixpoints. Comparison of the manual and the original Doppler coordinates of the fixpoints demonstrated that the average drift of the gyroscope was 0.71°/h. The average across-track error due to one 180° turn was found to be 94 m and the standard deviation 127 m. The along-track error $\triangle e$ in the original Doppler coordinates was, according to a model defined by the equation,

$$(22) \quad \triangle e = e_o + e_D\sqrt{L}$$

where L = length of the line (km), e_o = 110 m ± 70 m, e_D = 29 m ± 9 m. For a single Doppler fixpoint, the standard deviation of across-track error averaged 31 m.

In the above study, the manual x,y coordinates of the fixpoints were assumed to be error-free because the magnitude of the errors was not known. Boie (1970, p. 112) has reported an average error of 34 m for the manual x,y coordinates, but under flight

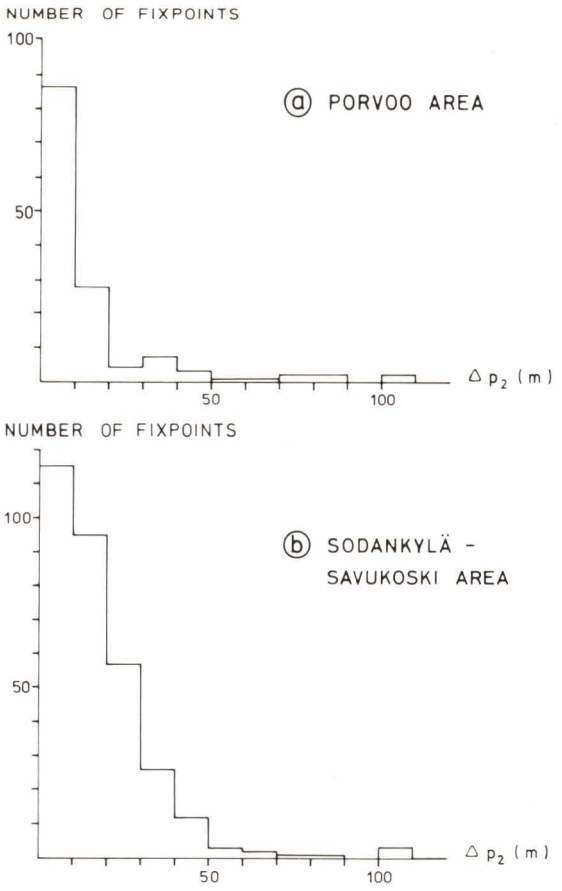

Fig. 16. Distribution of the position differences, Δp_2, between two fixpoint positionings. (a) The Porvoo survey area totalling 153 fixpoints. (b) The Sodankylä and Savukoski survey areas totalling 343 fixpoints.

conditions that were different than those upon which the above material is based. In the present work, errors in the manual fixpoint x,y coordinates of the DC-3 low-elevation flights were estimated on the basis of two different sets of data. The first consists of the same Porvoo 1975 data that were used as test material in the previous study. The navigation map of the survey area was compiled from aerial maps exceptionally on a scale of 1: 20 000, photographed in 1958–1959. Although quite old, the aerial maps were judged satisfactory owing to the highly

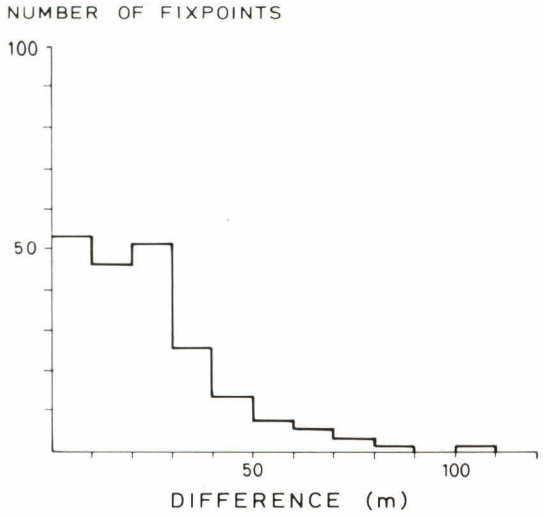

Fig. 17. Error distribution of the control points transferred from aerial photo mosaics to topographic maps. The Sodankylä survey area, total of 205 fixpoints compared.

detailed topography of the area. Of the fixpoints, 153 were repositioned by a different person from the one who made the original positioning. The difference between the new and old positions of the fixpoints is shown as a distribution histogram in Fig. 16a. The difference averages 13 m, and for 88 % of the points the difference is less than 30 m.

In the second comparison, the material studied comprises 1 140 line kilometres and 343 fixpoints from the Savukoski 1977 and Sodankylä 1977 survey areas in northern Finland. The navigation map was composed of aerial mosaics on a scale of 1: 10 000 that were enlarged copies of high-elevation aerial photos taken in 1971 and 1974. On account of extensive bogs and forests, the terrain is not so easy to recognise as in the Porvoo area, and the larger scale of the navigation map does not compensate for the larger errors in coordinates. In addition to the normal continuous-strip films, it was possible in this comparison to make use of the colour slides taken of each fixpoint with a single-exposure camera then in experimental use. Both cameras were fitted with the same type of lenses. The difference between the new and old positioning results is shown as a distribution histogram in Fig. 16b. The average difference for this material is 19 m, and for 78 % of the values the difference does not exceed 30 m. The differences are slightly higher than in the data on the Porvoo area.

In comparison with the topographic maps published for the Savukoski and Sodankylä areas, the errors in the aerial mosaics were studied by determining the coordinates for 205 control points from both types of maps and by computing the differences between the coordinates. The results are illustrated as a distribution histogram in Fig. 17. The average difference is 24 m, and for 73 % of the values the difference does not exeed 30 m. Note that the differences also include errors due to the compilation of the aerial mosaics and the positioning of the national x,y coordinate grid.

The position error estimates thus obtained can also be compared with the errors that can be deduced from the locations of the sharp AEM anomalies produced by power lines on the anomaly maps. For such anomalies the difference between the along-track location of the power line on the AEM anomaly map and the topographic map can be estimated within an accuracy of 10 m. The comparison for the 169 control points in the Tervo 1978 survey area gives an average of $\triangle p_3 = 16$ m, which also includes the effects of time constant and digital sampling. The result is of the same order of magnitude as that obtained in the fixpoint error analysis.

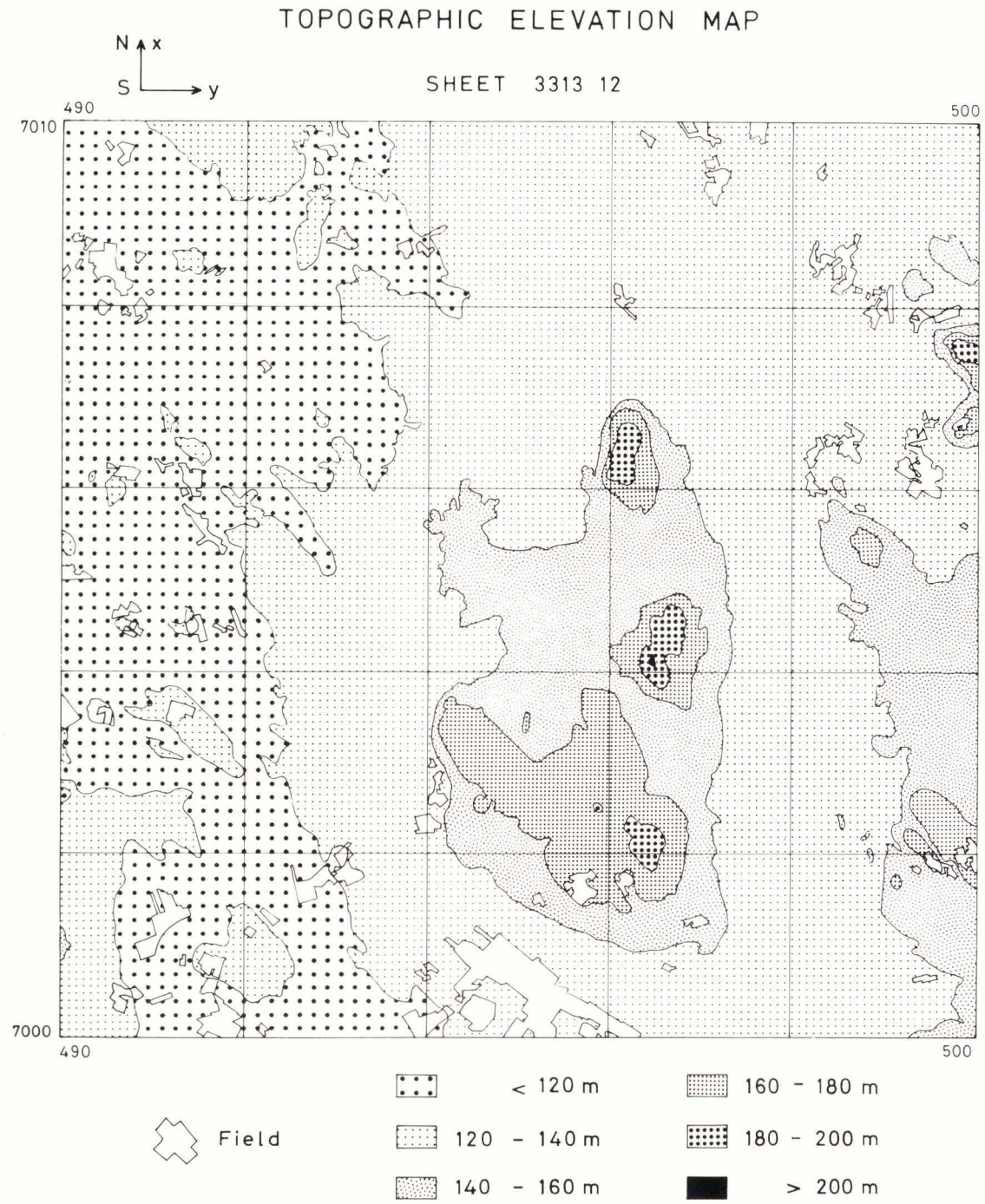

Fig. 18. Topographic elevation data and type of terrain from the Tervo survey area, map sheet 3313 12.

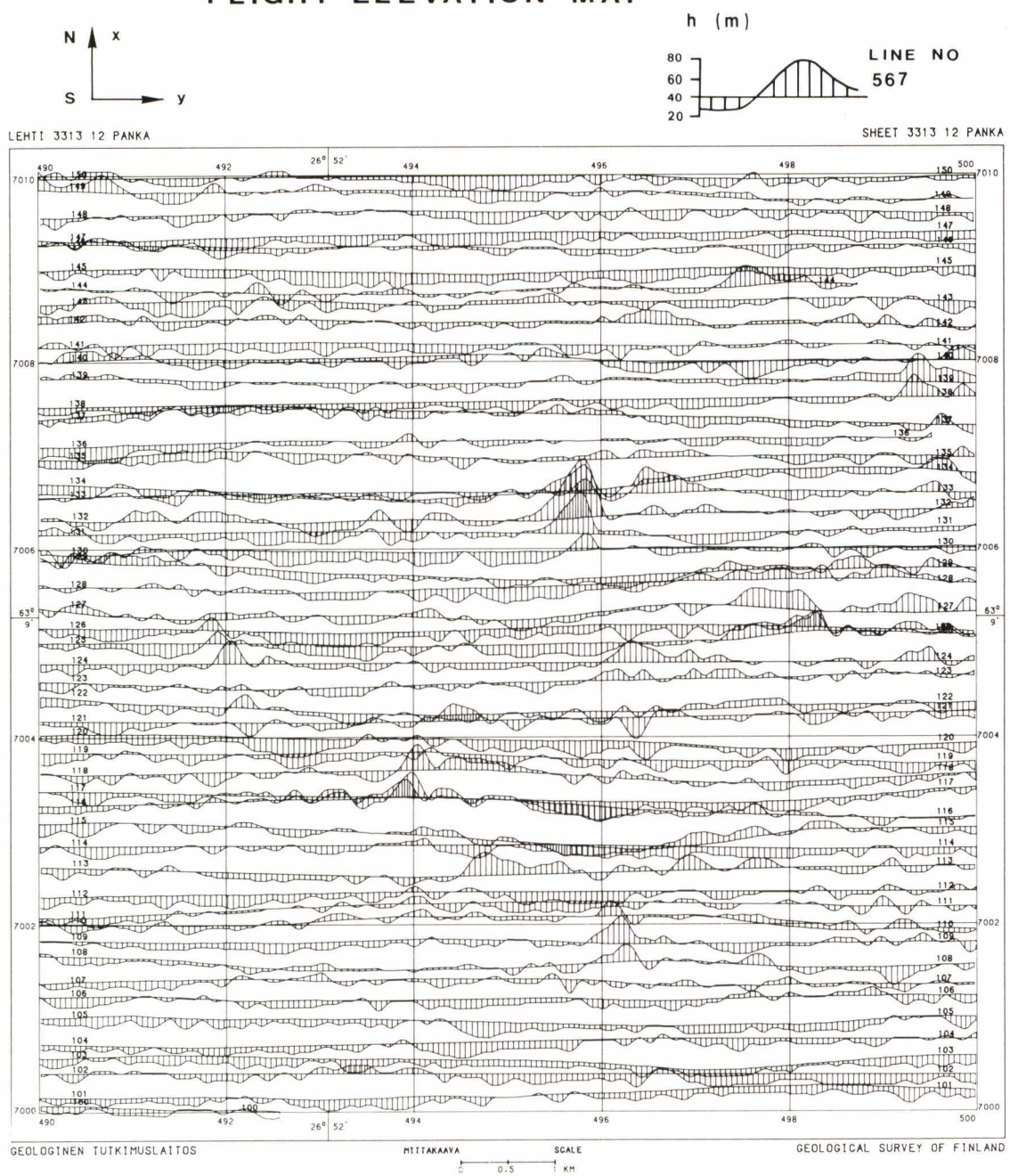

Fig. 19. Flight elevation map of the Tervo survey area, map sheet 3313 12.

Flight elevation

Low-elevation surveying by the Geological Survey aims at a flight elevation of 30 m (100 ft) from the obstacles, which, in practice, makes it 30 to 50 m from the ground surface. A constant flight elevation is very important for the quality of all aerogeophysical survey results because variations in flight elevation have a strong influence on survey data and cannot be exactly corrected in the anomaly values. The specifications call for great operational skill in flying and experienced and highly professional personnel. Likewise, the flying weather must meet strict conditions of wind, visibility and turbulence. Since the DC-3 aircraft is not designed specifically for low-elevation flying its specifications and characteristics had to be taken into consideration when planning the surveys. In practice, however, its performance turned out to be so good that only some fell regions in northern Finland had to be excluded from the surveying areas.

The flight elevation was measured with a radio altimeter and recorded in digital form at 0.5 s intervals with a ± 1 m resolution. The average flight elevations and standard deviations for the survey areas were calculated in the course of computer processing of the aerogeophysical data. The results from various areas differ mainly owing to differences in topography, because the variations in the flight weather tend to become smoothed. The influence of the topography is reflected in the averages $\bar{h}$ and standard deviations σ_h of the flight elevation data, as shown by Table 4. The highest areal average $\bar{h}$ was recorded in 1973 during the most difficult working conditions of the first operational year in the Sokli survey area, NE Finland, $\bar{h}$ = 48 m, σ_h = 9.2 m, and the lowest in 1975 in the Uusikaupunki survey area, SW Finland, $\bar{h}$ = 28 m, σ_h = 5.8 m.

Table 4

The average flight elevations $\bar{h}$ and the standard deviations σ_h measured by the DC-3 system in various survey areas. The average survey velocities $\bar{v}$ are also given.

Type of topography		Flight elevation		Velocity
Survey area (year)		$\bar{h}$ (m)	σ_h (m)	$\bar{v}$ (m/s)
Areas with flat topography				
Evijärvi	(1973)	34	5.7	55
Utajärvi I	(1974)	30	6.0	56
Pomarkku	(1975)	30	5.6	56
Korsnäs	(1976)	30	4.9	58
Areas with low or intermediate, yet sharp differences in elevation				
Vuokkijärvi	(1976)	33	5.7	58
Sotkamo	(1977)	39	7.2	59
Tervo	(1978)	40	7.8	58
Lieksa	(1979)	39	7.6	58
Areas in which the topography shows large differences in elevation although with varying gradient				
Tanhua	(1975)	33	9.4	57
Savukoski	(1977)	40	6.8	58
Tulppio	(1978)	40	7.1	60
Martti	(1979)	38	6.1	59

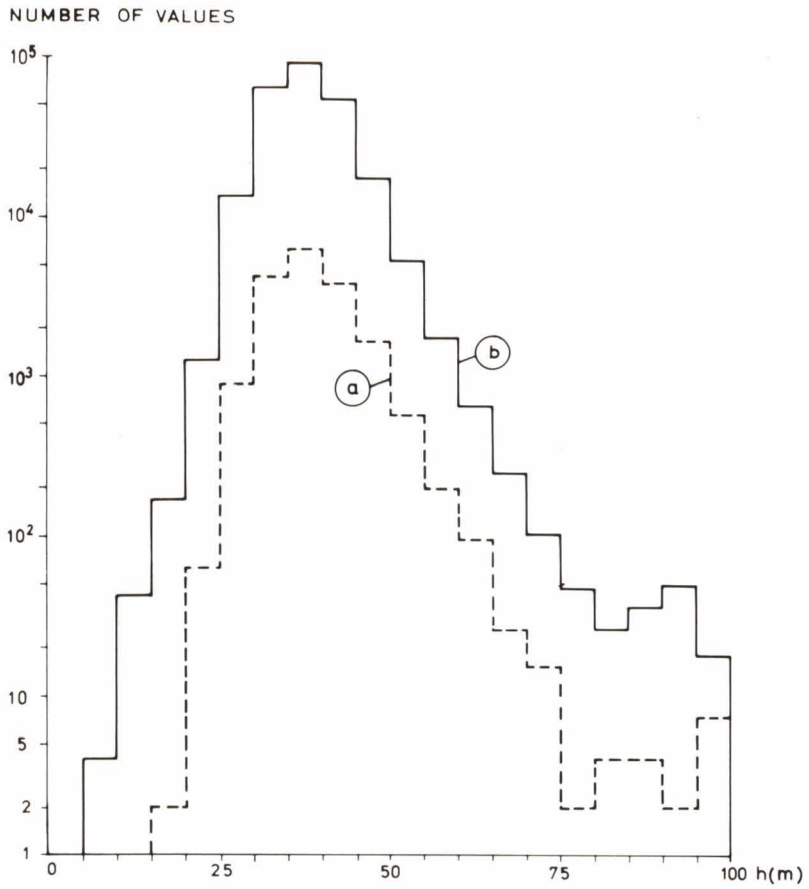

Fig. 20. Distribution of the flight elevation data h in the Tervo low-elevation airborne survey. (a) Calculated from the data on map sheet 3313 12 (Fig. 19). (b) Calculated from the data on the whole survey area (map sheet 3313).

An example of the correlation between flight elevation and topography is given by the results in Figs. 18 and 19. Fig. 18 illustrates the topographic elevation map (map sheet 3313 12 of the Tervo 1978 survey area) and Fig. 19 the flight elevation data of low-elevation DC-3 surveys in the same area. When comparing the results it is necessary to remember the principle on which the radio altimeter operates: on account of the high frequency of the device, f = 4 000 MHz, the data measured refer to the shortest distance to the reflecting object. Hence, the data usually show a jump at the boundary between forest and field. Otherwise the data behave as expected: owing to the flight technique the valleys exhibit maximum and the hills minimum values. A more detailed distribution of the flight elevation records is given in Fig. 20 for the data of the test map sheet (100 km²) and the whole survey area (1 200 km²). The distributions do not show a significant difference and, as expected, they are positively skewed over the greater values. The data contain 3.3 % flight elevations of over 50 m.

Turbulence

Flight conditions affect the quality of all aerogeophysical data, because the flight elevation (safety margin) has to be increased when conditions deteriorate and it becomes

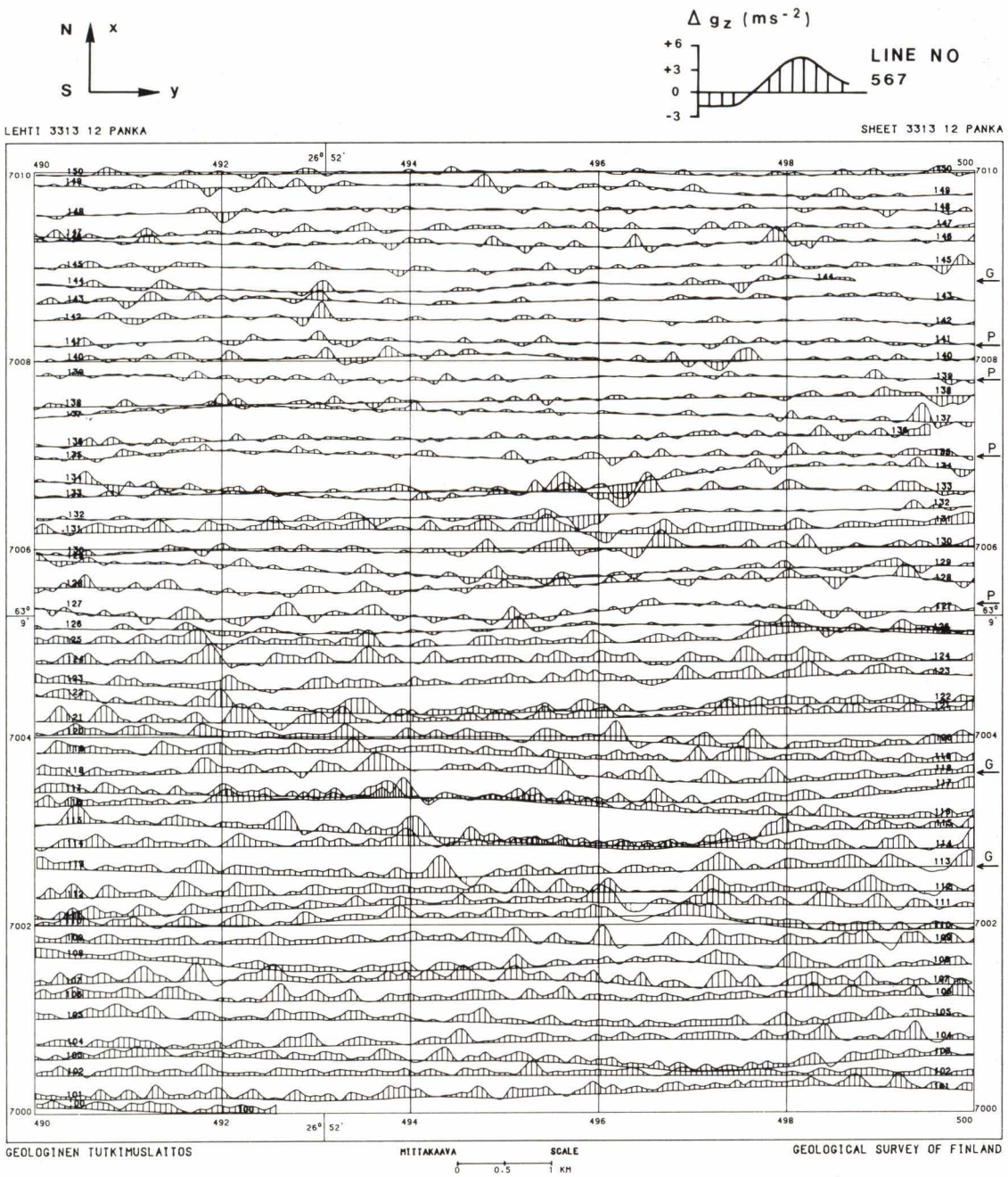

Fig. 21. Recorded changes in vertical acceleration of the DC-3 aircraft in the survey of map sheet 3313 12. G = good flying conditions, P = poor flying conditions.

more difficult to navigate the aircraft accurately along the desired profile. Turbulent flight conditions also affect the AEM data by excessively raising the noise level, particularly in wingtip coil systems. As pointed out on pages 17 and 33, motion-induced noise, which is one of the predominant sources of AEM noise, directly affects the quality of the results. In the DC-3 system, changes in the vertical acceleration of the aircraft due to the combined effect of turbulence and variations in topographic elevation were measured by means of a strain-gauge transducer whose data were recorded at intervals of 0.5 s with a resolution of ± 0.05 ms^{-2} (± 1 mV). The device measures relative values, and an increase in downward acceleration gives a positive deviation.

Fig. 21 gives the data on the vertical acceleration recorded in the area of the map sheet exhibited in Figs. 11, 18 and 19. The figure shows some adjacent line pairs along which the flight log-books reveal that the quality of the flight conditions varied from good to poor. Visual inspection of these data reveals no difference. To establish the AEM noise that is due solely to the variation in vertical acceleration, the data recorded under different flight conditions were studied in greater detail. The profile sections were the same as those used in the AEM noise calculations (Fig. 11). The average values for the changes in vertical acceleration $\overline{\triangle g_z}$ and the standard deviations $\sigma_{\triangle gz}$ for the test profiles are given in Table 3. The results demonstrate that the average $\overline{\triangle g_z}$ values correlate with flight weather, but there is no significant correlation between the $\overline{\triangle g_z}$ values and the standard deviations $\sigma_{\triangle gz}$, σ_{Re} and σ_{Im}. The variation in vertical acceleration does not affect the DC-3 AEM data so much that it can be distinguished in the AEM noise. On the basis of even more extensive material, Ruotoistenmäki (1980) has studied the correlations between the DC-3 AEM data, flight elevation and vertical acceleration. His results also suggest that the correlation between flight conditions and AEM data is not statistically significant. Hence, there is no need to correct the AEM anomaly data by means of the measured vertical acceleration. These results are good evidence of the degree of mechanical rigidity achieved in the installation of the DC-3 AEM coil supports.

COMPUTER PROCESSING OF DIGITAL AEM DATA

Background

When the low-elevation surveys began in 1972, automatic data processing (ADP) was in its initial stages at the Geological Survey of Finland and the production of aerogeophysical survey maps was their first large-scale ADP application. The computer system of the Geological Survey, a Hewlett Packard HP 2100A including peripherals, was installed in the autumn of 1971 in a configuration that included a central processing unit (CPU) with 16 k of 16-bit words, two magnetic tape stations, a graphic printer-plotter, and paper tape read and punch units. The operating system allowed one batch job to be run at a time. The hardware was extended and the operating system changed several times during the years 1972–1974.

During the initial stages of the low-elevation surveys even the development of the reading and checking program for the pri-

mary data tapes was a laborious task owing to the unusual packing density of the magnetic tape, 200 BPI, and the numerous recording errors on the tapes. The original version developed by Westerlund (1973) and Korhonen (1974) has since been supplemented and modified several times.

Owing to the limited capacity of the computer, the low-elevation survey data had to be handled on the basis of batch processing and separate data files, i.e. the desired component had to be picked out from the primary magnetic tape and treated separately. The data processing was started with data from low-elevation aeromagnetics. The appropriate application programs were developed by Korhonen (1974).

At the end of 1973 the Geological Survey acquired a set of computer programs developed at the Geological Survey of Canada for processing airborne gamma-ray survey data (Grasty 1972). In Canada the programs were run on a big CDC 6400 computer. Hence, in Finland, the programs could be brought into use more quickly when they were converted to fit the U1108 central computer of the Ministry of Education. At the same time the Geological Survey ordered a Calcomp 925/1036 drum plotter together with a contouring program for the graphic production of survey maps. The U1108 modification of the software for processing airborne gamma-ray survey data and the plotter were ready to be tested in the summer of 1974; the first low-elevation aeromagnetic and airborne radiometric maps were released by the end of the year.

In their systems design the computer programs for airborne radiometric data correspond to those applied at the Geological Survey of Canada. Owing to differences in instrumentation and methods, changes had to be made in the program versions at the Geological Survey of Finland (Peltoniemi 1975). The greatest changes were the processing of 36-channel gamma-ray spectrometer data and the inclusion of more detailed processing of the positioning data. When compared with the topographic map, the survey positioning data should be accurate to ± 50 m, as described on pages 41–45. Therefore, a set of programs was developed for that purpose by Kari Laakso, Martti Laasasenaho and the present author.

The software for handling the AEM data was developed in 1975 (Peltoniemi 1975) by making as much use as possible of the existing software for airborne radiometrics. The first AEM maps were released at the end of 1975.

Since the capacity of the HP 2100A was small, even after extensions, the Geological Survey decided to purchase a new and more efficient computer. The new one, a HP 3000 Pre-Cx, was installed at the end of 1974. The installation of the software for drawing contour maps was, however, more difficult than expected and thus the U1108-based versions continued to be used. The contouring software was transferred at the end of 1975 (Kaila 1976) and the remaining software during the winter of 1975–1976.

After these rather complicated arrangements had been completed, the computer-based map production of AEM low-elevation

Table 5

Number of in-phase and quadrature low-elevation AEM survey maps on a scale of 1 : 20 000 released from 1975 to 1981 by the Geological Survey of Finland.

Year	Survey area (km²)	Number of maps released
1975	235	8
1976	11880	266
1977	12455	258
1978	16670	350
1979	8945	188
1980	15865	312
1981	16700	464
Total	82750	1846

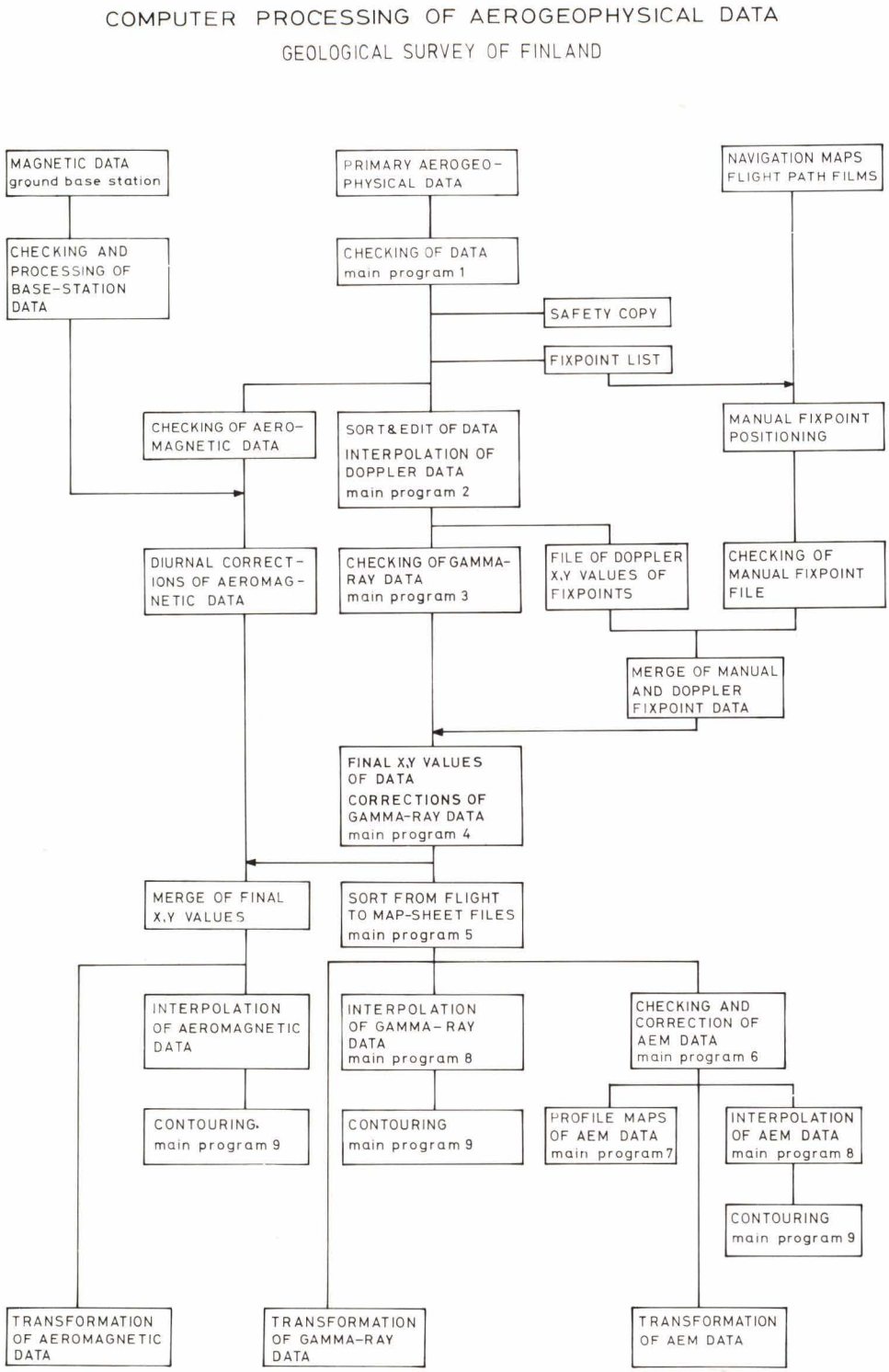

Fig. 22. Generalised flowchart of the basic ADP processing of the aerogeophysical survey data.

surveys got underway in the spring of 1976, and an effort was made to ease the backlog in the survey data. The number of AEM in-phase and quadrature component maps released on a scale of 1 : 20 000 in various years is shown in Table 5. By 1979 all the aerogeophysical low-elevation data had been sorted out. The computer processing of the annual low-elevation survey data into aeromagnetic, AEM and airborne radiometric anomaly maps equals about 10 million CPU seconds of processing time for the two HP 3000 minicomputers, and about 2 000 hours of plotting time for the drum plotter.

Description of basic software

In this context the basic processing of AEM data means the positioning and reduction of data and their presentation as anomaly profile or contour maps of in-phase and quadrature components. The flowchart of the basic processing sequence is shown in Fig. 22. The computer processing is common to all the aerogeophysical survey data in terms of initial checking, processing of the positioning data and contouring program. Moreover, for the reasons given above, the software for the AEM and airborne radiometric data is common in other respects as well except for the execution of methodic reductions.

The software for the AEM survey data includes nine main programs and auxiliary programs. The main programs undertake the processing and updating of survey data files. The data files are sequential, the data being in binary form except in the ASCII-formatted archives and security files. The first six main programs execute the initial processing for the last three plotter programs. The auxiliary programs (not marked in Fig. 22) include listing and line printer plotting programs, programs for processing the fixpoint data, for generating the control card decks and for undertaking safety-copying. Apart from the first main program, all the programs are coded in HP FORTRAN.

The CPU capacity required by the main programs varies, the highest being for the contouring program. This program needs such a large proportion of the capacity of the HP 3000 processor that no other programs can be executed at the same time. Since in the other main programs the data are processed by flight lines, the survey area has to be divided into subareas if the line length exceeds 70 km. The size of the data file that is processed in one run depends on the stage and varies between 1 and 10 megabytes. The input and output files must therefore be stored on magnetic tapes.

Method of reductions

The joint programs for processing airborne radiometric and AEM survey data (main programs 2–5 and 8, cf. Fig. 22) have already been released (Peltoniemi 1975); hence, in the following, only the concepts of the methodic AEM reductions (main program 6) are described in detail. In the input file the AEM survey data are arranged in flight lines in 1 s records that already include the final x, y coordinates. The formally erroneous records and the ones with coarse sporadic errors have been set to zero. The data are then corrected as follows (Peltoniemi 1978a):

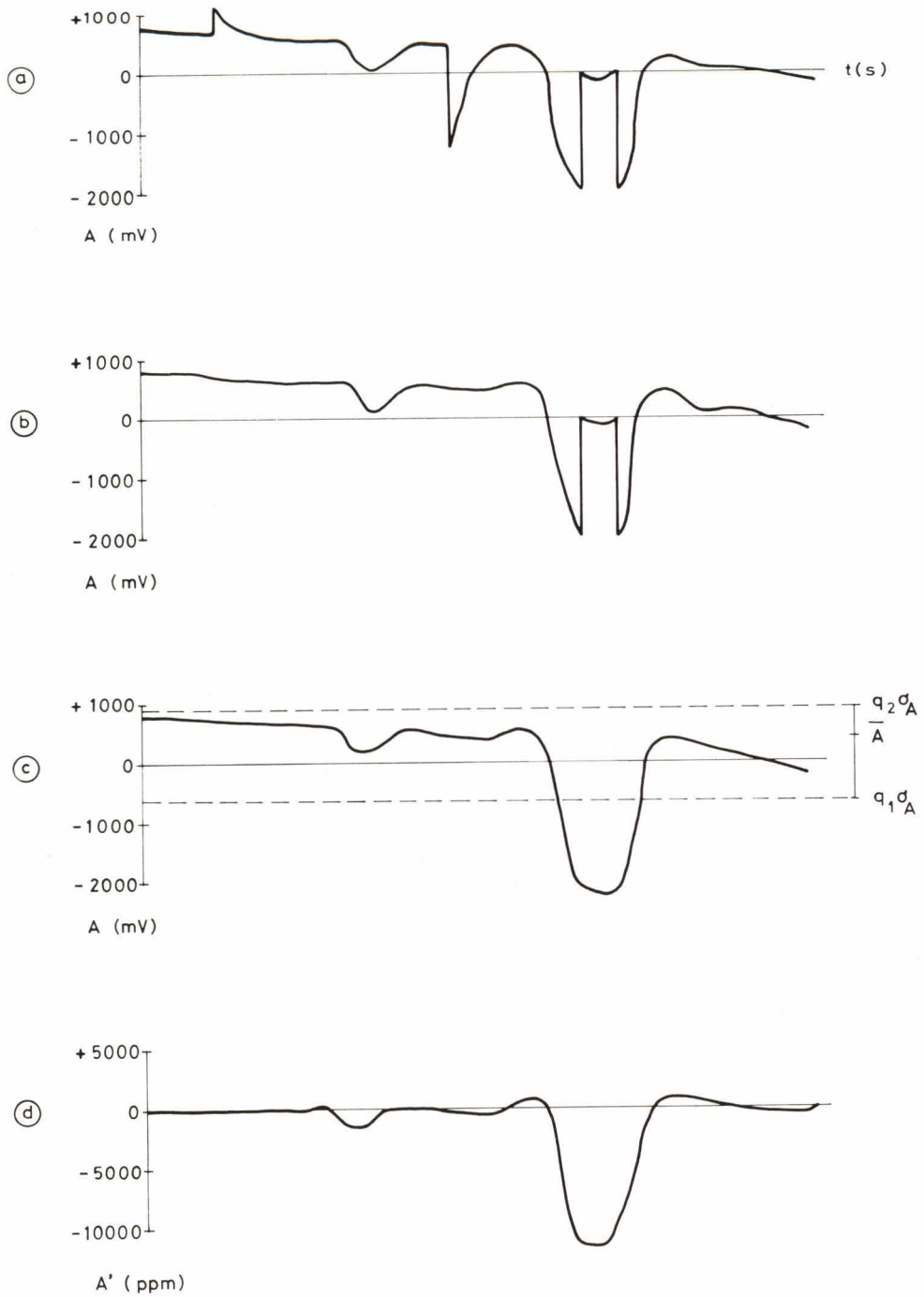

Fig. 23. Principle of the methodic reductions of AEM data. (a) Original survey data. (b) Survey data after spherics filtering. (c) Survey data after reducing the overflow of the ADC circuit. (d) Final AEM anomaly values after level and drift reductions.

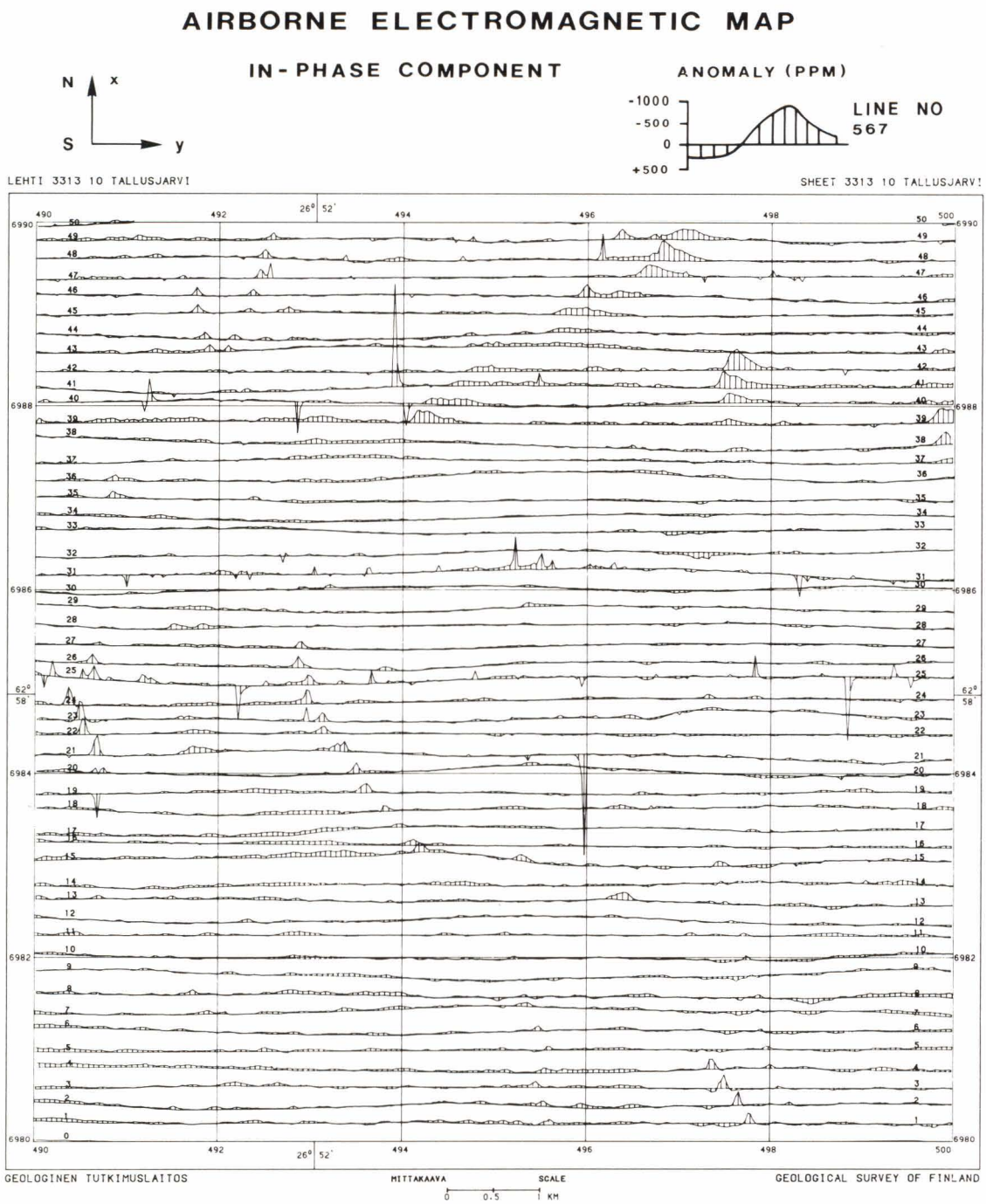

Fig. 24. Example of AEM data from the Tervo survey area (map sheet 3313 10) showing unusually abundant spherics transients. (a) In-phase anomaly values without spherics filtering. (b) In-phase anomaly values after spherics filtering. Portions of data where spherics transients have been removed are circled (see page 57).

AIRBORNE ELECTROMAGNETIC MAP

IN-PHASE COMPONENT

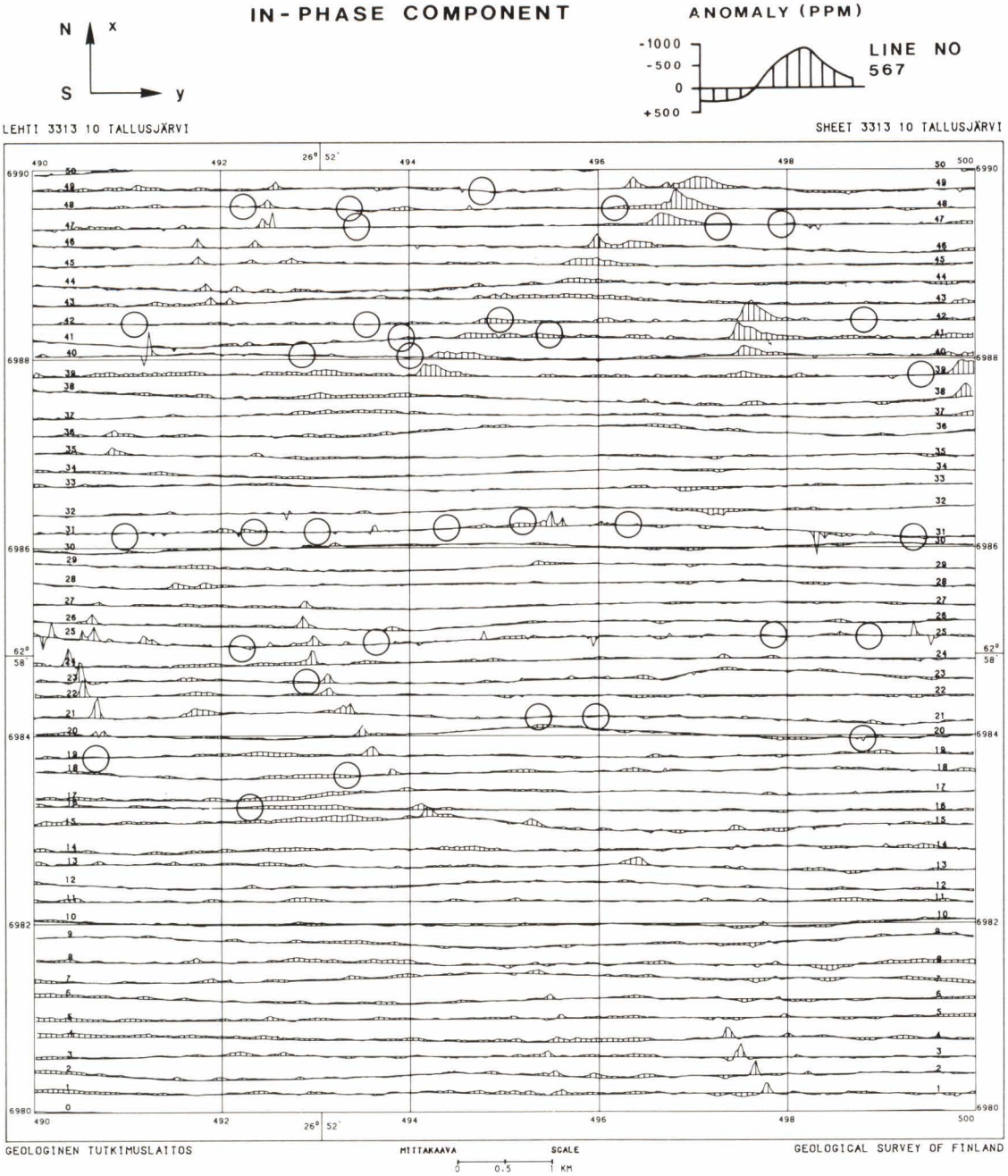

- Single recording errors and spherics transients are removed.
- Truncations of the anomaly peaks due to overflow of the analog-to-digital conversion circuit are corrected.
- The equation for the true zero level line of the anomaly curve is determined, and the level- and drift-corrected anomaly values are calculated.
- Anomaly values are converted by means of a calibration coefficient from voltage signals (mV) into final, relative anomaly values (ppm).

The various reduction stages are illustrated in Fig. 23. Fig. 23a shows a sample line of primary input data including the above components which require methodic corrections.

On account of the small time constant of the detector, the effect of the spherics transients is often seen as distinct anomalies in the AEM data. These must be filtered off sufficiently accurately before the contour maps can be drawn. The number of spherics transients varies with the survey weather and the season, the maximum being reached during long sunny periods at the height of the summer. At its worst, the number is so high that AEM surveying is impossible. Fig. 24a shows an example of uncorrected survey data with abundant spherics transients.

Several methods of eliminating spherics transients have been tried. Large transients can be detected simply through the differences between readings at successive points. Small transients, however, cannot be distinguished from true anomalies in this way. A comprehensive study was undertaken to establish the feasibility of numerical filtering of the transients based on spectral analysis (Tammenmaa & Peltoniemi 1979). The frequency analysis demonstrated, however, that the frequency spectra of transients and true anomalies overlap so strongly that filtering with a low-pass filter cannot be accomplished satisfactorily. Another drawback of the method would be the distortion of the true anomalies.

In practice, the best procedure found was to use a filter based on the shape of the transient. In transient recognition, good use can be made of the fact that the shape of transients is mostly characteristic and close to the impulse response of an RC-circuit (Fig. 25). If anomaly profiles have portions in which the ratios of the survey data are as shown in Fig. 25, the sections are identified as spherics transients and are eliminated by linear interpolation. The inspection is undertaken in the direction of increasing time for both inphase and quadrature components. The transients are always eliminated from the data on both channels, even though the identification is performed on only one of the two channels. The method has the advantage that the transient is detected irrespective of its amplitude, and that the application of the method has no effect on the values of the true anomalies. What is more, single-point recording errors can usually be rectified at the same time. As demonstrated by Fig. 24b, almost all the transients have been eliminated by filtering. Unfortunately, however, data sometimes include transients that differ in shape from the usual ones and cannot therefore be identified. The identification limits cannot be made too wide, because the true anomalies might then be affected.

If necessary, the spherics transients that escaped filtering can be eliminated by means of a separate spherics monitor (cf. p. 31). The monitor is dimensioned so that the output signal does not show the influence of the true conductor anomalies. Thus the data recorded on the monitor channel can be used directly as a correlation signal to eliminate the spherics transients. It has, however, not been possible to increase the sensitivity of the monitor so much that all the small transients are recorded. In practice, the use of numerical

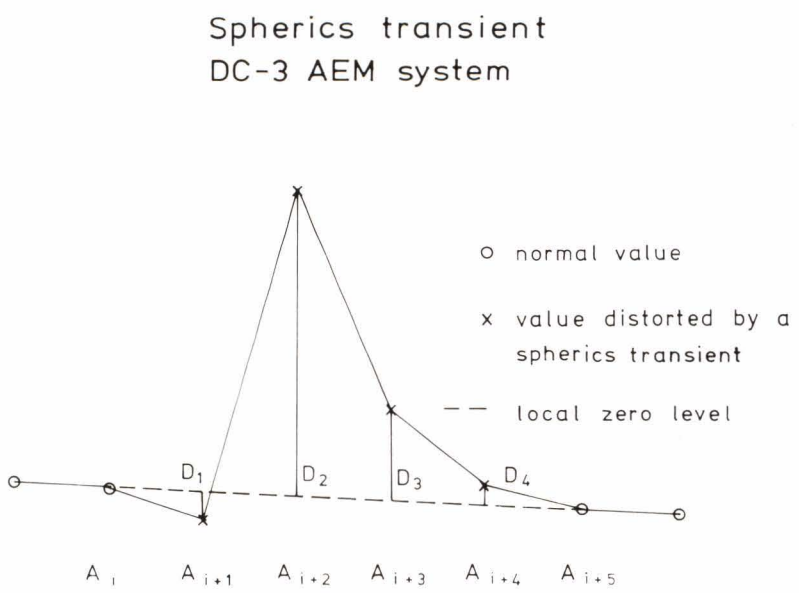

Fig. 25. Principle of the spherics filter (Tammenmaa & Peltoniemi 1979). A_i = original value, D_i = value with a local zero level at point i. If the successive values have ratios of $-0.10 \leq D_1/D_2 \leq 0.10$, $-0.10 \leq D_3/D_2 \leq 0.30$ and $-0.10 \leq D_4/D_2 \leq 0.10$, the data sequence is recognised as a spherics transient.

filtering is usually sufficient. For this reason and because of restrictions in the computer CPU capacity the outputs of the monitor channel have only occasionally been applied to filtering purposes.

In the next step of the reduction procedure the overflow of the voltage signals is corrected. Since the digital output from the analog-to-digital converter is recorded with 3 digits and a bit indicating the overflow, voltages exceeding ± 2 000 mV are truncated in the conversion, see Fig. 23a. In practice this is a rare event, because it requires anomaly amplitudes of at least 10 000 ppm. The overflow is identified by the magnitudes of and differences between successive survey data. The reduction itself is a trivial exercise, but its ADP procedure is somewhat hampered by the fact that, under such conditions, the true variation in the anomaly is usually high as well. Fig. 23c illustrates the survey data after they have been corrected for the overflow.

The most difficult methodical problem is how to determine accurately the true zero level of the anomaly data. As an instrumentation quantity the zero level of the voltage signal can be set arbitrarily. Changes in flight weather, such as temperature, cloud cover and wind, produce changes in the termal flow of the coils and other analog components and in the coil separation; hence, it is difficult in practice to wholly eliminate slow drift in the zero level. In the DC-3 AEM instrumentation the change is so slow and linear that it is not necessary to reset the zero level during a survey flight of normal duration. Hence, the drift can be accurately reduced by means of a correction equation that is a linear function of time. The correction coefficients could be manually determined for each flight line. The annual survey data, however, are so voluminous (c. 1 000 lines/a) that the coefficients should be determined by an automatic procedure if possible. The problem is, how to take the effect of the anomalies into account, because a direct least squares fitting for the

whole data gives an erroneous result; the more anomalous values there are along the line, the greater is the systematic error. Consequently, the computer program is based on the following procedure (cf. Figs. 23c and 23d):

- An average $\bar{A}$ and standard deviation σ_A are calculated for all the AEM survey data on a line.
- The values A_i that meet the condition

(23) $(\bar{A} - q_1\sigma_A) \leq A_i \leq (\bar{A} + q_2\sigma_A)$,

where q_1 and q_2 are constants determined experimentally, are picked out.
- A line is fitted with least squares method to the data A_i picked out

(24) $A_i = c_0 + c_1 t_i$,

where t_i = recording time of datum i (s), which gives the estimates for the correction coefficients c_0 and c_1.
- For each point along the line a reduced anomaly value Z_i' is calculated from the equation

(25) $A'_i = (A_i - c_0 - c_1 t_i) q_3$,

where q_3 = calibration coefficient (ppm/mV).

The method is applies separately to in-phase and quadrature components. It is simple and generally gives good accuracy provided all the data on the lines are not anomalous.

Visual interpretation and the use of profile maps are not disturbed by small errors in zero level and drift. When compiling the contour maps, however, it is imperative that the zero level be correct within ± 50 ppm. The requirement is strict and, as a consequence, about 2–5 % of the lines must be re-run on an additional reduction program before the data for contour maps can be interpolated. The reduction program, which also allows for non-linear drift, has been developed by Jouko Vironmäki.

After the methodical corrections, the AEM data are ready for the program that generates the stacked anomaly profiles (main program 7). The maps are produced on a scale of 1 : 20 000 in accordance with the Finnish topographic map division. The profiles have a linear scale for the anomalies with a scale coefficient of 400 ppm/cm or, in areas with large anomalies, 1 000 ppm/cm. The scale coefficient is the same for all the maps of a given survey area, and is given in the legend of the map. Examples of AEM profile maps are shown in Figs. 11a and 11b. It is worth noting that the data on the profile maps have not been submitted to any additional filtering except that resulting from the time constant of the detector (τ = 0.3 s) and spherics filtering. This preserves the original resolution of the data and allows the recognition of small anomalies. Anomalies caused by man-made noise (cf. p. 33) are not systematically deleted either, although some of them are eliminated in the spherics filtering.

The interpolation program of the AEM data (main program 8) is based on linear interpolation. At the same time the data are smoothed by a moving average procedure with binomial coefficients over a desired number of points (generally 5 points). The data are interpolated into a rectangular grid, an element measuring 25×200 m². In other words, the data matrix of a standard-sized map sheet of 10×10 km² has 53×401 = 21 253 points. The contours are generated from the gridded data by a commercial software package GPCP-II (California Computer Products Inc. 1972). The anomaly contours on the maps are shown on a progressive scale and the original plotting is produced in three colours. The contour values are listed in Table 6. Examples of the AEM contour maps are given in Figs. 54a and 54b. The specifications of the AEM device and data processing are listed in the legend of the maps (not reproduced here).

The question may be raised as to why both

Table 6

Numeric values and colours of the countour lines used in the plotting of the AEM contour maps. Owing to the small scale of reproduction possible in this context, some of the original contour levels have been omitted from the figures.

	Value (ppm)	
Colour	1.	2.
Blue	+100, +150, +200, . . .	+100, +300, +500, . . .
Black	+50, −100	−100
Red	−200, −300, −400, . . . −1000	−200, −600, −1000, −1500
	−1250, −1500, −1750, −2000, −2500, −3000, −3500, . . .	−2000, −3000, −4000, . . .

1. Original maps on a scale of 1 : 20 000
2. Maps reproduced here; all contours black (except Fig. 106)

Table 7

Capacity requirements (in terms of CPU time) of the HP 3000 Pre-CX computer used in the processing of the aerogeophysical low-elevation data, calculated as averages per one original record of data (cf. Table 2), one line km (averaging 35 points of AEM data) and one map sheet (530 line km). Numbers in brackets refer to the ADP flowchart in Fig. 22.

	CPU time (s)			%
	per 1 s record	per line km	per map sheet	
Basic data processing				
Main programs 1–5	0.80	14.0	7500	12.9
Safety copying	0.34	6.1	3200	5.5
Fixpoint data processing	0.06	1.2	600	1.0
Processing of AEM anomaly data				
Methodic corrections (6)	0.05	1.0	500	0.9
Profile map plotting (7)	0.23	4.1	2200	3.8
Gridding (8)	0.13	2.3	1200	2.1
Contouring (9)[1]	0.32	5.8	3100	5.3
Transformation of AEM data				
Transformation	0.06	1.0	600	1.0
Gridding (8)	0.13	2.4	1200	2.1
Code conversion	0.07	1.3	700	1.2
Contouring (9)[1]	0.61	11.0	5900	10.1
Processing of aeromagnetic data				
Correction of base station data	0.19	3.5	1800	3.1
Methodic corrections	0.59	11.0	5700	9.8
Single-sensor data gridding and contouring (9)[1]	0.38	6.9	3700	6.3
Gradient data gridding and contouring (9)[1]	1.26	23.0	12100	20.8
Processing of airborne gamma-ray data				
Gridding (8)	0.11	2.1	1100	1.9
Contouring (9)[1]	0.74	13.0	7100	12.2
Total (nominal)	6.07	110	58200	100
Repeats due to hardware and software failures (c. 40 % of total)	2.43	40	22800	
Total (effective)	8.5	150	81000	

[1]) The CPU time required in contouring depends on the number of contours generated.

profile and contour maps need to be produced from the same AEM data. In the opinion of the present author, there are advantages in both compilation techniques, and the results are complementary. The profile map displays the true position and value of each data point actually measured. Hence, the map gives a true representation of the original quality and noise level of the data, and makes it possible to distinguish between small signal and noise anomalies (geological conductor vs man-made anomaly source). On the other hand, the contour map makes it possible to display even the biggest anomalies in a readable form. As the contouring necessarily means a degree of smoothing of the original data, this may ease the visual interpretation of the results, as some of the short-wavelength signals are filtered off. These points are easily seen by comparing Figs. 12 and 81 (lower half), which are based on the same original data.

The ADP software developed serves the data processing of the AEM and airborne radiometric surveys and partly also of the aeromagnetic surveys. Thus there is no point in describing the use of the computer resources for AEM data processing alone. The average figures given in Table 7 hold for the data processing of one map sheet (100 km^2, 530 line kilometres). The figures are for the HP 3000 Series I and Pre-Cx computers of the Survey in 1980. The standard outputs comprise 2 profile and 2 contour maps for AEM data (in-phase and quadrature components), 3 contour maps for airborne radiometric data (total radiation, eU and eTh concentration maps) and 2 contour maps for aeromagnetic data (absolute values of magnetic total field intensity based on a single sensor or a transverse horizontal gradient).

The software described refers to the version applied at the Geological Survey of Finland in 1974–1980. Part of the same AEM software is also in use at the Geological Survey of Norway. In 1981 a new software package with an entirely redesigned and methodically improved set of programs was brought into use (Vironmäki & Multala 1981). The new software is faster, more flexible and more efficient than the one described in the present paper.

PRINCIPLES UNDERLYING THE APPLICATION OF AEM RESULTS

Physical properties causing AEM anomalies

When expressed in the SI system of units, the behaviour of electromagnetic fields in a medium is controlled by the following physical properties:

- Conductivity σ, dimension Sm^{-1}.
- Magnetic susceptibility k, dimensionless quantity.
- Relative dielectric permittivity ε_r, dimensionless quantity.

In AEM methods the physical property that most affects results is conductivity. The systems are generally dimensioned for exploration purposes so that only intermediate and good conductors produce anomalies. As pointed out on page 16, the lower limit of the conductivity aperture can be adjusted with the response parameter; in a rigid-coil system this is done most readily by changing the

transmitter frequency. The usefulness of AEM results in bedrock mapping and overburden studies is improved if indications are also obtained from weak, and even from poor conductors. This, however, entails an increase in the number of anomalies, and the explorational application of AEM data based merely on visual interpretation of anomalies becomes more difficult.

In practice, magnetic susceptibility, although in this context a secondary property in comparison with conductivity, often also produces AEM anomalies. According to Faraday's law, the eddy currents in a susceptive medium are proportional to the product

$$\mu \frac{\partial H_p}{\partial t}$$

Hence, the secondary field H_s generated by the eddy currents is directly proportional to the magnetic permeability μ and is in phase with the primary field H_p. Thus, a susceptive, resistive formation gives rise only to an in-phase component anomaly. This phenomenon can be put to good use within the limits of the sensitivity of the AEM method in the integrated application of AEM and aeromagnetic data, e.g. when interpreting the depth to the upper surface of the formation and the mode of magnetisation.

The effect of dielectric polarisation is negligible in audio frequency AEM methods; for example for the DC-3 AEM system the effect on a permittive half-space is a few ppm at most. The effect, which becomes measurable with AEM methods only at frequencies $f \geq 20$ kHz, has been utilised in permafrost studies and in exploration for resistive formations, such as gravel occurrences in a well-conductive environment (Sinha 1977a). The effect of induced polarisation (IP) has not been noted in the continuous wave AEM methods at audio frequencies. Some attempts have been made to interpret the AEM pulse transient results by taking into consideration the IP effect as well (Morrison, Phillips & O'Brien 1969, Lee 1981); such attempts are, however, still speculative.

Conductivities of Finnish rocks and soils

The average conductivities of Finnish rock and soil types, determined by means of galvanic earth resistivity measurements, are listed in Table 8. The values demonstrate that the conductivity of some rock and soil types is so high that in explorational applications they constitute a geological noise component in the AEM survey data. In Finland, particularly the following formations are marked producers of AEM anomalies:

- Marine clays, especially the saline Littorina Sea clays that cover the coasts of the Gulf of Finland and the Gulf of Bothnia and extend far inland, particularly in Bothnia.
- Graphite- and pyrrhotite-bearing schists (black schists), which are fairly common in the Precambrian bedrock.
- The preglacial weathering layer that is found in numerous localities in Lapland and whose conductivity at best approaches that of the saline clays.

The areal distribution of these conductive formations in Finland has been fairly well established thanks to the quantity of lithological and soil data gathered (e.g. Marmo 1960, Okko 1964, Kujansuu 1972). The utilisation of AEM data in exploration is, however, often hampered by the lack of sufficiently accurate in-situ conductivity data, particularly on soil,

Table 8

Electrical conductivities of some Finnish soil and rock types according to Puranen (1959) and Pernu (1979). The data refer to galvanic earth resistivity measurements.

Material type	Conductivity (Sm^{-1})	
Lake or stream water	0.002 – 0.01	
Sea water	0.2 – 1	
Coarse sand and gravel	0.0007 – 0.001	
Sand	0.001 – 0.002	
Silt	0.005 – 0.012	
Clay	0.015 – 0.03	
Till	0.002 – 0.005	
Peat	0.003 – 0.01	
Mud, gyttja, mould	0.007 – 0.012	
Saline or graphitic clay	0.02 – 0.5	
Weathered bedrock in situ	0.003 – 0.01	
Gabbro	0.00003 – 0.0001	rocks of low conductivity
Granite, limestone, Gneiss, mica schist, Quartzite, greenstone	0.00006 – 0.0002	rocks of low conductivity
Serpentinite	0.002 – 0.02	rocks of medium conductivity
Claystone	0.02 – 0.05	rocks of medium conductivity
Graphite- or pyrrhotite-bearing schist	0.02 – 10	rocks of high conductivity
Sulphide ores	0.1 – 100	rocks of high conductivity

NB Values of soils are valid for layers below groundwater level. Values of soils above groundwater level are approximately one order of magnitude lower.

because the conductivity measurements are undertaken only on a limited scale.

Anomalies due to magnetic susceptibility show up best in AEM results when they are associated with ultramafic and mafic rocks; they are most difficult to interpret when related to pyrrhotite-bearing black schists.

Methods of interpretation

The most common usage of AEM results is visual interpretation. When applied with experience, the method is both rapid and effective. The interpretation is based on the background information available on the lithology and soil geology of the study area as well as on the shape of the anomalies and their areal extension. Hence, the anomalies over a target can be classified, with a fair degree of confidence, as due to overburden or bedrock conductors. On the basis of the amplitude and in-phase/quadrature ratio of the anomalies, the conductors can further be classified into poor, intermediate and good conductors. Since the promising AEM anomalies in the exploration applications are generally measured in greater detail on the ground, there has been no attempt to interpret accurately the relations between the AEM anomaly and the conductor properties. Hence, visual interpretation is often very general and much checking is needed in the field.

When approaches more quantitative than

a visual interpretation are aimed at, the interpretation can be performed on the basis of the special points or curve fitting of the AEM anomaly. The application of the methods requires that the AEM responses to a variety of idealised conductor models, such as a conductive half-plane, have been determined either by numerical modelling or by scale model measurements as a function of the various parameters. With the aid of the modelling results, the interpretation can give more exact parameters, such as the conductivity-thickness product and the depth to the conductor. Manual interpretation utilising modelling results is arduous and hence much slower than visual interpretation.

Methodically the most advanced way of interpreting the AEM data would be to invert the survey data into a model that includes both the geometry and the physical properties of the conductors. The difficulties of inversion are, however, such that it has not been possible to apply the method in a general form. Even so, the method can already be partly used by fixing the geometry of the inversion model and by employing the theoretical solutions of the fixed model with the aid of a data bank. Palacky (1972) and Fraser (1978) were the first to apply the method to the interpretation of AEM data. In Finland, Valkeila (1978) has used the method in the computerised interpretation of slingram (horizontal loop) results. The method has also been applied in the present study. It has the advantage of allowing the anomaly values to be converted as an ADP application systematically and rapidly into apparent property values. On the other hand, the interpretation values are so strongly related to the fixed geometry of the model used that they cannot be more than a complementary way of presenting the AEM results.

So far, the interpretation of AEM data in Finland has been based almost exclusively on visual interpretation. In this study theoretical results and methodic examples are presented to demonstrate the feasibility of other methods as well. In the opinion of the present author, all the methods should be applied if the aim of AEM surveys is, even partly, to replace ground EM surveys.

Models used in interpretation

The interpretation of AEM anomalies has to be based on models with a simple geometry, because theoretical solutions allow only certain special cases to be resolved in closed form. Solutions of geologically more representative models must be searched for by means of numerical or scale modelling approximations. In this way some of the difficulties related to the models can be eliminated.

In the present work the AEM responses to the following models were studied in the DC-3 vertical coaxial coil system of the Geological Survey (cf. Fig. 26):

- One-layer model.
- Two-layer model.
- Half-plane.
- Sphere.

The one-layer (half-space) model corresponds to an extensive formation that is homogeneously conductive and/or susceptive within the lateral coverage and penetration of the AEM method. The formation may thus be either a bedrock that is exposed or covered by resistive overburden, or an electrically thick conductive overburden whose thickness exceeds penetration. The varied par-

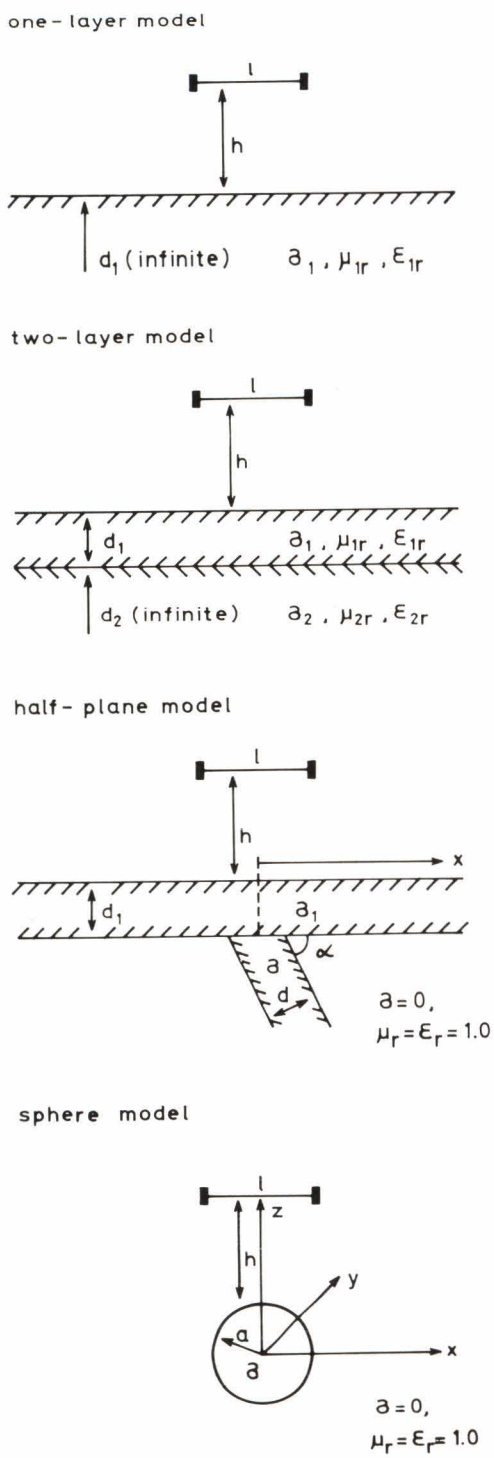

Fig. 26. Models and symbols of the variables used: (a) One-layer model. (b) Two-layer model. (c) Half-plane model. (d) Sphere model. σ_i = the conductivity, μ_{ir} = the relative permeability, ε_{ir} = the relative permittivity and d_i = the thickness of layer i, μ_0 = the permeability of vacuum $4\pi 10^{-7}$ Hm^{-1}, ε_0 = the permittivity of vacuum $8.854 \cdot 10^{-12}$ Fm^{-1}, h = the flight elevation, l = the coil separation, d = the thickness and α = the dip angle of the half-plane, a = the radius and z = the depth to the centre of the sphere.

ameters of the model include conductivity, susceptibility, and depth to the surface.

In Finland, the most important example of the two-layer model is a conductive and electrically thin blanket of overburden overlying resistive and possibly also susceptive bedrock. The parameters of the model are the conductivity-thickness product of the conductive layer, the depth to the upper surface of that layer and the susceptibility of the bedrock. The same model geometry but with an electrically thick layer of overburden can rarely be used in Finland, because its applicability is restricted by the geological conditions of the country. The multilayer earth models could also easily be solved; their use in Finland, however, seems only seldom to be possible.

A sheetlike bedrock conductor is modelled by an electrically thin, dipping half-plane. The conductor is assumed to be infinite along the strike, i.e. 2-dimensional. In the model, the conductivity of the country rock is taken as zero. The conductive overburden, however, can be included in the model with some restrictions. Experiments have also been performed on the model of an electrically thick half-plane, an important AEM model that has been subject to few studies to date. The varied parameters of the model are the depth to upper surface, the dip angle, the conductivity-thickness product of the half-plane and the conductivity-thickness product of the horizontal conductor.

A conductive sphere in a resistive environment, i.e. a local conductor in bedrock or soil, was studied as an example of a 3-dimensional model. The varied parameters of this model are conductivity, radius and the depth of the centre.

DC-3 AEM RESPONSES RESOLVED FOR VARIOUS MODELS

This chapter describes briefly how the model responses are solved and gives examples of the results for the vertical coaxial DC-3 AEM system. Previous studies of the models, as reported by other authors, and the accuracy of the modelling methods are also discussed. The results are given directly in accordance with the DC-3 AEM system; thus, the user does not have to transform the parameters. If desired, the results can also be transformed to suit other vertical coaxial coil systems by means of the response parameter, equation (13), and by scaling the linear dimensions (Grant & West 1965, pp. 548–551).

One- and two-layer models

The solutions to the one- and two-layer models can be written as formally exact special cases of a general multilayered earth model. The solutions, however, include oscillating infinite integral functions and hence the calculation of numerical results requires the use of numerical integration methods.

Previous studies

Conductivity effects

Theoretical solutions for a horizontal magnetic dipole above conductive one- and two-layer earth models have been given by Wait (1955, 1958). Malmqvist (1965) was the first to calculate numerical data for the one-layer model by means of series expansion methods. The results obtained with a computer program as numerically integrated values have been reported by Frischknecht (1967) in a study that gives in tables the response functions of the vertical and horizontal dipole at given values of the parameters. Since the number of parameters affecting the responses is high, the coverage of the tables, in spite of their large size, cannot be sufficient to meet all needs. This was noted at the start of the present study, when attempts were made to calculate characteristic diagrams for the high-elevation AEM systems of the Survey on the basis of the tables. Ward and Hood (1969, Fig. 25) and Fraser (1978, Fig. 7) have compiled characteristic diagrams for the one-layer model from the tabulated values of the response function. The characteristic diagrams calculated by Malmqvist are, however, still of the most general use.

Peltoniemi (1977, Fig. 12) and Pitcher, Barlow and Lewis (1980, Fig. 13) have published characteristic diagrams for the conductive two-layer earth model. Both sets of graphs have been produced by employing the computer program reported by Sinha and Collett (1973).

Wait (1962) has presented a theoretical solution to the multilayer earth model. On the basis of this, Sinha and Collett (1973) published their computer program which, however, omits the effect of displacement currents. By means of the program, responses have been calculated for one- and two-layer earth models of all the AEM systems in use in Finland; the results have been reported as characteristic diagrams (Peltoniemi 1977,

1978b). The program was further developed so that it can be applied to other towed-coil (e.g. dual frequency) systems as well.

Susceptibility effects

Few theoretical studies have been published to date on the effect of magnetic susceptibility on the results of electromagnetic and AEM survey methods. The first study reported was that by Ward (1953), in which he showed the responses to a conductive, susceptive sphere in a homogeneous primary field. Later, Ward (1959) demonstrated that in order to interpret the dimensions and properties of the source, measurements must be undertaken at several frequencies so that use can be made of the information relevant to the resistive and inductive limit of the response function. Thomas (1977) has studied the effect of susceptibility on the results of ground electromagnetic survey in a multifrequency dip-angle method. He has also calculated the effect for the one-layer model in a helicopter-borne AEM system. As a result, he gives k = 0.004 as the limit of sensitivity in the susceptibility determinations of the AEM system in question. Lodha and West (1976, Fig. 8) give some response values for a susceptive, conductive sphere in an AEM vertical coaxial system. Fraser (1973) and Sequin (1975) have reported case histories of experimental interpretation procedures for AEM data in prospecting for taconite iron ores. Finally, Fraser (1981) has presented a magnetite mapping technique for a horizontal coplanar AEM system. The technique is based on a resistive half-space model and an empirical relationship between susceptibility and magnetite content.

Since remanent magnetisation is a static property, the measuring of induced magnetisation by electromagnetic methods presents a means of discriminating directly between these two mechanisms of magnetisation by ground or airborne surveys, provided that the electromagnetic survey is sensitive enough. The first study on this subject was probably that undertaken by Goldstein and Ward (1966), who utilised the micropulsations of the Earth's natural electromagnetic field. Later, Peltoniemi (1981b) gave examples of the application of the method in the combined interpretation of AEM and aeromagnetic data.

The special case of a homogeneous, susceptive half-space with zero conductivity can be readily solved with a method of images. The results thus calculated for various coil configurations have been reported, for example, by Keller and Frischknecht (1966, Fig. 201) and for the slingram method more extensively by Ketola and Puranen (1967, Fig. 75).

Solution method and its accuracy

A new version of the computer program for the multilayer earth model has been published for permafrost studies (Sinha 1977b), in which the displacement currents generated by dielectric polarisation are also taken into account. Although the effect of magnetic polarisation was omitted from the original version, its addition to the solution and to the new computer program did not entail too large alterations. The addition of the magnetic permeability μ_i of the layer i as a variable requires that it be taken into account in the boundary conditions on the surfaces between the layers and in the values of the skin depth and propagation constant. The boundary conditions determine the equations of the reflection coefficients, which can be deduced for the electric and magnetic polarisation mode from the solutions reported by Sinha. The equations are transformed into the form reported earlier (Peltoniemi 1980a).

In the calculations for the horizontal conductor (two-layer earth) model, the conductivity of the lower layer σ_2 was taken as $\sigma_2 = 0.001 \cdot \sigma_1$. The contrast was selected experimentally to be so high that, within the sensitivity limits of the method, the model corresponds to a horizontal conductor layer in a highly resistive environment. Since information on the shape of the anomaly is not available for the layered earth model, the characteristic diagrams describe all the information included in the model results.

The values of the relative dielectric permittivity can be varied in the program and hence a value of $\varepsilon_{ir} = 10$ was used for all the layers in the calculations. Compared with $\varepsilon_{ir} = 1.0$, the effect on the DC-3 AEM data is negligible, a few ppm at most.

After the changes the program was tested as follows:

- On the inductive limit the conductivities of the layers are the predominant parameters. Hence the results on the in-phase anomaly must, at high conductivity, approach the same limit values that can also be calculated with the method of images. As Table 9 demonstrates, the responses already approach the limit value at $\sigma_1 = 50$ Sm^{-1}, and yet the effect of susceptibility is still recognisable. The limit value is reached in practice at a conductivity of $\sigma_1 \geq 500$ Sm^{-1}.
- On the resistive limit the susceptibility values are the predominant parameters. Hence the results should approach the limit values calculated with the method of images when very low conductivity values σ_1 are used. The results in Table 9 demonstrate that this condition, too, is met excellently.

Table 9

Comparison of responses to conductive and/or susceptive earth in the DC-3 AEM system, solved by means of the computer program and the method of images at a flight elevation of h = 30 m.

(a) Inductive limit.

μ_{ir}	Computer program						Method of images	
	$\sigma = 50$ Sm^{-1}		$\sigma = 500$ Sm^{-1}		$\sigma = 5000$ Sm^{-1}		$\sigma = \infty$	
	Re (ppm)	Im (ppm)	Re (ppm)	Im (ppm)	Re (ppm)	Im (ppm)	Re (ppm)	Im (ppm)
1.0	−15430	−408	−15700	−126	−15780	−40	−15820	0
1.01	−15420	−410	−15700	−127	−15780	−40		
1.1	−15410	−428	−15690	−133	−15780	−42		
1.5	−15330	−501	−15670	−155	−15770	−49		
2.0	−15260	−580	−15650	−179	−15770	−56		

(b) Resistive limit.

μ_{ir}	computer program						method of images	
	$\sigma = 0.001$ Sm^{-1}		$\sigma = 0.0001$ Sm^{-1}		$\sigma = 0.00001$ Sm^{-1}		$\sigma = 0$	
	Re (ppm)	Im (ppm)	Re (ppm)	Im (ppm)	Re (ppm)	Im (ppm)	Re (ppm)	Im (ppm)
1.0	−54.6	−286	−1.6	−33.9	0.8	−3.6	0	0
1.01	23.5	−228	77.1	−34.2	79.5	−3.6	79	0
1.1	692	−311	752	−37.1	754	−4.0	753	0
1.5	3080	−396	3162	−48.2	3166	−5.2	3165	0
2.0	5164	−476	5271	−59.0	5276	−6.4	5274	0

Sinha (1977b, p. 9) reports that the accuracy of the calculation in the original program is so good that »accuracies of 1 ppm or better are realized in most cases». The above checks also show that the accuracy is very good. Therefore, the usefulness of the computed results depends on the compatibility of the model (layered earth structure) with true geological formations.

The calculation accuracy and time are proportional to the accuracy in the numerical evaluation of the infinite integrals involved in the solution. The accuracy of the method of integration – Gaussian Quadrature method, 96 calculation points per area between successive zeros of the integrand – is good, although the computing time required is relatively long. The lower the elevation h of the coil pair from the ground, the greater is the number of terms that must be taken into the solution. On the boundary h = 0 the integrals diverge. As an example, the computing time on the U1108 computer for the response curve in Fig. 28 (h = 30 m, $\mu_{1r} = 1.01$, 19 σ_1-values) was 50 CPU-seconds.

Results

The set of characteristic diagrams shown in Figs. 27–34 were calculated for the DC-3 AEM system with the modified program. Corresponding results for the vertical coplanar coil configuration have been reported elsewhere (Peltoniemi, 1980a).

Comparison of Figs. 28, 29 and 31, 32 demonstrates that, on the resistive limit, an almost linear correlation on a logarithmic scale prevails between the susceptibility and the amplitude of the in-phase anomaly. The sign of the in-phase component is reversed in comparison with the conductor response, whereas the quadrature component remains almost constant at low values of σ_1 or $\sigma_1 d_1$. The change from a positive response determined by susceptibility to the normal negative response controlled by conductivity takes place within a rather narrow range of conductivity or conductivity-thickness product. After a further increase in conductivity, the response is determined entirely by the conductivity of the medium within the measuring accuracy of the system.

Figs. 27 and 30 demonstrate that the sign of the quadrature component becomes positive at $h \leq 20$ m and at high values of σ_1 or $\sigma_1 d_1$. Since flight elevations that low are unusual in practice, use cannot be made of this diagnostic effect.

As stated previously (page 00), the average noise level of the DC-3 AEM system is N = 25 ppm. In accordance with the generally accepted definition of the anomaly detection limit $\bar{S_d}$ (11), the minimum recognisable anomaly of the system is 100 ppm. Fig. 28 (flight elevation h = 30 m, one-layer model) shows that, in terms of susceptibility, this means a detection limit of about k = 0.01. A k-value like this corresponds to a magnetite content of about 0.3 volume %, and a static anomaly of about 250 nT. The sensitivity of AEM methods to detect the variations in susceptibility is thus essentially lower than that of magnetic surveying. However, if the magnetisation is strong enough, the results described present a means of testing preliminarily whether the static anomaly is due to induced or remanent magnetism. The k-value derived from the interpretation of the aeromagnetic data can namely be applied with the theoretical AEM results. Thus, assuming that the magnetism is entirely induced, it is possible to compare the interpreted and measured magnitudes of the in-phase component anomaly in the AEM data (see examples on pp. 207–220). The comparison cannot be made if the magnetised formation is also

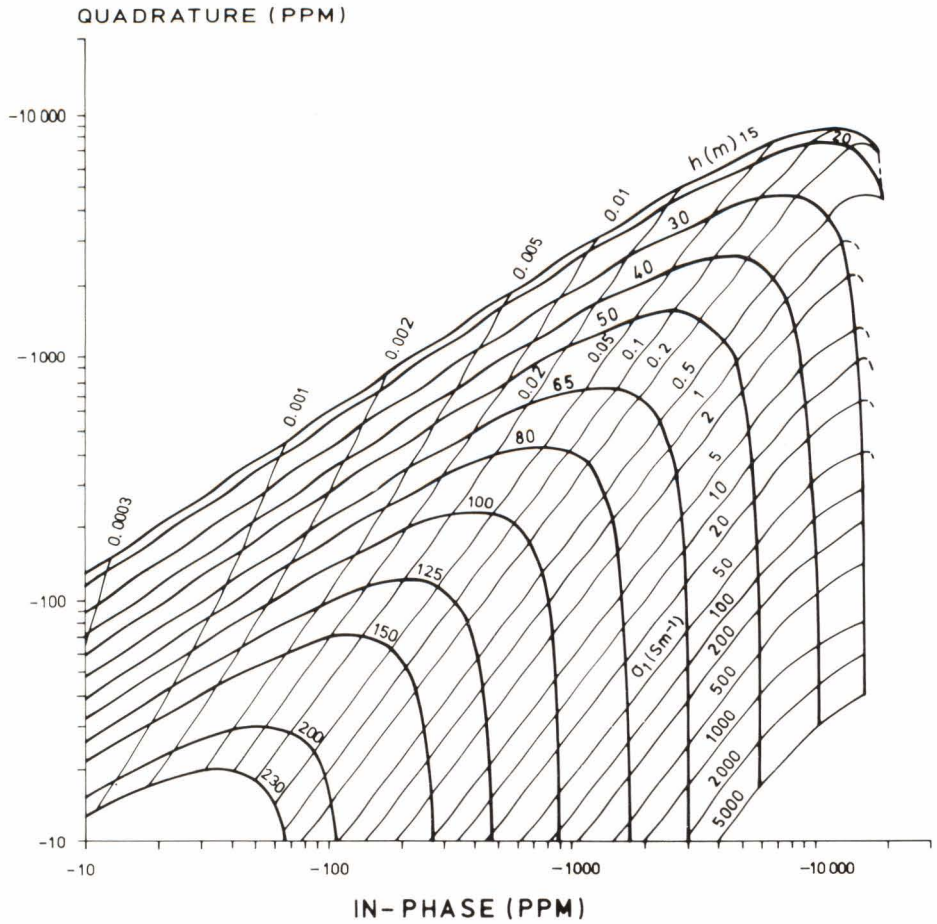

Fig. 27. In-phase and quadrature anomalies caused by a conductive half-space in the DC-3 AEM system as a function of the flight elevation h and the conductivity σ_1 of the half-space.

highly conductive, because the response is then determined by the conductivity.

Characteristic AEM anomalies due to susceptibility are more frequently encountered in low-elevation than in high-elevation AEM data. The difference is due to the higher survey elevation and the larger coil separation in the high-elevation systems. The response parameter θ_1 of the one-layer model

(26) $\theta_1 = \sigma_1 \mu_1 \omega l^2$

receives essentially higher values than it does in the low-elevation systems at the same $\sigma_1 \mu_1$ values, and the higher frequency of the low-elevation systems does not compensate the difference. Thus, in the high-elevation surveys, the inductive limit of the response function is approached more easily and conductivity becomes the predominant factor.

An outcome for the practical interpretation of electromagnetic survey data is that the susceptibility attenuates the in-phase anomaly of the conductor, and too low values of interpreted conductivity or conductivity-thickness product are then obtained from Figs. 27 and 30 (k = 0).

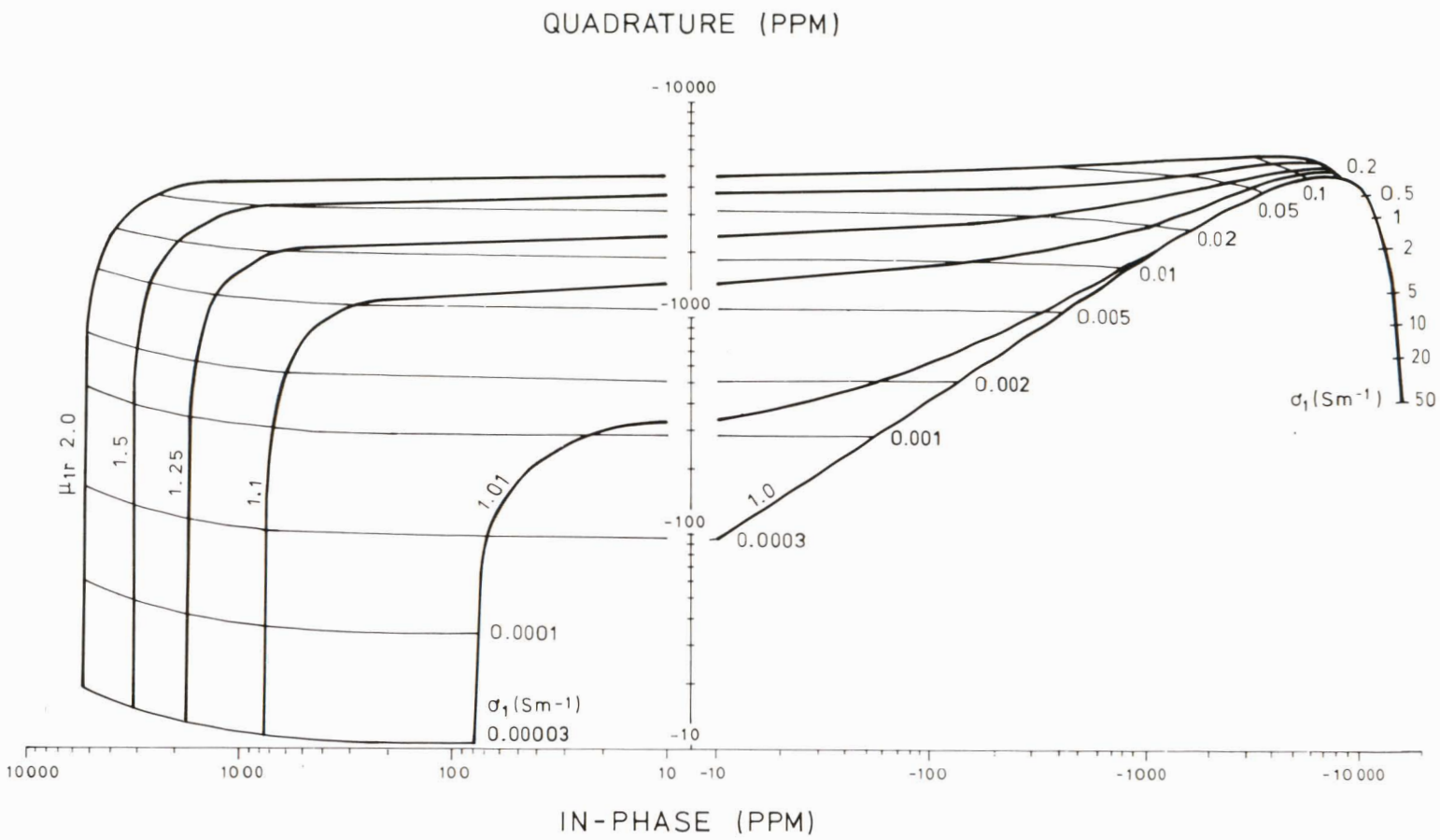

Fig. 28. In-phase and quadrature anomalies produced by a conductive and susceptive half-space in the DC-3 AEM system as a function of the conductivity σ_1 and the relative permeability μ_{1r} of the half-space. The flight elevation h = 30 m is constant.

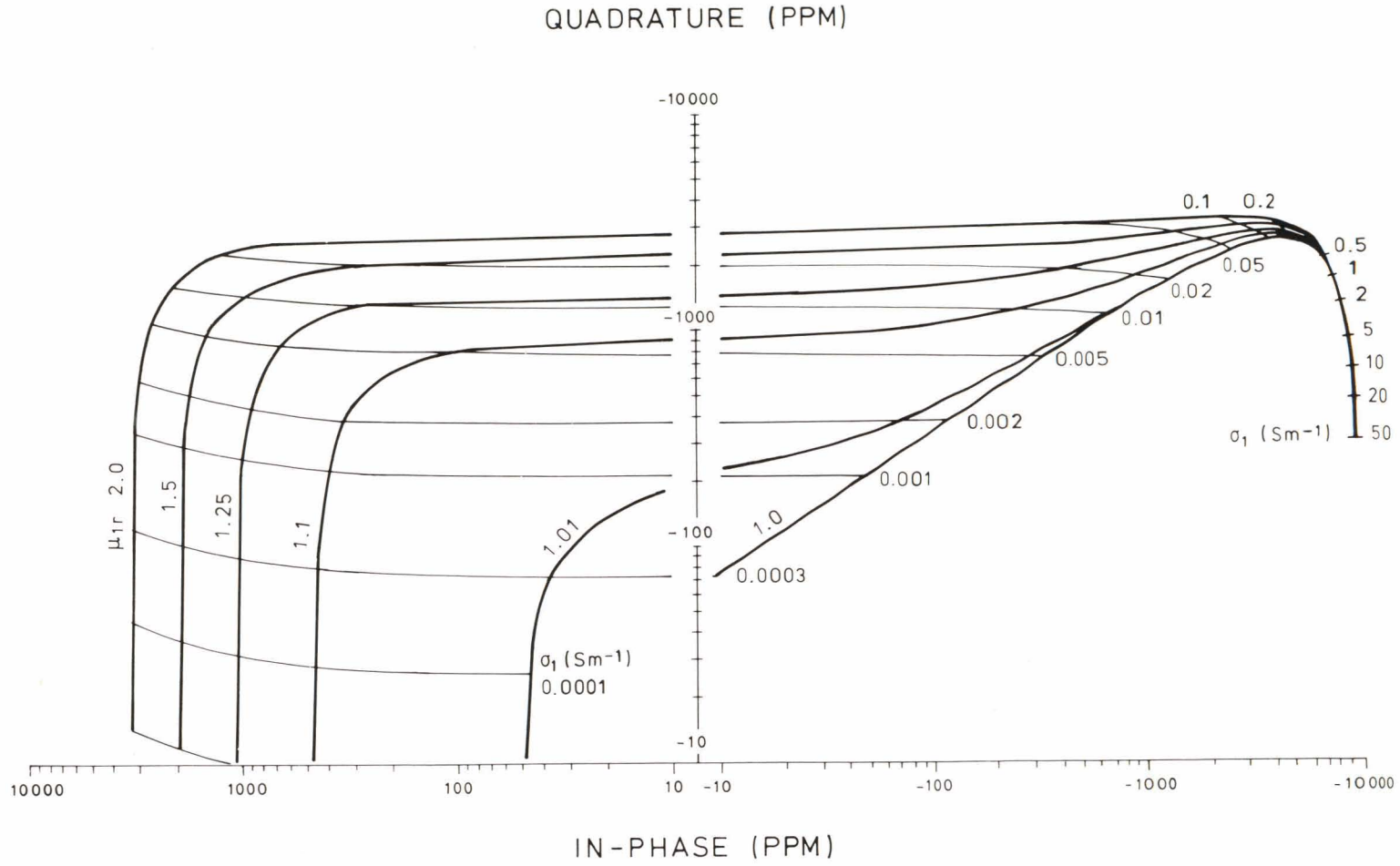

Fig. 29. In-phase and quadrature anomalies produced by a conductive and susceptive half-space in the DC-3 AEM system as a function of the conductivity σ_1 and the relative permeability μ_{1r} of the half-space. The flight elevation h = 40 m is constant.

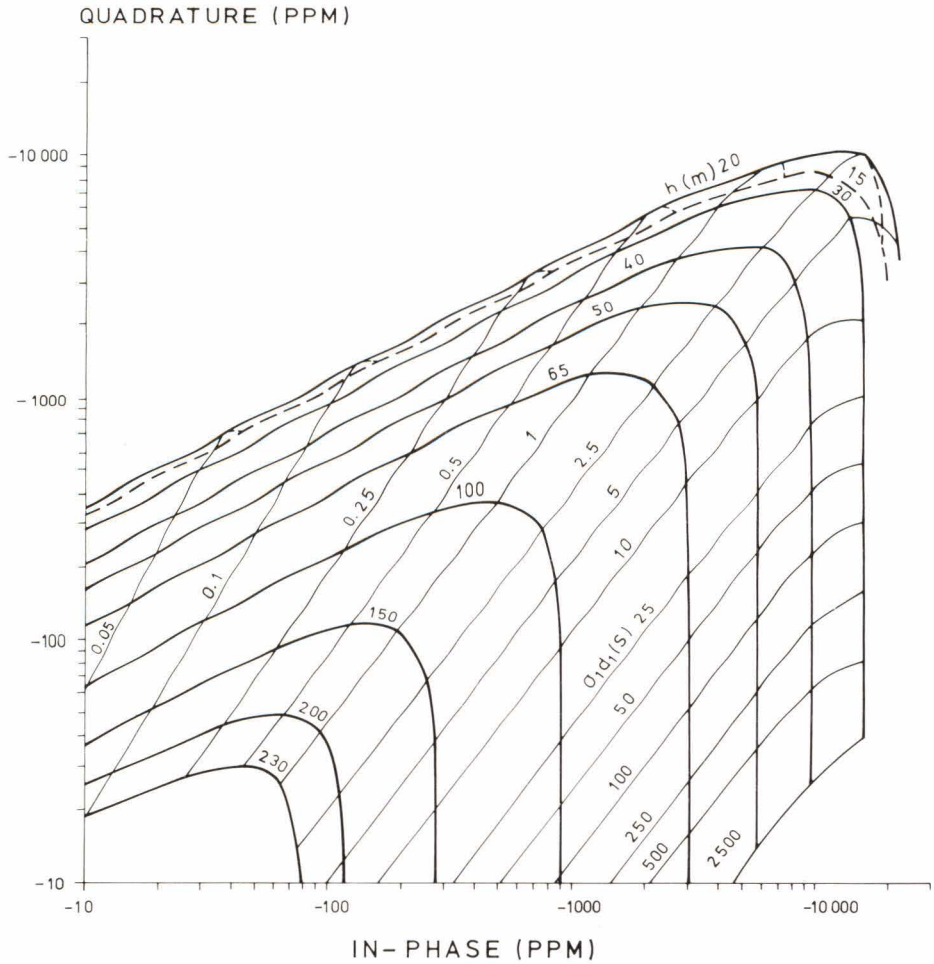

Fig. 30. In-phase and quadrature anomalies produced by a thin conductive horizontal layer in the DC-3 AEM system as a function of the depth to the upper surface h and the conductivity-thickness product $\sigma_1 d_1$ of the horizontal layer.

Table 10

Effect of conductivity and susceptibility on the behaviour of the response functions in the DC-3 AEM system. One-layer and two-layer models, survey flight elevation h = 30 m.

Source of dominant effect	One-layer model	Two-layer model
Susceptibility	$\sigma_1 < 0.001$ Sm^{-1}	$\sigma_1 d_1 < 0.04$ S
	0.001 Sm$^{-1} \leq \sigma_1 < 0.01$ Sm^{-1} and $\mu_{1r} > 1.15$	0.04 S $\leq \sigma_1 d_1 < 0.4$ S and $\mu_{2r} > 1.2$
Conductivity, conductance	$\sigma_1 > 0.05$ Sm^{-1}	$\sigma_1 d_1 > 0.6$ S

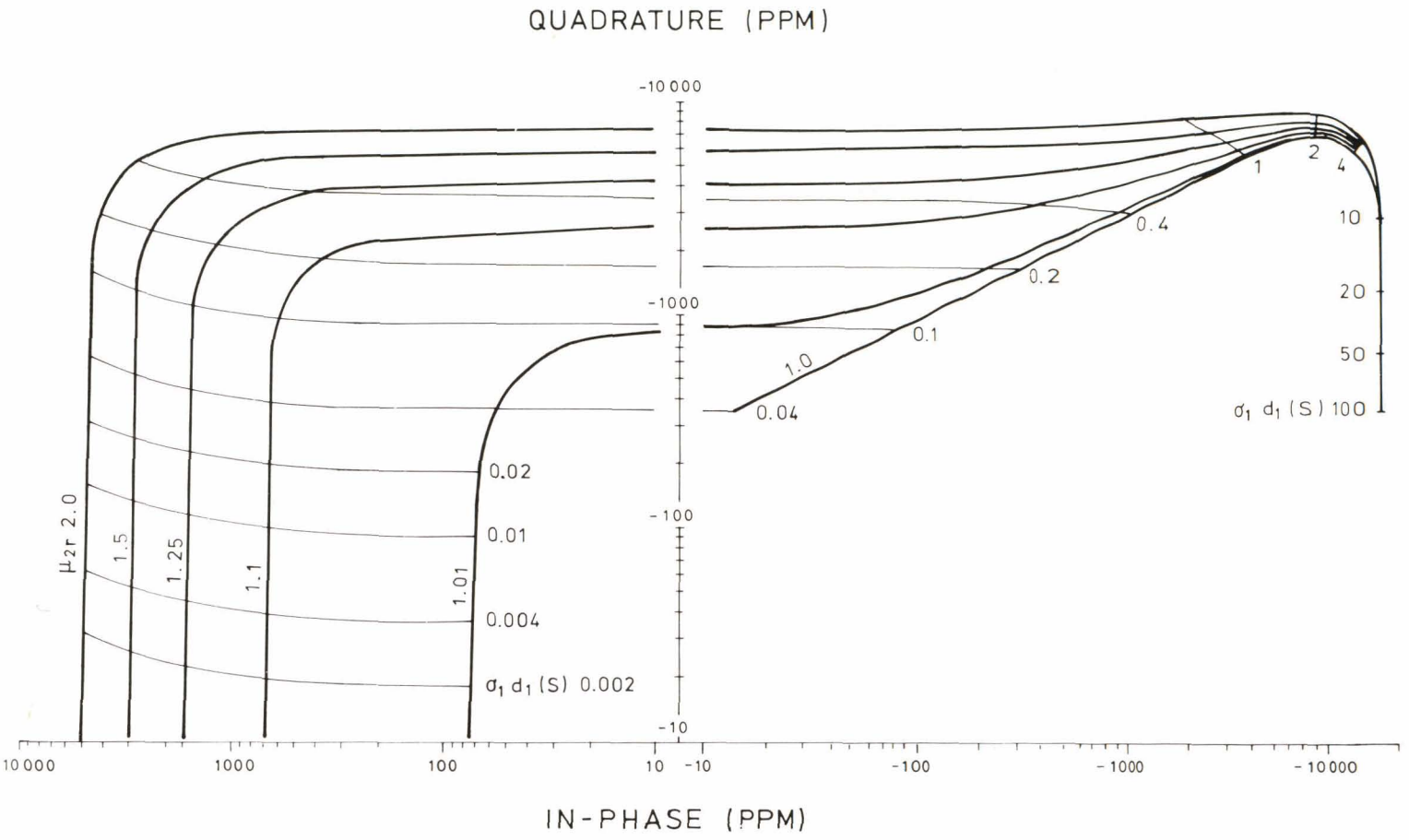

Fig. 31. In-phase and quadrature anomalies produced by a susceptive half-space covered by a thin conductive horizontal layer in the DC-3 AEM system as a function of the conductivity-thickness product $\sigma_1 d_1$ of the horizontal layer and the relative permeability μ_{2r} of the half-space. The flight elevation, i.e. the depth to upper surface of the conductive horizontal layer h = 30 m is constant.

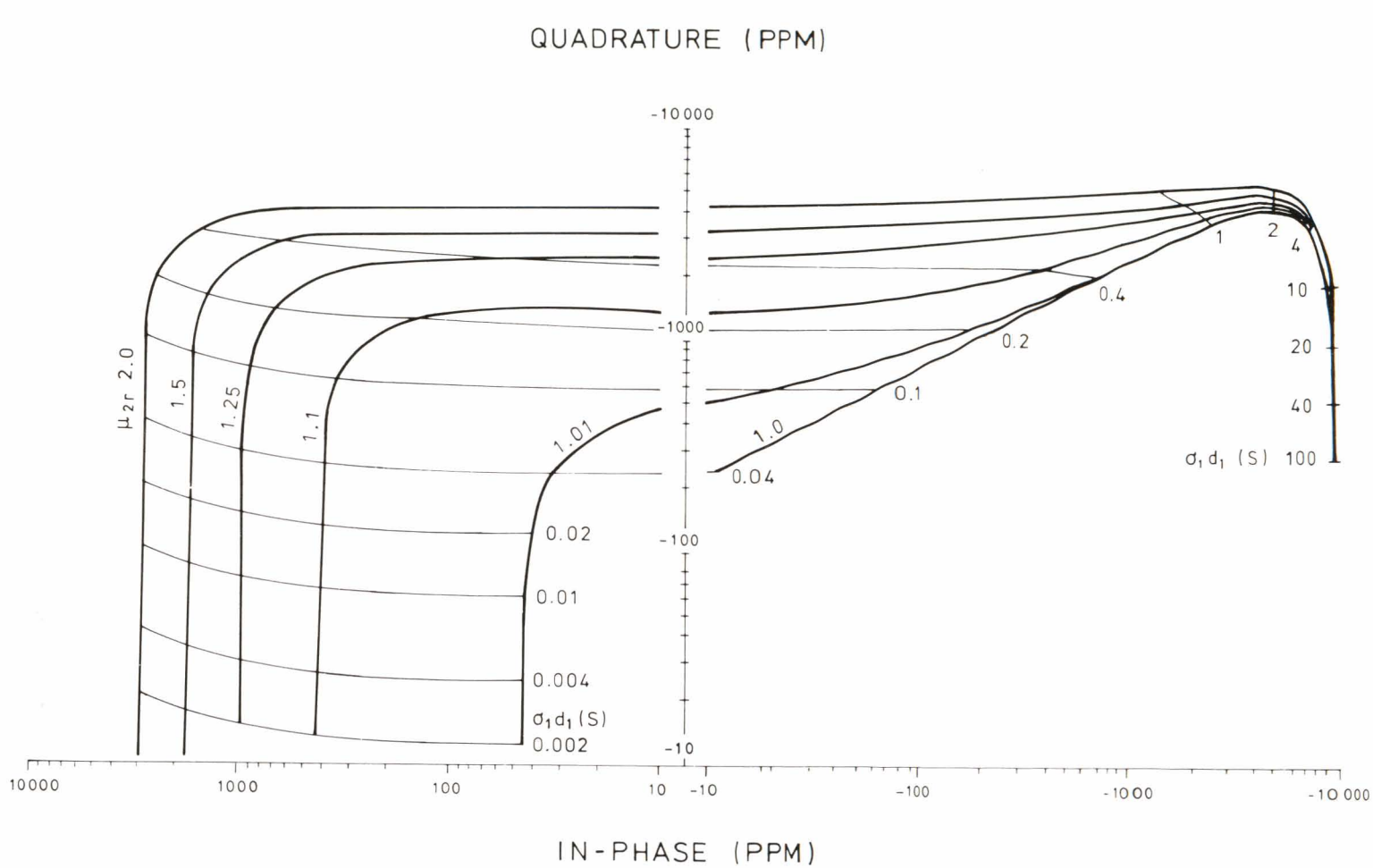

Fig. 32. In-phase and quadrature anomalies produced by a susceptive half-space covered by a thin conductive horizontal layer in the DC-3 AEM system as a function of the conductivity-thickness product $\sigma_1 d_1$ of the horizontal layer and the relative permeability μ_{2r} of the half-space. The flight elevation, i.e. the depth to the upper surface of the conductive horizontal layer h = 40 m is constant.

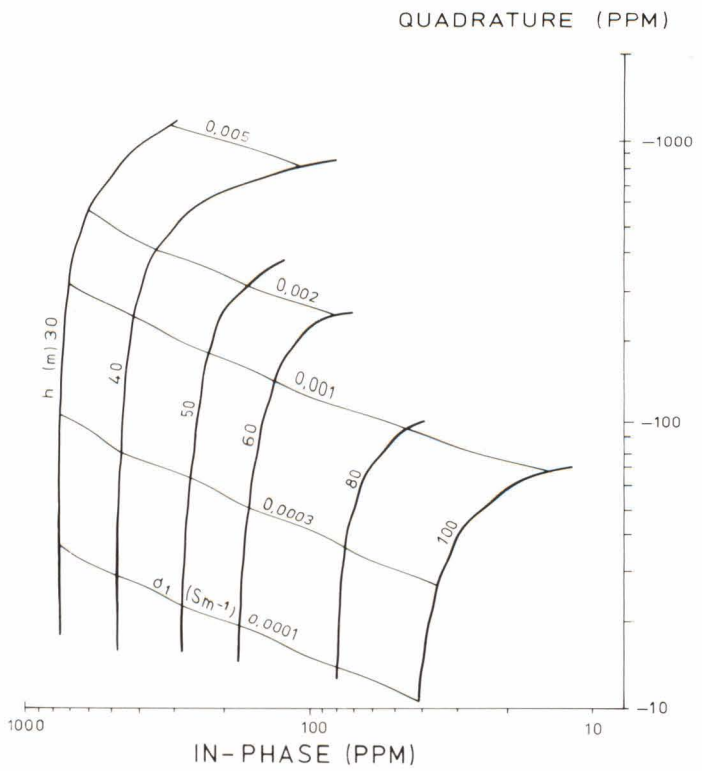

Fig. 33. In-phase and quadrature anomalies produced by a conductive and susceptive half-space in the DC-3 AEM system as a function of the flight elevation h and the conductivity σ_1. The relative permeability of the half-space $\mu_{1r} = 1.10$ is constant.

Based on the data in Figs. 28 and 31, Table 10 shows the limit values of the conductivities and conductivity-thickness products at which the DC-3 AEM responses grade from those controlled by susceptibility into those controlled by conductivity. The results demonstrate that in the case of a homogeneous half-space, when the conductivity $\sigma_1 \leq 0.001$ Sm^{-1}, the anomalies are always controlled by susceptibility. At conductivity $\sigma_1 \geq 0.05$ Sm^{-1}, the anomalies are controlled by conductivity, and in the intervening range both properties have a significant influence. The effect of conductive soil begins at conductivity-thickness products $\sigma_1 d_1 > 0.04$ S and becomes predominant at $\sigma_1 d_1 \geq 0.6$ S.

It was suggested above that there are possibilities for using the AEM susceptibility responses for interpreting the mode of magnetisation. The lack of a characteristic in-phase anomaly over an anomalously magnetised formation does not, however, necessarily imply that the magnetisation is remanent. In practice, the in-phase anomaly may be lacking simply because the outcrop of the magnetised formation is too deep for the penetration of the AEM method. Fig. 33 illustrates the influence of the depth of the subsurface outcrop on the results of the DC-3 AEM system in the case of the one-layer model. The figure illustrates the variation in response as a function of the depth h and the conductivity σ_1, when the susceptibility is constant, $\mu_{1r} = 1.10$. The anomaly detection limit (100 ppm) is reached with a depth value of h = 75 m. When μ_{1r} is 1.25, the detection limit value is increased to h = 100 m.

The characteristic diagram in Fig. 30 refers to an electrically thin horizontal conductive layer. Fig. 34 shows the effect of the thickness d_1 and the conductivity σ_1 of the horizontal conductor on the DC-3 AEM data, when the

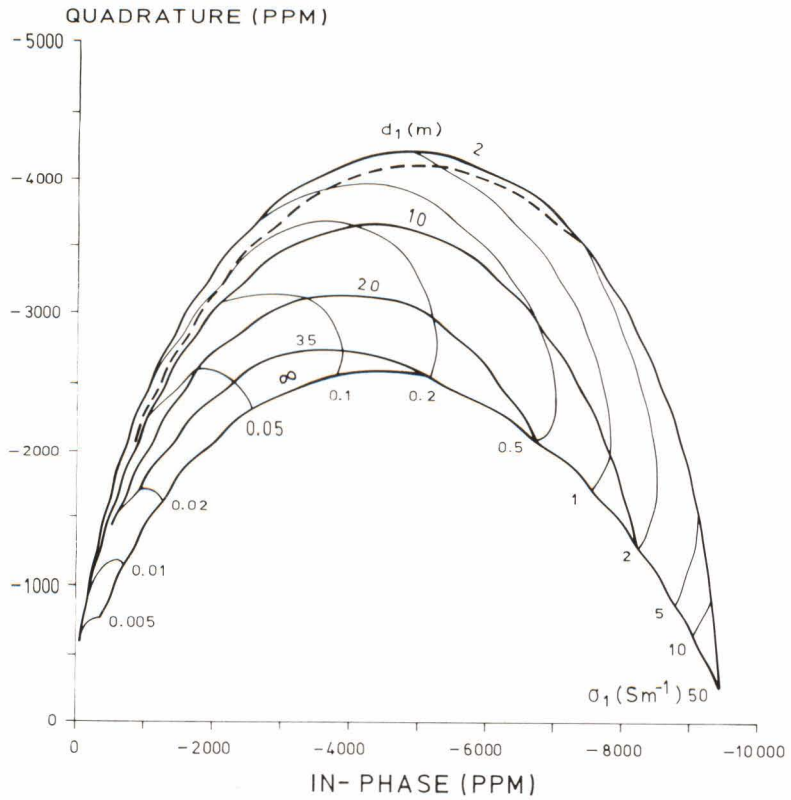

Fig. 34. In-phase and quadrature anomalies produced by a thick conductive horizontal layer in the DC-3 AEM system as a function of the conductivity σ_1 and the thickness d_1 of the horizontal layer. The flight elevation h = 40 m is constant. Dashed line = the lower limit of interpretability as given by equation (31).

flight elevation h = 30 m and the susceptibilities ($\mu_{1r} = \mu_{2r} = 1.0$) are constant. The result indicates the theoretical possibilities for interpreting the thickness of a conductive layer. The practical application of the result, however, requires that also the depth to the upper surface of the conductor be accurately known; otherwise it would not be possible to discriminate between the characteristic diagrams in Figs. 30 and 34 (changes in h or d_1). The discrimination would be possible by applying a multifrequency method of AEM surveying.

Half-plane model

A widely-used interpretation model in explorational applications of AEM data has been a thin conductive half-plane in a resistive environment. Modelling with the finite conductivities of the half-plane must be conducted on scale models. Only if the conductivity of the half-plane is infinite can the anomalies produced by the model be solved numerically.

Previous studies

Wieduwilt (1962, Fig. 6b) and Podolsky (1966, Fig. 5) were the first to report the results of scale model measurements on a vertical coaxial coil system. Brant, Dolan and Elliot (1966, Fig. 10) have extended the characteristic diagram of the vertical half-plane published by Wieduwilt to cover also the h/*l* -ratios between 0.25–1.0. A comprehensive scale model study of different AEM systems has been undertaken by Ghosh and West (1971) and Ghosh (1972). In the latter paper, Ghosh also discusses the change in the half-plane response caused by a conductive horizontal layer of overburden. Of the scale model measurements conducted at the Geological Survey of Finland, a treatise by Hämäläinen (1977) and a larger one by Ovaskainen and Peltoniemi (1979) deal with this coil configuration.

Results for a thin, vertical half-plane of infinite conductivity, solved by numerical modelling methods, have been reported by Hjelt (1964), Paterson (1971) and Jain (1973).

EM scale model responses to a susceptive half-plane model have been reported for the slingram coil configuration only (Ketola 1968, Figs. 22–26). The papers by Wieduwilt (1962), Fraser (1973) and Seguin (1975) give examples of anomalies due to susceptive bodies in AEM field survey data.

The most realistic 2-dimensional model for EM data interpretation would be a conductive half-plane in a medium of poor, but finite conductivity. This would best allow for the complicated interaction and current channeling effects between the overburden, country rock and half-plane. Owing to modelling difficulties, results of this model structure are scarce in the literature. Gaur, Verma and Gupta (1972) and Gaur and Verma (1973) have shown examples of the changes caused by conductive overburden and/or country rock on the responses to a thin half-plane in a vertical coaxial coil configuration. Their results suggest that, even with low conductivity, the environment clearly affects the quadrature component of the anomalies. It would also be important to establish the responses, which likewise have not been reported in the literature, to the thick half-plane in the AEM fixed-coil systems. Thus, the need for future scale model studies still exists, in spite of the number of studies already undertaken and the significant contribution of the available results to the interpretation of AEM data.

AEM scale model measurements and results play a minor role in the present study. Some data relevant to the DC-3 AEM system are, however, presented on the basis of a report by Ovaskainen and Peltoniemi (1979). The results seek to demonstrate the effect of the conductive overburden and the detector time constant on the half-plane data and to illustrate the responses to the electrically thick half-plane.

Solution method and its accuracy

The scale model measurements were undertaken with the modelling facilities of the Laboratory of Economic Geology at the Helsinki University of Technology. The construction and accuracy of the instrumentation have been described by Ovaskainen (1976). The data relevant to the models and the measurements are listed in Table 11. The measurements with different σd values were undertaken by varying the values of the response parameter θ_3 of the half-plane

(27) $\theta_3 = \sigma\mu_0\omega l d$,

where d = the thickness of the half-plane (m), between $\theta_3 = 0.25$ and 750, and for the hori-

Table 11

Properties of the instrumentation and models used in the scale model measurements (partly according to Ovaskainen 1976 and Kurimo-Salminen 1979).

	Specifications
Instrumentation	
Principle	fixed coils, moving model
Coils	diameter 18 mm, length 8 mm, 1875 turns, electrostatic shielding
Coil separation	10–20 cm
Model velocity	0–10 cm/s
Oscillator	HP Model 201C Audio oscillator
Frequency	1000–15000 Hz, adjustable
Detector	PAR Model 129A Lock in Amplifier
Recorder	Philips Model PM 8010 2-line flat bed recorder
Models	
Thin half-planes	aluminium foils and sheets thickness 0.01–2 mm, area 1 × 1 m² conductivity $3.15 \cdot 10^7$ Sm^{-1}
Horizontal sheets	aluminium foils thickness 0.005–0.01 mm, area 1 × 1 m² conductivity $3.15 \cdot 10^7$ Sm^{-1}
Thick half-planes	graphite slabs No 1: 5 × 29 × 51 cm³ No 2: 10 × 23 × 51 cm³ No 3: 30 × 22 × 51 cm³ conductivity $1.0 \cdot 10^5$ Sm^{-1}
Accuracy	
Along-track accuracy of model	5 mm
Accuracy of model depth	1 mm
Accuracy of dip angle	1 degr.
Recorder resolution	2 ppm
Noise level	20 ppm (original), 5 ppm (digitised) } on the most sensitive scale

zontal conductor between $\theta_2 = 0.12$ and 3.7, when the response parameter of the horizontal conductor is defined by

$$\theta_2 = \sigma_1 \mu_0 \omega l d_1, \quad (28)$$

where d_1 = the thickness of the horizontal conductor (m). In practice, variations in θ_2 or θ_3 values were achieved by varying either the conductor thickness or transmitter frequency.

By keeping the scaling factor $\tau v/l$ constant in field and scale model measurements, it was possible to scale the effect of the time constant to meet true flight conditions. The depth to the upper surface of the half-plane was varied as $h/l = 1.0$, 1.5 and 2.0. Hence, in this respect, the measurements complement those undertaken by Ghosh and West (1971), in which the h/l ratio was ≥ 2.0. Experimental measurements on the thick half-plane were conducted with graphite conductor models, cf. Table 11. The properties of and responses to these models in the slingram coil configuration have been reported by Kurimo-Salminen (1979).

Table 12

Comparison of the scale and numerical modelling results for the vertical coaxial coil system as published by various investigators.

(a) Thin half-plane with dip angle $\alpha = 90°$, depth/coil separation $h/l = 2.0$ and time constant $\tau = 0$ s.

σdf/10³	Wieduwilt (1962)		Brant *et al.* (1966)		Ghosh (1972)		Ovaskainen & Peltoniemi (1979)	
(SHz)	Re (ppm)	Im (ppm)	Re (ppm)	Im (ppm)	Re (ppm)	Im (ppm)	Re (ppm)	Im (ppm)
3.6	−110	−250	−60	−200	−85	−230	−110	−240
12	−450	−510	−400	−400	−310	−410	−460	−390
36	−920	−500	−800	−280	−810	−480	−770	−290
120	−1220	−200	−950	−140	−1200	−320	−950	−150
360	−1260	−67	−1000	−35	−1300	−200	−1000	−50
∞ (calc.)	−1380	0			−1380	0		

(b) As in (a) but $h/l = 3.0$.

σdf/10³	Podolsky (1966)		Ghosh (1972)	
(SHz)	Re (ppm)	Im (ppm)	Re (ppm)	Im (ppm)
3.6	−60	−130	−40	−95
12	−230	−190	−125	−150
36	−390	−150	−280	−140
120	−500	−90	−370	−80
360	−560	−40	−410	−50
∞ (calc.)			−460	0

(c) As in (a) but $\alpha = 0°$.

σd	Ovaskainen & Peltoniemi (1979)		Peltoniemi (1980a)	
(S)	Re (ppm)	Im (ppm)	Re (ppm)	Im (ppm)
0.37	−80	−800	−400	−1150
0.74	−450	−1400	−1050	−1800
1.78	−1700	−2300	−2300	−2400
3.70	−3400	−2100	−3900	−2000
7.42	−4800	−1330	−5200	−1200
11.9	−5100	−980	−5600	−950
37	−5200	−370	−5700	−310
55	−5200	−180	−5700	−230

The accuracy of the measurements was studied by comparing the results of different measurements as given in Table 12. The results clearly show that the absolute accuracy of different measurements is poor, because each study has suffered from different systematic errors, and because the accuracy requirements are very high: maximum anomalies measure only 0.01–1 % of the primary field H_p. The results for the vertical half-plane show systematic differences of 100–400 ppm and for the horizontal conductive thin sheet 100–600 ppm. However, the relative precision of results within each study is acceptable, because the systematic errors are constant for the same modelling facility.

Results

Fig. 35a shows the characteristic diagram of the DC-3 AEM system for a vertical thin half-plane conductor in a resistive environment. The effect of the time constant has been omitted from the results. In contrast, the diagram in Fig. 35b refers to results with $v = 58$ m/s, $\tau = 0.3$ s. Figs. 36a and 36b illustrate the corresponding results of the model measurements when the dip angle of the half-plane is $\alpha = 30°$. In the results of Fig. 37 the model includes a vertical thin half-plane and a horizontal conductor. The vertical and the horizontal models were not in galvanic contact in the measurements. The effect of the

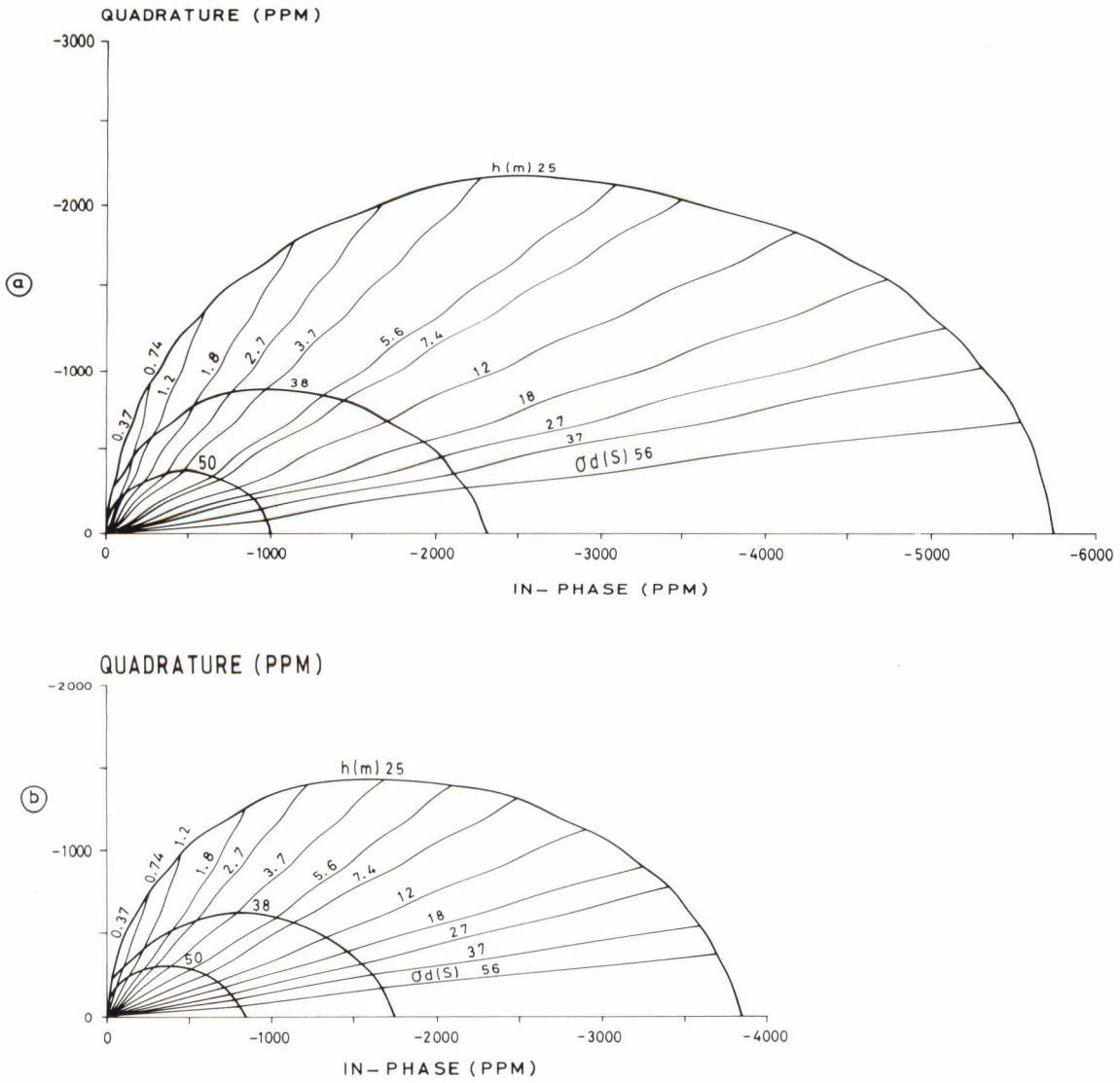

Fig. 35. In-phase and quadrature anomalies produced by a thin conductive half-plane in the DC-3 AEM system as a function of the depth to the upper surface h and the conductivity-thickness product σd of the half-plane. The dip angle $\alpha = 90°$ of the half-plane is constant. (a) The time constant of the detector $\tau = 0$ s. (b) The time constant of the detector $\tau = 0.3$ s.

dip angle and the detector time constant on the thin half-plane model curves are studied in Fig. 38. Finally, model curves of a thick conductive half-plane are shown in Fig. 39.

In all the diagrams in Figs. 35–37 the characteristic values are the peak values of the in-phase and quadrature anomalies digitised from analog curves. In the results including an overburden model the peak anomalies are defined in relation to the local zero level produced by the conductive overburden. On account of the difficulties encountered in modelling, measurements on the thick half-plane are still too limited to warrant the compiling of characteristic diagrams.

Comparison of Figs. 35a and 35b demon-

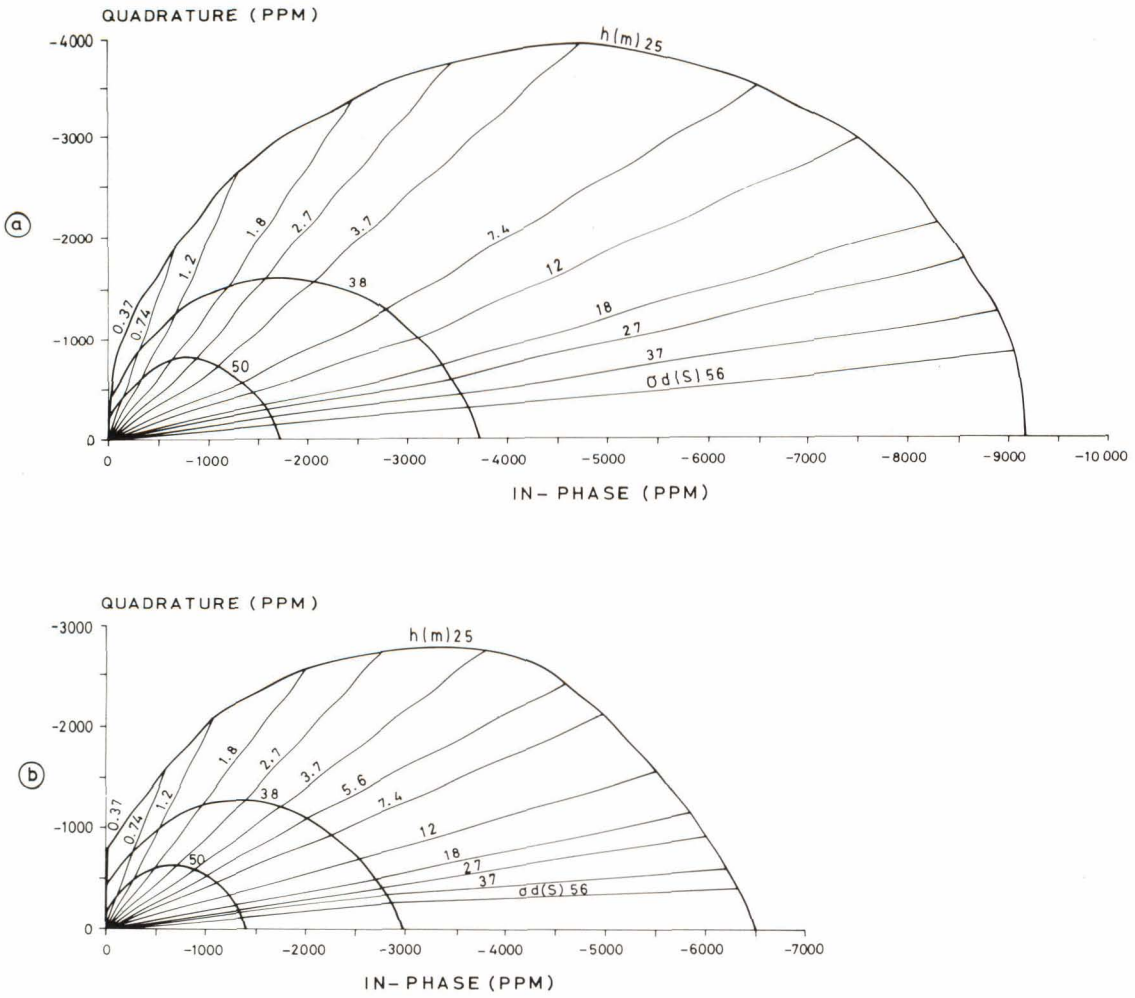

Fig. 36. In-phase and quadrature anomalies produced by a thin conductive half-plane in the DC-3 AEM system as a function of the depth to the upper surface h and the conductivity-thickness product σd of the half-plane. The dip angle $\alpha = 30°$ of the half-plane is constant. (a) The time constant of the detector $\tau = 0$ s. (b) The time constant of the detector $\tau = 0.3$ s.

strates that the influence of the time constant on the anomaly values is not negligible at small survey elevations ($h/l \leq 1.5$) even if the condition (21) given on page 41 holds.

The effect of the dip angle on the anomaly amplitude is very clear as a comparison of Figs. 35 and 36 shows. In practice, however, the interpretation of the dip angle is hindered by the fact that the effect of the dip angle on the anomaly shape may be difficult to recognise from the field data.

Fig. 37 demonstrates that the influence of the conductive overburden is stronger on the quadrature component. At high $\sigma_1 d_1$ values of the horizontal conductor, the phase angle changes so that the sign of the quadrature component turns positive in relation to the local zero level. Use could be made of the phenomenon even in visual interpretation, because positive quadrature anomalies like these do not normally occur in survey data.

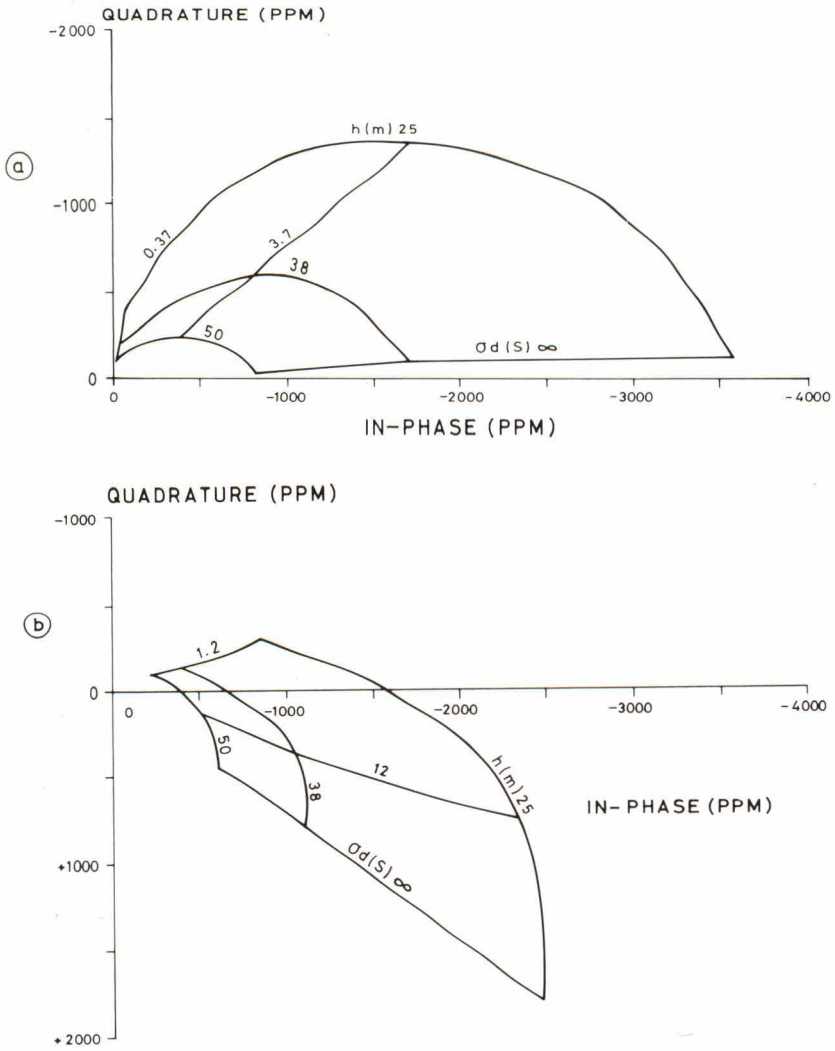

Fig. 37. In-phase and quadrature anomalies produced by a thin conductive half-plane in the DC-3 AEM system when the half-plane is covered by a thin horizontal conductor. The dip angle of the half-plane $\alpha = 90°$ and the time constant of the detector $\tau = 0.3$ s are constants, whereas the depth to the upper surface of the horizontal conductor h and the σd product of the half-plane vary. (a) The conductance of the horizontal conductor s = 0.19 S. (b) The conductance of the horizontal conductor s = 1.2 S.

Comparison of the thin and thick half-plane model curves in Figs. 38 and 39 clearly shows that the increase in half-plane thickness leads to very complicated forms in the anomaly profiles. This fact gives support to the further modelling needs of the thick half-plane conductors.

Preliminary data on the dependence of the anomaly half-width values on the thickness, conductivity and depth of the half-plane are given in Fig. 40. The data qualitatively outline the behaviour of anomalies for the thick half-plane model. The point is of practical importance, because fixed-coil AEM systems easily reach values of $d/l > 1$ even for sheet-like bedrock conductors. In such cases, the thin half-plane model is a poor approximation. On the other hand, the importance of the time constant decreases with increasing values of half-plane thickness. The data in Fig. 40 indicate that for a thin half-plane the anomaly half-width values of $w_{1/2}$ increase with decreasing σd value or increasing depth to outcrop. In both cases, however, the change in $w_{1/2}$ value is very small. For a thick half-plane the $w_{1/2}$ values increase with increasing σd value and depth, and the change is significant.

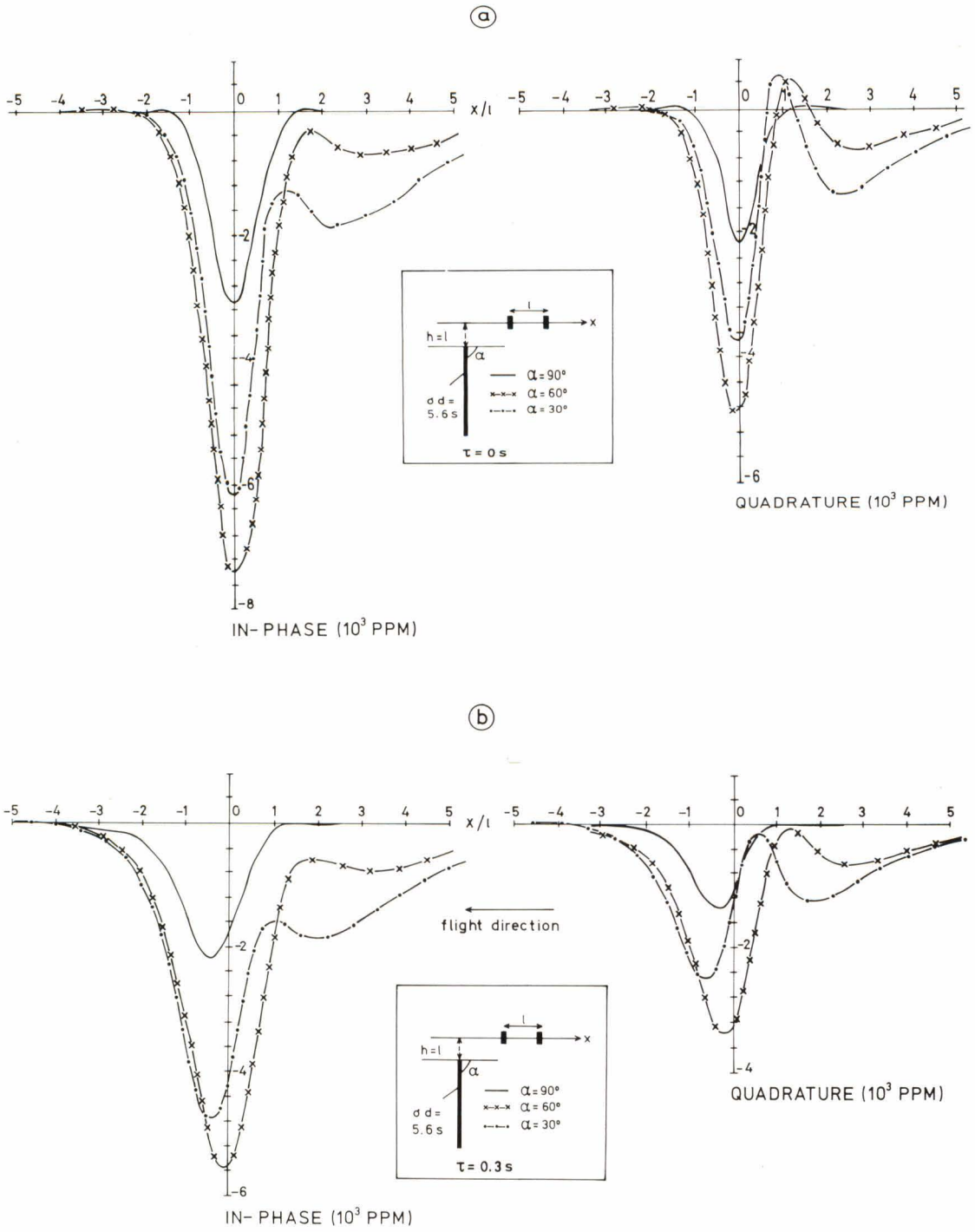

Fig. 38. In-phase and quadrature anomaly curves produced by a thin conductive half-plane in the DC-3 AEM system when the dip angle α varies. The depth to the upper surface h = 25 m and the σd product of the half-plane = 5.6 S are constants. (a) The time constant of the detector τ = 0 s. (b) The time constant of the detector τ = 0.3 s.

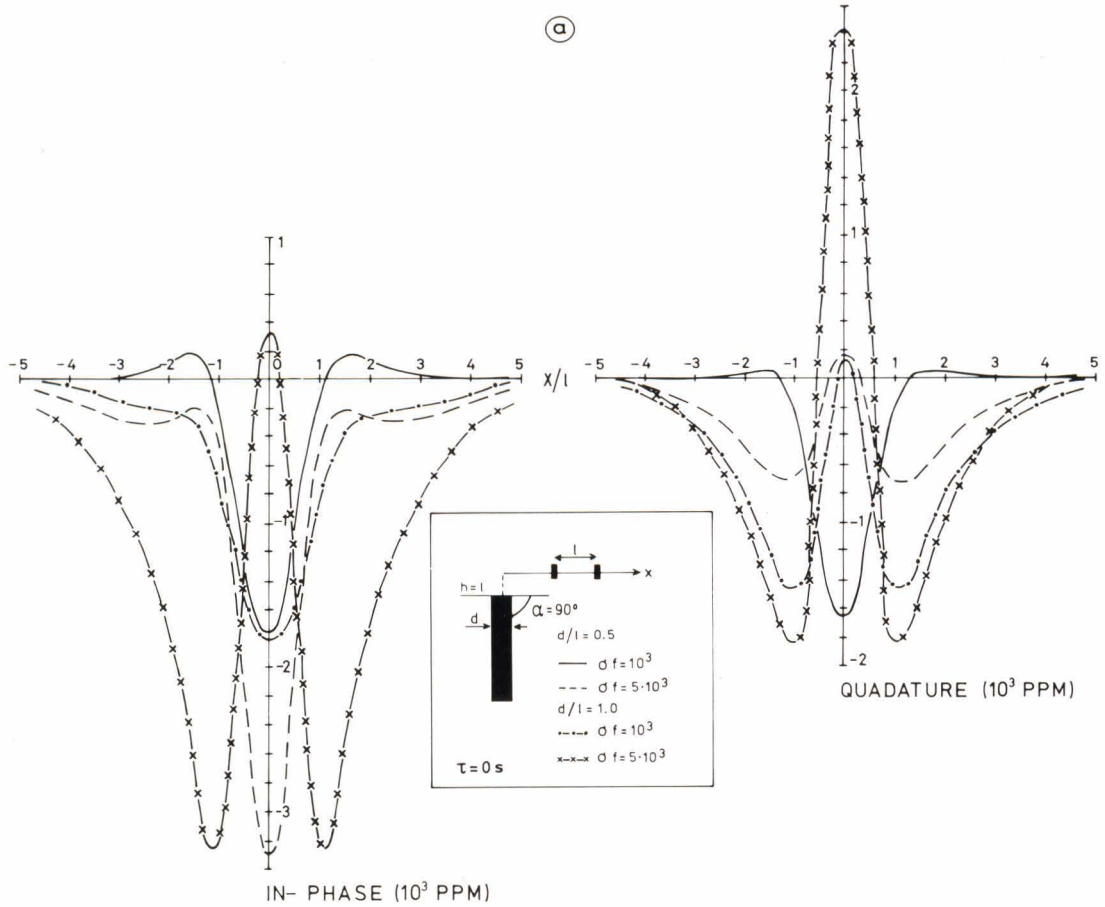
a
X/l
h=l
d
α=90°
d/l = 0.5
σ f=10³
σ f=5·10³
d/l = 1.0
σ f=10³
σ f=5·10³
τ=0 s
IN- PHASE (10³ PPM)
QUADATURE (10³ PPM)

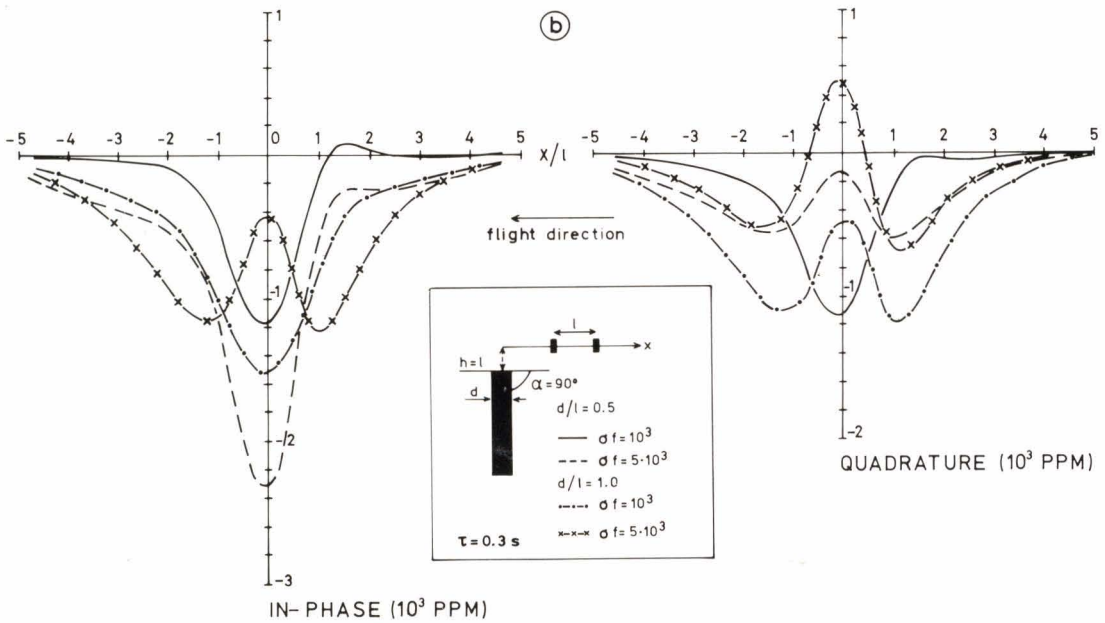
b
X/l
flight direction
h=l
d
α=90°
d/l = 0.5
σ f=10³
σ f=5·10³
d/l = 1.0
σ f=10³
σ f=5·10³
τ=0.3 s
IN- PHASE (10³ PPM)
QUADRATURE (10³ PPM)

Fig. 39. Scale model results of a thick conductive half-plane in the DC-3 system as in-phase and quadrature anomaly curves. The depth to the upper surface h = 25 m is constant, whereas the thickness d and the conductivity σ of the half-plane vary. (a) The time constant of the detector τ = 0 s. (b) The time constant of the detector τ = 0.3 s.

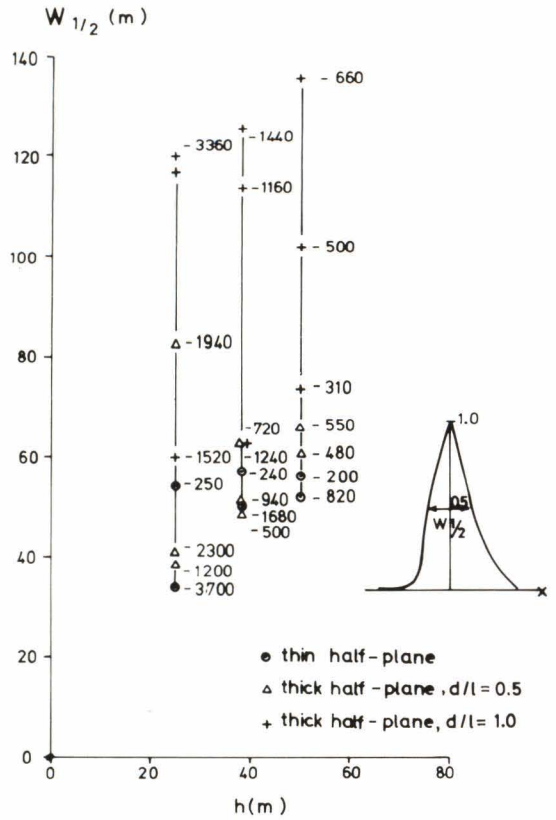

Fig. 40. Half-width $w_{1/2}$ of the in-phase component anomaly curve produced by a conductive half-plane as a function of the half-plane thickness d and the outcrop depth h in the DC-3 AEM system. The columns at h = constant show the effect of the half-plane thickness on the half-width. The data adjacent to the columns refer to the in-phase anomaly peak values with the corresponding h, d and $w_{1/2}$ combinations. The dip angle of the half-plane α = 90° and the time constant of the detector τ = 0.3 s are constants.

Sphere model

In the interpretation of the AEM anomalies produced by locally restricted conductors, theoretical model results are also needed for the responses to the 3-dimensional conductors. The model that is most studied by numerical methods is the conductive sphere, and even that is troublesome to solve up to a numerical outcome. Although geologically strongly idealised, the model still gives useful interpretational information on local conductors.

Previous studies

A theoretical solution for the EM response to the conductive sphere in a dipole field was given by March (1953). Approximative numerical results have been reported by Wait

(1953). Lodha (1974) presented the first accurate results applicable to the interpretation of AEM survey data in the form of characteristic diagrams. The general solution, which also allows for transversal dipole sources, was published by Best and Shammas (1979).

Solution method and its accuracy

The theory of the solution has been given in detail by Best and Shammas (1979) and it is referred to in this context only in so far as is needed for the discussion on accuracy. The secondary field generated by the transmitter dipole source is solved by differentiating the secondary field caused by the magnetic pole at the transmitter source point. The solution is achieved by the equations of the secondary field inside and outside the sphere, which are fitted, with the aid of the boundary conditions, to be continuous on the surface of the sphere. The solution consists of an infinite series of multipoles in the centre of the sphere. Each multipole produces a sum term in the response function, whose amplitude and phase depend on the ratio of the radius of the sphere to the distance to the transmitter dipole, and on the value of the response parameter of the sphere. In his calculations, Lodha used $p_i = 15$ as the number of multipole terms; the corresponding figure for Best and Shammas was $p_i = 20$.

The numerical results in this study were calculated with the computer program developed by Best and Shammas (1979), which Shell Canada Resources Ltd. kindly put at the disposal of the Geological Survey of Finland. The program is run on a U1108 computer and is very fast in execution: the computing time for all the results given in this study totals 400 CPU seconds.

The accuracy of the computing method and the program was studied as follows. The formal operation of the program was checked with the aid of the test data and by comparing the results with those published by Lodha, and by Best and Shammas. The results were identical.

The accuracy of the numerical solutions depends also on the computational accuracy of the modified Bessel function $I(\lambda)_{i+1/2}$ and its derivative $I'(\lambda)_{i+1/2}$ incorporated in the solution. The values of the functions were calculated from series expansions or recursion relations that vary depending on the value of the formal parameter λ. The program operates correctly with the values of the response parameter of the sphere $\bar{\theta}_4 > 1.0$, where

$$\bar{\theta}_4 = \sigma\mu\omega a^2, \quad (29)$$

and a = the radius of the sphere (m). This has somewhat restricted the coverage of the calculated characteristic curves.

The accuracy of the program was also examined by comparing the results with the anomaly values calculated by the method of images: when the conductivity of the sphere tends to infinity, the first multipole term in the series expansion can be solved by placing an image dipole in the centre of the sphere. The anomaly values calculated with this method, described in detail by Lodha (1974, Appendix I), were compared with those calculated with the computer program in Table 13, part a. The compatibility of the results is excellent.

As another method of comparison, the anomaly produced by the sphere can be studied by increasing the radius of the sphere so that it is very large in relation to the coil separation and flight elevation. The anomaly should then approach the anomaly caused by a conductive half-space. Results of such an approach are shown in Table 13, part b,

Table 13

Comparison of responses to a conductive sphere in the DC-3 AEM system at a flight elevation of h = 30 m. (a) Values of the first multipole term of the AEM in-phase and quadrature anomalies, calculated by means of the computer program and the method of images. The data refer to the observation point x = 12.5 m, y = 0. The conductivity of the sphere is constant, $\sigma = 5000$ Sm^{-1}, and the detector time constant $\tau = 0$ s. The radius a and the depth to the centre z of the sphere vary.

a (m)	z (m)	Computer program		Method of images	
		Re (ppm)	Im (ppm)	Re (ppm)	Im (ppm)
50	80	−1183	−4.5	−1187	0
100	130	−683	−1.3	−684	0
150	180	−355	−0.4	−355	0
200	230	−200	−0.2	−200	0
250	280	−122	−0.1	−122	0
300	330	−79.5	−0.0	−79.6	0

when the numbers of the multipole terms are $p_i = 20$ and $p_i = 27$. The comparison demonstrates that, with short radius values, the convergence with different p_i-values is good up to radius a = 150 m. The radius of the sphere is, however, still too short to approximate the half-space. When the length of the radius is increased, the anomalies increase up to a = 350 m, but thereafter begin to decrease. The reduction is caused by the fact that the number of the multipole terms $p_i = 27$ is still not large enough. On account of this limitation, the results of the program with $a \geq 200$ m would be inaccurate and the relative error increases with the increase in radius and in conductivity. The relative error

(b) Comparison between the AEM in-phase and quadrature anomalies of the sphere and half-space. The number of multipoles p_i and the conductivity σ and radius a of the sphere vary. For the sphere, the values are maximum anomalies along profile y = 0. The detector time constant equals $\tau = 0.3$ s.

a (m)	z (m)	Computer program $p_i = 20$						Computer program $p_i = 27$					
		$\sigma = 10$ Sm^{-1}		$\sigma = 100$ Sm^{-1}		$\sigma = 1000$ Sm^{-1}		$\sigma = 10$ Sm^{-1}		$\sigma = 100$ Sm^{-1}		$\sigma = 1000$ Sm^{-1}	
		Re (ppm)	Im (ppm)	Re (ppm)	Im (ppm)	Re (ppm)	Im (ppm)	Re (ppm)	Im (ppm)	Re (ppm)	Im (ppm)	Re (ppm)	Im (ppm)
100	130	−5240	−420	−5550	−152	−5660	−48	−5240	−418	−5550	−152	−5650	−48
150	180	−7300	−575	−7700	−183	−7830	−58	−7160	−507	−7480	−152	−7580	−47
200	230	−9120	−824	−9740	−277	−9930	−89	−8620	−649	−9070	−205	−9190	−63
300	330	−11310	−1065	−12120	−363	−12370	−118	−11120	−1015	−11890	−344	−12130	−111
700	730	−6680	−375	−6950	−124	−7040	−40	−9960	−697	−10470	−233	−10630	−75
∞	(1-layer model)							−14920	−935	−15540	−286	−15730	−89

in the data given in the present paper ($a \leq 170$ m) is 0.01 ··· 1.0 % at the most, depending on the length of the radius and the conductivity. The accuracy is satisfactory and the usefulness of the results depends on how well the sphere model corresponds to true geological formations.

Results

The present study supplements the results reported by Lodha (1974) and later by Lodha and West (1976) for a conductive sphere in the vertical coaxial coil system. The results published by the above investigators cover the flight elevation/coil separation range of $5 \leq h/l \leq 14$. For the DC-3 AEM system, data are needed for lower h/l values; in the present study they were therefore calculated for $h/l \geq 0.8$. The effect of the time constant on the anomaly values has also been taken into account for the same reasons as in the half-plane model.

The peak values of the in-phase and quadrature anomalies were collected from the computed sets of anomaly profiles and compiled into characteristic diagrams. All the data refer to the profile y = 0, (cf. Fig. 26d). The

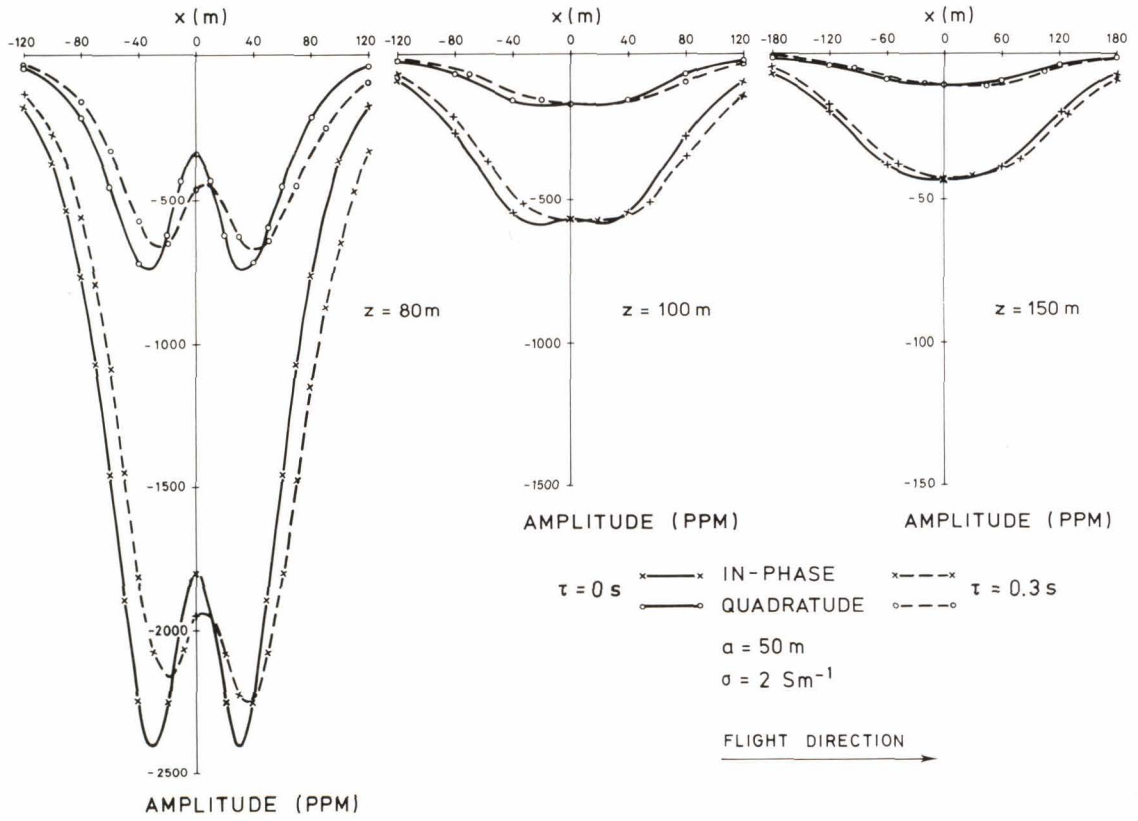

Fig. 41. Examples of AEM modelling results on a conductive sphere in the DC-3 AEM system as in-phase and quadrature anomaly curves. The radius of the sphere a = 50 m, its conductivity $\sigma = 2$ Sm^{-1} and the across-track coordinate of the flight line y = 0 are constants, whereas the depth to the centre of the sphere z varies.

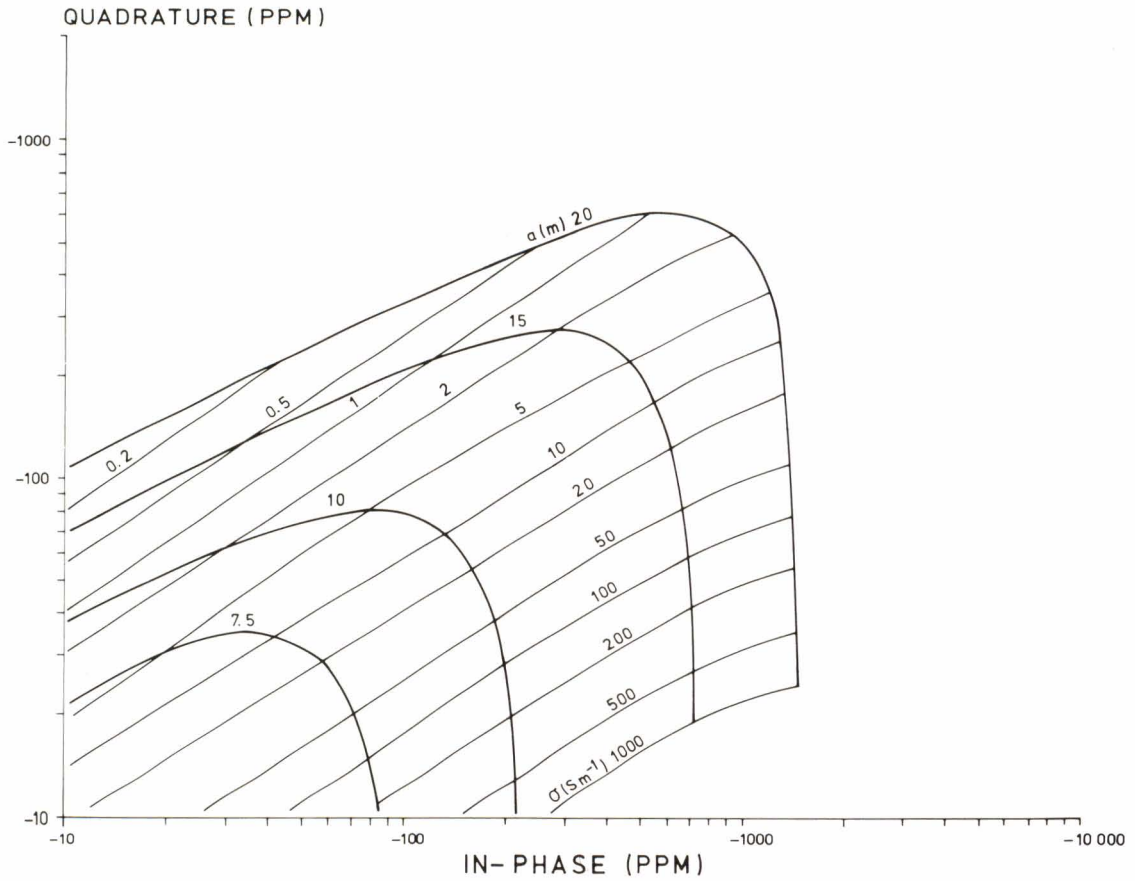

Fig. 42. In-phase and quadrature anomalies produced by a conductive sphere in the DC-3 AEM system as a function of the radius a and the conductivity σ. The depth to the centre of the sphere z = 40 m is constant.

point separation Δx was either 10 m or 20 m. The effect due to the time constant of the low-pass filter in the amplifier was taken into consideration by convolving the original anomaly profiles with the impulse response of the low-pass filter. An example of the original and the convolved profiles are given in Fig. 41.

For each characteristic diagram, the depth of the centre of the sphere z is constant, whereas the conductivity of the sphere and the radius vary. The diagrams were compiled for five values of z, and the graphs are shown in Figs. 42–46. The results are given directly in accordance with the DC-3 AEM system. Corresponding diagrams with $\tau = 0$ s for the vertical coaxial and coplanar coil configurations have been reported elsewhere (Peltoniemi 1980b).

In a vertical coplanar AEM system the anomaly amplitude attains a single maximum above the sphere. Apart from the maximum amplitude the single anomaly profile does not contain any other information except the anomaly half-width (or corresponding parameter), which indicates primarily the depth of the sphere. In the vertical coaxial coil system the situation is made more difficult by

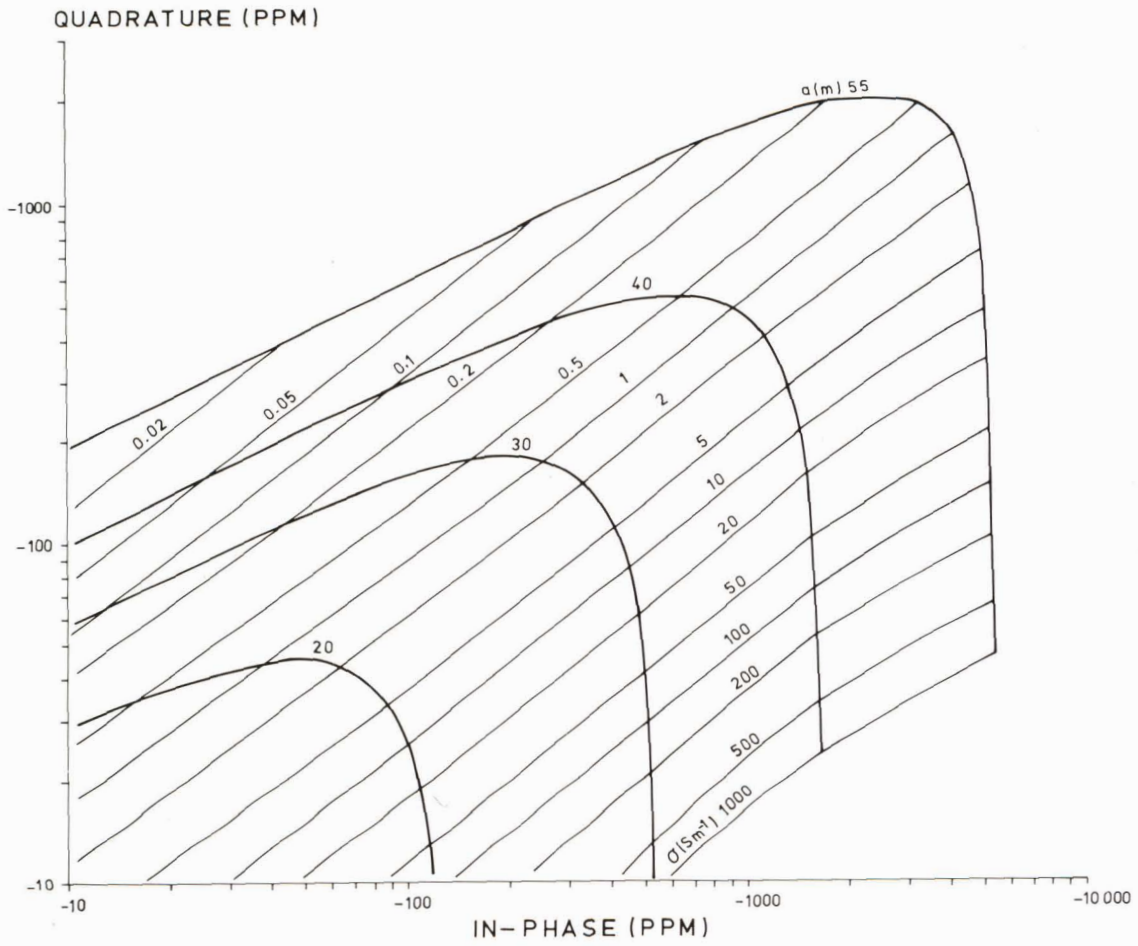

Fig. 43. In-phase and quadrature anomalies produced by a conductive sphere in the DC-3 AEM system as a function of the radius a and the conductivity σ. The depth to the centre of the sphere z = 75 m is constant.

the fact that the anomaly shape becomes more complicated when the depth to coil separation ratio, z/l, is small. In these cases, the anomaly curves exhibit an intervening maximum whose magnitude depends on the z/l ratio, the radius of the sphere and conductivity, as exemplified by Fig. 41. For this reason and because of the effect of the time constant, the characteristic diagrams no longer show the beautiful analogy reported by Lodha and West (1976, Fig. 7).

The application of the modelling results to the interpretation of survey data requires, in addition to the model curves depicted in Figs. 42–46, a selection criterion to find the correct graph. The selection is best made with the aid of the half-width value of the anomaly. The half-width values were calculated for all the anomaly profiles, and the half-width values of the in-phase components are compiled in Fig. 47. In practice, the AEM field survey results can be interpreted in the following steps:

- The possible z values are found in Fig. 47 by means of the half-width value $w_{1/2}$ of the measured in-phase anomaly.
- If several depths correspond to the measured $w_{1/2}$ value, as they often do,

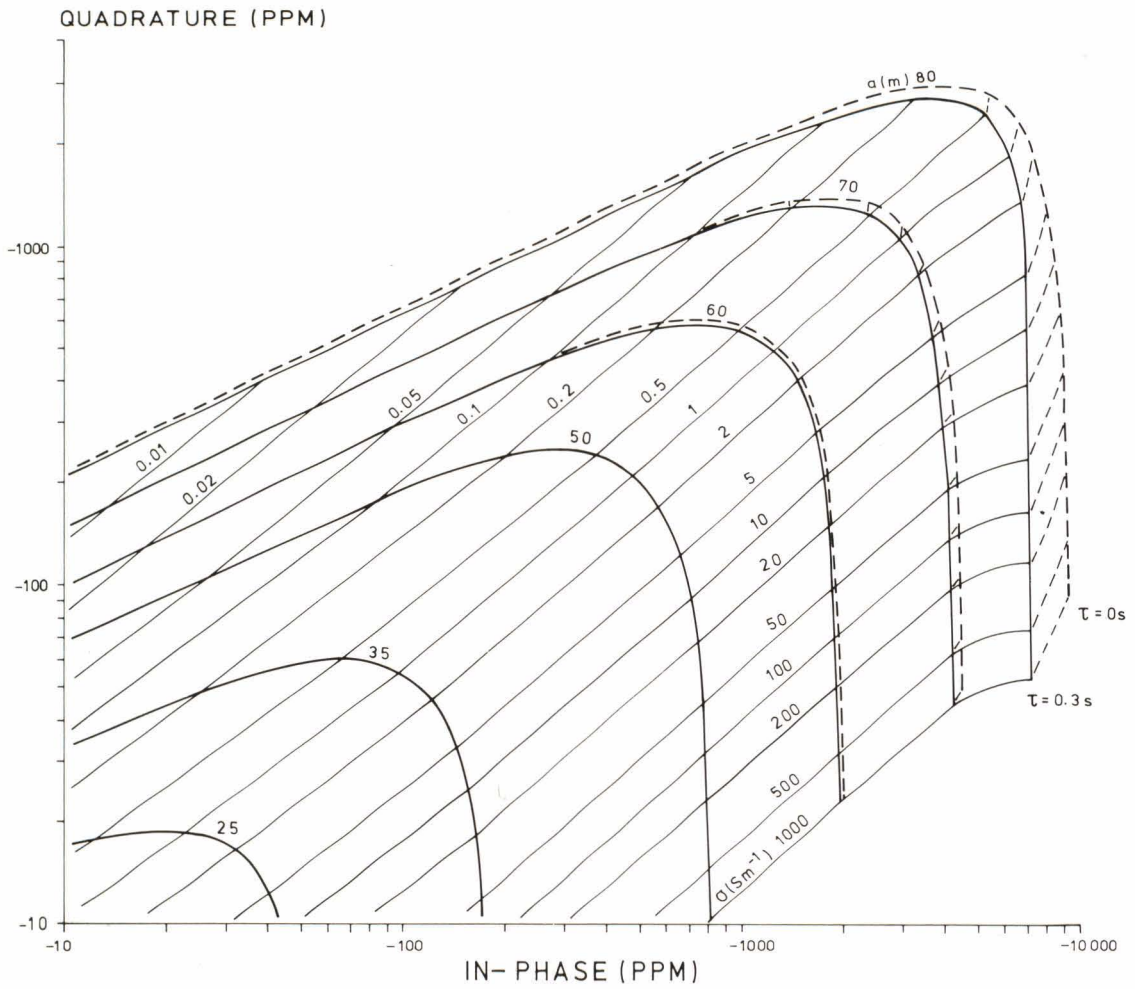

Fig. 44. In-phase and quadrature anomalies produced by a conductive sphere in the DC-3 AEM system as a function of the radius a and the conductivity σ. The depth to the centre of the sphere z = 100 m is constant.

the right one can be selected by using as an additional criterion the amplitude of the in-phase anomaly, whose values for the z and $w_{1/2}$ combinations in question are also marked in Fig. 47.

- The radius and conductivity of the sphere corresponding to the amplitudes of the in-phase and quadrature anomalies can now be read from the characteristic diagram selected.

Hence, with the aid of the three parameters – the in-phase and quadrature anomalies and the half-width of the in-phase anomaly – it is possible to interpret the depth, radius and conductivity of the sphere. With regard to the accuracy in field survey results, however, the outcome of the interpretation is ambiguous.

The results in Fig. 47 indicate that the wavelength of the anomalies of the sphere decreases when the conductivity of the sphere increases and the other variables re-

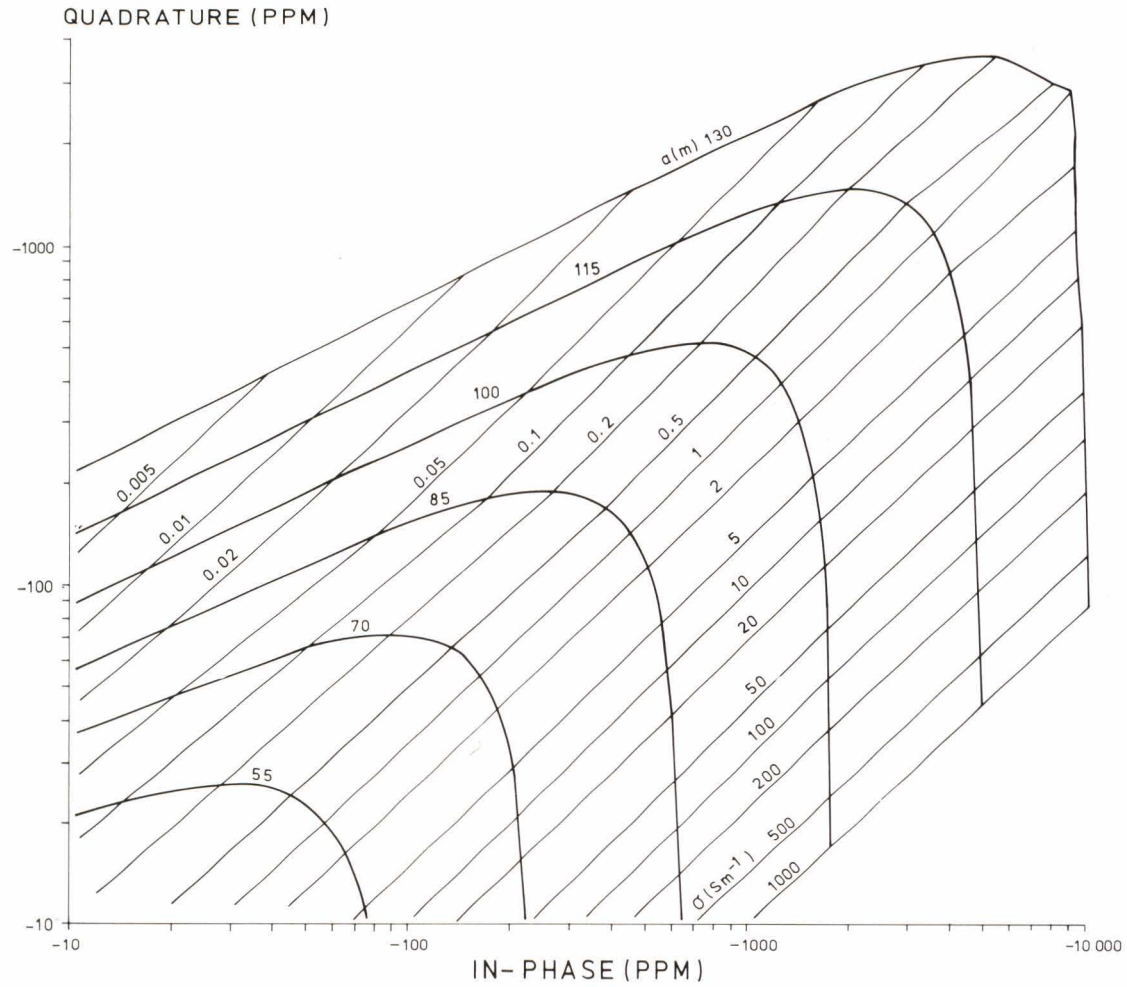

Fig. 45. In-phase and quadrature anomalies produced by a conductive sphere in the DC-3 AEM system as a function of the radius a and the conductivity σ. The depth to the centre of the sphere z = 150 m is constant.

main constant. Exceptions are the responses when $h < 30$ m, in which case the wavelengths start to increase again with increasing conductivity values. Modelling results of the vertical coplanar coil system (Peltoniemi 1980b) demonstrate that, particularly at low z values, the wavelength of the anomalies is shorter than in the vertical coaxial coil system when the model is the same. Moreover, with z as constant, the change of the wavelength as a function of the sphere radius is much larger in the vertical coplanar coil system. Hence, the resolution of adjacent conductors in this system is better but the discrimination ability in terms of z poorer than in the vertical coaxial coil system. As a consequence, in the vertical coplanar coil system, either the flight speed or the interval of the digital sampling must be reduced to keep the sampling frequency in relation to the anomaly wavelength comparable with that in the vertical coaxial coil system.

The graph in Fig. 42 is important from a practical point of view. It allows the estima-

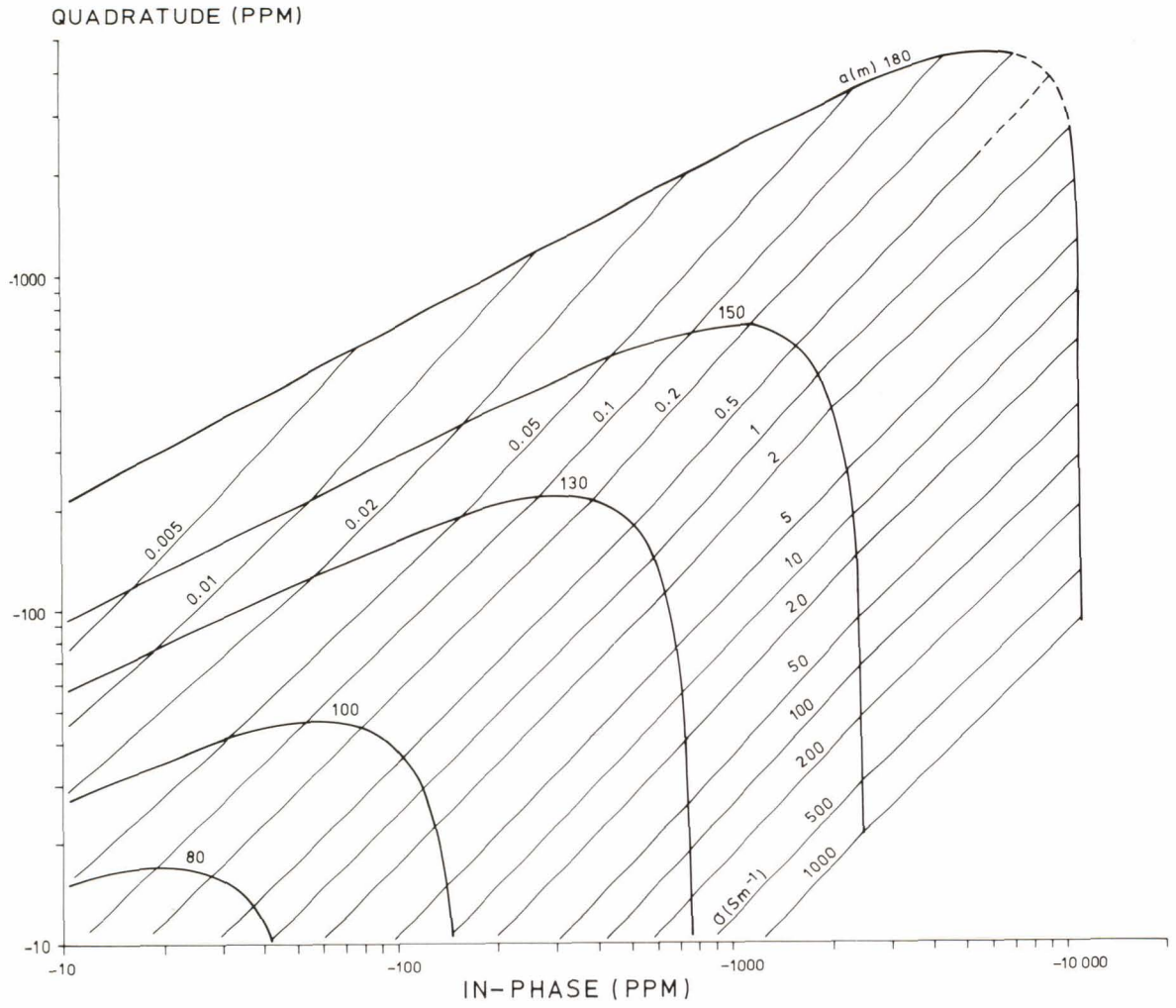

Fig. 46. In-phase and quadrature anomalies produced by a conductive sphere in the DC-3 AEM system as a function of the radius a and the conductivity σ. The depth to the centre of the sphere z = 200 m is constant.

tion of the minimum dimensions that a small conductor located right on the flight line must have in order to produce an anomaly detectable from the noise. It is seen that the minimum radius required in the DC-3 AEM system is a = 8 m for the highly conductive sphere. Similarly, Fig. 44 demonstrates that the radius of the highly conductive sphere located between the flight lines (separation 200 m) must be a $\geq$ 35 m to make the anomaly detectable from the noise. At the other limit of size discrimination, even a sphere with radius a = 150 m gives only half of the anomaly (cf. Table 13) measured over a half-space of the same conductivity.

For the sake of comparison, characteristic response values with $\tau = 0$ s have also been marked in Fig. 44. It is seen that with a low depth to outcrop, the differences in results between $\tau = 0.3$ s and $\tau = 0$ s are significant.

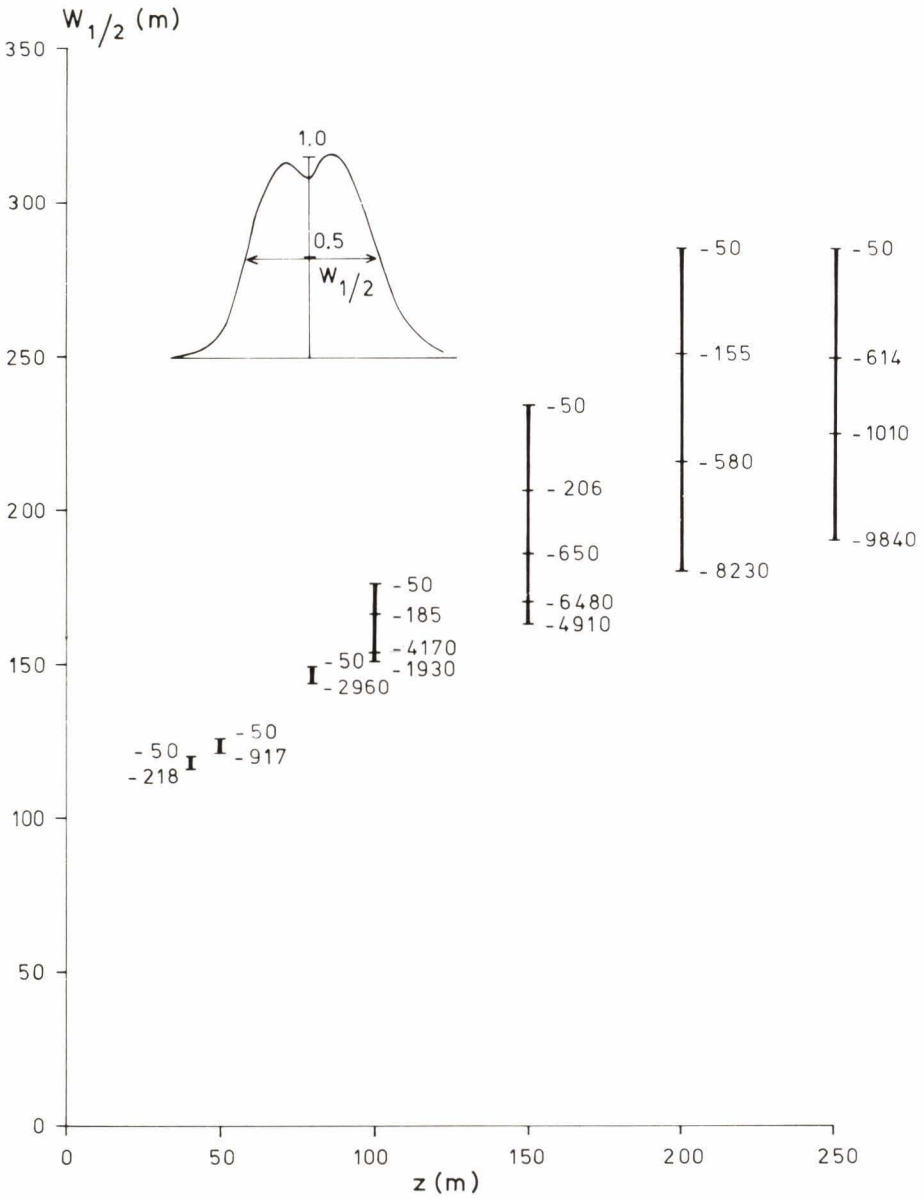

Fig. 47. Half-width $w_{1/2}$ of the in-phase component anomaly curve produced by a conductive sphere as a function of the depth to the centre of the sphere z in the DC-3 AEM system. The columns at z = constant show the effect of the sphere radius on the half-width. The data adjacent to the columns refer to the in-phase anomaly values with the corresponding z and $w_{1/2}$ combinations.

ANALYSIS OF MODELLING RESULTS

Electrical thickness of the conductor

By definition (cf. p. 15), an electrically thin conductor is one whose conductivity σ and thickness d cannot be determined separately from the electromagnetic survey data owing to the finite accuracy in field measurements; only the value of product σd (conductance) is obtainable. Hence, measurements undertaken at two different frequencies and resulting in different in-phase and quadrature anomalies lead to the same σd value in the characteristic diagram. In contrast, conductivity and thickness can be separately determined for an electrically thick conductor provided that two components, e.g. in-phase and quadrature anomaly values, are available. In AEM surveys, use must also be made of the elevation data or the nominal flight elevation must be assumed.

The limit value of the layer thickness d_{lim} at which the conductive layer passes from thin to thick in terms of the EM method depends on the true thickness of the conductive layer d, its electrical thickness in δ units and the properties of the survey system. The problem has not been treated very rigorously in the literature. Parasnis (1971, p. 167) defines the limit for the vertical half-plane in slingram surveys

(30) $d_{lim} = 1\delta$ (m).

Seigel and Pitcher (1978, p. 567) have suggested limit values $d_{lim} = 50-10$ m for a horizontal conductor in a vertical coplanar, three-frequency AEM system when the conductivity varies $\sigma = 0.01-1$ Sm^{-1} and the layer thickness in relation to flight elevation d = (0.1−1)h. Peltoniemi (1978b) has proposed an interpretation range for a thick horizontal conductor in the DC-3 AEM system to be approximately between the limit

(31) $d_{lim} = 0.25\delta$ (m)

and the inductive saturation limit. The lower limit given by equation (31) is marked as a dashed line in the characteristic diagram for the thick horizontal conductor in Fig. 34.

When the theoretical interpretability of a thick layer is considered in terms of the conductivity and thickness of the overburden in Finland, only the thickest saline clay deposits can be interpreted as thick horizontal conductors. With the conductivity $\sigma = 0.2$ Sm^{-1} (the maximum conductivity of the saline clays) the required thickness of the layer would be $d_{lim} \geq 5$ m. Hence, the theoretical results of the electrically thick horizontal layer have not been further discussed in the present study, and only one practical example (Fig. 61) is given.

Conductivity and conductivity-thickness apertures

On the basis of the definition of the anomaly detection limit S_d, equation (11), and the theoretical model results, the σ and σd apertures of the DC-3 AEM system can be determined for different conductor models. Figs. 42–46 demonstrate that the electrical equivalence does not hold for a conductive sphere: when the conductivity σ and radius a change in such a way that the product σa^2 remains constant, the anomalies change. For the detection limit to be unambiguously applicable on the conductive sphere as well, the constant radius of the sphere that is used in the consideration must be defined. Since the mass of a sphere with radius a = 50 m and density $3.5 \cdot 10^3$ kg/m³ is 2 million tons, an

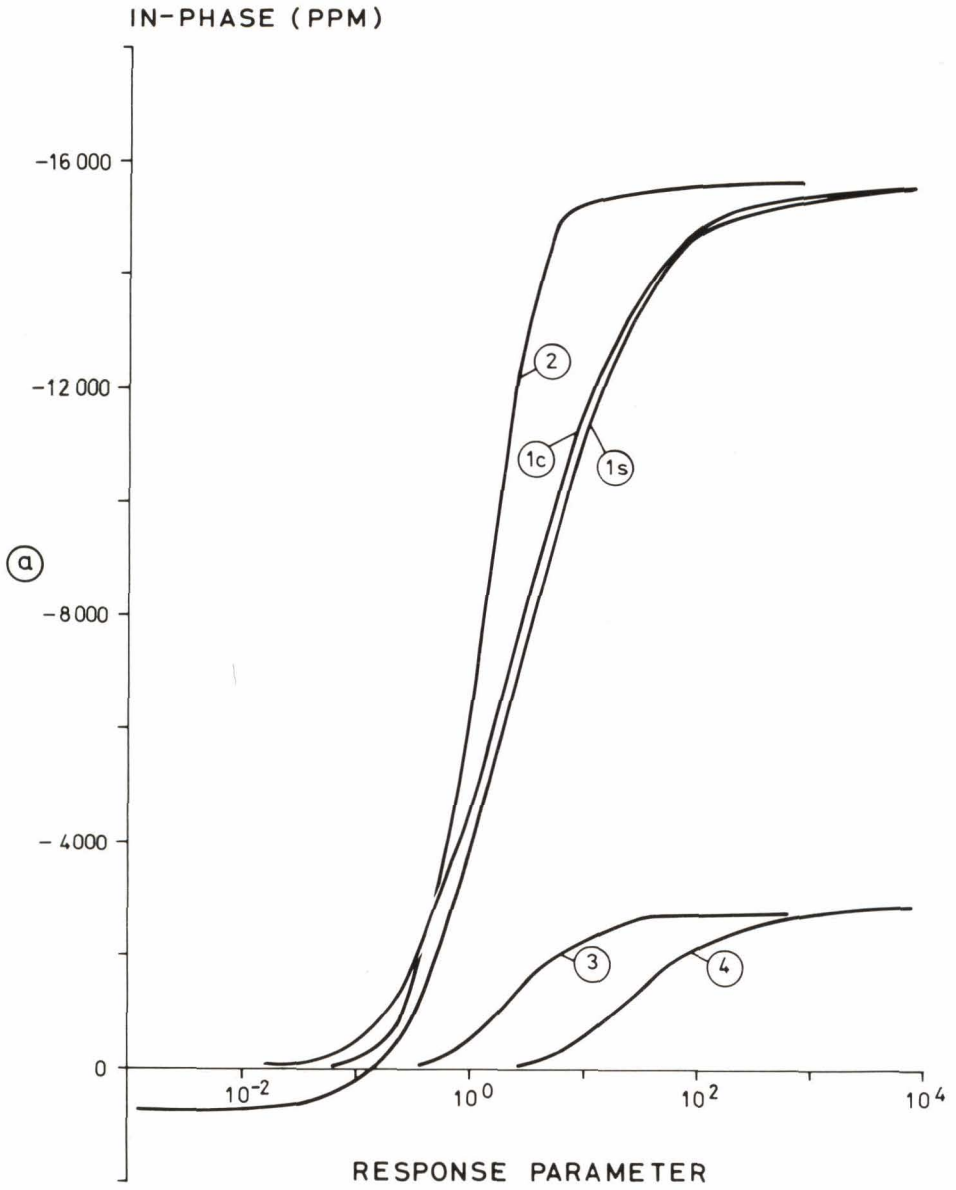

Fig. 48. Response functions of various conductor models in the DC-3 AEM system for a constant survey elevation of h = 30 m. Symbol lc stands for the response function of a conductive half-space and ls for a susceptive half-space ($\mu_{1r} = 1.10$), 2 refers to the response function of a thin horizontal conductor and 3 to that of a vertical thin half-plane ($\tau = 0.3$ s). Symbol 4 stands for the response function of a sphere (a = 50 m, $\tau = 0.3$ s). The response parameters $\theta_1 - \theta_4$ of different conductors have been defined by equations (26)–(29). (a) The in-phase parts of the response functions. (b) The quadrature parts of the response functions (see page 99).

appropriate choice for the constant radius would be a = 50 m. The response functions of the different conductor models under consideration can now be displayed and compared as in Figs. 48a and 48b. The figures illustrate the difference in range within which

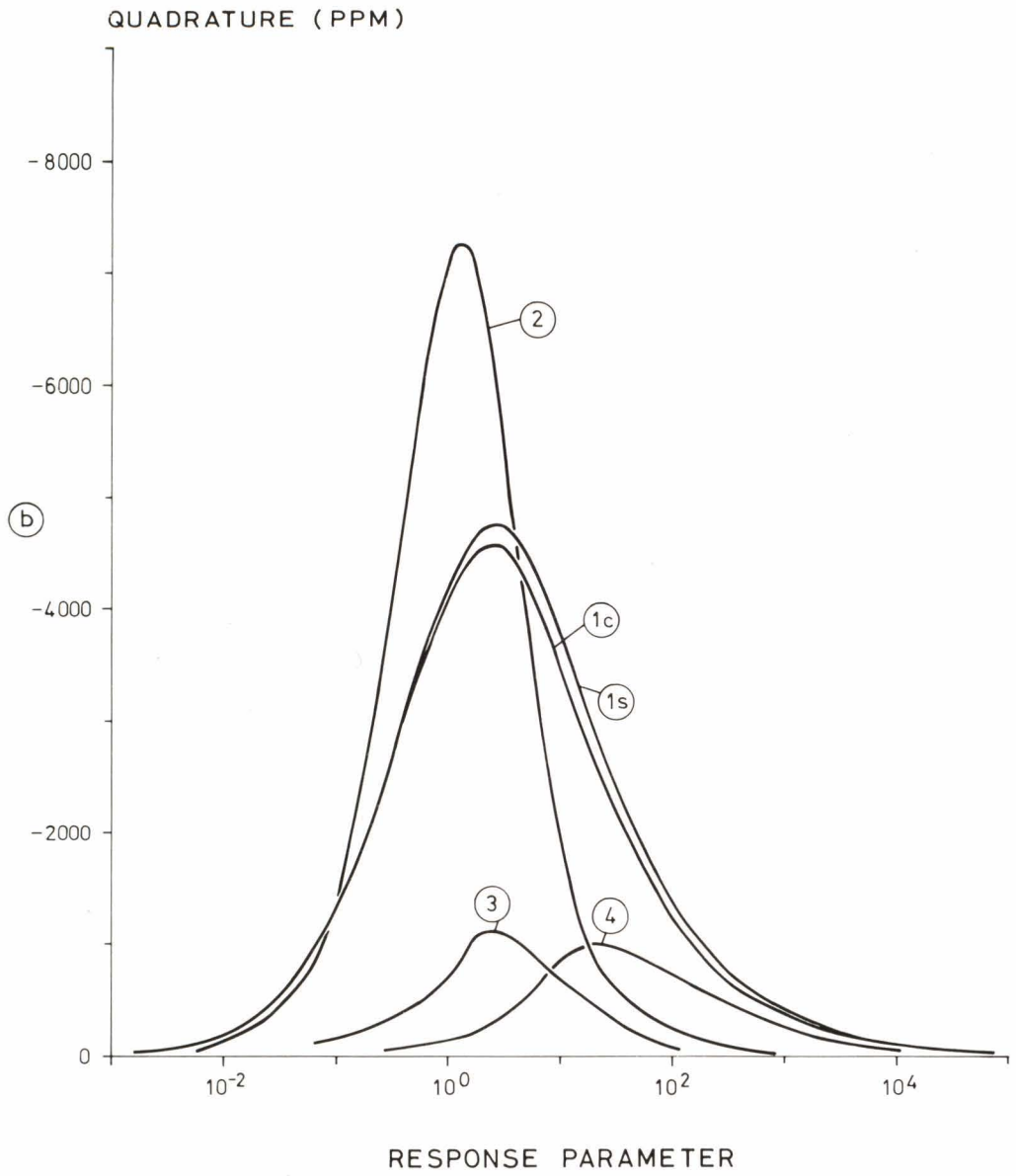

the response function varies depending on the conductor geometry, although in principle it retains its behaviour as already shown in Fig. 2.

When the detection limit $S_d = 4N$ is applied to the data in Figs. 48a and 48b the limit values listed in Table 14 are obtained for the σ and σd apertures of the DC-3 AEM system. Note that because the upper limits are not detection limits but discrimination limits, the maximum in-phase anomaly Re_{max} is still obtained on the inductive limit. The anomaly,

however, remains constant irrespective of the increase in the response parameter. Furthermore, with the specifications of the system used, a large range of conductivity or conductance is covered. This allows the anomaly data to be transformed into values of apparent conductivity and conductivity-thickness product as is shown in the following chapter. On the other hand, a large aperture means that change into a multifrequency AEM system would not have any significant advantages, at least not under the geological conditions prevailing in Finland. The search for new interpretational possibilities, if needed, should rather be directed towards multicomponent systems (Fraser 1979) or plane wave VLF methods (Arcone 1979).

Table 14

Conductivity and conductance apertures of the DC-3 AEM system for various conductors when the survey flight elevation h = 30 m and the anomaly detection limit $S_d^- = 4N$, i.e. 100 ppm, are constants. Note: if the elevation h is increased, the apertures are shifted towards higher σ and σd values.

Formation	Aperture
Conductors (k < 0.01)	
Half-space	$3 \cdot 10^{-4} - 3 \cdot 10^{2}$ Sm^{-1}
Thin horizontal sheet	$10^{-2} - 4 \cdot 10^{2}$ S
Thin vertical half-plane ($\tau = 0.3$ s)	$0.2 - 10^{2}$ S
Sphere with a radius of 50 m ($\tau = 0.3$ s)	$10^{-2} - 10^{2}$ Sm^{-1}
Susceptive formations (σ low)	
Half-space	0.01 – 1 SI-units

Penetration

A criterion of the usability of the AEM system is its penetration. Before an objective comparison can be drawn between the penetration values of different systems, the concept must be defined exactly. The definition is derived from the detection limit in accordance with equation (11) (Paterson 1971). Hence the penetration of the system is the maximum depth to the outcrop of the conductor, which produces an anomaly distinguishable from the noise. The change in the signal S as a function of depth can be deduced from the modelling data, and the noise value N from the field survey results. For the layered model conductors it is enough to define the conductivity of the conductive layer $\sigma = \infty$ as a supplementary parameter. The thickness of the conductive layer has no effect, i.e. the same penetration value is obtained for one-layer and two-layer models. For the half-plane model, the examination is undertaken with a vertical, thin half-plane with infinite conductivity. If the time constant of the system is so high that it affects the anomaly of a thin half-plane in field surveying, then the influence of the time constant must also be taken into account. The penetration for the sphere model could be defined in the same way as the response function aperture described above. Thus, for a sphere, the penetration equals the maximum depth to the upper surface of a perfectly conductive sphere, 50 m in radius, at which the equation of the detection limit (11) is valid when the smoothing effect of the time constant is once more taken into account.

In accordance with the above principles, the penetration values for various conductor models were determined for the DC-3 AEM system and are listed in Table 15. The table also includes penetration values for susceptive formations (from page 77). It is seen that the dimensions of the conductive formations strongly affect the penetration of the AEM system. The time constant $\tau = 0.3$ s has only a slight effect on the penetration for 2- and

Table 15

Penetration of the DC-3 AEM system for large conductive or susceptive formations when the anomaly detection limit S_d = 4N, i.e. 100 ppm, is constant.

Formation	Penetration (m)
Conductors (k < 0.01, σ = ∞)	
Half-space	210
Thin horizontal sheet	210
Thin vertical half-plane (τ = 0 s)	125
Thin vertical half-plane (τ = 0.3 s)	123
Sphere with a radius of 50 m (τ = 0 s)	85
Sphere with a radius of 50 m (τ = 0.3 s)	85
Susceptive formations (σ low)	
Half-space with k = 0.1	75
k = 0.25	100
k = 1.0	145

3-dimensional conductors, because the wavelength of the anomaly is increased with increasing depth to conductor outcrop.

The penetration values obtained are only valid if the conductor is in a resistive environment. The conductive overburden attenuates both the primary and secondary EM fields in proportion to the conductance $\sigma_1 d_1$, thus reducing the values in Table 15. Peltoniemi (1978b) has studied the penetration in a case when an extensive conductor is overlain by conductive overburden. In the study, the maximum penetration of the DC-3 AEM system was determined as follows. On the basis of the two-layer model data (Fig. 30), the limit thickness of the conductive overburden was determined as a function of the conductivity σ_1 so that with the maximum thickness of layer d_1 the anomalies are identical with the structure $d_1 = \infty$, i.e. with the one-layer model, within the detection limit of the anomaly (S_d, 100 ppm). Hence, at depths greater than this, a large underlying conductor at least cannot produce a detectable change in the anomaly. The results of the examination are given in Table 16. They show, for example, that overburden with conductivity 0.2 Sm^{-1} and thickness 40 m masks all the conductors in the bedrock in

Table 16

The maximum thicknesses d_{1max} of the conductive horizontal layer for various conductivities σ_1 on condition that the difference between the one-layer model data and the two-layer model data exceeds 100 ppm. The survey flight elevation of the DC-3 AEM system is h = 30 m.

Conductivity σ_1 (Sm^{-1})	d_{1max} (m)	d_{1max} (in δ units)
0.01	78	0.88
0.02	70	1.1
0.1	49	1.7
0.2	35	1.8
1.0	13	1.5

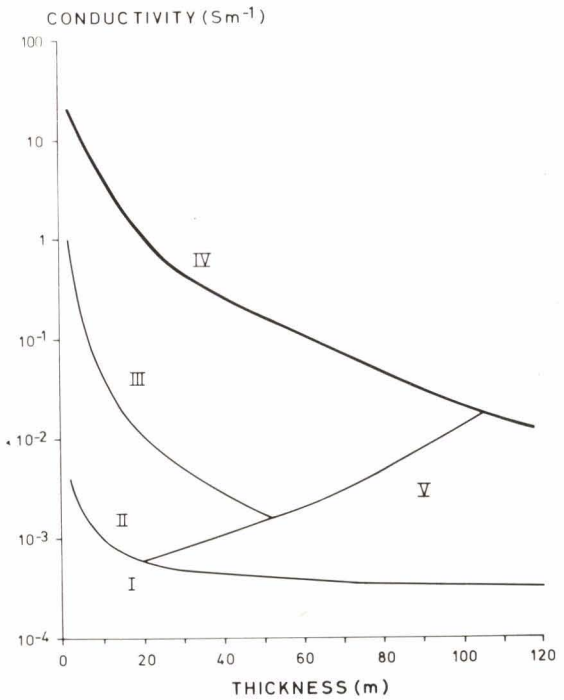

Fig. 49. Discrimination and penetration of the DC-3 AEM system as a function of the thickness and conductivity of the overburden, based on analysis of the computed modelling data. The flight elevation h = 30 m and the detection limit S_d = 4N, i.e. 100 ppm, are constants. For explanation see text on page 102.

such a way that they do not produce a recognisable AEM anomaly.

Attempts were also made to examine the method for the half-plane conductor below a conductive overburden by studying the relevant results of scale model measurements. At least within the limits of the results available, these comparisons corroborate the maximum penetration approach given above. The effect of the conductive country rock is, however, unknown and may, owing to the channeling of the induction currents (Gaur & Werma 1973), even increase the penetration values listed in Table 16.

As a summary of the model studies, Fig. 49 shows in compact form the discrimination properties of the DC-3 AEM system for a conductive horizontal layer. Marked by symbol I in the figure is the area in which the anomaly is below the detection limit S_d, i.e. no recognisable anomaly can be obtained from the combinations of thickness and conductivity. Symbol II refers to the area in which the anomaly is distinguishable from the noise; with the aid of Fig. 30, however, only a thin-layer interpretation is possible. Symbol III marks the area in which the anomalies allow the interpretation of a thick layer. The boundary between areas II and III is approximated by equation (31). Symbol IV denotes the area in which anomalies due to various conductivity and thickness combinations are of equal and maximum magnitude within the given measuring accuracy. The boundary between areas III and IV thus shows the maximum penetration of the system whenever conductive overburden covers an extensive conductor. If the conductivity of the overburden is $\sigma_1 < 0.1$ Sm^{-1}, the penetration is controlled by geometric attenuation instead of electrical attenuation. Symbol V indicates the area in which a detectable anomaly is obtained, but which is so low in intensity that the discrimination ability of the system allows no differentiation between one- and two-layer earth models.

Sensitivity

The penetration values given above correspond to the sensitivity of the system at the detection limit. The sensitivity values at the nominal flight elevation can also be deduced from the modelling results of different conductor types and are given in Table 17. The results show that the sensitivity values of horizontal conductors are much higher than those for a half-plane and a sphere. This fact explains the large contribution horizontal overburden conductors make to the geological noise in the application of AEM data to exploration purposes. In contrast to penetration, the time constant has a decisive influence on sensitivity values, owing to the shorter wavelengths of anomalies at nominal survey elevation.

The characteristic properties of the DC-3 AEM system are also studied in the examples of the field survey results.

Table 17

The signals S and sensitivities S_{nom} of the DC-3 AEM system for various conductors ($\sigma = \infty$) at the nominal survey elevation h = 30 m.

Formation	S (ppm)	S_{nom}
Horizontal conductive layer	−15820	633
Vertical thin half-plane (τ = 0 s)	−3600	144
Vertical thin half-plane (τ = 0.3 s)	−2700	108
Sphere with a radius of 50 m (τ = 0 s)	−3290	132
Sphere with a radius of 50 m (τ = 0.3 s)	−3040	122

COMPUTER-BASED UTILISATION OF LAYERED-EARTH MODEL DATA

Principles

The results of the various conductor models presented above can be used manually although tediously as a set of characteristic diagrams. If the system is dimensioned like the DC-3 AEM system, in which the intermediate conductors also give rise to anomalies, the number of detectable responses readily becomes too high to be interpreted manually. The modelling results, however, make it possible to transform all the anomalous in-phase and quadrature survey data into more meaningful apparent properties. The systematic application of such a transformation requires the use of computer data processing techniques. For the transformation to be feasible the survey data must be reduced for level, drift and spherics with sufficient accuracy; in the present study the accuracy aimed at was 10 to 40 ppm, depending on the component and survey area.

Palacky (1972) was the first to develop methods for the computerised transformation and interpretation of AEM data for the pulse transient method. Later, Fraser (1978) and Seigel and Pitcher (1978) gave examples of ADP-based transformations for multicomponent and multifrequency systems based on modelling results of a conductive half-space. Seigel and Pitcher also used models of electrically thin and thick horizontal conductors in the transformation.

All of the transformation methods developed so far are applicable to multichannel AEM systems. With the quality of the data in mind, a study was implemented to apply the transformation method to the two-channel DC-3 AEM results. A set of computer programs was developed to transform the in-phase and quadrature anomaly values of the DC-3 AEM system into the apparent conductivity σ_a of a half-space or into the apparent total conductance s_a of an electrically thin horizontal conductor. As a result of the transformation, the apparent depths to the upper surface of the conductor da_1 (one-layer model) and da_2 (two-layer model) are also obtained. It has not been considered worthwhile in Finland, for the reasons given on pages 78 and 101, to include the model of the thick horizontal conductor in the transformation. If necessary, it can be readily added to the software. The first version of the software was developed in 1978 (Peltoniemi 1979a) and an improved one in 1980–1981.

The transformed results have the following advantages:

- The results of the different AEM systems are easier to compare, because the differences between the dimensions and recording parameters of the systems are partly eliminated.
- They are more illustrative and closer to the physical properties of the anomaly source than the in-phase and quadrature anomaly values, whose relation to source geometry and conductivity is complicated. For this reason, the processing of slingram results into Re/Im ratio maps has already been practised for quite a long time (Hattula 1970).
- They make it easier to assess the type of conductor that produces the anomaly, i.e., whether it is an overburden or a bedrock conductor.
- The method allows some of the distortions introduced into the survey data by the variation in flight elevation to be eliminated.

Method of transformation and its accuracy

The computer programs use the numerical modelling results in Figs. 27 and 30 as comparative values digitised and stored in a data bank matrix. With the aid of these values, the survey data are transformed into σ_a, da_1 or s_a, da_2 values of one-layer or two-layer models. Hence, the programs read the output file of the basic processing stage 6 (cf. Fig. 22) as input data and perform the following tasks:

- The smoothing of the input, i.e. the in-phase and quadrature survey data if desired, either by a moving average method with binomial coefficients or by recursive filtering.
- Should both in-phase and quadrature anomaly values exceed given threshold values Re_{min}, Im_{min}, the corresponding transformation results are sought. It is checked that the in-phase and quadrature values fall within the definition range covered by the characteristic curves. If this requirement is met, that cell of elements of the data bank matrix is sought to which the measured in-phase, quadrature data pair belongs. By means of linear interpolation, σ_a, za_1 or s_a, za_2 values corresponding to the data pair are calculated from the cell values.
- In special cases (when only one of the anomaly values exceeds the threshold, or the in-phase, quadrature data pair falls outside the definition area of the matrix) the transformation results are determined on the basis of the higher anomaly value and the measured flight elevation alone. The transformation is then always undertaken towards the conservative, i.e. lower, σ_a or s_a values.
- If both anomaly values are so low (below the threshold) as not to warrant accurate transformation, the transformation results are given constant values. These are $\bar{\sigma_a} = 0.0002$ Sm^{-1} and $\bar{s_a} = 0.005$ S. In this case, the apparent depth values za_1 or za_2 are made equal to the flight elevation at the survey point in question.
- The measured flight elevation h is subtracted from the transformation results za_1 or za_2. The difference da_1 or da_2, which is the apparent depth of burial to the conductor outcrop, can have a value higher than, equal to or lower than zero. The conductive half-space is not a suitable model if $da_1 < 0$. Similarly, the conductive overburden is not a suitable model if the apparent depth to the conductive overburden $da_2 < 0$. Thus it is possible to obtain useful diagnostic information for interpretation even from negative apparent depth values.
- The results are coded into integer variables and transferred into an output file, which is processed in the same way as the anomaly data: the transformation results are interpolated into a rectangular grid, the data are decoded and the logarithmic values are contoured and plotted. If desired, the results can also be plotted directly as survey profiles.

The methodically unnecessary coding of the transformation results into integer variables is caused by the limited size of the CPU memory of the HP 3000 minicomputer. The alternative would have been to develop a new interpolation program.

A transformation program based on the above concepts is fast to execute. When operated in an HP 3000 Pre-Cx environment it requires about 1.0 CPU seconds per line kilometre (cf. Table 7). Hence the transformation

takes only 5 % more computing time than the methodic reductions (main program 6). By the end of 1981, data from four AEM survey areas, totalling 12 500 line kilometres, had been processed with the software. The ϱ_a and da_1 maps in Fig. 89 and the s_a and da_2 maps in Fig. 55 exemplify transformed AEM results.

The accuracy of the method is affected mainly by the accuracy of the input data and errors due to the digitisation of the characteristic curves. The lower the anomaly values, the lower is the relative accuracy of the input data. The results from the test areas show that, in some cases, the threshold values of the anomalies (20 to 60 ppm) were too low. This is revealed as a noise of low σ_a or s_a values on the output maps. The test data suggest that a reliable threshold value would have been 20 to 80 ppm, depending on the area. This would still be less than the 100 ppm detection limit in visual anomaly recognition.

The error resulting from the digitisation of the characteristic curves consists of errors generated during the original building up of the data bank matrices and the linear interpolation of the intervening points. The modelling data are stored in the data bank matrices 10 points/decade. Thus the size of the one-layer model matrices is 26 × 36 points and that of the two-layer model 27 × 46 points. The linear interpolation is accomplished within such small subareas that the error produced in it is negligible compared with the other sources of error. Checking with theoretical results demonstrates that the error incorporated in the transformation values is the higher of the values:

for σ_a data ± 0.0005 Sm^{-1} or 5 %,
for s_a data ± 0.01 S or 5 %.

In practice, the most important source of error is greatly simplified model geometry. If the conductor dimensions are less than the lateral coverage and penetration of the system, the transformed values exhibit large systematic deviations from true conductivity and conductance values.

As was pointed out on page 103 and will be demonstrated in the following chapters, the transformation results obtained have some indisputable advantages. The present author, however, feels that transformation cannot be the only way of presenting the AEM results for the following reasons:

- The relative accuracy of the transformation data is poor at low conductivity or conductance values because the in-phase anomaly values are then low.
- Since the structural models used in the transformation are 1-dimensional, the σ_a, s_a results for noise-free anomalies of 2- or 3-dimensional conductors are invariably too low. However, for noisy field data with very low anomaly amplitudes, the Re/Im ratio may change so that erroneously high σ_a, s_a values are obtained.
- Compared with galvanic earth resistivity measurements, the transformation method poses the additional difficulty that, for the model of the homogeneous half-space, it is not possible to transform all the data into σ_a values. For example, some of the anomaly values of a thin conductive horizontal layer fall outside the definition area of the half-space. This can be seen by comparing Figs. 27 and 30. The situation, although informative in terms of interpretation, complicates the calculation of the σ_a transformation values.

The addition of 2- and 3-dimensional models to the transformation software would in itself be a rather small task, because much of their theoretical modelling results have already been given above. The use of the method would then, however, require development

of interactive, graphic software and significantly more effective computer hardware than that currently available at the Geological Survey.

EXAMPLES OF THE INTERPRETATION AND APPLICATION OF DC-3 AEM RESULTS

In the following chapters the interpretability and applicability of the DC-3 AEM results are illustrated by examples from field surveys. The examples refer to the following applications:

- Conductance determinations of the overburden, with Seinäjoki and Tervo Utrianlahti-Talluskylä as targets.
- AEM anomalies due to black schists, todether with their classification, with Seinäjoki and Sotkamo as targets.
- Interpretation of the AEM anomalies produced by a high-grade sheet-like sulphide conductor, with Pielavesi Säviä as target.
- Comparison between the AEM transformation, galvanic earth resistivity and IP survey results, with Tervo Luvelahti as target.
- Interpretations of 3-dimensional conductive bodies, with Savukoski Miekkaoja and Pielavesi Ilokangas as targets.
- Information gained from AEM data in the interpretation of susceptive bodies, with Savukoski Sokli, Savukoski Kuollutvaara and Ylivieska as targets.

The location of the target areas is shown on the index map (Fig. 50). Although the emphasis is on the AEM anomaly and transformation data, other geophysical data have also been used whenever they have contributed towards solving the problem in question. Extensive data are available from the target areas. Consequently, all other data, including the geological ones, can be presented only briefly.

The other geophysical data were interpreted with the following methods:

- The total conductance s_a was calculated asymptotically from the direct current (DC) earth resistivity sounding data (Keller & Frischknecht 1966, p. 115), and the sounding curves were interpreted with the interactive interpretation program of the layered earth model developed by Jokinen and Vironmäki (Vironmäki 1977).
- Slingram data were studied with the aid of scale model results and characteristic diagrams as reported by Ketola and Puranen (1967), Ketola (1968) and Kurimo-Salminen (1979). The slingram modelling data needed in the interpretation of the sphere and layered earth models were computed with the ADP programs described on pages 68–70. Since the reading accuracy of the older one- and two-layer characteristic diagrams (Ketola & Puranen 1967 Figs. 73 and 74, Malmqvist 1965 Fig. 5a) is low for small anomaly values, additional results were elaborated by means of the computer program, and the enlarged parts of the characteristic diagrams are shown in Fig. 51.
- The VLF-R data were interpreted with layered earth models using the characteristic diagrams given in the report TN-1 of Geonics Limited (1975).

  The double dipole EM detector data were interpreted with the aid of the numerical modelling results reported by Peltoniemi (1981a). In addition to

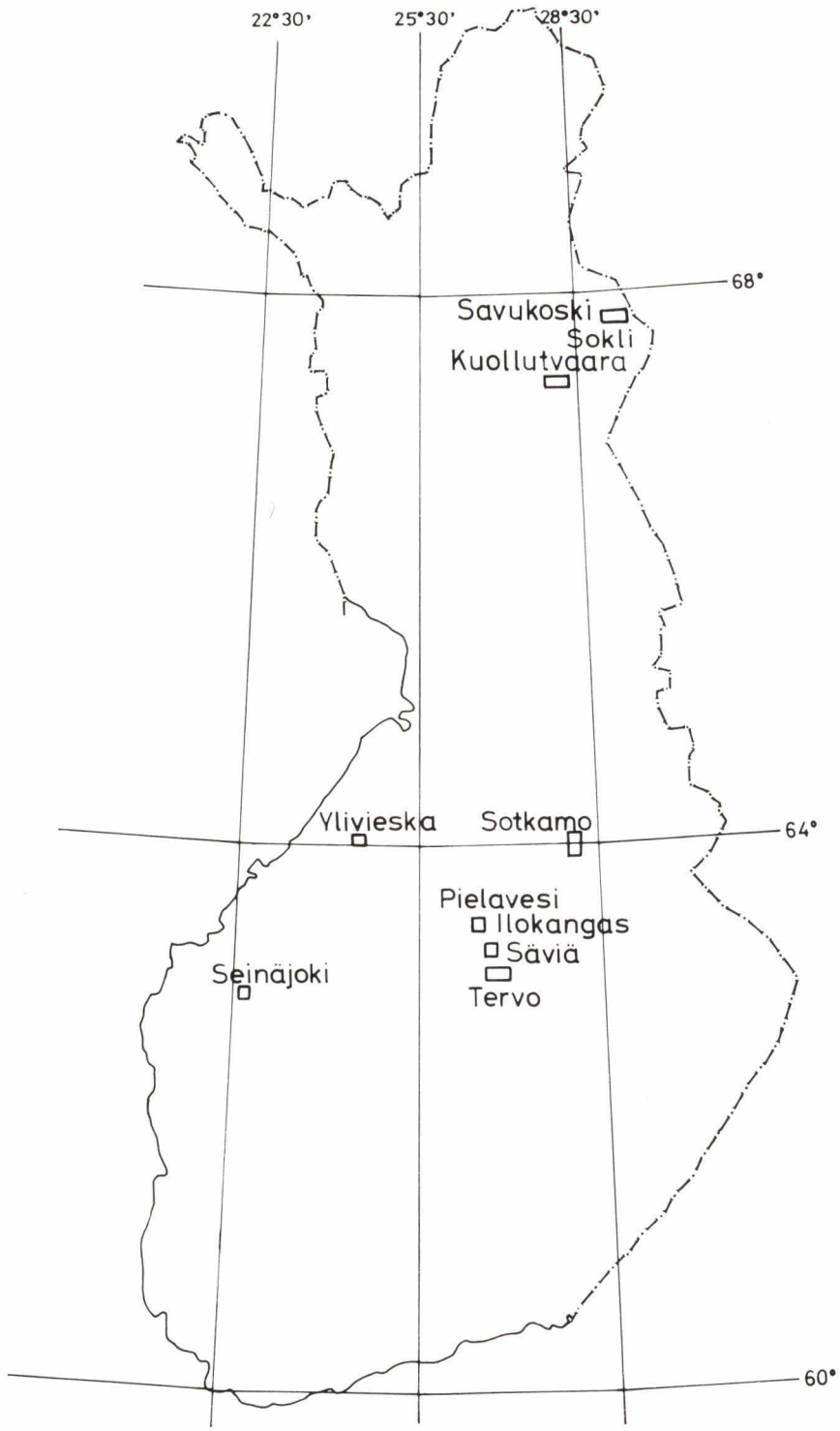

Fig. 50. Index map showing location of the target areas studied in the examples.

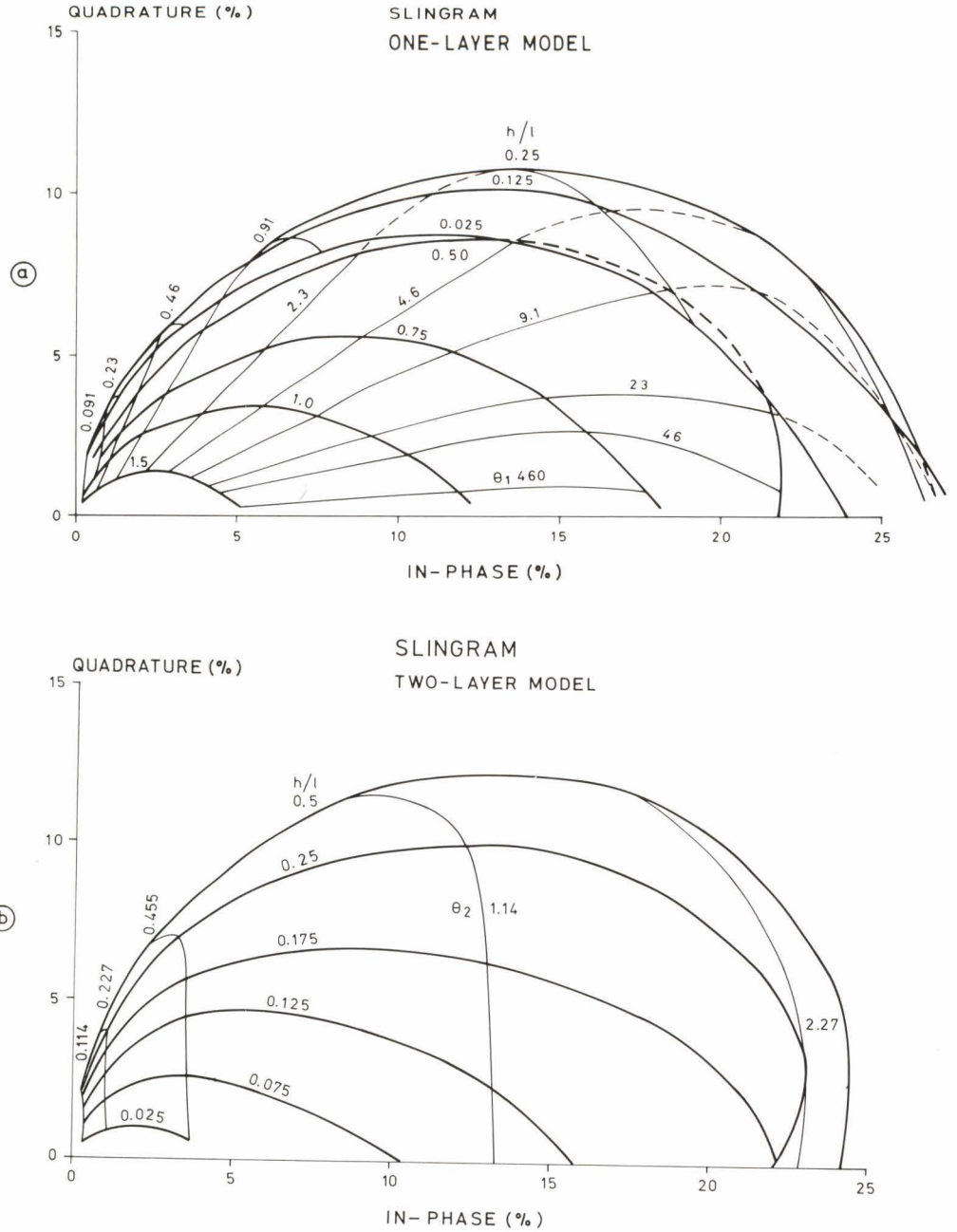

Fig. 51. In-phase and quadrature anomalies as a function of the depth/coil-separation ratio h/*l* and the response parameter θ in the slingram method. (a) The conductive half-space model, $\theta_1 = \sigma_1\mu_0\omega l^2$. (b) The conductive horizontal layer model, $\theta_2 = \sigma_1 d_1 \mu_0 \omega l$.

boulder tracing, this light-weight portable instrument is occasionally used in the preliminary follow-up studies of AEM anomalies. A combined characteristic diagram of one- and two-layer models for the Apex MK I double dipole

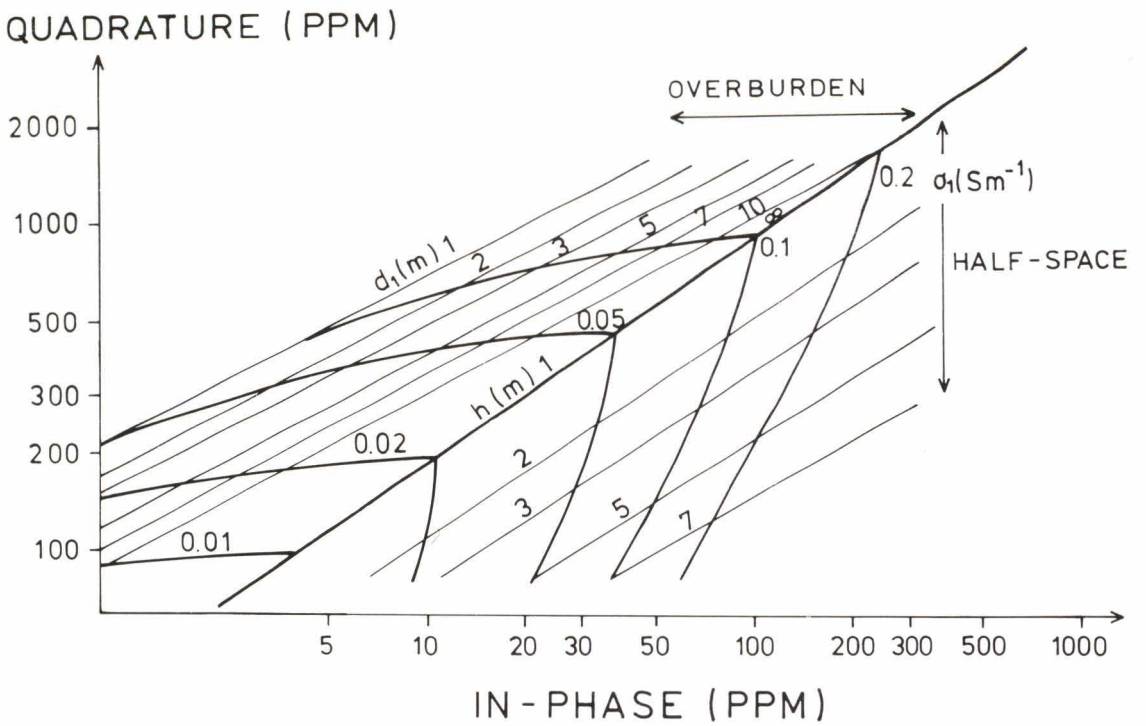

Fig. 52. In-phase and quadrature anomalies produced by a conductive half-space and a conductive horizontal layer in a double dipole EM (Apex MK I) survey as a function of the depth to the upper surface h, the thickness d_1 and the conductivity σ_1 of the conductor. The coil separation l = 1.22 m, frequency f = 8 000 Hz, and the coil inclination angles $\beta_1 = \beta_3 = 54.7°$ are constants.

EM detector used in the measurements is reproduced in Fig. 52.

- The aeromagnetic data were interpreted using the interactive interpretation program developed by Jokinen (1979). The program is based on the anomaly solutions for a thick plate and a prism derived by Hjelt (1972, 1973) and on the computer algorithms developed by Vironmäki (1977).

Seinäjoki: Conductive overburden and bedrock layers

The Seinäjoki area (map sheet 2222 06 Munakka) was selected as a target for study because the AEM survey data on the area exhibit anomalies due to both conductive overburden (sulphide-bearing Littorina clays) and bedrock conductors (black schists). In the middle of the study area the conductors occur close to each other and the anomalies are partly summed up. To investigate the AEM anomalies in closer detail, diverse geophysical ground surveys were undertaken in the area, the results of which have been reported by Peltoniemi (1981a). The example illustrates:

- How the AEM anomaly data can be transformed in practice into s_a and da_2 values applying the thin horizontal conductor model.

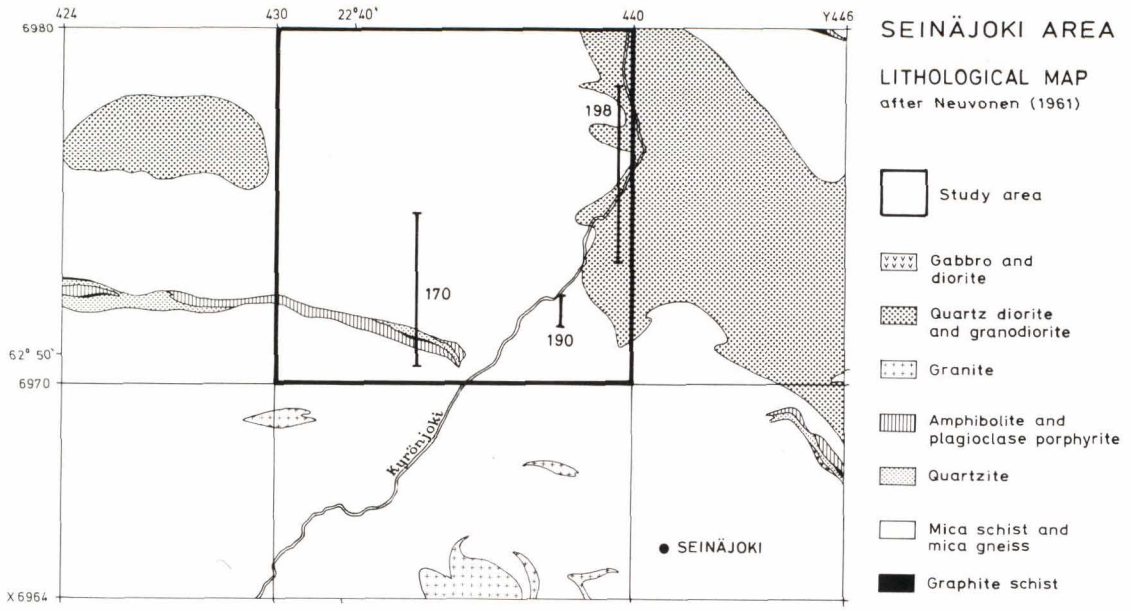

Fig. 53. Generalised version of the lithological map by Neuvonen (1961) covering map sheet 2222 06. Test lines 198, 190 and 170 are marked on the map.

- What other interpretational information the transform results contain apart from that obtained by the visual interpretation of the in-phase and quadrature data.
- How the AEM results given by transformation with the horizontal conductor model are applicable to narrow, sheet-like conductive zones in bedrock.
- How the conductance aperture of the DC-3 AEM system corresponds in practice to the theoretical results in Table 14.
- How the resolution, conductance aperture and penetration of the AEM, EM and electrical ground surveys compare with each other in practice.

The geological map by Neuvonen (1961) (simplified version in Fig. 53) shows that the test area is part of the Bothnia schist belt with mica schist and mica gneiss as predominant rock types. On the SW margin of the area there is, however, a narrow amphibolite and quartzite zone with intervening graphite and iron sulphide layers. Plutonic rocks, quartz diorite and granodiorite are encountered on the eastern margin of the test area. Consequently, except for the black schists, the bedrock in the area is poorly conductive.

The clay deposits around the river Kyrönjoki are conductive soil formations typical of the test area. Postglacial clays contain abundant dark saline and sulphide-bearing layers and cover large tracts. The clays in this area are very acidic in chemical properties (Romu 1980) and electrically highly conductive, as is indicated by the results of geophysical surveys and electrochemical analyses. Laboratory determinations on the conductivity of clay suspension for samples collected from the adjacent map sheet 2222 08 gave an average conductivity of $\sigma = 0.16 \pm 0.05$ Sm^{-1} (Romu 1980, p. 51).

Aerogeophysical low-elevation surveys

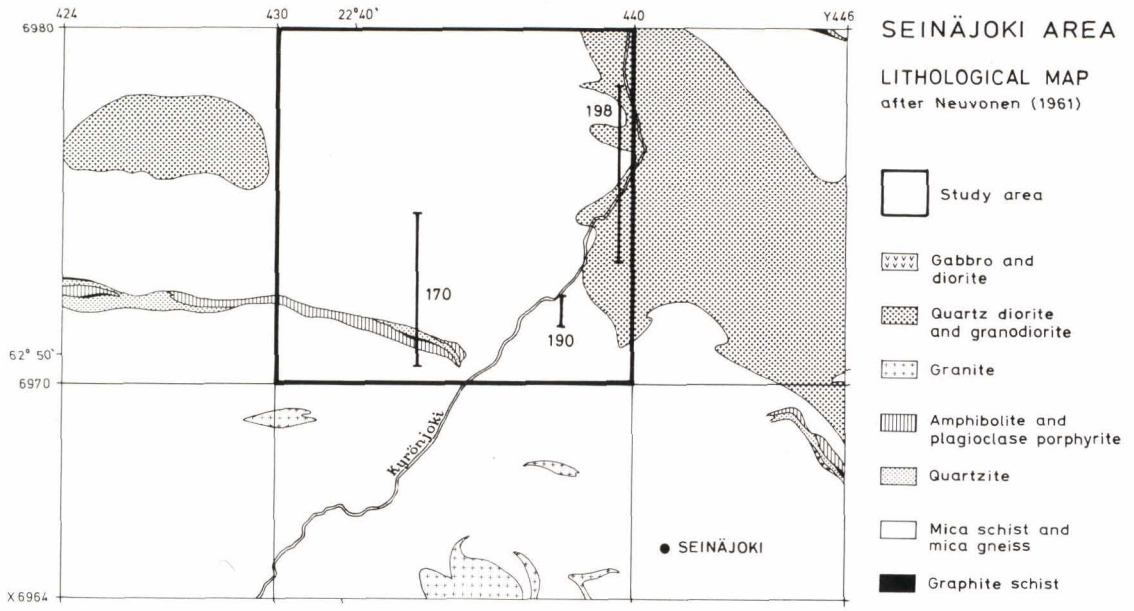

Fig. 53. Generalised version of the lithological map by Neuvonen (1961) covering map sheet 2222 06. Test lines 198, 190 and 170 are marked on the map.

- What other interpretational information the transform results contain apart from that obtained by the visual interpretation of the in-phase and quadrature data.
- How the AEM results given by transformation with the horizontal conductor model are applicable to narrow, sheet-like conductive zones in bedrock.
- How the conductance aperture of the DC-3 AEM system corresponds in practice to the theoretical results in Table 14.
- How the resolution, conductance aperture and penetration of the AEM, EM and electrical ground surveys compare with each other in practice.

The geological map by Neuvonen (1961) (simplified version in Fig. 53) shows that the test area is part of the Bothnia schist belt with mica schist and mica gneiss as predominant rock types. On the SW margin of the area there is, however, a narrow amphibolite and quartzite zone with intervening graphite and iron sulphide layers. Plutonic rocks, quartz diorite and granodiorite are encountered on the eastern margin of the test area. Consequently, except for the black schists, the bedrock in the area is poorly conductive.

The clay deposits around the river Kyrönjoki are conductive soil formations typical of the test area. Postglacial clays contain abundant dark saline and sulphide-bearing layers and cover large tracts. The clays in this area are very acidic in chemical properties (Romu 1980) and electrically highly conductive, as is indicated by the results of geophysical surveys and electrochemical analyses. Laboratory determinations on the conductivity of clay suspension for samples collected from the adjacent map sheet 2222 08 gave an average conductivity of $\sigma = 0.16 \pm 0.05$ Sm^{-1} (Romu 1980, p. 51).

Aerogeophysical low-elevation surveys

were undertaken in the Seinäjoki area in 1975. AEM survey data from the study area are shown as contour maps in Fig. 54. The terrain in the test area is flat, the elevation fluctuating gently between 40 and 60 m above sea level. The average flight elevation in the whole area was $\bar{h}$ = 29 m, the standard deviation being 5.8 m. Power transmission and telegraph lines abound. High-elevation AEM surveying has not been conducted in the area.

The predominant features of the AEM anomaly maps (Fig. 54) are the extensive and high-amplitude anomaly zones around the river Kyrönjoki. The anomaly values exceed Re $\leq -3\,000$ ppm, Im $\leq -4\,000$ ppm over large areas, the minimum values being Re = $-8\,500$ ppm and Im = $-5\,500$ ppm. The anomaly zone in the southern part of the area, which trends SE–NW and is caused by the narrow black schist layers, is not readily distinguishable on the contour map as a different conductor from the clay beds. In contrast, the difference in the in-phase/quadrature ratio between the clay and black schist area is easily seen on the profile maps. The AEM data suggest that the black schist layers extend farther eastwards under the overburden than is indicated on the geological map on the basis of the scarce exposure observations.

The AEM anomaly data were transformed into apparent conductance s_a and depth da_2 values of an electrically thin horizontal conductor by means of the computer program described in the previous chapter. The transformation was undertaken by setting the anomaly threshold values at $Re_{min} = -60$ ppm, $Im_{min} = -60$ ppm. Mutual comparison of the anomaly and transformation maps (Figs. 54 and 55) indicates that the method of transformation is feasible in practice and that the output maps are technically acceptable. The transformed results show distinctly the difference between the various conductive formations: the s_a values for the clay areas are $s_a \leq 3$ S, whereas the values for the black schist layers are $s_a \approx 10-30$ S. The pattern of the map in Fig. 55a demonstrates that even by transforming the data on the standard model (horizontal conductor) it is possible to establish the difference in conductance between different types of conductors. The s_a values are highest for the black schist layers, in which the in-phase/quadrature ratio is highest, and not for the clay beds, in which the anomaly amplitudes are highest.

The depths to the upper surface of the conductive layer (Fig. 55b) are reasonable within large conductor areas ($da_2 \approx 3-20$ m), but unrealistically high (70–150 m) for small conductor sources. These maximum da_2 values are associated with anomalies small in size and low in intensity, but which exceed the given in-phase and quadrature thresholds. At low in-phase, quadrature values one operates close to the origin of the characteristic diagram (Fig. 30), and even a slight change in the in-phase/quadrature ratio produces large changes in the interpreted s_a, da_2 values. Thus, the usability of the apparent depth map in everyday practice is probably restricted to the evaluation of the fitness of the transformation model. This is well illustrated by the profile in Fig. 70 and the contour maps in Fig. 55.

The AEM data can best be studied and compared with other data if shown as profiles. Marked on Fig. 53 are the locations of the three test lines, 198, 190 and 170. The results of these lines will be examined more closely in the following.

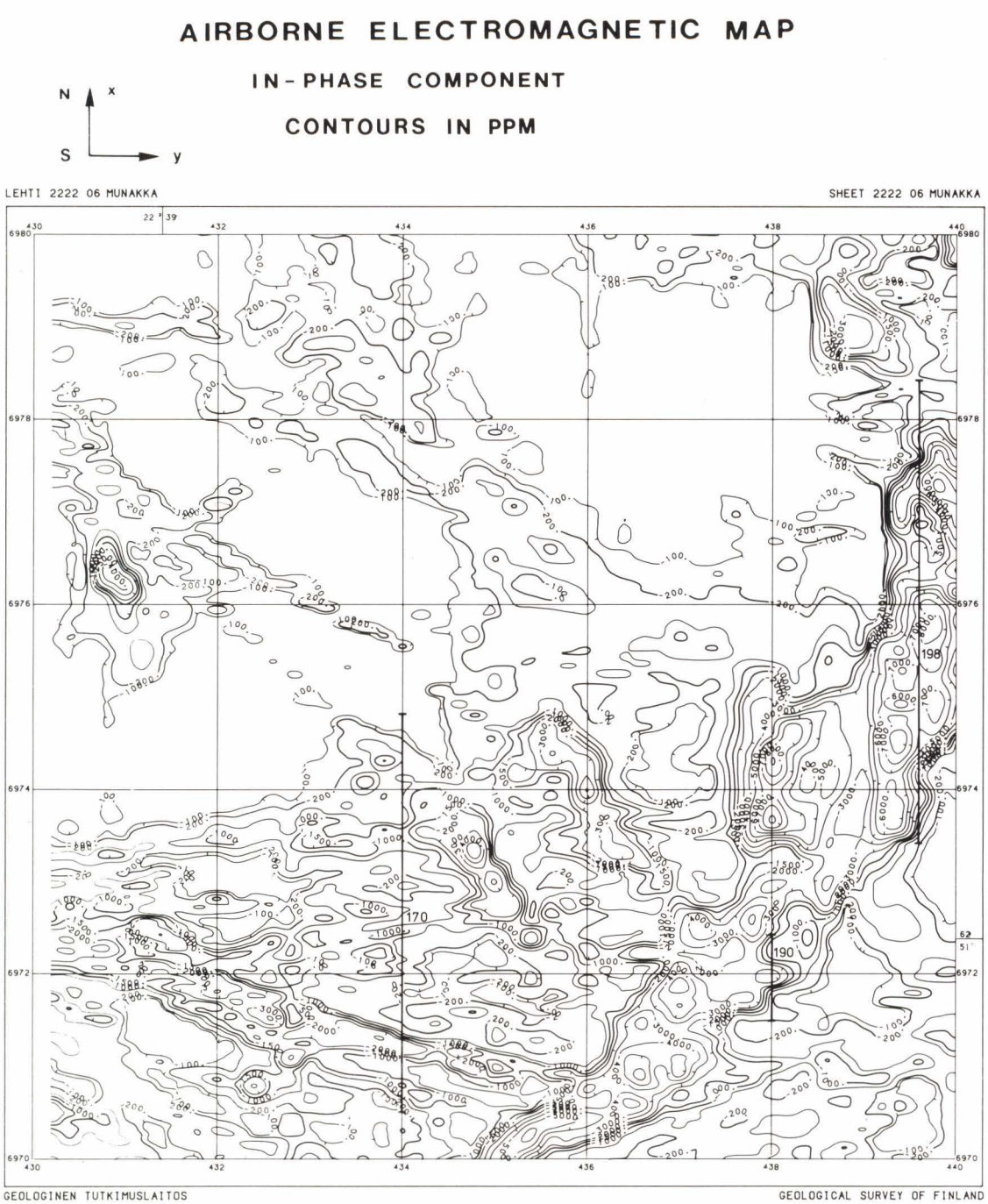

Fig. 54. DC-3 AEM survey data, map sheet 2222 06 (Seinäjoki area). Flight direction N–S, line spacing 200 m. Test lines 198, 190 and 170 are marked on the maps. (a) In-phase component. (b) Quadrature component (see page 113).

AIRBORNE ELECTROMAGNETIC MAP

QUADRATURE COMPONENT

CONTOURS IN PPM

LEHTI 2222 06 MUNAKKA

SHEET 2222 06 MUNAKKA

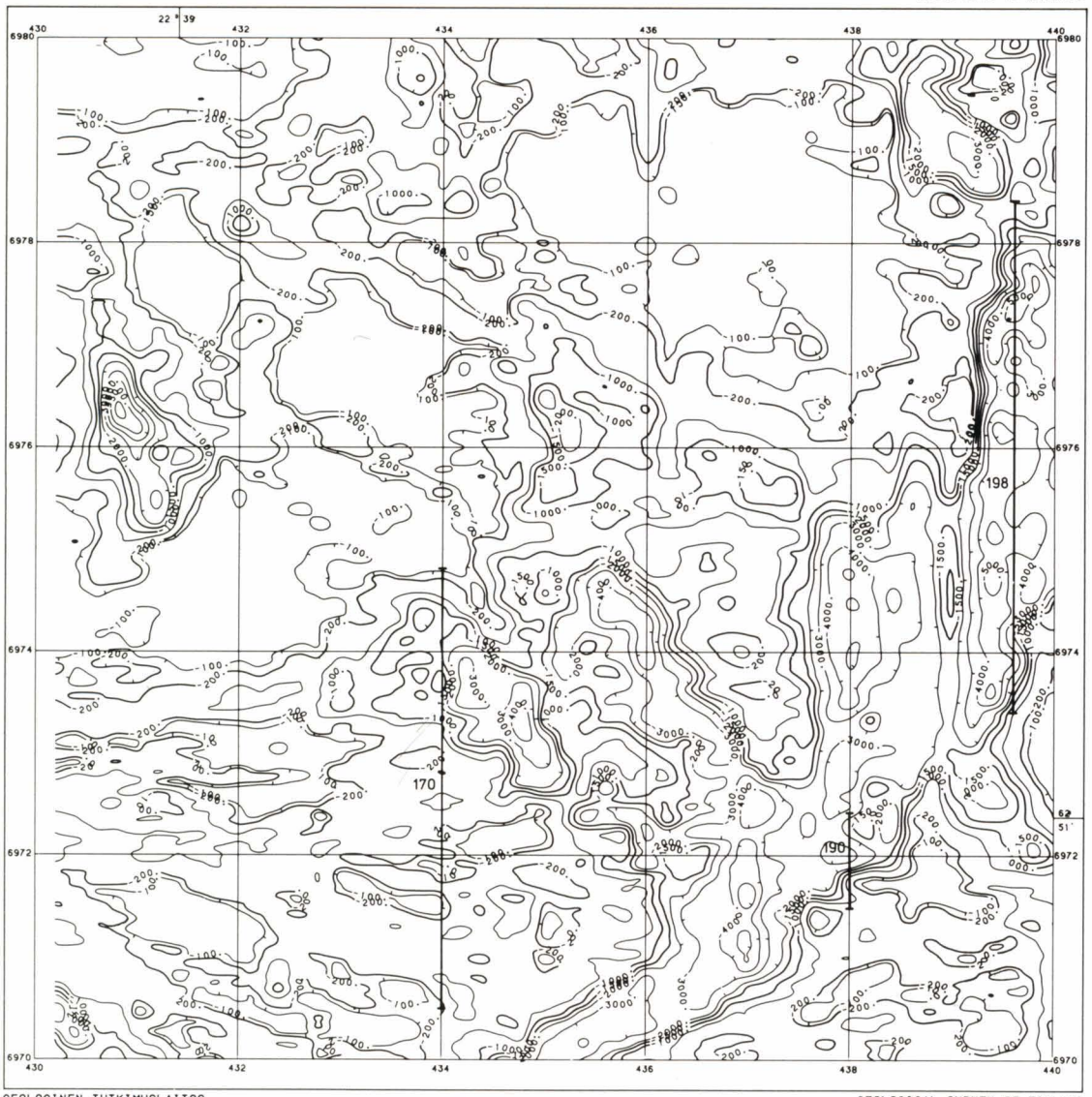

GEOLOGINEN TUTKIMUSLAITOS

GEOLOGICAL SURVEY OF FINLAND

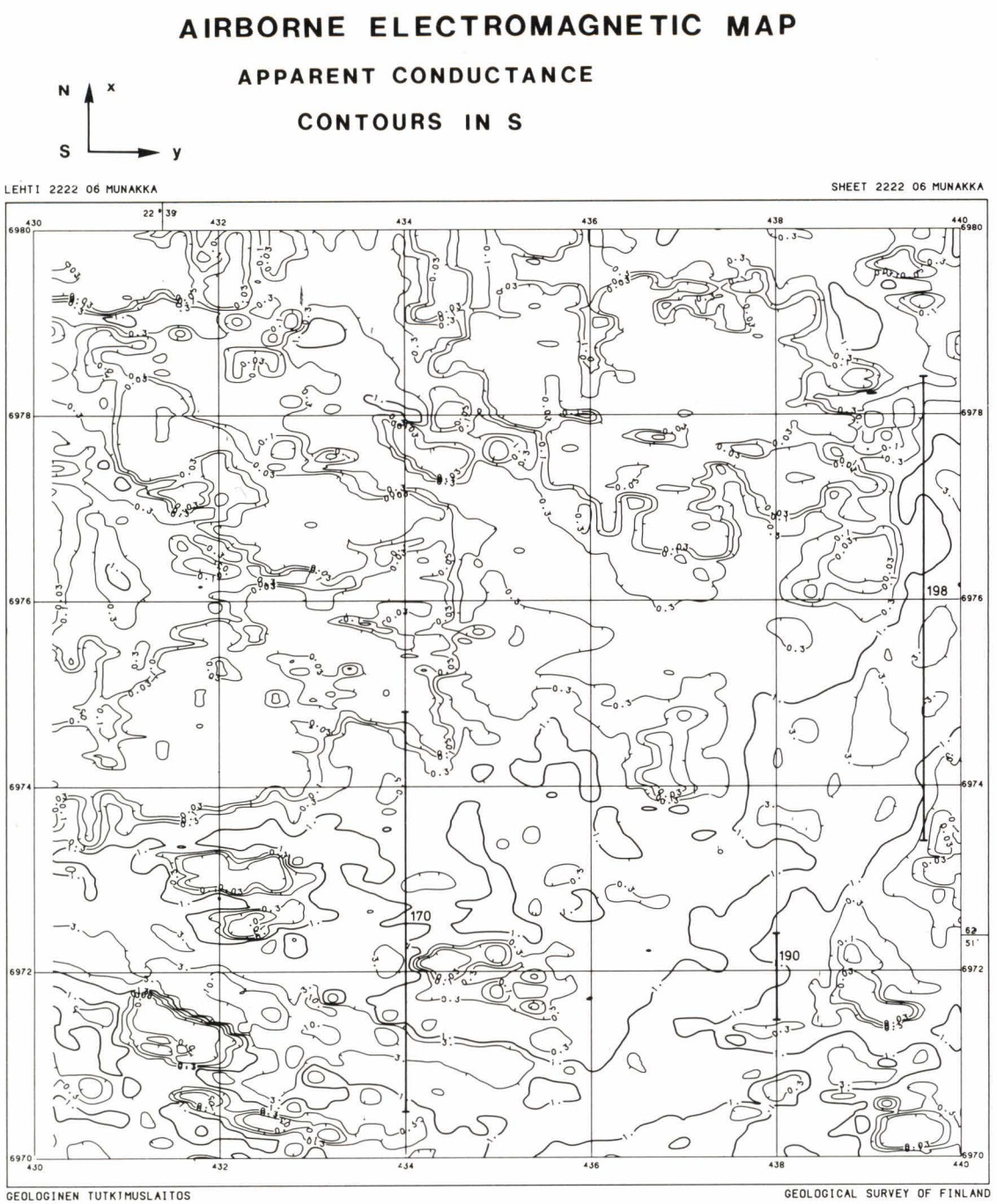

Fig. 55. Transformation results for map sheet 2222 06 (Seinäjoki area) calculated from the original AEM data in Fig. 54 by means of the 2-layer model (a thin conductive horizontal layer). Test lines 198, 190 and 170 are marked on the maps. (a) The apparent conductance values s_a. (b) The apparent depths to the upper surface of the conductive layer da_2 (see page 115).

AIRBORNE ELECTROMAGNETIC MAP

APPARENT DEPTH, 2-LAYER MODEL

CONTOURS IN m

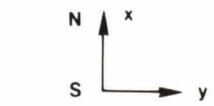

LEHTI 2222 06 MUNAKKA

SHEET 2222 06 MUNAKKA

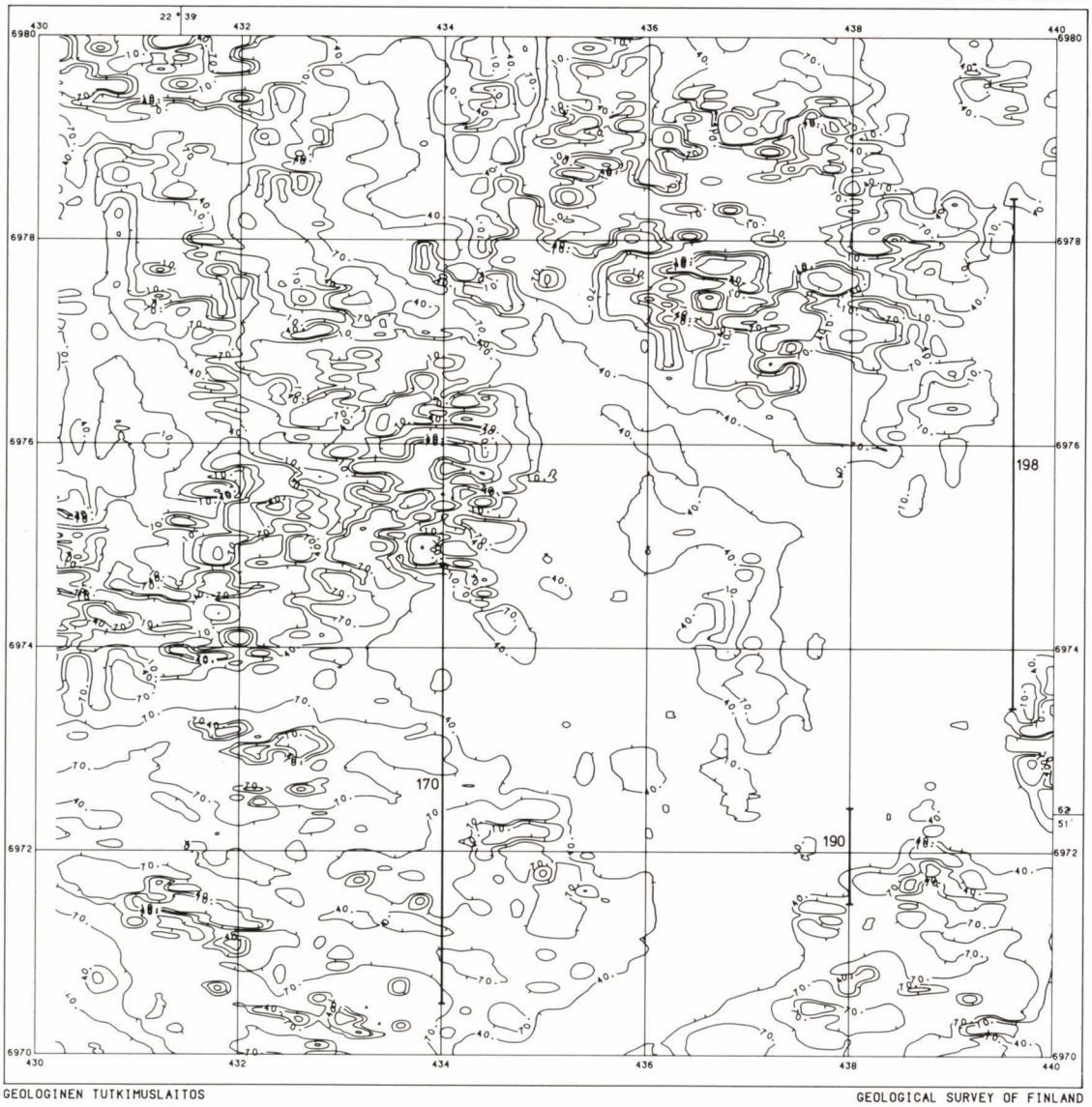

GEOLOGINEN TUTKIMUSLAITOS

GEOLOGICAL SURVEY OF FINLAND

Line 198

The following measurements were made on test line 198 (y = 439.6, between x = 6973.400–6978.420):

- AEM and aeromagnetic measurements, results in Fig. 56a.
- Slingram measurements with coil separation l = 40 m at f = 3 600 Hz, results in Fig. 56b.
- Measurements with Apex Mk I double dipole EM detector, coil separation l = 1.22 m, f = 8 000 Hz, results in Fig. 56c.
- VLF-R measurements (between x = 6973.400–6975.150) with a Geonics EM16R instrument, transmitter JXZ, f = 16 kHz, results in Fig. 57a.
- Measurements of VLF magnetic total field components H (horizontal) and V (vertical), with GT-04,-05 instruments, transmitter JXZ, f = 16 kHz, results in Fig. 57b.
- Direct-current resistivity soundings with an ABEM Terrameter instrument and a Schlumberger electrode configuration at three points 198/1, 198/2 and 198/3, results in Fig. 58.
- Seismic refraction survey (between x = 6973.530–6974.530) with a 12-channel ABEM Trio instrument, interpretation results in Fig. 59.

The aeromagnetic survey data (Fig. 56a) indicate weak, homogeneous magnetisation of the bedrock. The biggest anomaly, +200 nT around x = 6975.4, is located on the river Kyrönjoki and is interpreted here as a fracture zone controlling the placement of the river valley. Another small +40 nT anomaly is situated south of the river on x = 6974.2, where also a seismic sounding profile was shot. The propagation velocity v_s of the acoustic waves at the site is so low that interpretation of a fracture zone at this site, too, is justified. Since the predominant conductor is a conductive soil, i.e. an extensive horizontal layer, the VLF-H, V components do not show any clear anomalies apart from that due to the southern fracture zone.

To ease comparison, some of the EM survey data are recompiled in Fig. 60. In spite of the diversity of methods applied the quadrature component data of various EM measurements are surprisingly concordant. The quadrature component of the slingram measurements exhibits the most complex behaviour, the sign of the phase angle (and that of the quadrature component) being reversed when the conductance of the horizontal conductor increases.

Attempts were made to determine the total conductance s_a of the horizontal conductor from all the results. The values given by the various methods at resistivity sounding points are listed in Table 18. Also shown in the table are the interpretation results for the seismic data at the same points. The locations of the resistivity soundings were chosen on the basis of AEM data so that there would be only a thin conductive layer at point 198/2. Even so, the double dipole EM data suggest that, even at this point, the overburden shows such a high $\sigma_1 d_1$ product that its conductance value cannot be determined from Fig. 52 (upper half). This is exhibited in the survey data by the fact that the in-phase-quadrature data pairs always remain below the family of two-layer curves, i.e. within the definition area of the conductive half-space model. When the values of and variations in the in-phase component are very small, the one-layer characteristic diagram in Fig. 52 is not readily applicable either. Nonetheless, it has been applied to interpret the variation in the depth to the upper surface and the conductivity of the sulphide clay. Thus interpreted, the double dipole EM data and their good qualitative correlation with other data,

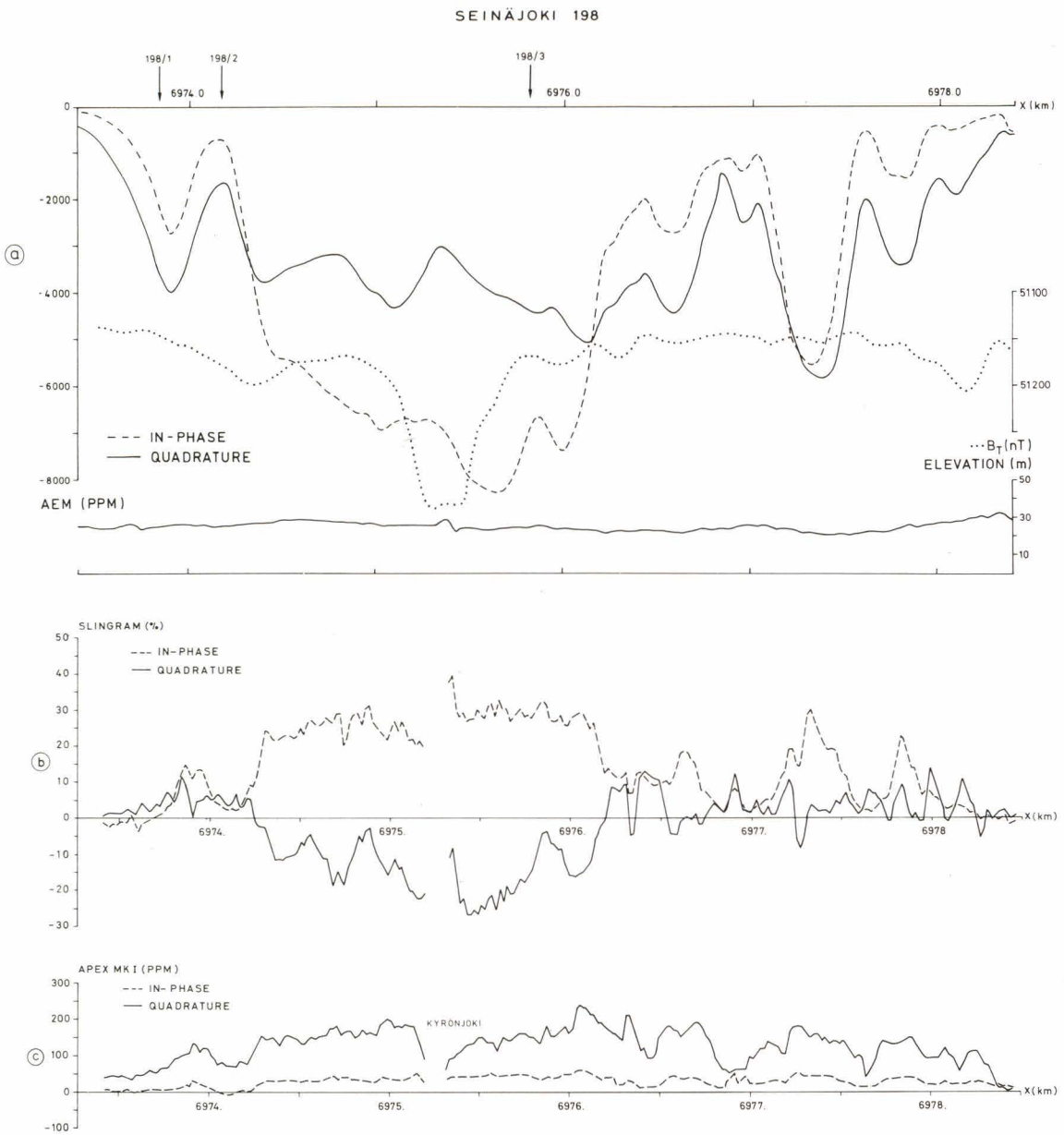

Fig. 56. Survey data by various EM methods from test line Seinäjoki 198. (a) DC-3 aerogeophysical survey, AEM, aeromagnetic and flight elevation data, point spacing $\Delta x = 28$ m. (b) In-phase, quadrature data of slingram survey, $\Delta x = 20$ m. (c) In-phase, quadrature data of double dipole EM (Apex MK I) survey, $\Delta x = 20$ m.

above all with the AEM results, become understandable. Fig. 61a shows the AEM and double dipole EM data on the test profile transformed with the aid of the one-layer model (Figs. 27 and 52). The transform results, which are given as apparent resistivity values, show moderate correlation. Fig. 61b exhibits the AEM data transformed into con-

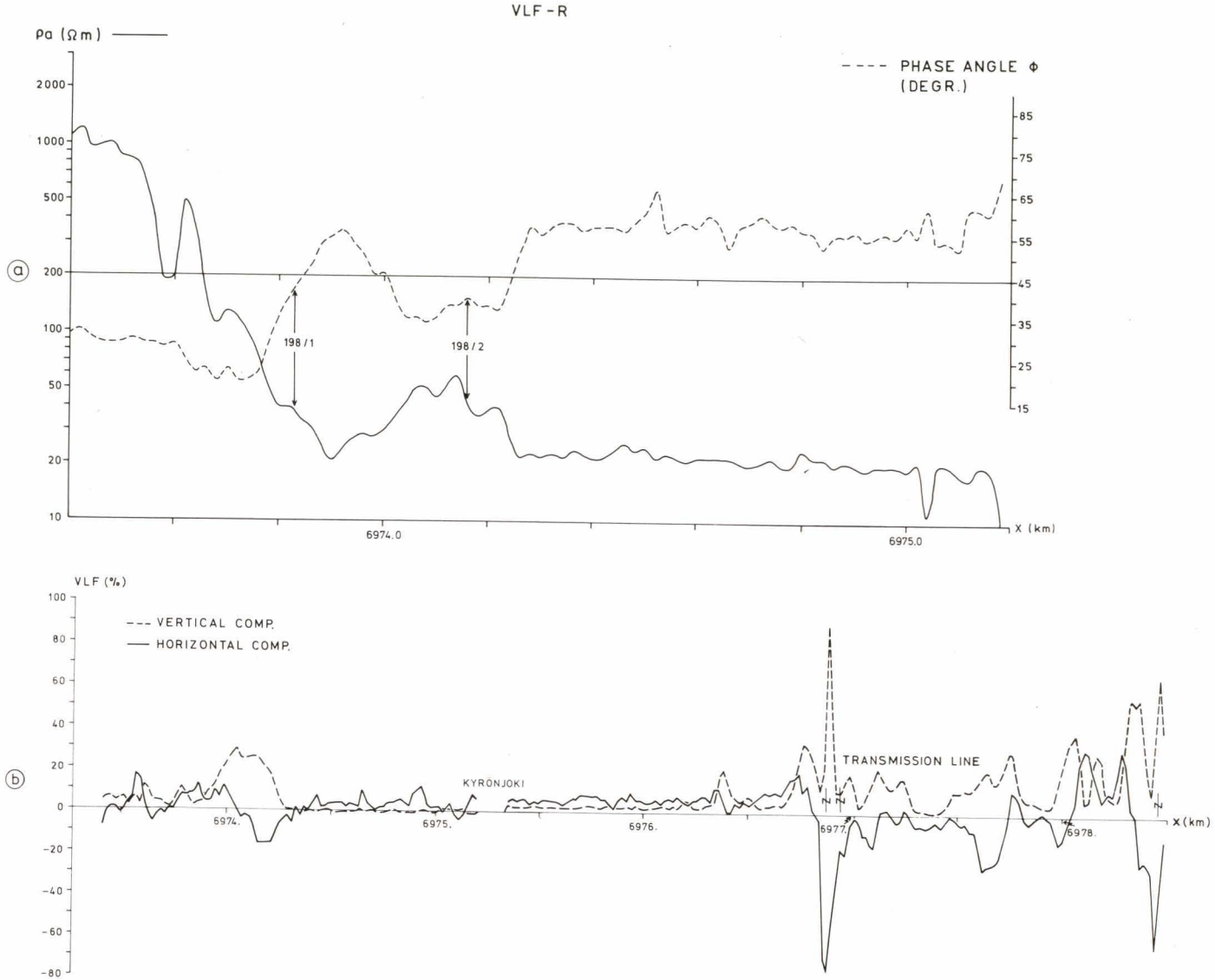

Fig. 57. Test line Seinäjoki 198, VLF survey data, $\Delta x = 20$ m. (a) VLF-R survey, apparent resistivity ϱ_a and phase angle Φ (only the southern part of the test line was surveyed). (b) VLF survey, vertical (V) and horizontal (H) components of the magnetic total field intensity.

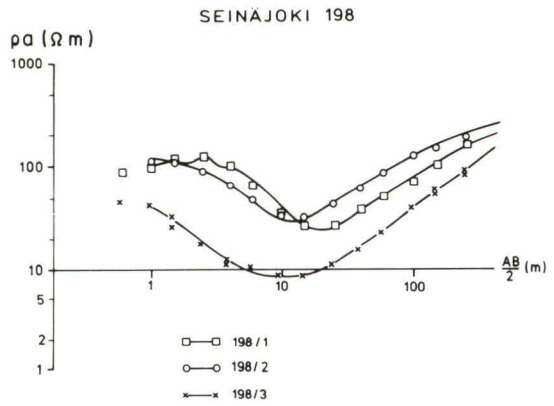

Fig. 58. Test line Seinäjoki 198, DC earth resistivity sounding results at points 198/1, 198/2 and 198/3. Half-value of the current electrode separation = AB/2, Schlumberger electrode configuration. Discrete points refer to survey data, curves denote the theoretical model results with the parameters of the models as listed in Table 18.

ductance values with the aid of the thin-layer model (Fig. 30).

An attempt was also made to interpret the AEM data with the thick-layer model results given in Fig. 34. The interpretation results, which are given in Fig. 61c, are inaccurate and a constant elevation model (h = 40 m) could not be applied to the whole set of data.

At survey points 198/1 and 198/2 the total conductance s_a of the overburden was determined by means of resistivity sounding, AEM, VLF-R and slingram methods. As shown by Table 18, the values are fairly close to each other. The VLF-R results demonstrate that at x = 6973.9 and x = 6974.3–.9, the phase angle ϕ exceeds 45°. According to the characteristic diagrams, this means that, at these sites, the penetration of the VLF-R method is not sufficient to intersect the clay layer. The total conductance of the overburden s_a increases farther northwards, and at point 198/3 it is too high even for the penetration of the slingram method with 40 m coil spacing and 3600 Hz frequency. Thus it is not possible to use the characteristic diagram (Ketola & Puranen 1967 Fig. 73) of

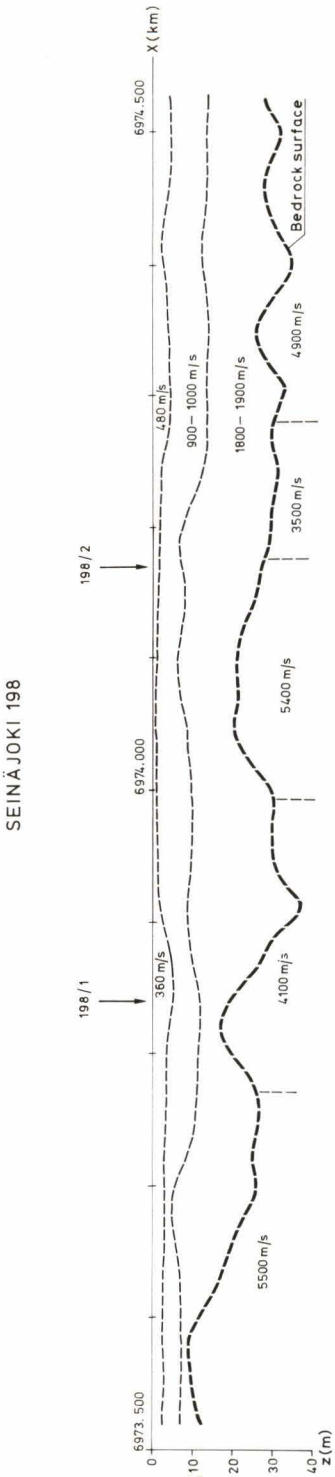

Fig. 59. Test line Seinäjoki 198, seismic refraction survey results: interpreted values of layer thickness and propagation velocity of the acoustic waves. Geophone spacing = 10 m. Interpretation according to Järvimäki (1977).

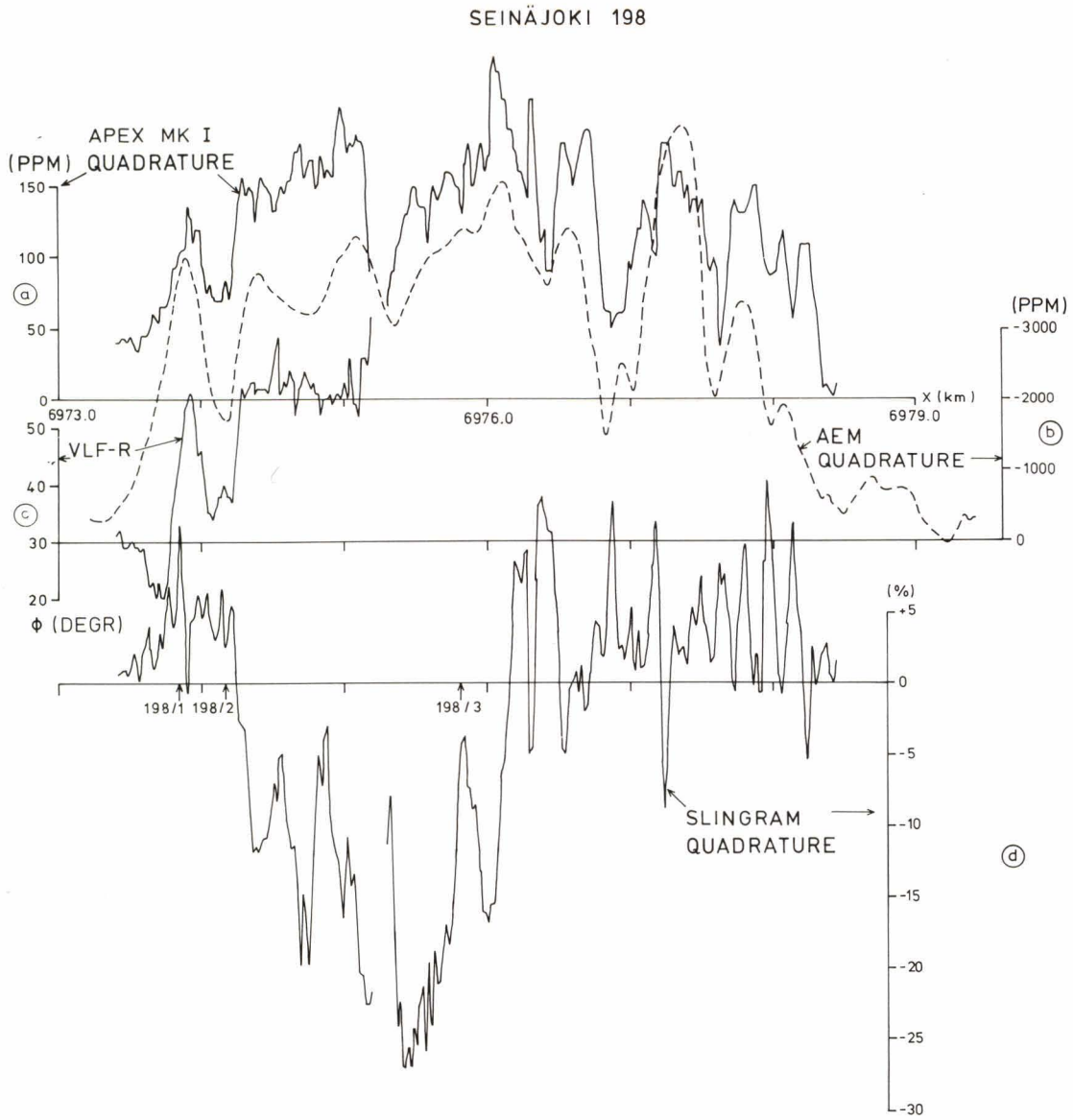

Fig. 60. Test line Seinäjoki 198, combination of various EM survey data. (a) Double dipole EM (Apex MK I) survey, quadrature component (from Fig. 56c). (b) AEM survey, quadrature component (from Fig. 56a). (c) VLF-R survey, phase angle ϕ (from Fig. 57a). (d) Slingram survey, quadrature component (from Fig. 56b).

the thin horizontal conductor, as the data points fall outside the definition area of the diagram. The same holds for the results of the half-space model; the reason for this behaviour is unexplained. The resistivity sounding data and the AEM data, however, make interpretation possible and the total conductance s_a can be determined even within this range.

According to the seismic and resistivity sounding data, the overburden on the test line has at least three layers:

Table 18

Test line Seinäjoki 198, interpretation results at earth resistivity sounding points 198/1, 198/2 and 198/3.

(a) Values of the total conductance σd (S) interpreted by various methods.

Method	Total conductance (S)		
	Point 198/1	Point 198/2	Point 198/3
Earth resistivity sounding (ERS)	1.33	0.67	1.92
AEM	0.82	0.49	2.93
Slingram	1.02	0.53	not defined
VLF-R	0.76	0.61	not measured
Double dipole EM	not defined	not defined	not defined

(b) Interpretation of various EM data by means of the one-layer model. The depth to the upper surface of the conductor = da_1, apparent resistivity = ϱ_a.

Method	Point 198/1		Point 198/2		Point 198/3	
	da_1 (m)	ϱa (Ωm)	da_1 (m)	ϱa (Ωm)	da_1 (m)	ϱa (Ωm)
AEM	−6	54	2	110	6	5.9
Slingram	19	14	10	90	5	3.7
Double dipole EM	2.8	33	2.5	50	4.5	11

(c) Interpretation of the earth resistivity sounding (ERS) survey and seismic refraction survey data by means of a multilayer model. Thickness of layer = d, apparent resistivity = ϱ_a and the propagation velocity of the acoustic wave = v_s.

Layer	Point 198/1				Point 198/2				Point 198/3			
	ERS		Seismic s.		ERS		Seismic s.		ERS		Seismic s.	
	d (m)	ϱa (Ωm)	d (m)	v_s (m/s)	d (m)	ϱa (Ωm)	d (m)	v_s (m/s)	d (m)	ϱa (Ωm)	d (m)	v_s (m/s)
1	0.2	90	4.3	360	0.2	90	1.7	480	0.9	45		
2	3.0	120	7.7	900−1000	1.7	120	6.7	900−1000	3.9	9	not	
3	16	16	5.3	1800−1900	10	21	18.3	1800−1900	14	7	measured	
4	∞	340	∞	4100	∞	340	∞	5400	∞	1000		

- organic soil, $v_s \approx 300-700$ m/s, $\varrho_a \approx 45-120$ Ωm;
- sulphide clay and gyttja, $v_s \approx 700-1\,100$ m/s, $\varrho_a \approx 7-21$ Ωm; and
- till, $v_s \approx 1\,500-2\,800$ m/s, $\varrho_a > 340$ Ωm.

Comparison of the interpreted thicknesses of the layers (Table 18) shows clearly that electrical equivalence has made the interpretation of the resistivity sounding data so difficult that only the total conductance values s_a are reliable if used alone without related control (e.g. drilling) data. The same was evident when the preliminary results of the manual interpretation based on partial curve matching were compared with the results of the ADP interpretation program. Apart from those for the clay layer, the results were in good agreement. The s_a values of the clay layer were also close to each other, but the σ and d values separately showed marked

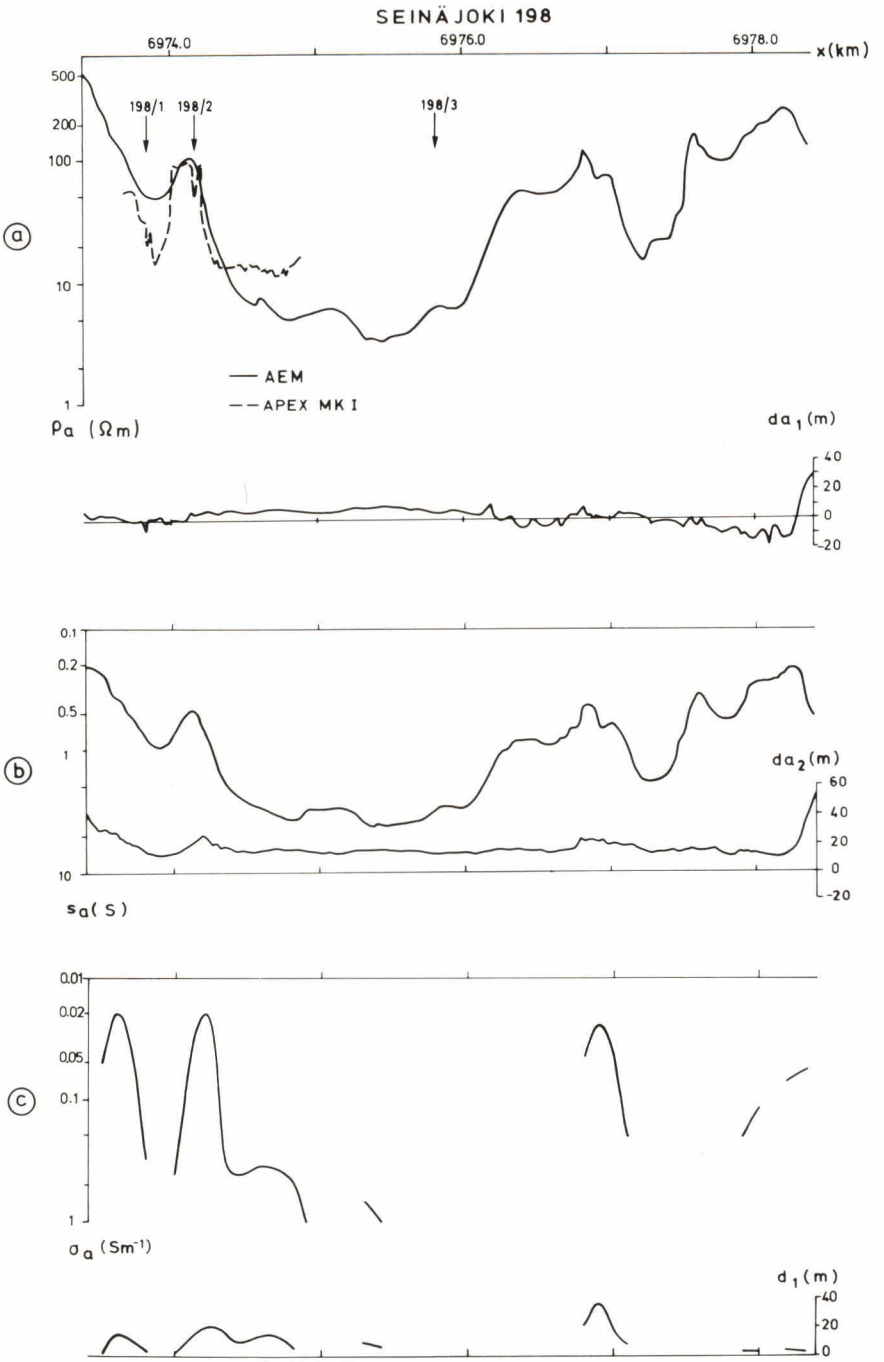

Fig. 61. Test line Seinäjoki 198, transformed EM data. (a) The values of apparent resistivity ϱ_a and apparent depth to the surface da_1 calculated from AEM data by means of the conductive half-space model. Some ϱ_a values obtained with the double dipole EM (Apex MK I) data from the southern end of the line are also shown. (b) The values of apparent conductance s_a and apparent depth to the upper surface da_2 calculated from AEM data by means of the conductive horizontal thin-layer model. (c) The values of apparent conductivity σ_a and thickness d_1 calculated from AEM data by means of the conductive horizontal thick-layer model.

differences when interpreted by different methods.

The AEM in-phase, quadrature and s_a interpretation results (Figs. 56a and 61b) show that the conductance obtains maximum values $s_a = 4.2$ S at x = 6975.380. In these circumstances the method approaches the inductive limit of the response function; the quadrature component has already passed its maximum and decreases in this range when the conductance increases.

Line 190

The following surveys were undertaken on test line 190 (y = 438.0, between x = 6971.550 −6972.450):

- AEM survey, results in Fig. 62a.
- Slingram surveys with coil separation of l = 20 m and l = 40 m, results in Figs. 62b and 62c. The in-phase anomaly values measured were corrected for level offset in the data compilation.

Table 19

Test line Seinäjoki 190, interpretation results at earth resistivity sounding points 190/1, 190/2 and 190/3.

(a) Values of the total conductance σd (S) interpreted by various methods.

Method	Total conductance (S)		
	Point 190/1	Point 190/2	Point 190/3
Earth resistivity sounding	< 0.11	2.63	1.82
AEM	1.04	1.92	0.91
Slingram (l = 20 m)	not defined	3.34	0.70
(l = 40 m)	not defined	not defined	0.88
VLF-R	0.11	not defined	0.68
Double dipole EM	not defined	not defined	not defined

(b) Interpretation of various EM data by means of one-layer model. The depth to the upper surface of the conductor = da_1, apparent resistivity = ϱ_a.

Method	Point 190/1		Point 190/2		Point 190/3	
	da_1 (m)	ϱa (Ωm)	da_1 (m)	ϱa (Ωm)	da_1 (m)	ϱa (Ωm)
AEM	22	37	5	16	1	45
VLF-R	not applicable		6.6	10	not applicable	
Double dipole EM	not defined		5	5	5	10

(c) Interpretation of the earth resistivity sounding data by means of a multilayer model. Thickness of layer = d, apparent resistivity = ϱ_a.

Layer	Point 190/1		Point 190/2		Point 190/3	
	d (m)	ϱa (Ωm)	d (m)	ϱa (Ωm)	d(m)	ϱa (Ωm)
1	4.0	150	1.3	35	0.6	42
2	∞	950	4.8	12	1.8	18
3			16	4	13.2	11
4			∞	10000	∞	300

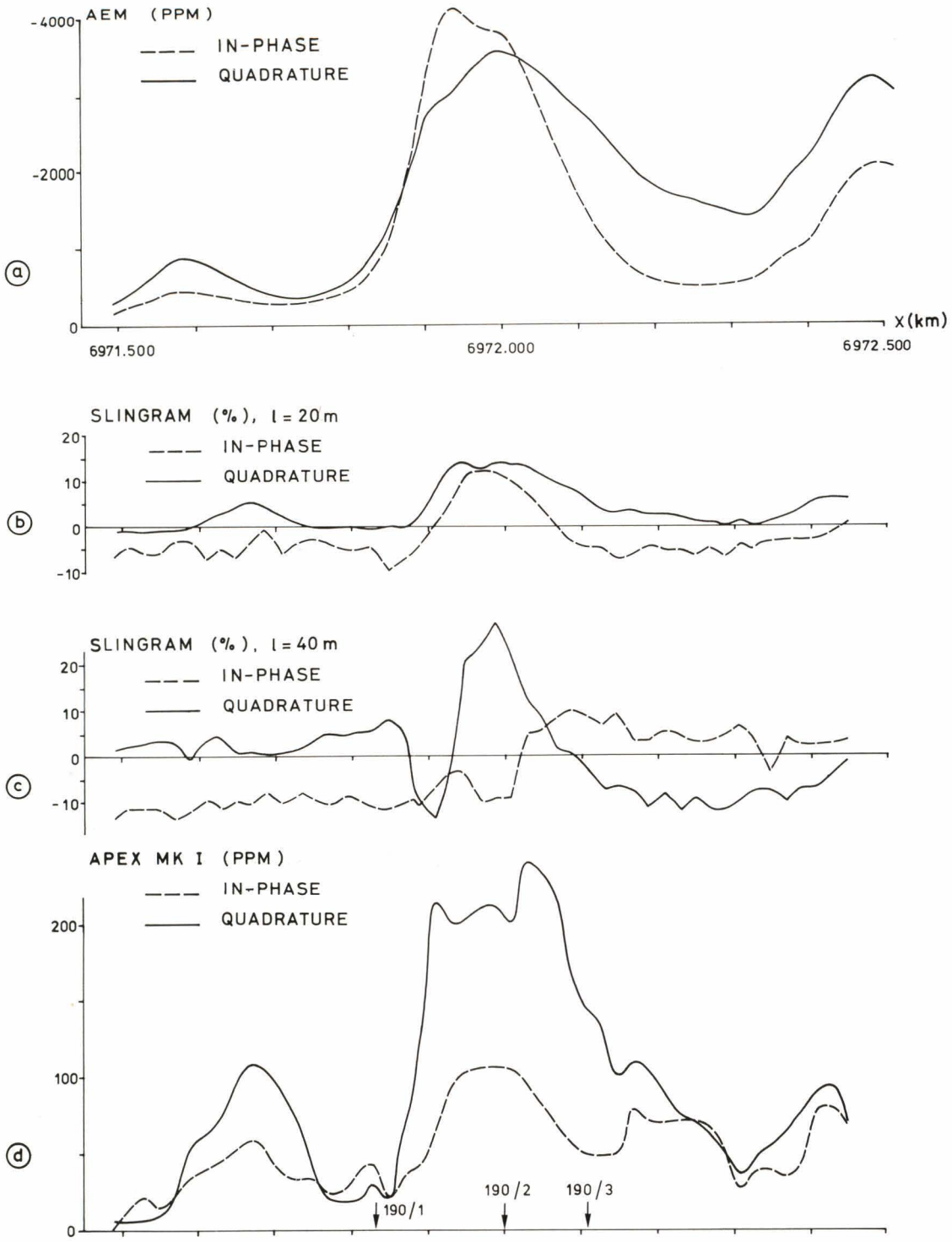

Fig. 62. Test line Seinäjoki 190, results of various EM methods. (a) AEM survey in-phase and quadrature data, point spacing $\Delta x = 28$ m. (b) Slingram survey in-phase, quadrature data with coil separation $l = 20$ m, $\Delta x = 20$ m. (c) Slingram survey in-phase, quadrature data with $l = 40$ m, $\Delta x = 20$ m. (d) Double dipole EM (Apex MK I) survey in-phase, quadrature data, $\Delta x = 20$ m.

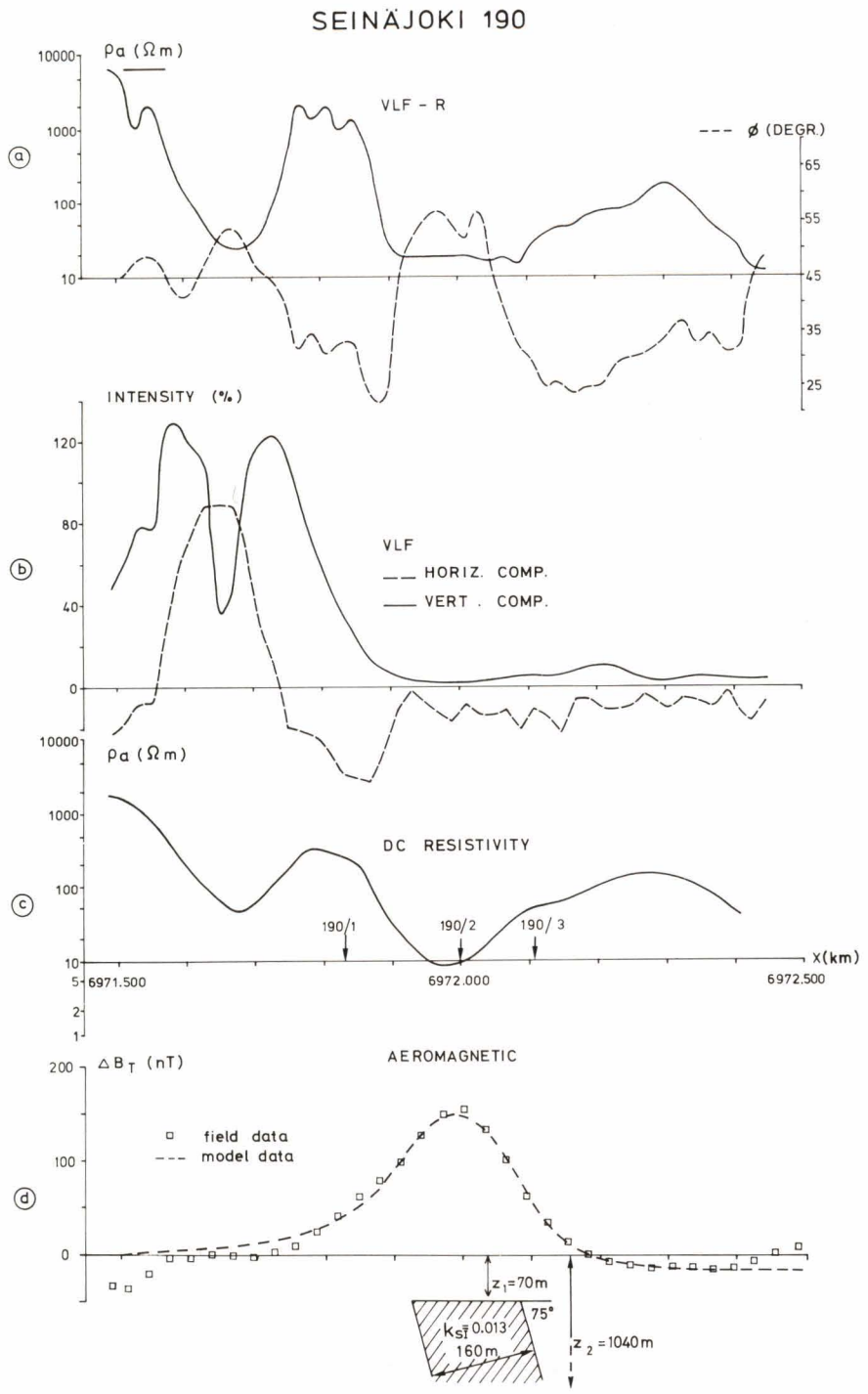

Fig. 63. Test line Seinäjoki 190, results of various methods. (a) VLF-R survey ϱ_a, Φ data, point spacing $\Delta x = 20$ m. (b) VLF survey H- and V-component data, $\Delta x = 20$ m. (c) DC earth resistivity profiling data, $\Delta x = 40$ m. (d) Aeromagnetic survey data, $\Delta x = 28$ m: anomaly values of the magnetic total field ΔB_T and their plate-model interpretation.

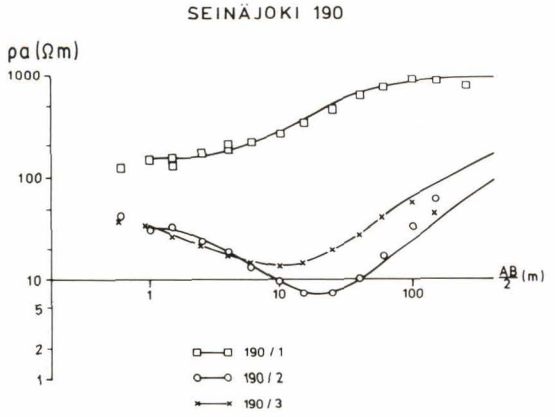

Fig. 64. Test line Seinäjoki 190, DC earth resistivity sounding results at points 190/1, 190/2 and 190/3. Half-value of the current electrode separation = AB/2, Schlumberger electrode configuration. Discrete points refer to survey data, curves denote the theoretical model results with the parameters of the models as listed in Table 19.

- Double dipole EM survey, results in Fig. 62d.
- VLF-R survey, results in Fig. 63a.
- VLF-H, V survey, results in Fig. 63b.
- Direct current resistivity profiling with Schlumberger electrode configuration (MN = 5 m, AB = 40 m), results in Fig. 63c.
- Aeromagnetic survey, results and interpretation in Fig. 63d.
- Resistivity soundings at three points, 190/1, 190/2 and 190/3, results in Fig. 64.

If not explicitly given, the specifications of the different survey methods were the same as on test line 198.

The test line was originally planned to exemplify an area with a gradual increase in the conductivity of the overburden. Later interpretation (cf. Fig. 63d) of the magnetic data, however, indicated the possibility of a deep-buried, steeply dipping and magnetised (black schist?) zone around x = 6972.0. It could explain the difficulties encountered in the application of layered earth models to the interpretation of EM, especially slingram, data.

The interpretation results of the conductive overburden at the resistivity sounding points are shown in Table 19. The result for sounding point 190/1 demonstrates that sulphide clay is absent and that the total conductance of the soil is low, $s_a < 0.1$ S (the asymptotic value has not yet been reached). Even so, it is still not possible to interpret the double dipole EM data with the two-layer model, but only with the half-space model. Since the anomaly values of the double dipole EM data are very low at this site (in-phase and quadrature values ≤ 40 ppm), the results are unreliable for the latter model as well. The value of the total conductance at this point is so low that the anomaly values produced by the slingram survey are below the noise level of the instrument.

At sounding points 190/2 and 190/3 the composition of the overburden is similar to that on test line 198, i.e. it includes a conductive ($\varrho \leq 10\ \Omega$ m) clay layer. Thus, at point 190/2 the conductance is so high that the penetration of the VLF-R method is insufficient and the method gives no more than an estimate of the depth to the upper surface and of the conductivity of the clay layer (Table 19). The change in the coil separation in the slingram surveys from 20 m to 40 m shifts the data points beyond the definition area of the characteristic diagrams of one-layer and two-layer models. At point 190/3 the penetration of all the methods, the double dipole EM method excluded, is sufficient to establish the total conductance.

The total conductance values interpreted from the various measurements on the test line and covering the whole profile are shown in Fig. 65. The data indicate that by combining the slingram and VLF-R methods the conductance can be interpreted along the whole profile. Alone, neither of the methods is sufficient. Within the region 0.5–1.0 S both methods work well and the results are in good agreement. The interpreted AEM sur-

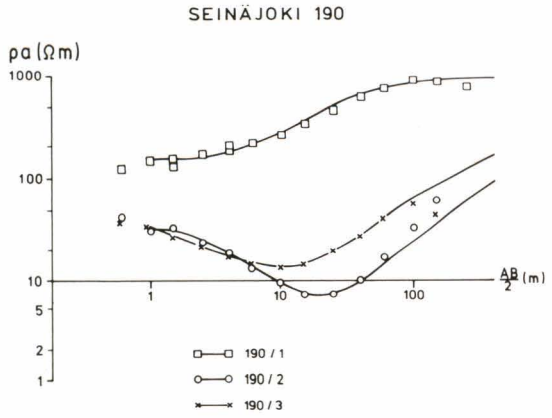

Fig. 64. Test line Seinäjoki 190, DC earth resistivity sounding results at points 190/1, 190/2 and 190/3. Half-value of the current electrode separation = AB/2, Schlumberger electrode configuration. Discrete points refer to survey data, curves denote the theoretical model results with the parameters of the models as listed in Table 19.

- Double dipole EM survey, results in Fig. 62d.
- VLF-R survey, results in Fig. 63a.
- VLF-H, V survey, results in Fig. 63b.
- Direct current resistivity profiling with Schlumberger electrode configuration (MN = 5 m, AB = 40 m), results in Fig. 63c.
- Aeromagnetic survey, results and interpretation in Fig. 63d.
- Resistivity soundings at three points, 190/1, 190/2 and 190/3, results in Fig. 64.

If not explicitly given, the specifications of the different survey methods were the same as on test line 198.

The test line was originally planned to exemplify an area with a gradual increase in the conductivity of the overburden. Later interpretation (cf. Fig. 63d) of the magnetic data, however, indicated the possibility of a deep-buried, steeply dipping and magnetised (black schist?) zone around x = 6972.0. It could explain the difficulties encountered in the application of layered earth models to the interpretation of EM, especially slingram, data.

The interpretation results of the conductive overburden at the resistivity sounding points are shown in Table 19. The result for sounding point 190/1 demonstrates that sulphide clay is absent and that the total conductance of the soil is low, $s_a < 0.1$ S (the asymptotic value has not yet been reached). Even so, it is still not possible to interpret the double dipole EM data with the two-layer model, but only with the half-space model. Since the anomaly values of the double dipole EM data are very low at this site (in-phase and quadrature values ≤ 40 ppm), the results are unreliable for the latter model as well. The value of the total conductance at this point is so low that the anomaly values produced by the slingram survey are below the noise level of the instrument.

At sounding points 190/2 and 190/3 the composition of the overburden is similar to that on test line 198, i.e. it includes a conductive ($\varrho \leq 10$ Ω m) clay layer. Thus, at point 190/2 the conductance is so high that the penetration of the VLF-R method is insufficient and the method gives no more than an estimate of the depth to the upper surface and of the conductivity of the clay layer (Table 19). The change in the coil separation in the slingram surveys from 20 m to 40 m shifts the data points beyond the definition area of the characteristic diagrams of one-layer and two-layer models. At point 190/3 the penetration of all the methods, the double dipole EM method excluded, is sufficient to establish the total conductance.

The total conductance values interpreted from the various measurements on the test line and covering the whole profile are shown in Fig. 65. The data indicate that by combining the slingram and VLF-R methods the conductance can be interpreted along the whole profile. Alone, neither of the methods is sufficient. Within the region 0.5–1.0 S both methods work well and the results are in good agreement. The interpreted AEM sur-

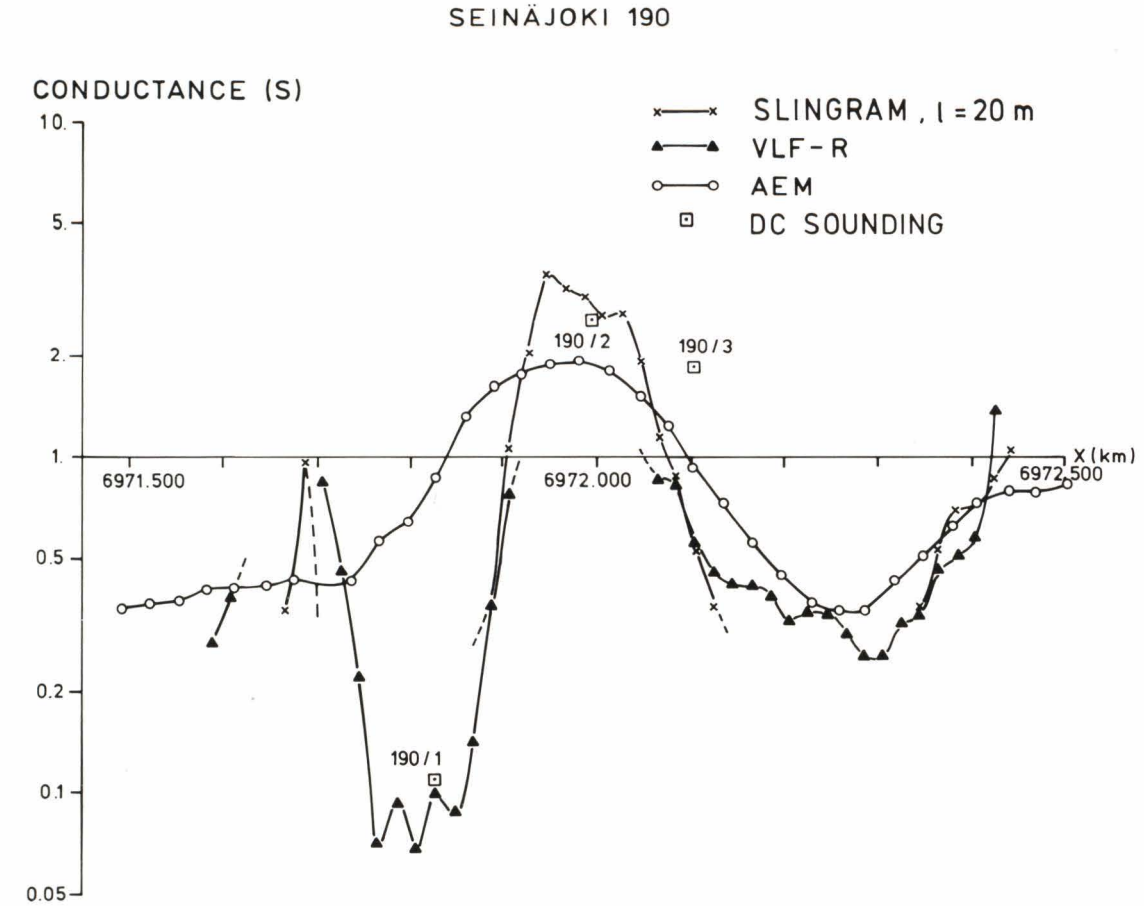

Fig. 65. Test line Seinäjoki 190, the values of apparent conductance s_a of the conductive horizontal thin-layer model calculated from the data of various methods.

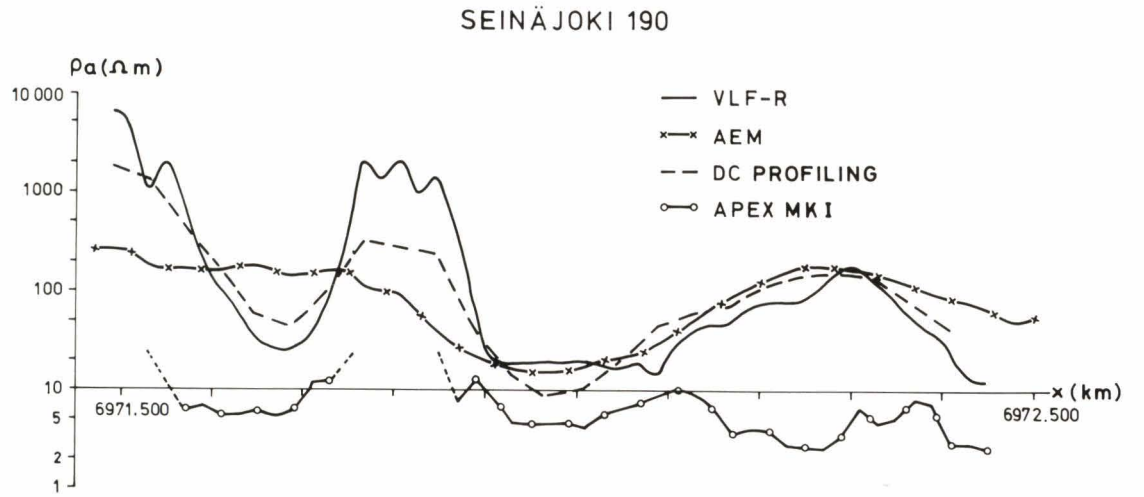

Fig. 66. Test line Seinäjoki 190, the values of apparent resistivity ϱ_a of the conductive half-space model calculated from the data of various methods.

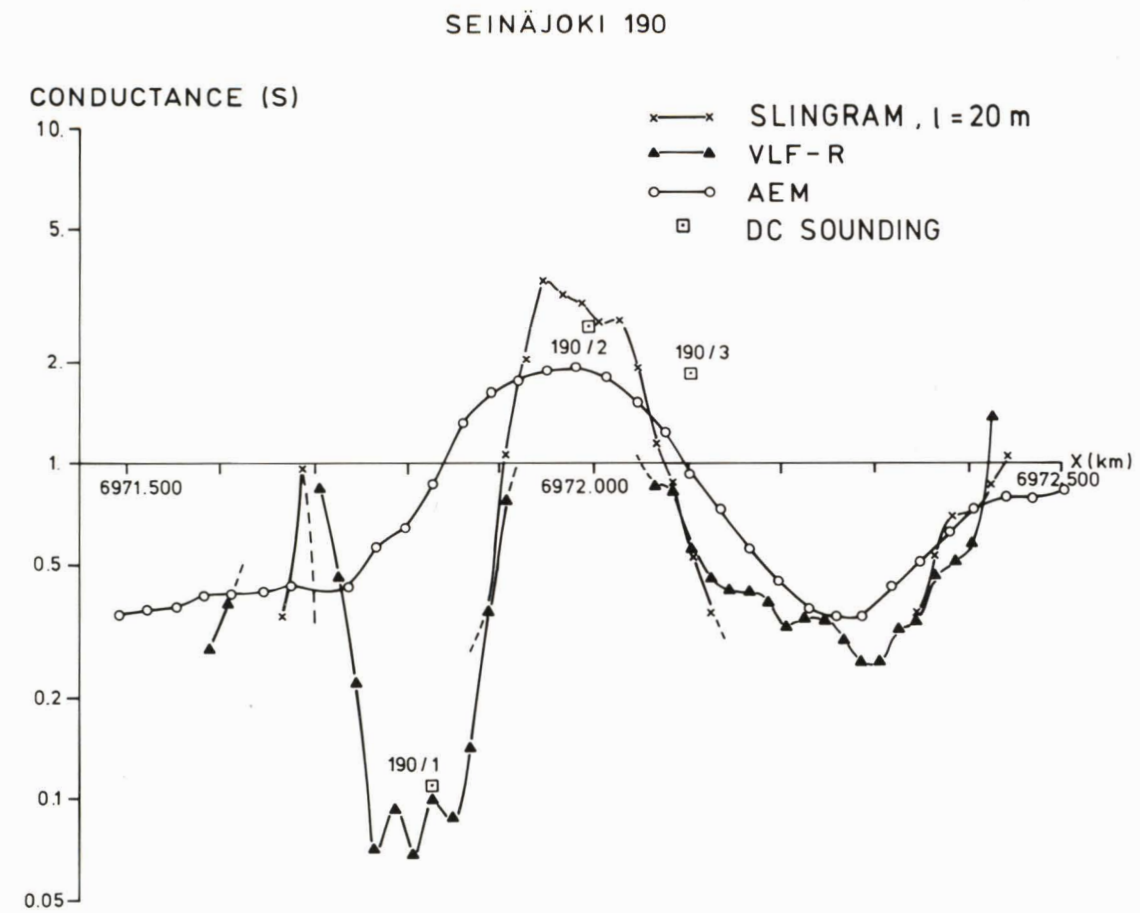

Fig. 65. Test line Seinäjoki 190, the values of apparent conductance s_a of the conductive horizontal thin-layer model calculated from the data of various methods.

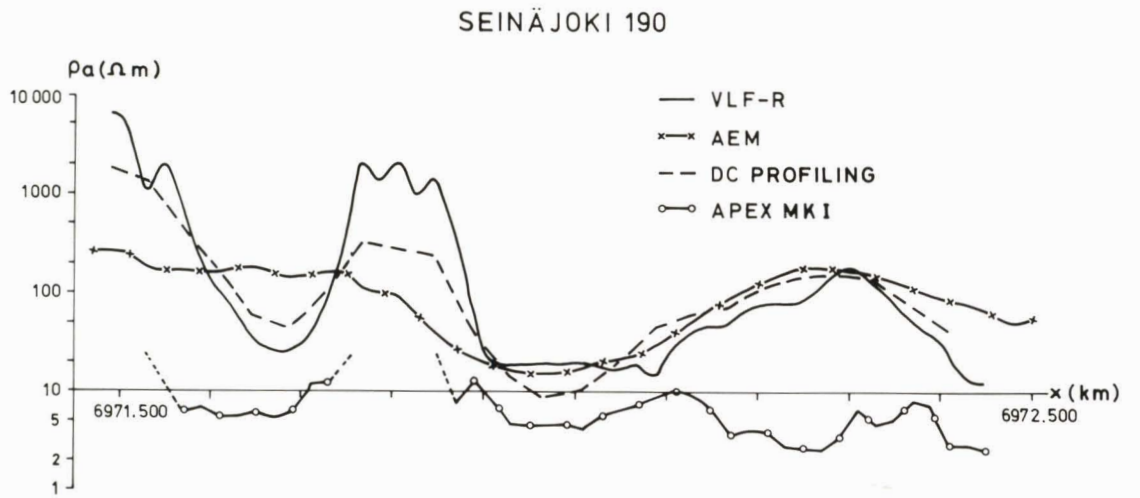

Fig. 66. Test line Seinäjoki 190, the values of apparent resistivity ϱ_a of the conductive half-space model calculated from the data of various methods.

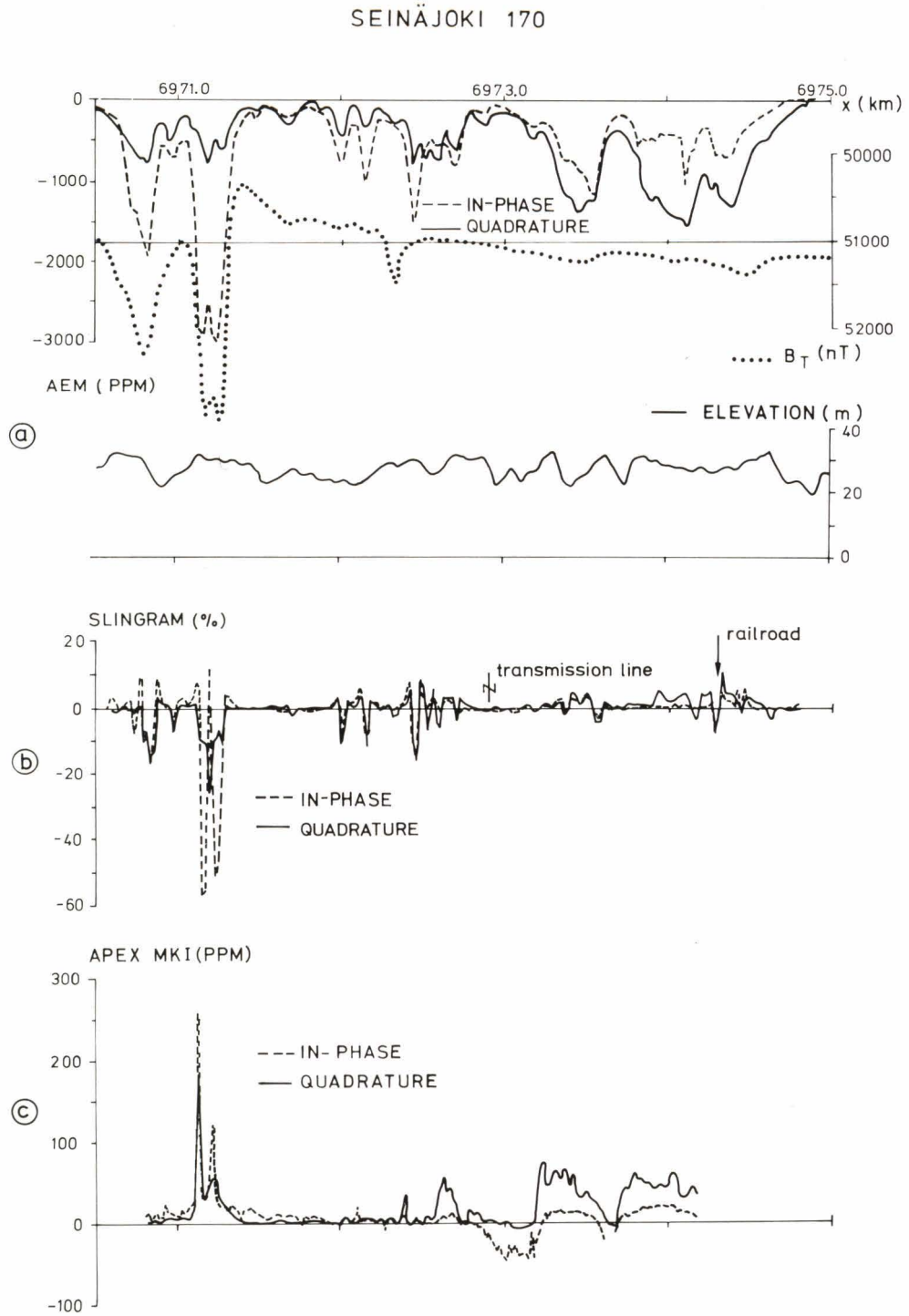

Fig. 67. Test line Seinäjoki 170, results of various geophysical methods. (a) DC-3 aerogeophysical survey, AEM, aeromagnetic and flight elevation data, point spacing $\Delta x = 28$ m. (b) Slingram in-phase, quadrature data, $\Delta x = 20$ m. (c) Double dipole EM (Apex MK I) survey in-phase, quadrature data, $\Delta x = 10$ m.

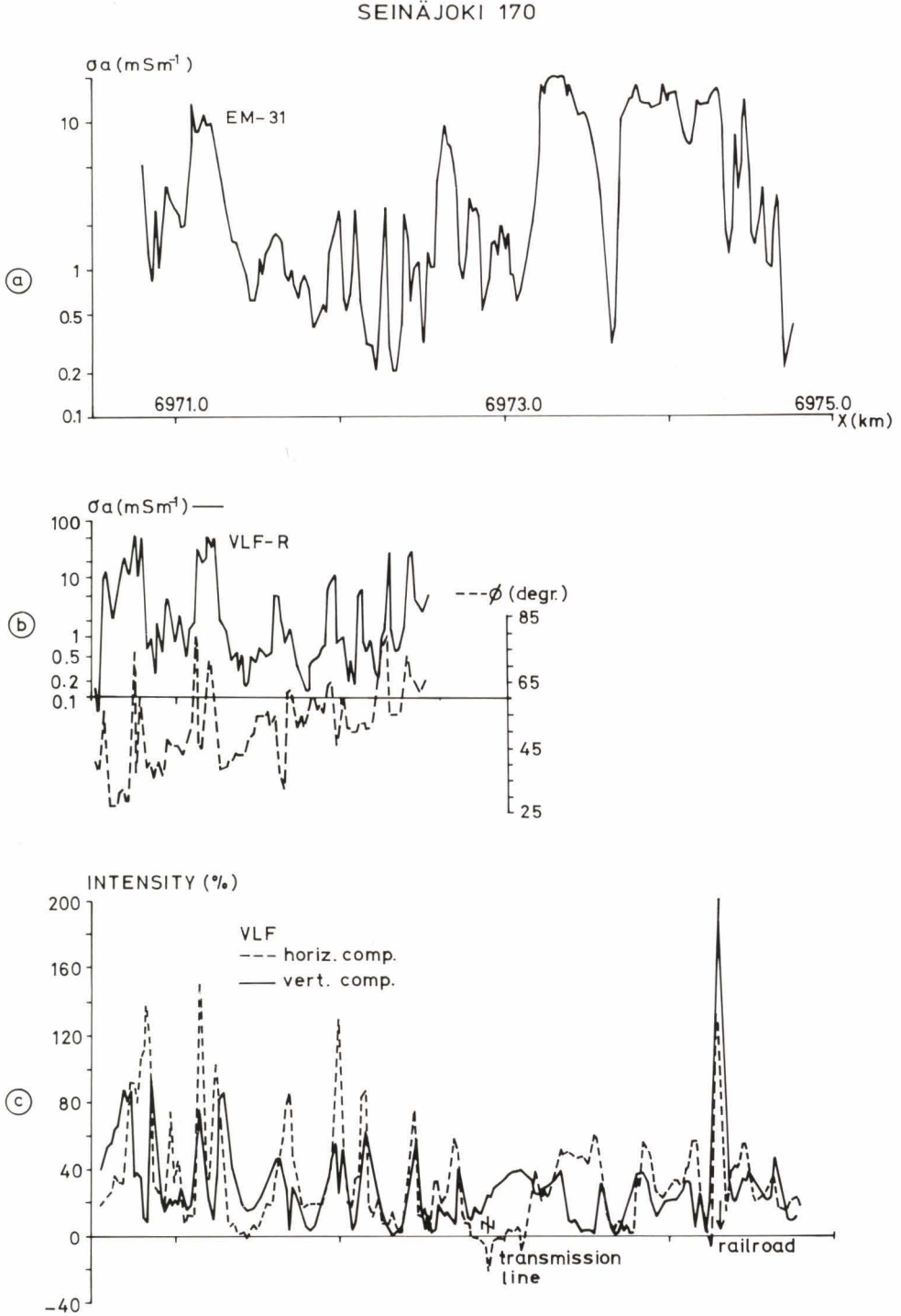

Fig. 68. Test line Seinäjoki 170, results of various EM measurements. (a) Geonics EM-31 data, values of apparent conductivity σ_a, point spacing $\Delta x = 10$ m. (b) VLF-R survey σ_a, ϕ data, $\Delta x = 20$ m. (c) VLF survey H- and V-component data, $\Delta x = 20$ m.

vey data also correlate well with the ground survey data at the northern end of the profile. On account of the flight elevation and the data processing method (five-point smoothing), the resolution of the AEM data is poorer, and the narrow resistive area between x = 6971.75–.85 is not shown by the AEM results.

The measured and interpreted (one-layer model) values of the apparent resistivity are shown in Fig. 66. The ϱ_a values of the VLF-R and DC resistivity profiling survey correlate very well with each other and fairly well with the AEM ϱ_a values. The VLF-R survey data also provide the values of the phase angle Φ, and hence the interpretability of the data (cf. Fig. 65) is better than in the DC resistivity profiling. The operational costs of the method are also lower and thus, in soil studies, VLF-R surveying could evidently largely replace DC resistivity profiling. At the southern end of the profile the ϱ_a interpretation results of the double dipole EM survey (Fig. 66) exhibit a variation similar to that of the other data. The ϱ_a values obtained are about a decade smaller than those given by other methods. This means a zero-level difference of about 10–30 ppm in the in-phase component values and thus illustrates the accuracy needed in adjusting and reading the instrument.

Line 170

The following measurements were undertaken on test line 170 (y = 434.0, between x = 6970.500–6974.800):

- AEM and aeromagnetic survey, results in Fig. 67a.
- Slingram survey with coil separation l = 40 m, results in Fig. 67b.
- Double dipole EM survey, results in Fig. 67c.
- Survey with a Geonics EM-31 electromagnetic conductivity meter with l = 3.66 m and f = 8 kHz, results in Fig. 68a.
- VLF-R survey (between x = 6970.500–6972.500), results in Fig. 68b.
- VLF-H, V survey, results in Fig. 68c.

The test line is located in an area in which the overburden lacks saline clay beds, although there are soils of weaker conductivity in the northern part of the test line. In the southern part there are several isolated narrow black schist layers in the bedrock that generate strong EM and magnetic anomalies. The difference in conductivity between the northern and southern parts of the test line can be directly seen as a change in the Re/Im ratio on the AEM and slingram data, but not on the EM-31 and VLF data. The anomalies measured with different methods coincide well with each other. The observation point spacing in the ground surveys was either 10 m or 20 m and hence, the results do not differ markedly in resolution. The EM results can, however, be arranged in order of declining resolution so that the VLF-R and EM-31 methods have the best resolution and the slingram method the next best. The poorest resolution is shown by the VLF-H, V method. The resolution of the AEM data (h = 30 m, Δx = 28 m) is only slightly poorer than that of the slingram data.

The AEM data were transformed into apparent resistivity values with the one-layer model, and the results are shown in Fig. 69. The measured ϱ_a values of the EM-31 survey are also shown in the figure. It can be claimed that the discrimination ability of the transformed AEM data exceeds that of the EM-31 and VLF-R results. In the northern part of the test line the ϱ_a values with different methods agree well with each other. For the southern part with black schist conductors the EM-31 and VLF-R ϱ_a values are about two

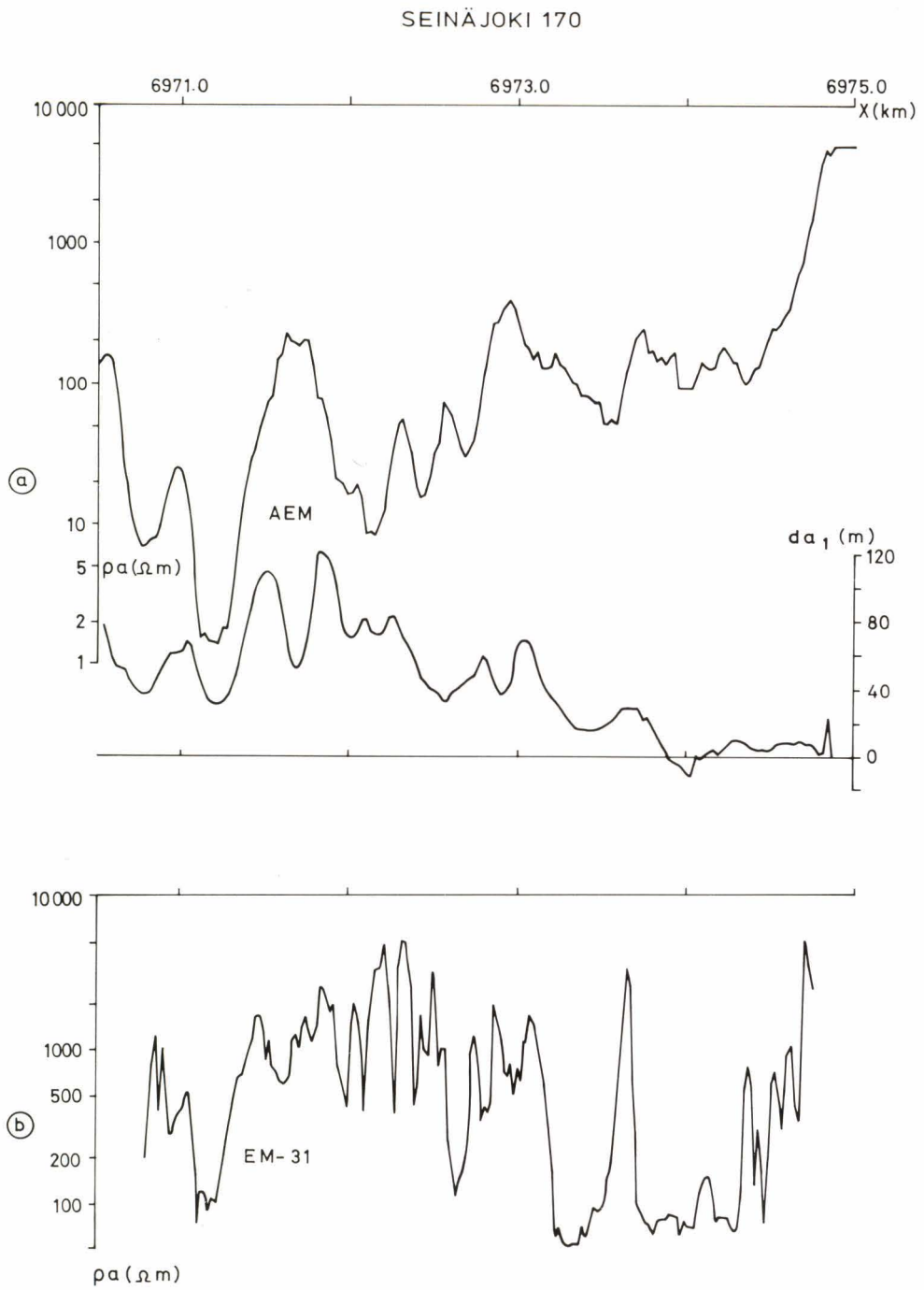

Fig. 69. Test line Seinäjoki 170, comparison of EM results. (a) Values of apparent resistivity ϱ_a and apparent depth da_1 calculated from AEM data by means of the conductive half-space model. (b) Values of apparent resistivity ϱ_a measured with a Geonics EM-31 conductivity meter.

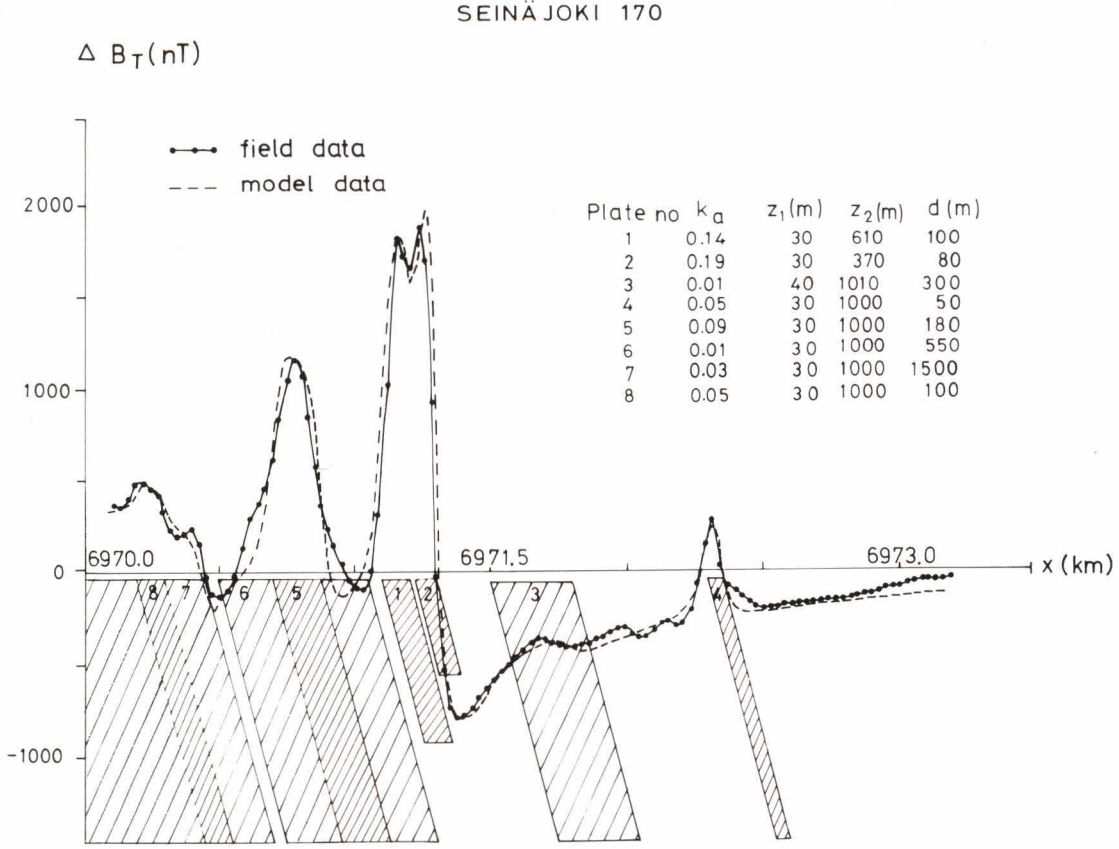

Fig. 70. Test line Seinäjoki 170, aeromagnetic survey data: anomaly values of the magnetic total field ΔB_T and their plate-model interpretation, point spacing Δx = 28 m. The dip angle α = 75° N is constant.

decades higher than the AEM transform values. The difference must be due to the greater penetration of the AEM method. For this reason and in spite of the unsuitability of the theoretical model, the transformed data could give conductivity values of the right order of magnitude even for the sheet-like, dipping conductors in the bedrock.

The aeromagnetic data for the southern part of the test line have been interpreted with plate models, and the outcome is given in Fig. 70. According to the results, the black schist layers are covered with a thin layer of overburden and dip steeply northwards. The two strongest adjacent sources of EM and aeromagnetic anomalies around x = 6971.2 have smaller depth extents than the other formations. The AEM and slingram anomalies of these sources have been tentatively interpreted with a combination of thick and thin half-plane models in Fig. 71. The modelling results are not extensive enough to allow a good fit between the measured and the model data.

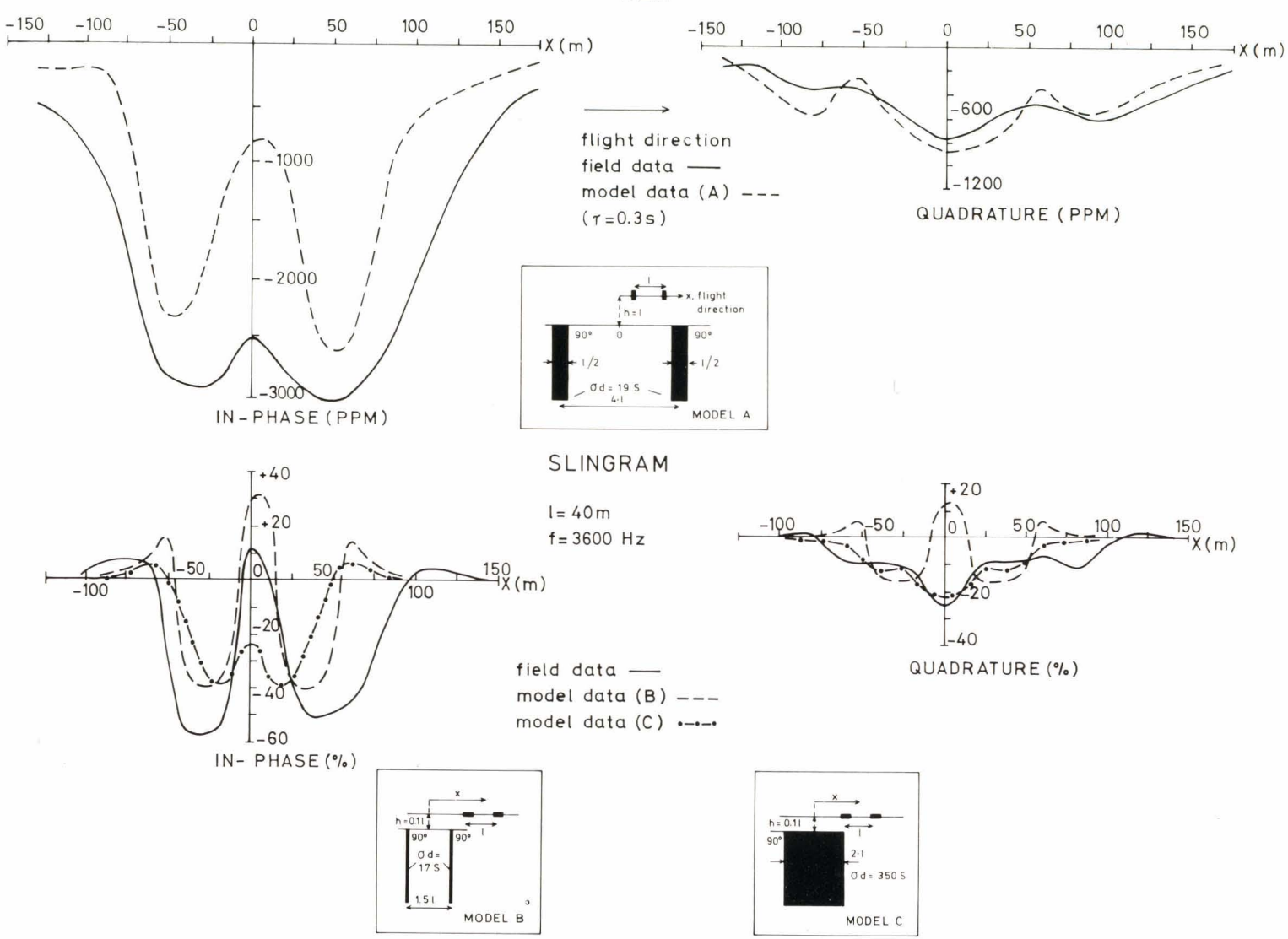

Fig. 71. Test line Seinäjoki 170, interpretation of the AEM and slingram anomalies around x = 6971.2 (see Fig. 67) with different half-plane conductor models.

Summary of the results for the Seinäjoki test area

The results for the Seinäjoki test area can be summarised as follows:

- The transformation of the AEM data by means of one-layer and two-layer models was feasible in practice and made the classification of the different types of conductors easier than when it was based on the original anomaly data. The small size of the conductor is emphasised in the apparent depth values, and in other respects, too, the usability of the apparent depth map seems to be restricted.
- Comparison between the various EM data shows that the compatibility of the quadrature component values is surprisingly good considering the differences in coil separation and distance to the conductor. The differences in penetration between the methods are due to the behaviour of the signal/noise ratio as a function of the h/*l*-ratio, which, in the slingram and AEM data, is significantly better than in the double dipole EM-data.
- The results for the test area show that the total conductance of the overburden can be interpreted by various methods as follows: the double dipole EM data can usually be interpreted only visually; the VLF-R survey data were applicable up to s_a values of about 1 S and the slingram survey data (l = 20–40 m, f = 3 600 Hz) up to about 4 S. For the AEM survey and the DC resistivity sounding data, the upper limit is still higher and was not reached during the measurements.
- Total conductance appears to be the most reliable result of interpretation of conductive overburden for all the electromagnetic measurements. The σ and d values cannot be obtained separately, except as very rough estimates, even if the results of various methods are combined. Thus, for example, the solution of the three-layer model

  d_1 σ_1 (low, e.g. organic soil)
  d_2 σ_2 (high, e.g. clay)
  σ_3 (low, e.g. till)

  would be theoretically possible as a combination of the VLF-R and slingram or AEM methods (d_1 and σ_2 are obtained by interpreting VLF-R data, $d_2\sigma_2$ by interpreting the slingram or AEM data), but the results obtained in practice were not reliable.
- For the conductive overburden and within the limits of penetration, the VLF-R survey seems to be more advantageous than the DC resistivity profiling method in both interpretability and operation costs.
- Provided that the survey is done carefully, the double dipole EM data can be interpreted to some extent with the aid of the one-layer model.

Tervo: Conductive zones in bedrock overlain by poorly conductive overburden

The target, which covers map sheets 3313 08 Utrianlahti and 3313 11 Talluskylä, is an example of AEM anomalies caused by different types of bedrock conductors overlain by poorly conductive glacial soils. The example includes the response to a buried conductor in the Sorosuo area and the comparison of AEM and induced polarisation (IP) survey data on the Luvelahti area.

The bedrock of the study area is part of

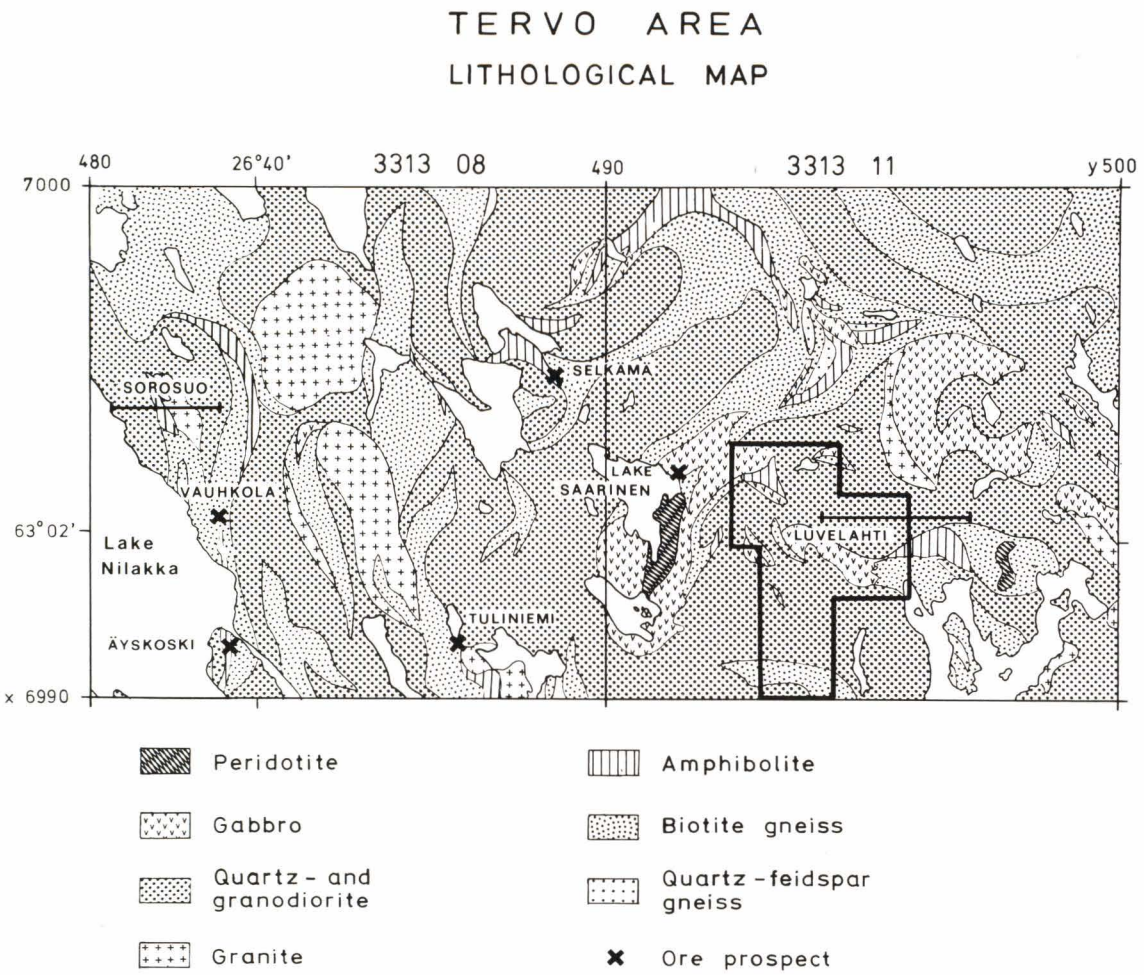

Fig. 72. Lithological map of the Tervo area according to Ekdahl (1976b). The target areas of Sorosuo and Luvelahti are marked on the map.

the Savo schist zone and is composed mainly of various gneisses, amphibolites, quartz diorites, granodiorites and granites, as shown by the geological map by Ekdahl (1976b) in Fig. 72. In places the gneisses contain garnet, cordierite and anthophyllite. The western part of the study area (map sheet 3313 08) exhibits a few small mafic bodies, and the eastern part (map sheet 3313 11) the larger Saarinen-Luvelahti zone of mafic and ultramafic rocks. The Quaternary geology of the area is characterised by moraine cover (Tenhola 1979). The till layers average from a few metres up to 10 m in thickness, but reach 30 to 40 m in the drumlins. At least two till beds of different ages have been established. The Koivulahti-Pulkonkoski zone, the predominant esker formation, has been classified as an end moraine. Topographically, the area is fairly flat although relatively large local variations in elevation (50–70 m) occur due to drumlins and eskers. There is a high proportion of lakes and bogs in the surface area, and the lake sediments include, at least in some places, clay and gyttja.

The schists and mafic rocks in the area

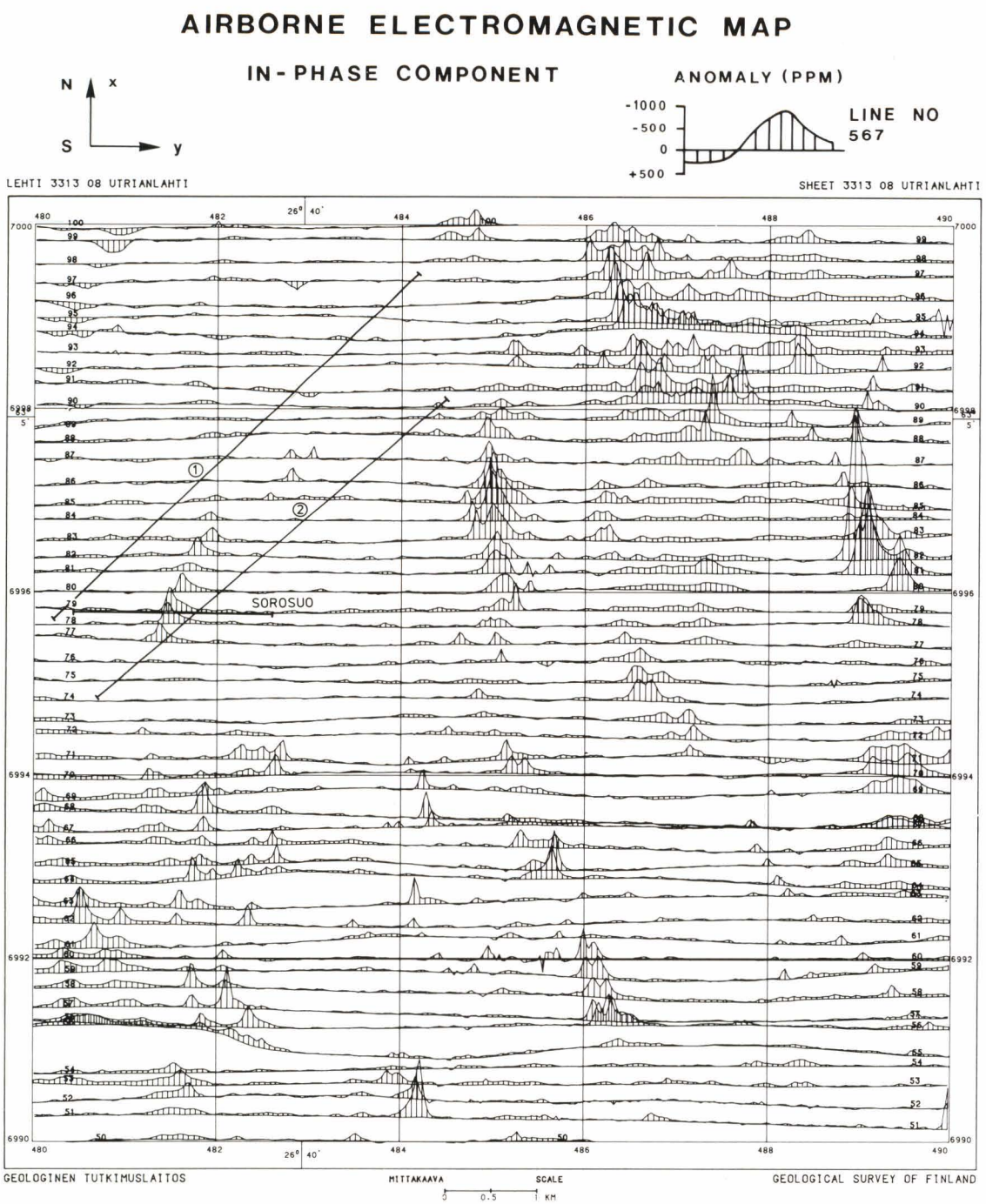

Fig. 73. DC-3 AEM survey data, map sheets 3313 08 and 3313 11 (Tervo area). The target areas of Sorosuo and Luvelahti and the till sampling profiles (1,2) are marked on the maps. (a) In-phase component (see pages 136–137). (b) Quadrature component (see pages 138–139).

AIRBORNE ELECTROMAGNETIC MAP

IN-PHASE COMPONENT

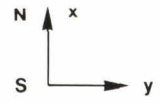

ANOMALY (PPM)

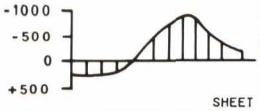

LEHTI 3313 11 TALLUSKYLÄ

SHEET 3313 11 TALLUSKYLÄ

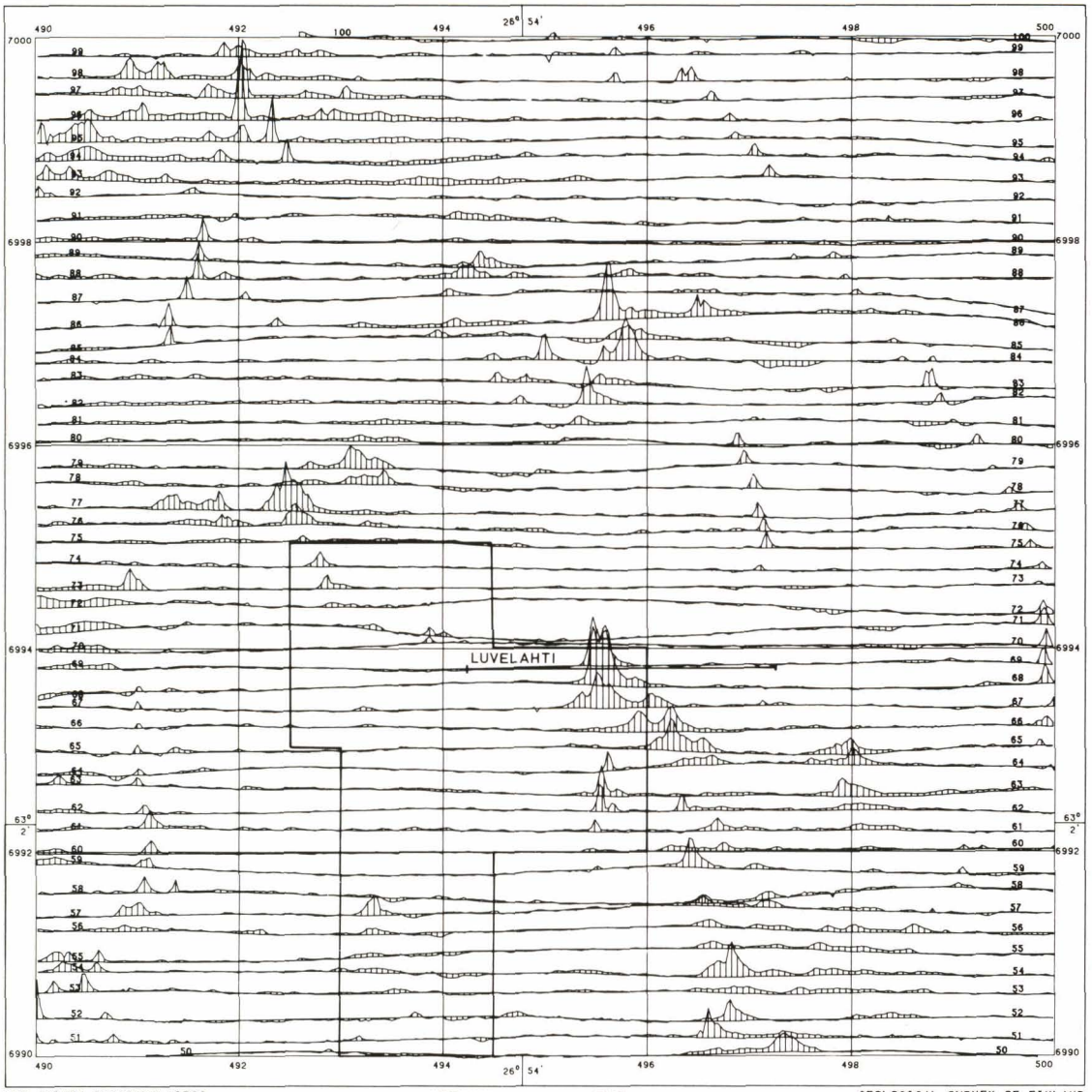

GEOLOGINEN TUTKIMUSLAITOS

MITTAKAAVA SCALE

0 0.5 1 KM

GEOLOGICAL SURVEY OF FINLAND

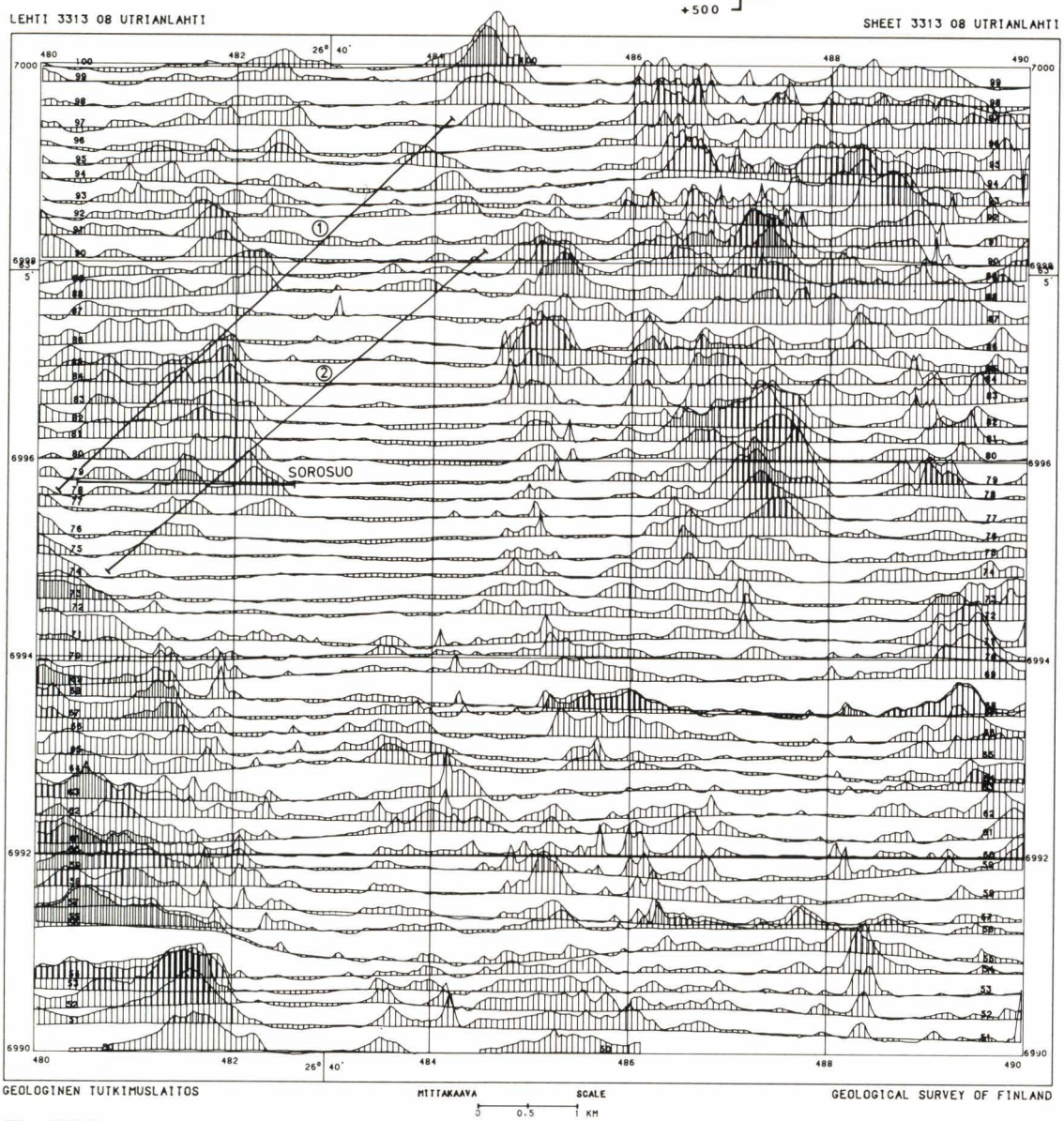
AIRBORNE ELECTROMAGNETIC MAP
QUADRATURE COMPONENT
ANOMALY (PPM)
-1000
-500
0
+500
LINE NO
567
N
S
x
y
LEHTI 3313 08 UTRIANLAHTI
SHEET 3313 08 UTRIANLAHTI
SOROSUO
①
②
480
482
484
486
488
490
6990
6992
6994
6996
7000
26° 40'
GEOLOGINEN TUTKIMUSLAITOS
GEOLOGICAL SURVEY OF FINLAND
MITTAKAAVA
SCALE
0 0.5 1 KM

Fig. 73 b)

AIRBORNE ELECTROMAGNETIC MAP

QUADRATURE COMPONENT

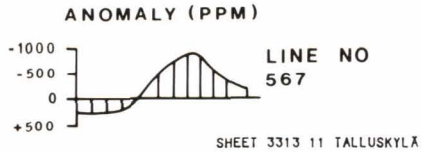

LEHTI 3313 11 TALLUSKYLÄ

SHEET 3313 11 TALLUSKYLÄ

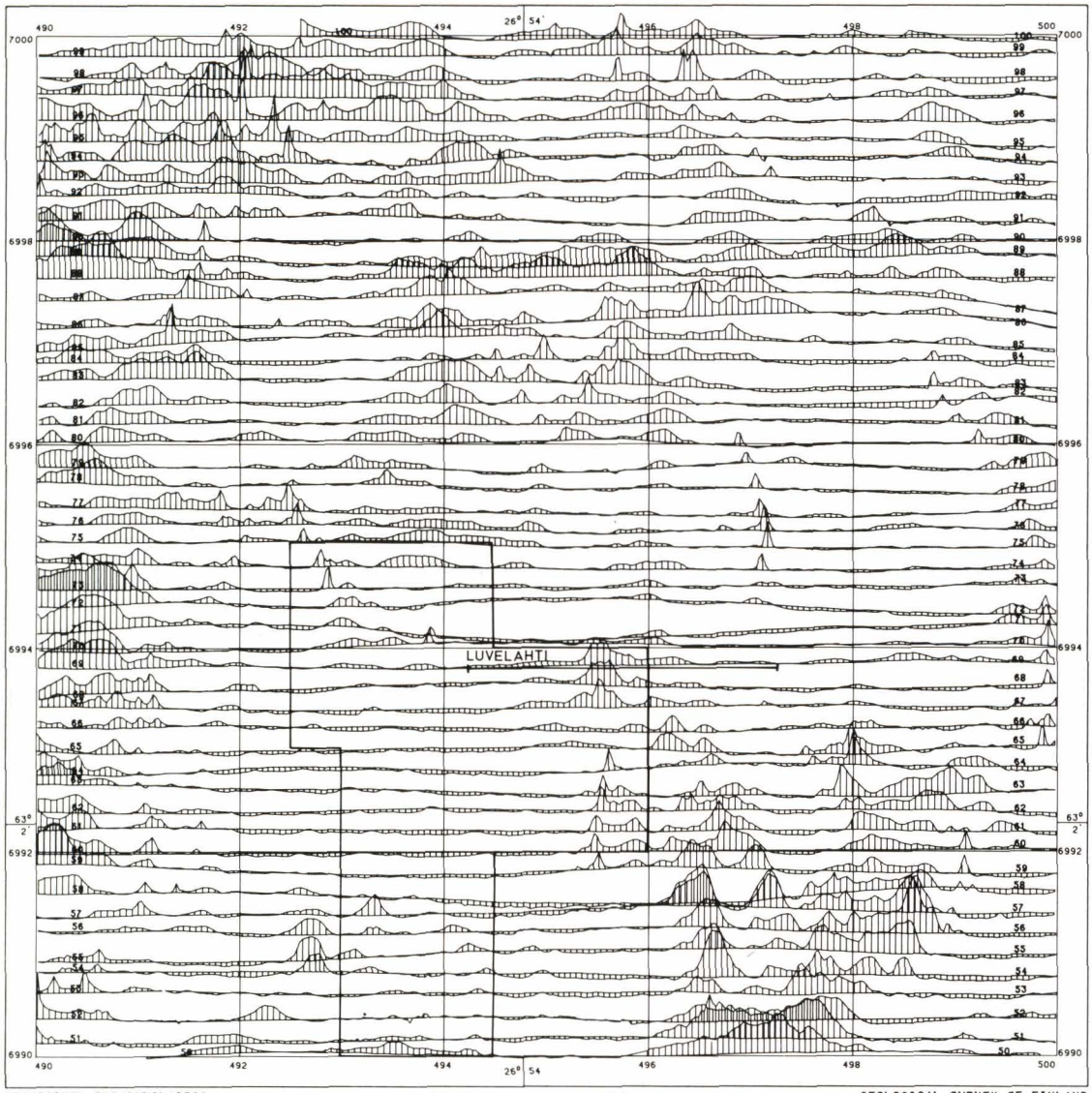

GEOLOGINEN TUTKIMUSLAITOS

MITTAKAAVA SCALE 0 0.5 1 KM

GEOLOGICAL SURVEY OF FINLAND

Fig. 73 b)

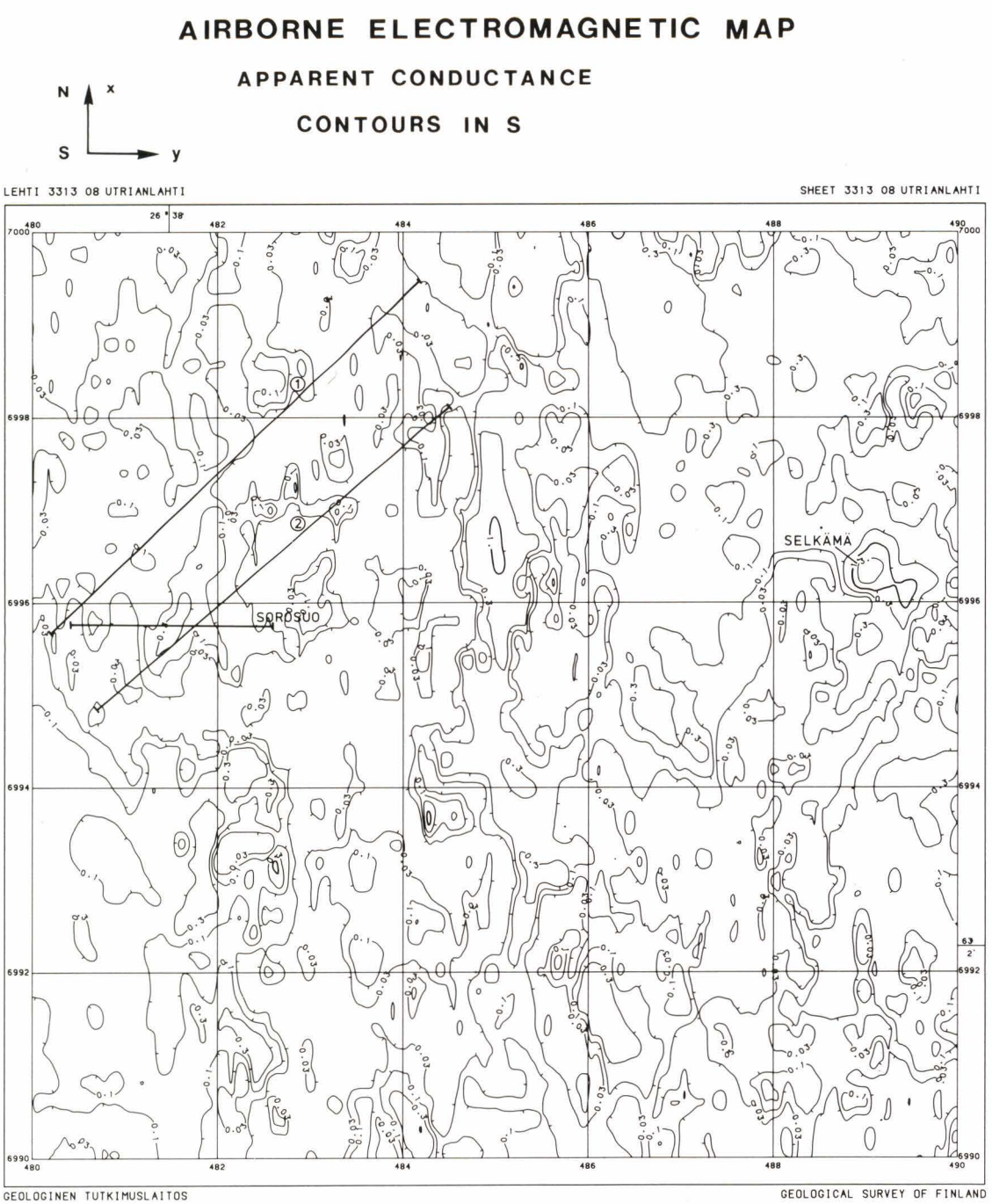

Fig. 74. The values of apparent conductance s_a of map sheets 3313 08 and 3313 11 (Tervo area) calculated from the AEM data in Fig. 73 by means of a thin conductive horizontal layer model. The target areas of Sorosuo and Luvelahti and the till sampling profiles (1,2) are marked on the map (see pages 140–141).

AIRBORNE ELECTROMAGNETIC MAP

APPARENT CONDUCTANCE

CONTOURS IN S

LEHTI 3313 11 TALLUSKYLÄ

SHEET 3313 11 TALLUSKYLÄ

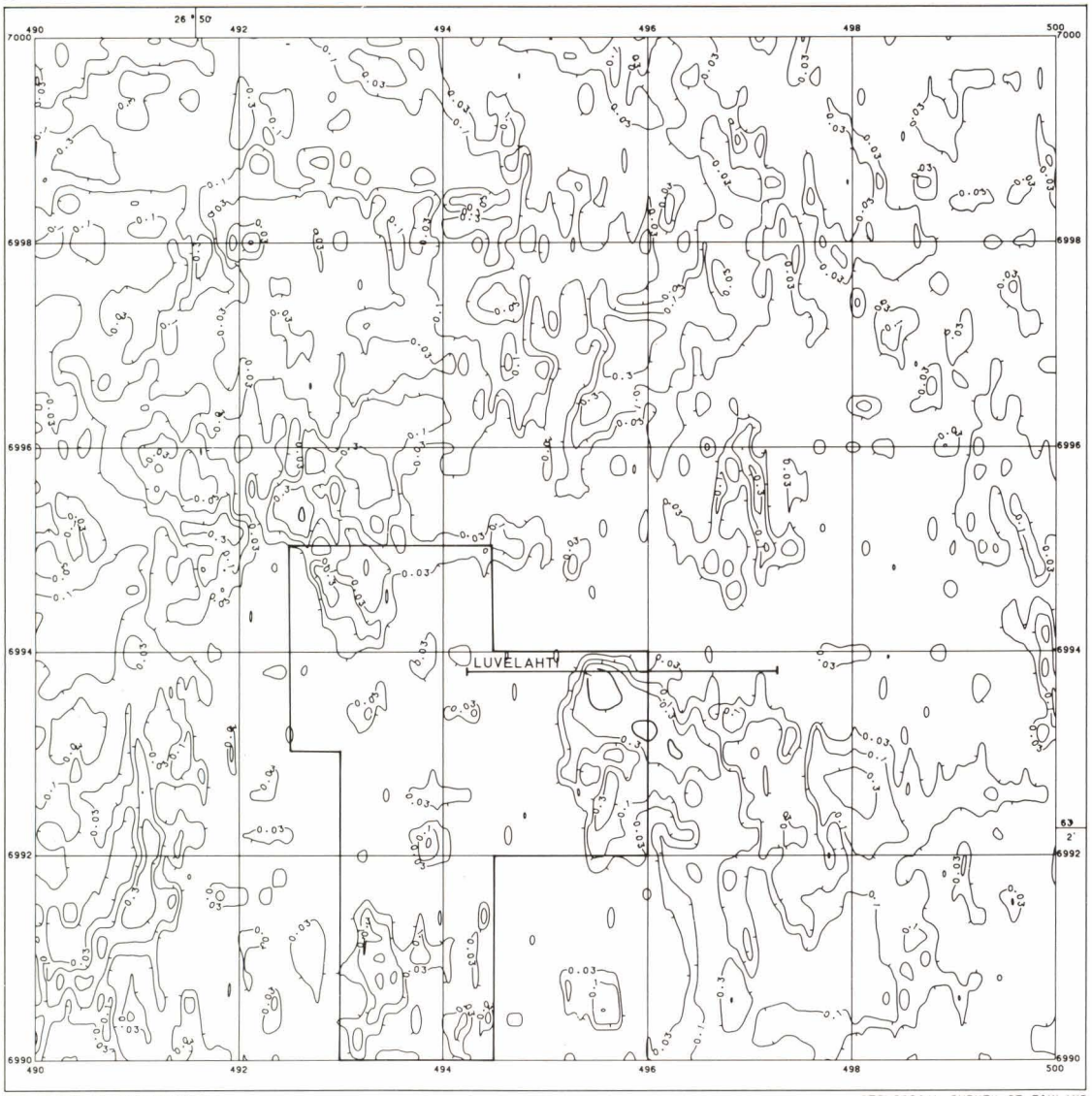

GEOLOGINEN TUTKIMUSLAITOS

GEOLOGICAL SURVEY OF FINLAND

have been subject to exploration since the 1950's. The major prospects have been the Äyskoski and Vauhkola Zn mineralisations and the Saarinen-Luvelahti Ni–Cu mineralisation. Several smaller prospects and some high-grade Zn, Cu and Ni floats, whose source has not yet been established, are also known in the area (Ekdahl 1976b, Västi 1978). The Säviä Cu–Zn deposit described on pages 172–186 is located in the same schist zone, some 15 km north of the test area.

The area was studied with AEM high-elevation survey in 1960 and low-elevation survey in 1978. The outcome of the latter is shown as profile maps in Fig. 73. Apart from the airborne surveys, diverse and extensive ground measurements have been conducted in the area; some targets have been tested with diamond-core drilling. Geochemical till sampling has been extended over the whole area. In the western part (map sheet 3313 08) the samples were taken from the greatest depth possible using a light percussion drill (Tenhola 1979). The maximum depth attained was 10 m.

In the AEM anomaly maps, the effects of the extensive weak conductors manifest themselves as large quadrature component anomaly zones in which the amplitudes vary between −200 and −1 000 ppm. The zones are related to the lake and bog areas, i.e. conductive overburden. The in-phase component data (Fig. 73a) differ distinctly from the quadrature component data, the anomalies being better defined and areally much more restricted. Except for the zone of positive in-phase anomalies in the NW corner of the area, which is caused by susceptive schists that contain disseminated magnetite, most of the in-phase anomaly bands are due to bedrock conductors. The in-phase anomaly map reveals that there are AEM anomalies associated with most of the ore showings and prospects located in the study area. For exploration applications, the in-phase component data are significantly more useful than the quadrature component data in the delineation of the bedrock conductor zones and in the appraisal of the anomalies. This conclusion is supported by other examples of the DC-3 AEM data.

If the anomaly maps are compared with the transformation map (Fig. 74) produced by applying the horizontal conductor model, the transformation can be judged as technically successful, although the original anomaly values are much lower than in the previous example. In the resistive areas the s_a values are ≤ 0.01 S, in the areas of poorly conductive overburden 0.01–0.1 S, and over the bedrock conductors generally 0.1–3.0 S. The Selkämä conductor around x = 6996.4 and y = 489.0, which produces a small but strong anomaly, shows the best conductance. In this test area, however, the conductance map does not yield as much useful exploratory information as do the original in-phase component data; rather, it must be pointed out that conductors that generate a very small indication, such as the Cu showing in the Saarisenjärvi gabbro, do not show up in the s_a values owing to smoothing and the contour map form of presentation.

The transformation map demonstrates that the conductance values also fluctuate somewhat in poorly conductive till-covered areas. If the sensitivity of the AEM results were high enough, they might possibly be of assistance in the planning of geochemical till sampling. Fig. 75 shows a comparison between the penetration of the till blanket at the sampling points along the two test profiles and the corresponding values of quadrature component AEM data. It must be noted that from the 67 sampling points along the test profiles, only 2 reached the bedrock surface. Even so, the variables are moderately correlated with each other. Test line 1 does not cross any known bedrock conductors. On test line 2 the correlation is also clear,

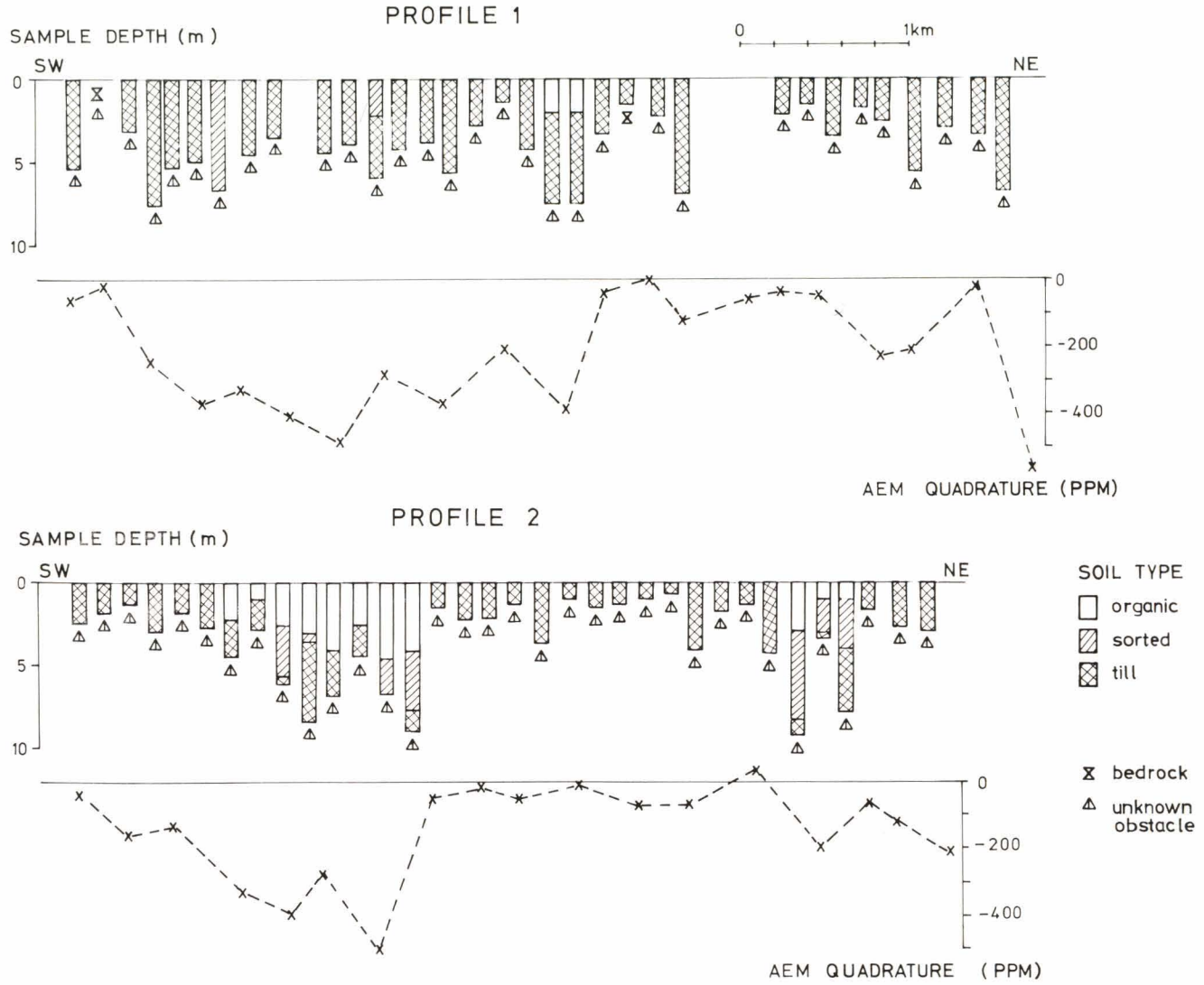

Fig. 75. The values of AEM quadrature component anomaly data compared with the composition and thickness data of the overburden at the sampling points of the geochemical till sampling profiles in map sheet 3313 08 (western half of the Tervo area).

although the interpretation is now more difficult owing to the bedrock conductors which also contribute to the AEM anomalies. The lower, older basal till encountered in the area contains silt and clay (Hirvas & Nenonen 1978). Another possible source of AEM anomalies are layers of weathered rock, which have also been found in the test area. The results in Fig. 75 indicate that it might be feasible, under favourable conditions, to map the areal distribution of these types of poorly conductive soils by means of AEM results.

Sorosuo: conductive half-plane covered by thick overburden

In spite of extensive studies, the source of all the Zn-rich floats in Utrianlahti has not been established; one possible source is farther off to the north-west in the Sorosuo-Hirviniemi area (Ekdahl 1976b). The bedrock is covered by bog and has no exposures, which makes exploration difficult. The slingram survey (l = 40 m, f = 3 600 Hz) conducted earlier in the Sorosuo area did not

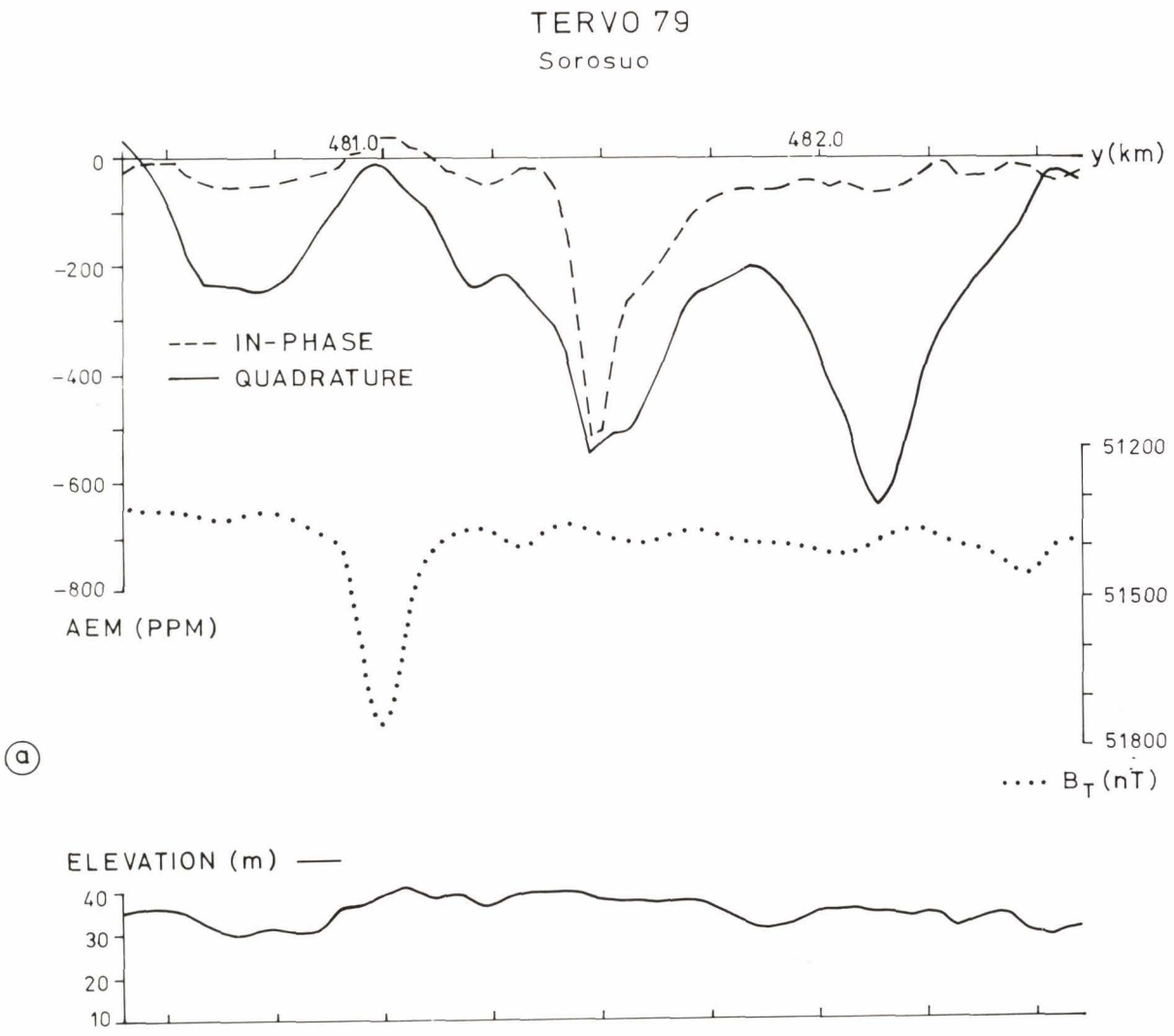

(a)

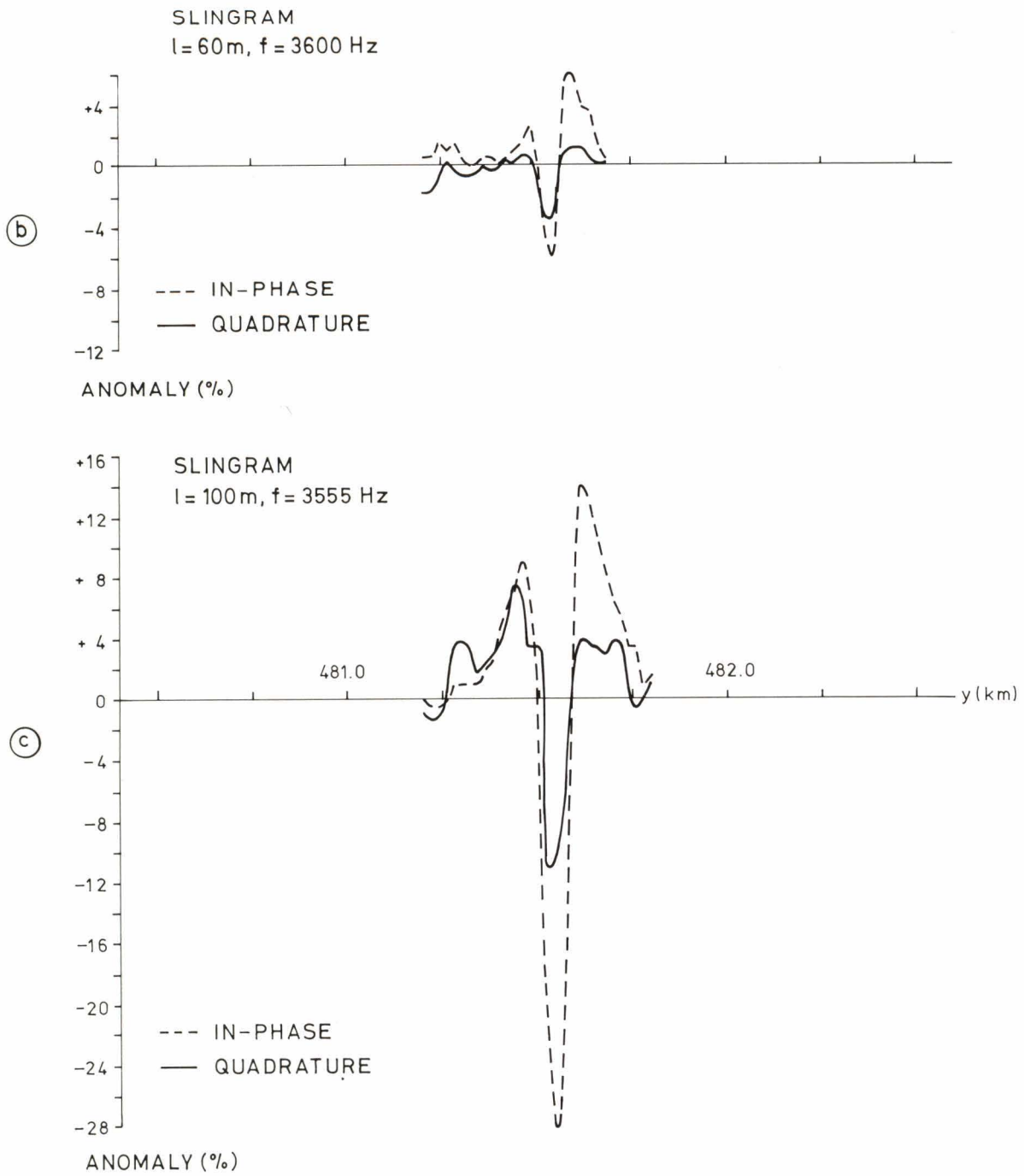

Fig. 76. Test line Tervo 79 (Sorosuo target), results of various geophysical methods. (a) DC-3 aerogeophysical survey, AEM, aeromagnetic and flight elevation data, point spacing $\Delta y = 29$ m (see page 144). (b) Slingram survey, in-phase and quadrature data, coil separation $l = 60$ m, frequency f = 3 600 Hz, $\Delta y = 20$ m. (c) Slingram survey, in-phase and quadrature data, $l = 100$ m, f = 3 555 Hz, $\Delta y = 20$ m.

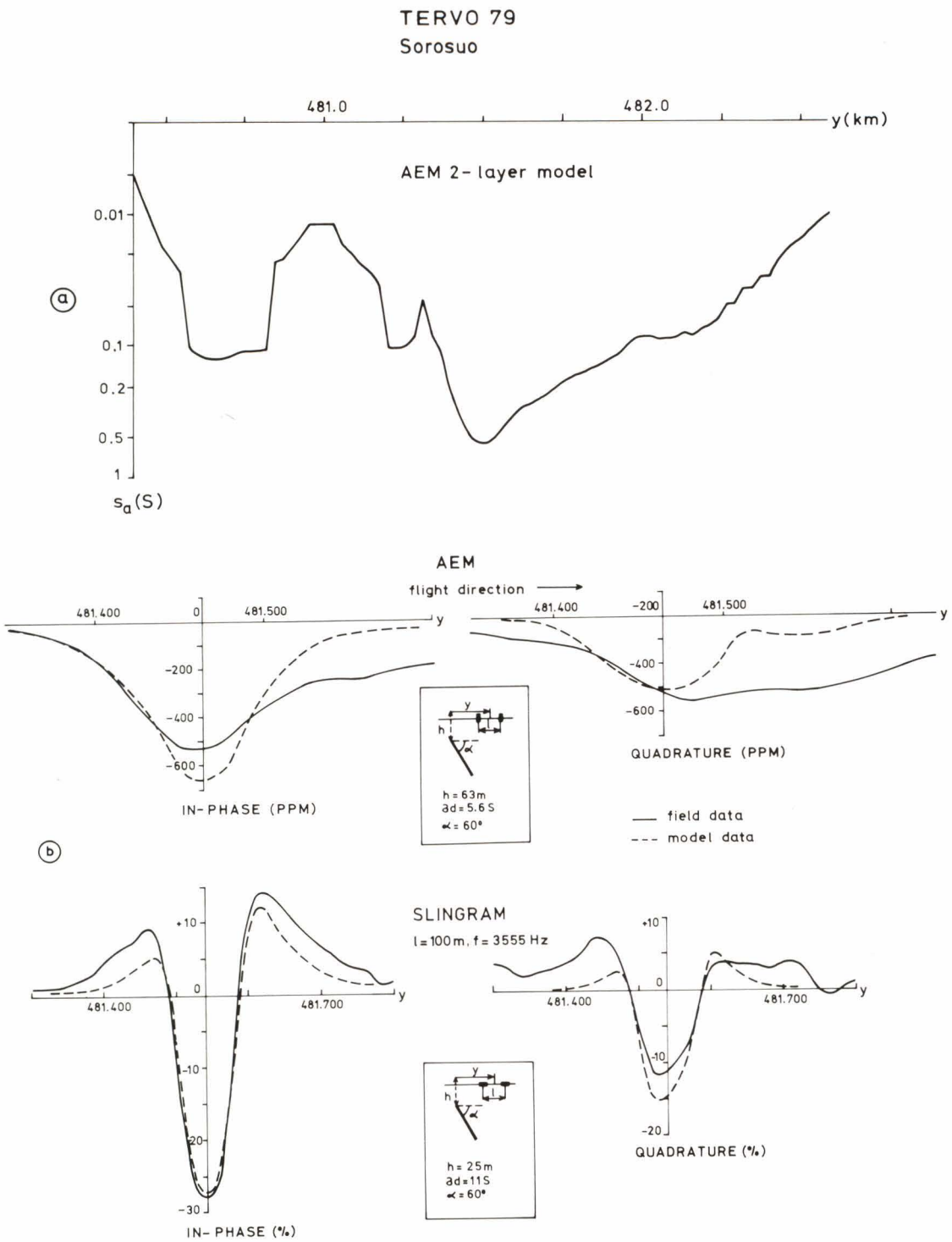

Fig. 77. Interpretation of the EM data from the Sorosuo target. (a) The values of apparent conductance s_a calculated from AEM data (Fig. 76a) by means of a thin horizontal layer model. (b) Interpretation of the AEM and slingram data with a thin half-plane model.

produce any indications. Magnetics, however, revealed weak anomalies in the area, and the AEM and new slingram surveys produced a distinct conductor indication, as shown by Figs. 73, 74 and 76.

Various EM data on the flight line 79 (x = 6995.8 between y = 480.400–482.600) are shown in Fig. 76. The new slingram data demonstrate that the anomaly shows up vaguely when the coil separation is l = 60 m; it is clearly distinguishable only when the coil separation is l = 100 m. The interpretation of different results is given in Fig. 77. By means of Fig. 35b and the original scale modelling profiles, the interpretation of the AEM data, in phase = −520 ppm, quadrature = −320 ppm, gives 5.6 S for the σd product of the conductor and da_3 = 63 m−38 m = 25 m for the depth to the outcrop of the conductor from the ground surface. An eastward dip of the conductor can be anticipated from the in-phase anomaly profile. Slingram interpretation gives correspondingly σd = 11 S, da_3 = 25 m and α = 60°. The AEM data show that the conductance of the horizontal conductor is low, s_a = 0.01–0.1 S. Its thickness is, however, so high that the penetration of the slingram method is sufficient only when $l \geq$ 60 m. In comparison, sampling depths up to 8 m have been reached in regional till sampling in the Sorosuo area (cf. Fig. 75, test line 2). Studies on the target are underway and more data to test the interpretation are not yet available.

Luvelahti: conductive zone in bedrock

Explorational activities were initiated at Luvelahti in 1960 by the discovery of chalcopyrite-bearing gabbro floats, whose source was established in the eastern portion of the Saarinen-Luvelahti gabbro massif. The source of the best floats, however, cannot yet be considered fully established and follow-up studies, which include IP surveying, have been conducted in the environment of the gabbro massif. In Fig. 78 the transformed AEM data calculated with the half-space (one-layer) model are compared with the values of apparent resistivity and phase angle measured by the IP method with a gradient electrode array. Both methods give anomalies indicating adjacent conductors east of the gabbro massif. Considering the differences in the methods, the apparent resistivity values of the various methods are in surprisingly good agreement. All the resistivity lows mapped with the AEM method can be found in gradient array results as well (areas 1–6 in Fig. 78). A strong anomaly, area 7 around x = 6992.4 and y = 495.0, in gradient data does not have any correspondence in the AEM, aeromagnetic or slingram data. As the ϱ_a values measured in the boundary points with the next set of current earthings are a hundred times higher, the anomaly must be a spurious one.

One of the drawbacks of the gradient array is that it is not easy to combine the data measured with different current earthings. The more serious hindrance in this case, however, is due to the highly abnormal negative phase angle values (up to −670 mrad) in the resistive zone between the conductors (area 4 in Fig. 78c). These values are obviously caused by too low values of electric field intensity in the resistive zone. The phenomenon makes it difficult to interpret the phase angle data (Lehtimäki 1981). It can be concluded that, in this particular case, the transformed AEM data are as good as, if not better than, the IP data at localising the conductors. The results of the various methods for a test line are shown in profile form in Fig. 79. The data refer to survey line 68 (x = 6993.6, between y = 494.250–497.250). The AEM, slingram and IP resistivity data confirm that the main indication around y = 495.5 is due to two separate conductors. The difference in resolu-

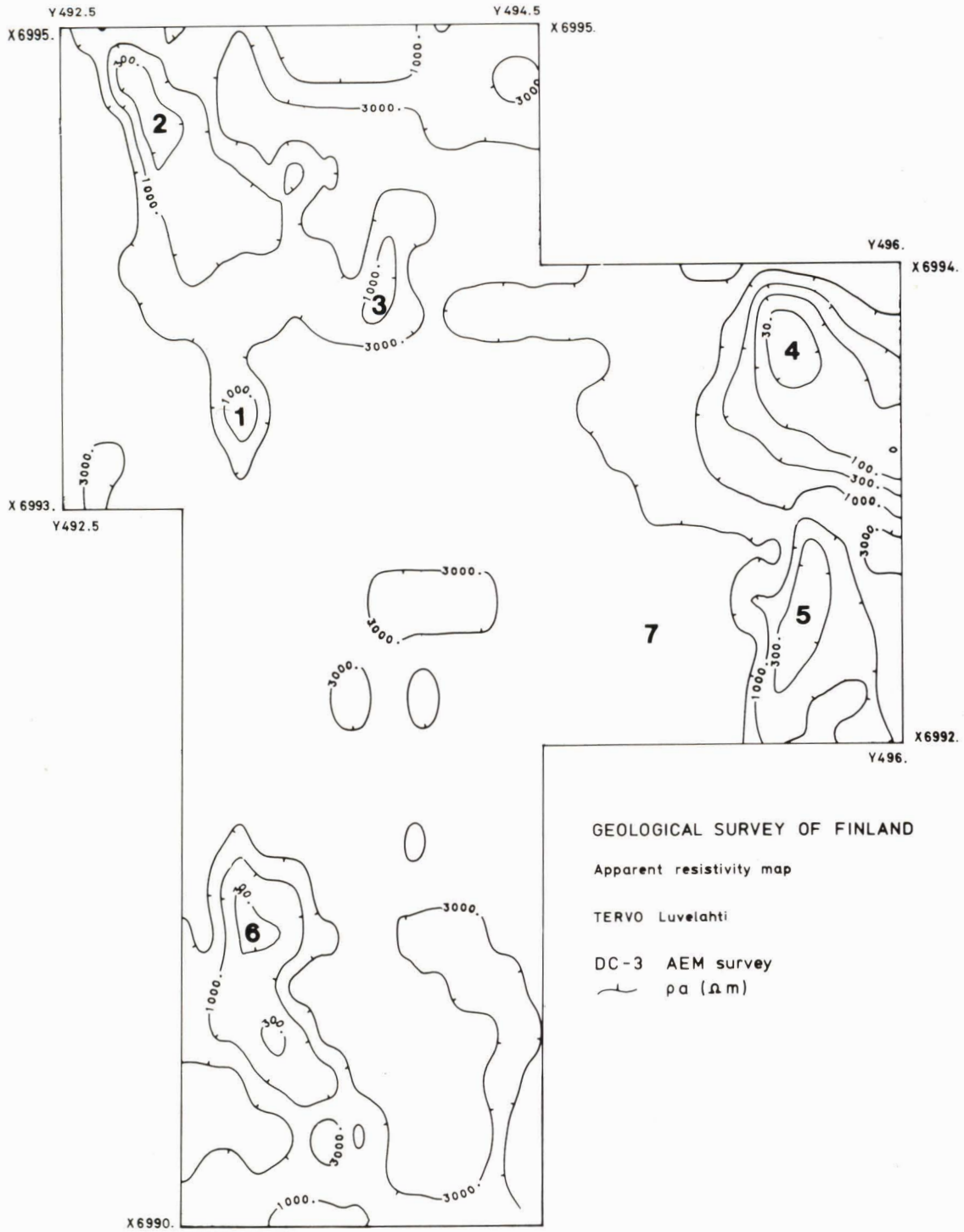

Fig. 78. Tervo area (Luvelahti target), comparison between AEM and IP surveys. Numbers 1–7 indicate areas of low resistivity. A gradient array with AB ≥ 2 000 m, MN = 20 m, line spacing = 100 m or 50 m and point spacing Δy = 20 m was applied in the IP survey. Phase-angle IP equipment model FP was used in the measurements with f = 1 Hz, I = 400 mA. (a) The values of apparent resistivity ϱ_a calculated

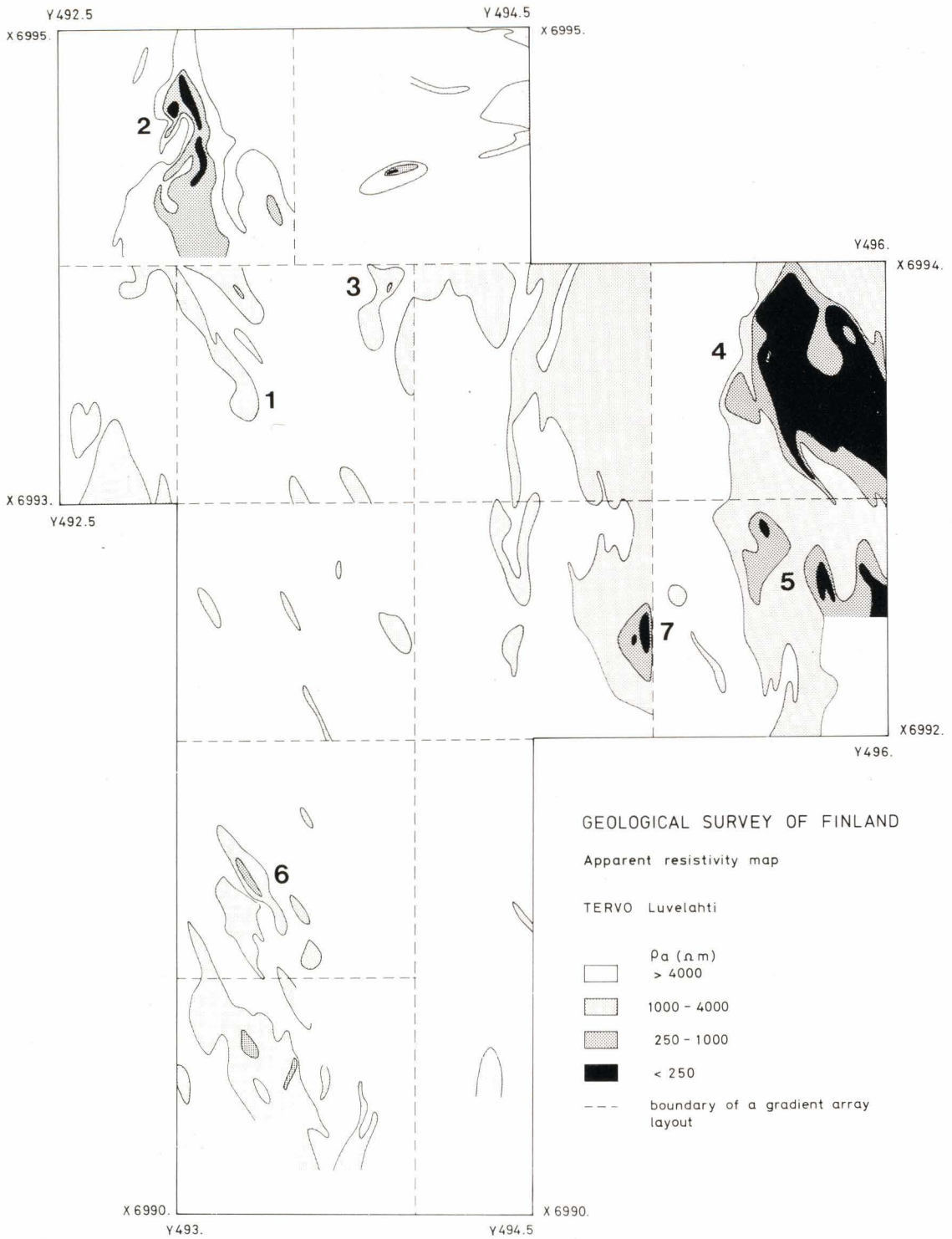

from AEM data with a conductive half-space model. (b) The values of apparent resistivity ϱ_a calculated from IP survey data. (c) IP survey data, phase angle values ϕ (see page 150).

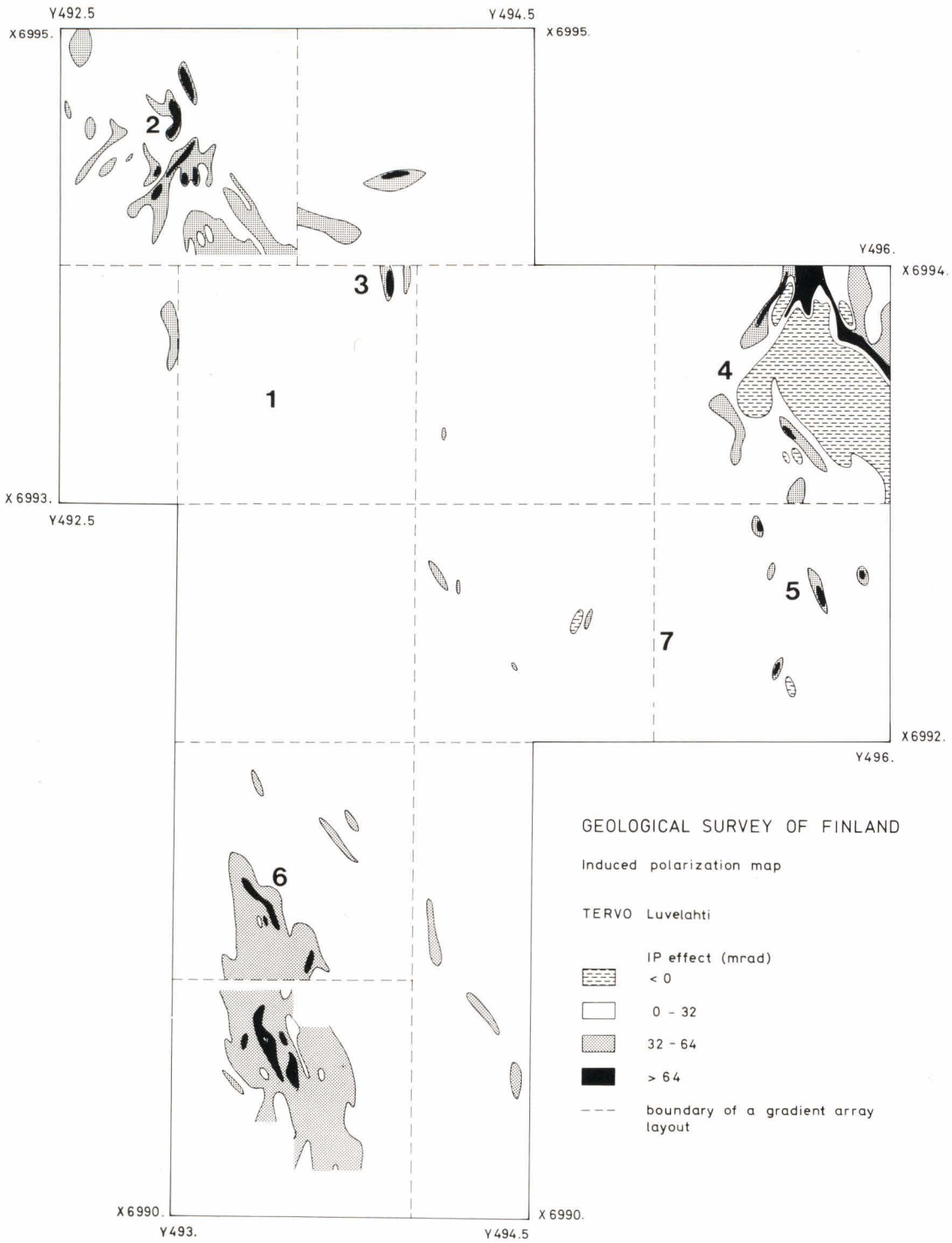
Y492.5
Y494.5
X6995.
X6995.
Y496.
X6994.
X6993.
Y492.5
X6992.
Y496.
X6990.
Y493.
Y494.5
X6990.
1
2
3
4
5
6
7
GEOLOGICAL SURVEY OF FINLAND
Induced polarization map
TERVO Luvelahti
IP effect (mrad)
< 0
0 - 32
32 - 64
> 64
boundary of a gradient array layout

Fig. 78 c)

tion of ϱ_a and IP phase angle data, measured with a gradient or a dipole-dipole electrode array, is clearly seen in Fig. 79. The nearest exposures show that cordierite-bearing gneiss rocks occur in the area. According to Ekdahl (1976b), this rock type contains graphitic portions, a fact that could explain the EM and electrical indications at the target.

Summary of the results for the Tervo study area

Examination of the results for the target area shows that:

- The transformation of DC-3 AEM data is technically feasible, even in areas in which the conductance of the overburden shows the moderately low values typical of till in Finland.
- The penetration of the AEM method exceeded that of the slingram method with a coil separation of l = 40 m and rather matched a value of l = 60 m.
- The relatively low and small indications produced by the bedrock conductors were recognised in the transformed data as well; not, however, with the

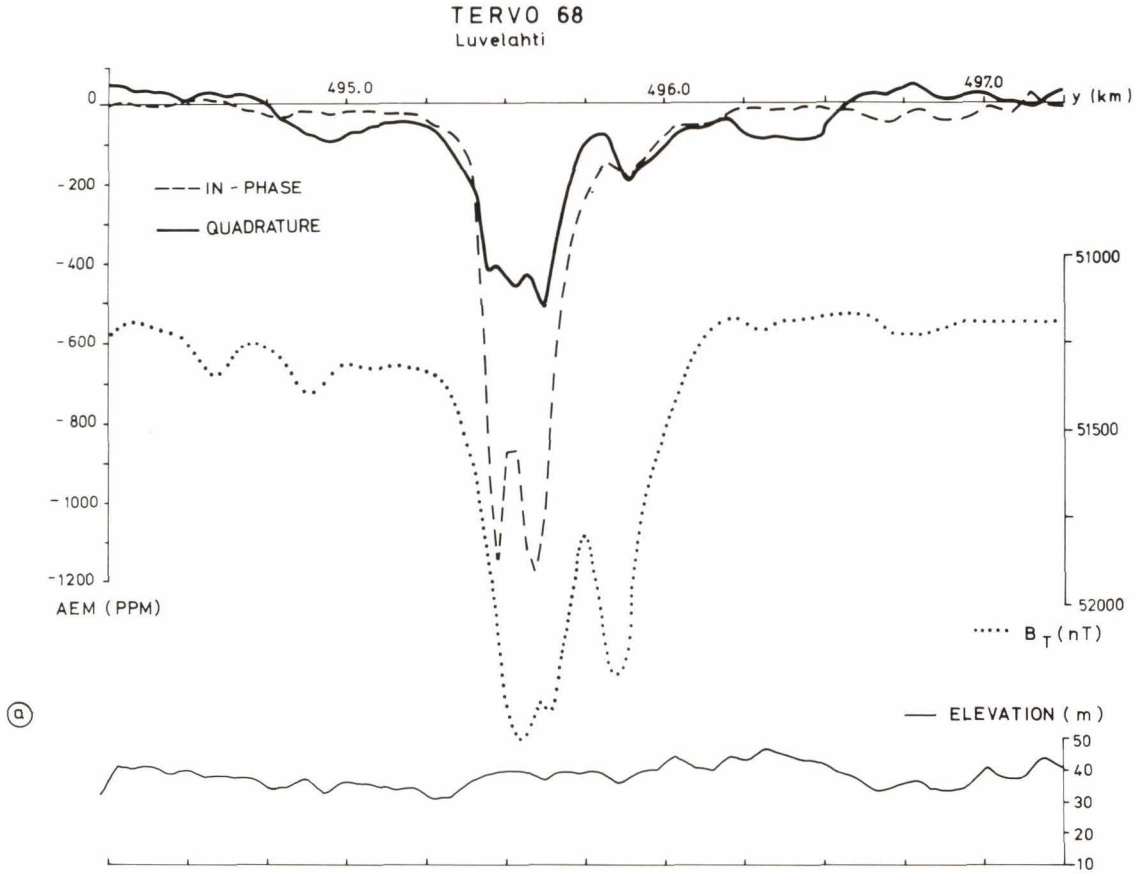

Fig. 79. Test line Tervo 68 (Luvelahti target), results of various geophysical methods. (a) DC-3 aerogeophysical survey, AEM, aeromagnetic and flight elevation data, point spacing Δy = 29 m. (b) Slingram survey, in-phase and quadrature data, coil separation l = 60 m, frequency f = 3 600 Hz, Δy = 20 m. (c) IP survey, the values of phase angle ϕ measured with gradient and dipole-dipole arrays, Δy = 20 m. IP equipment model FP and an electrode array with AB = 20 m, MN = 20 m and dipole separation = 60 m were applied in the dipole-dipole measurements. (d) IP survey, the values of apparent resistivity ϱ_a measured with gradient and dipole-dipole arrays. The ϱ_a values calculated from the AEM data are also shown for comparison (see page 152).

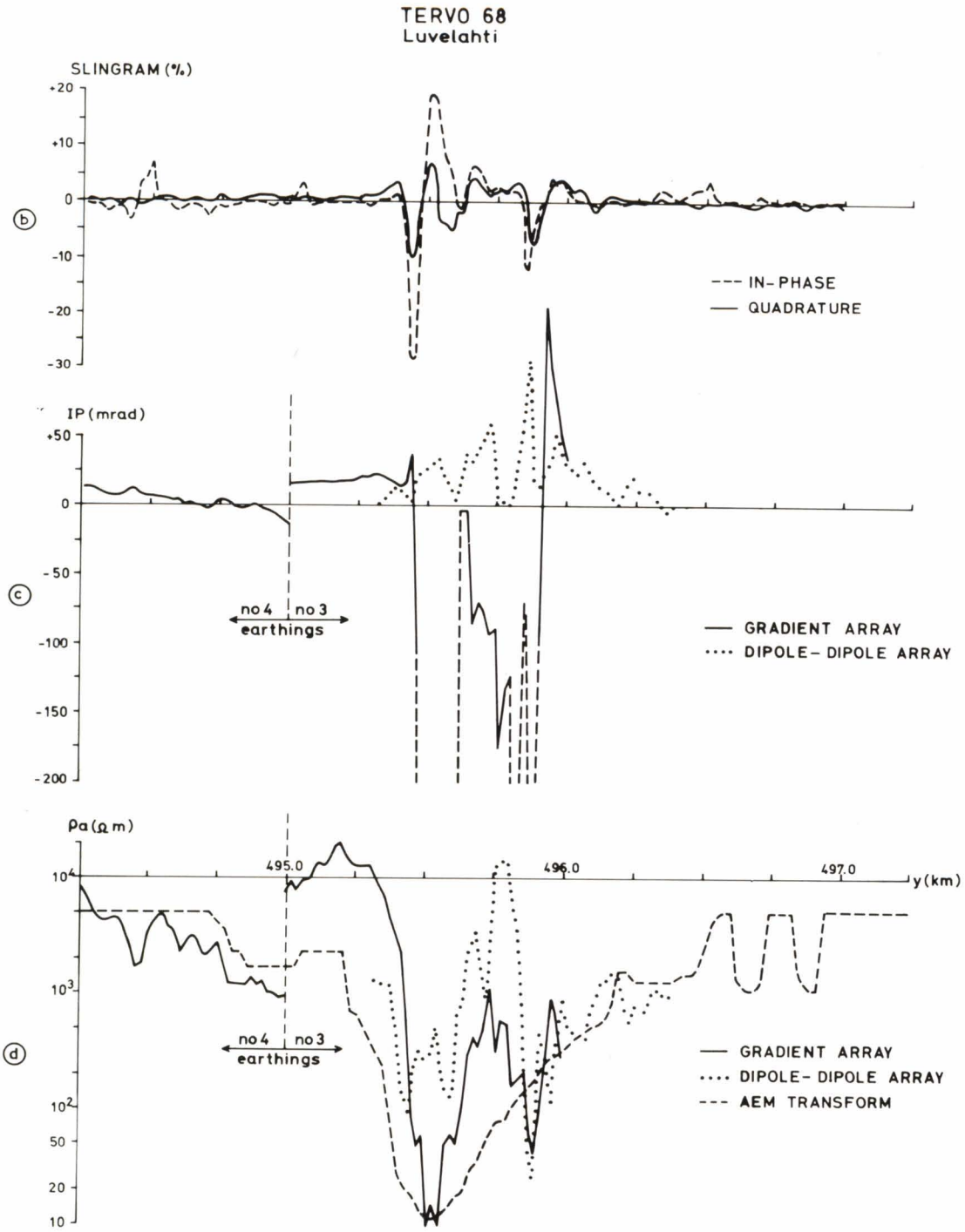
TERVO 68
Luvelahti
SLINGRAM (%)
+20
+10
0
-10
-20
-30
b
--- IN-PHASE
— QUADRATURE
IP (mrad)
+50
0
-50
-100
-150
-200
c
no 4
no 3
earthings
— GRADIENT ARRAY
···· DIPOLE-DIPOLE ARRAY
ρa (Ω m)
10⁴
10³
10²
50
20
10
495.0
496.0
497.0
y (km)
d
no 4
no 3
earthings
— GRADIENT ARRAY
···· DIPOLE-DIPOLE ARRAY
--- AEM TRANSFORM

resolution of the original in-phase anomaly values.
- The values of the apparent resistivity ϱ_a calculated from the AEM data correspond well with the ϱ_a values deduced from the gradient array measurements.
- On account of the good penetration of the AEM method, explorationally useful information was obtained, even from this area which had long been submitted to ground studies more diverse and detailed than the AEM survey.

Sotkamo: Extensive black schist formation of varying conductivity

Owing to their high conductivity, black schist zones are readily indicated by various EM methods. When they occur as extensive formations, however, they are such dominant sources of anomaly that it is not generally considered possible to study their internal structure in detail on the basis of AEM data nor to assess the explorational priority of the anomalies. Nonetheless, such a methodic trial will be made in this example. It will also be demonstrated that, with transformed data, it is possible to reduce the variations in anomaly values caused by the large variations in topography and flight elevation so that the transformed data are considerably more useful than are the original anomaly values.

The target area is part of the western margin of the Kainuu schist belt. According to Heino and Havola (1980), the bedrock in the area is composed of three major groups (Fig. 80): the Presvecokarelian gneiss complex, Karelian schists and intrusive rocks. The Presvecokarelian gneiss complex is granodioritic or granitic in composition. The Karelian schists include quartzites, black schists and mica schists, all of which also occur together as intervening layers. The intrusive rocks are rare and occur mainly as metadiabase dykes in the western margin of the schist formation.

On the basis of the sulphides present, the large black schist formation in Sotkamo can be subdivided into four major types (Ervamaa & Heino 1980):

- Pyrite-predominant black schist (type 1).
- Pyrrhotite-predominant black schist (type 2).
- Ni–Cu–Zn-bearing black schist (type 3).
- Mn-bearing black schist (type 4).

The black schists average 8–20 % sulphides and about 7 % graphite. Only a small proportion of the sulphides are ore minerals, and in the exploration studies the limit of the type 3 has been at 0.25 % Cu+Ni.

The Geological Survey of Finland has undertaken exploration in the area several times, most intensely in 1977–1979 (Ervamaa & Heino 1980). The problem has been how to distinguish black schist types 3 and 4, which contain valuable metals, from types 1 and 2, which do not contain such metals; the types differ only in trace metal content. A decisive contribution to solving the problem was made through petrophysical studies and subsequent slingram measurements. The results of the geophysical ground surveys made in 1977 (Tervo 1980) and the low-elevation airborne survey made in the same year are dealt with in the present context.

On account of the quartzites the topography varies sharply, particularly in the eastern part of the area. This made it rather difficult to conduct low-elevation survey flights. The

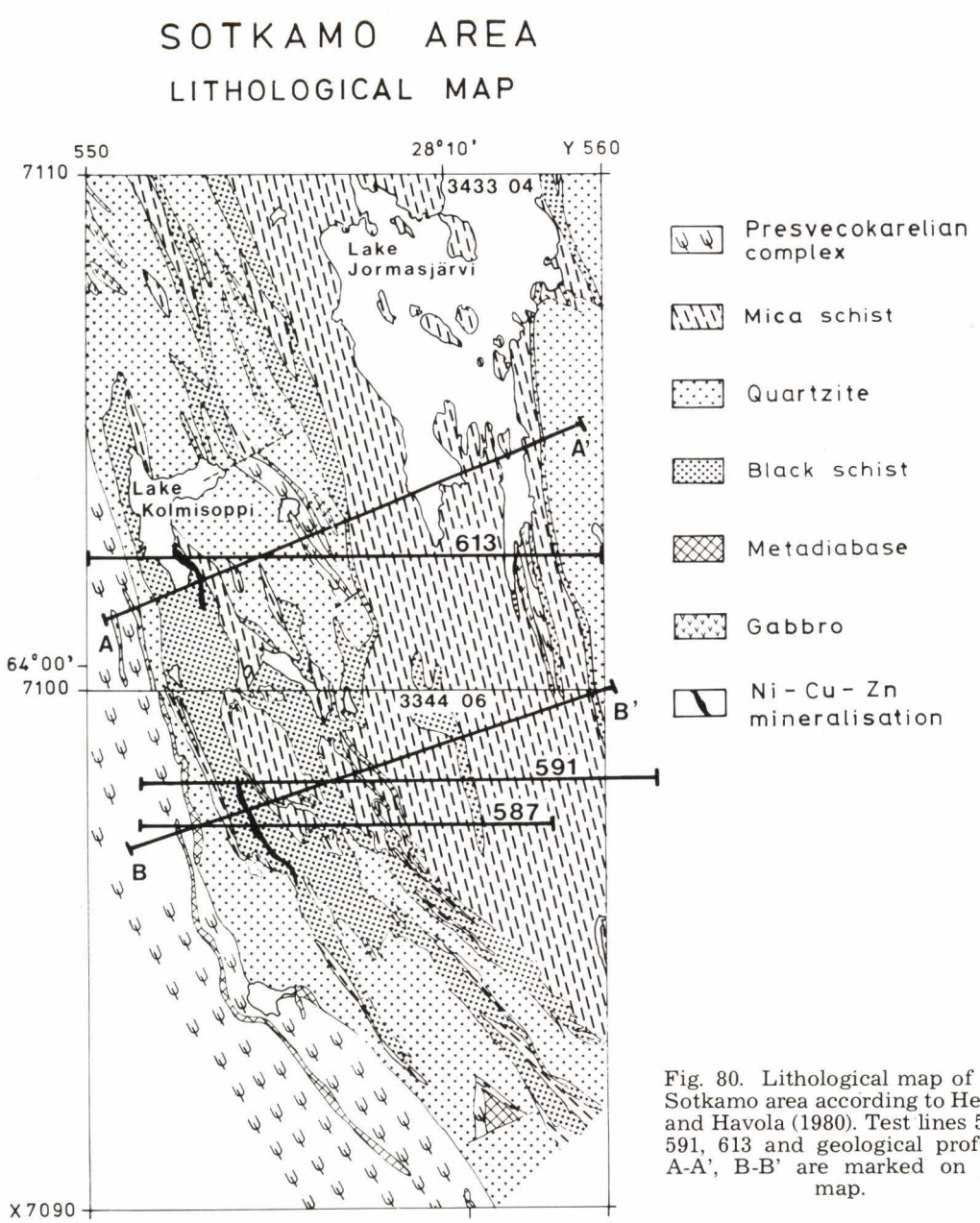

Fig. 80. Lithological map of the Sotkamo area according to Heino and Havola (1980). Test lines 587, 591, 613 and geological profiles A-A', B-B' are marked on the map.

average flight elevation was $\bar{h} = 32$ m, the standard deviation being $\sigma_{\bar{h}} = 7.2$ m. The overburden is predominantly till that varies in thickness between 1 and 5 m with maximum recorded values of 15 m. The western margin of the black schist formation is well exposed; elsewhere exposures are scarce.

Most, but not all, of the schist formations are also strongly magnetised. Interpretation of magnetic data is, however, complicated by a strong remanent magnetisation. The Q values measured from 26 samples average Q = 15.6 in intensity, and the directions are widely scattered (Tervo 1980, p. 9). Because

of remanence, the separation of black schist zones into different types is not possible on the basis of magnetic data. This is indicated by a visual inspection of the aeromagnetic profiles shown in Figs. 83a, 85a and 86a.

AEM anomaly maps for the whole area are shown in Fig. 81. As expected, the black schist responses dominate the AEM data. The largest in-phase anomalies, (in-phase $< -10\,000$ ppm), are around the lakes Kolmisoppi and Kuusilampi. Another visually clearly distinct anomaly group are the positive in-phase anomalies produced by metadiabases. The other rock types in the area do not show up on the AEM maps as separate units. The quadrature component map shows extensive weak anomalies also due to poorly conductive soil layers. The original AEM quadrature component data in this area have an abnormally high noise level, averaging 50–150 ppm.

The anomaly values, transformed into apparent conductivity data, are shown in Fig. 82. The results demonstrate that the black schist zone is highly conductive; the transformation has led to maximum apparent conductivity values of $\sigma_a \geq 10$ Sm^{-1}. The curve $\sigma_a = 0.1$ Sm^{-1} approximately delineates the contact between the black schist zone and the resistive country rock. Closer comparison of the maps in Figs. 81 and 82 shows further that the in-phase and σ_a maxima do not coincide everywhere. Fig. 80 also shows the areas occupied by the Cu–Ni–Zn-bearing black schist (type 3) as deduced from the exploration data available to date. The σ_a maxima on the transformation map coincide well with the known occurrences of the type-3 black schist. The transformation results also suggest that the likelihood of extensive black schist portions of type 3 is unlikely in the vicinity of the Taattola pit (x = 7100.5, y = 554.1), where exploration started.

Considering the geological environment, the use of the conductive half-space model is well motivated in this area. The anomaly data were also transformed by applying the model of a thin horizontal conductor. The map obtained is analogous to that in Fig. 82.

The slingram surveys were originally undertaken in the whole area with a coil separation of $l = 60$ m and at a frequency of f = 3 600 Hz. On account of the shorter point and line spacings the resolution is slightly better than in the AEM data. The discrimination ability, however, is poor, because in the black schist area the data are on the inductive limit of the response function of the system (in-phase = -100 %, quadrature = $-1 \cdots -10$ %), and the internal differences in the conductivity of the formation cannot be detected. Measurements of drill-core samples showed that the conductivity of type-3 black schist is still higher than that of the other types. Hence, multifrequency and multicoil-separation surveys with the slingram method (f = 222–3 555 Hz, $l = 60$–160 m) were undertaken in the area. The measurements delineated the portions of the formation with the highest conductivity and thus directed the follow-up studies to limited targets in the Kolmisoppi–Talvivaara area (Tervo 1980). In that respect the value of the transformed AEM results is only that of a methodic comparison, because they were produced too late to aid in prospecting. For more detailed comparison, results of three survey lines are examined.

Line 587

Fig. 83 shows survey data on various methods from survey line 587 (x = 7097.4 between y = 551.000–559.000). The flight elevation was fairly constant, h = 30 ± 10 m, along this line.

The positive AEM in-phase anomalies indicate the metadiabase dykes in the contact zone marked by 1a and 1b in Fig. 83. The AEM anomaly produced by the black schist

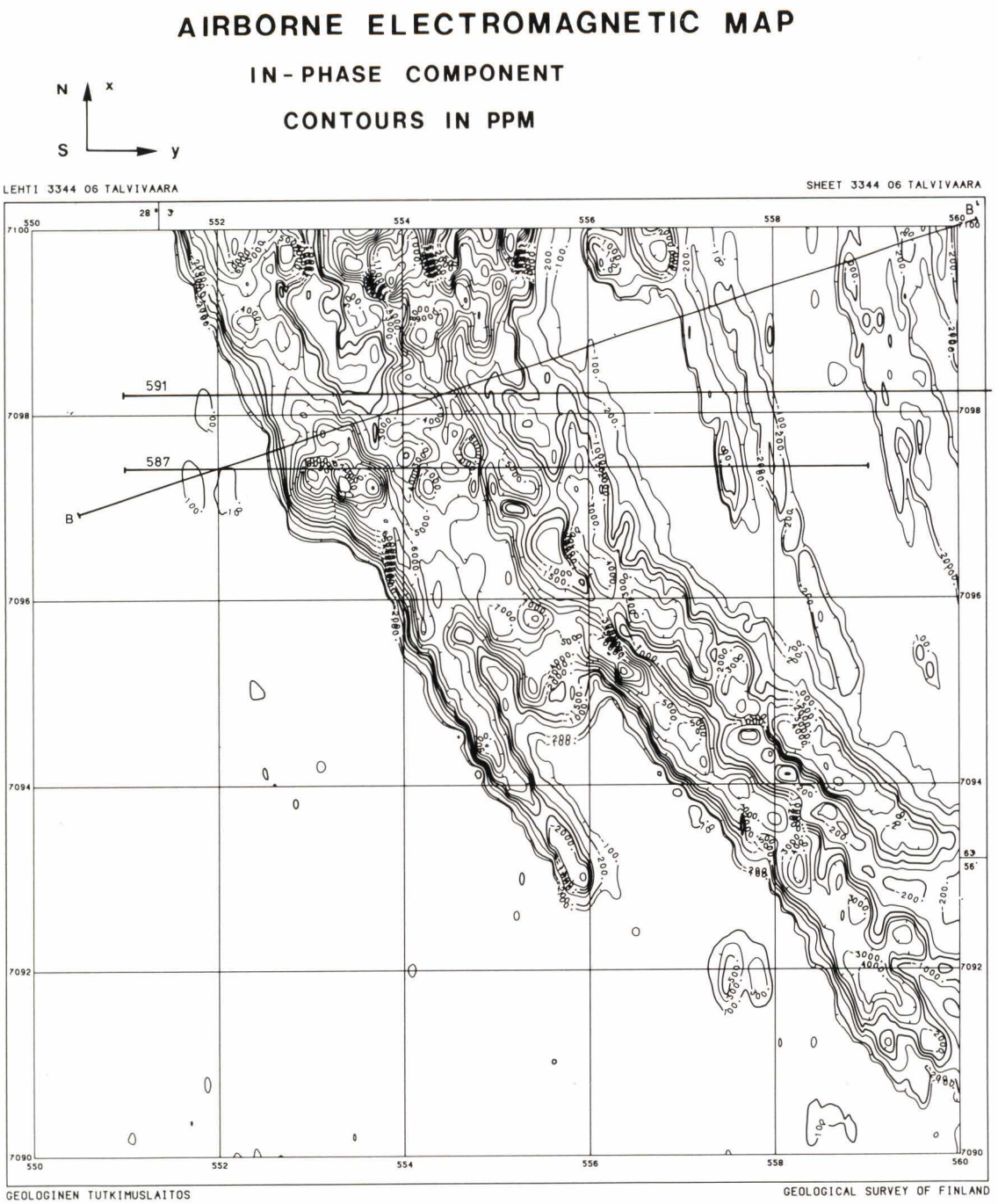

Fig. 81. DC-3 AEM survey data, map sheets 3344 06 and 3433 04 (Sotkamo area). Flight direction E–W, line spacing 200 m. Test lines 587, 591, 613 and geological profiles A-A', B-B' are marked on the maps. (a) In-phase component (see pages 156–157). (b) Quadrature component (see pages 158–159). Note: the data relevant to the southern map sheet (3344 06) are shown as profile maps in Fig. 12.

AIRBORNE ELECTROMAGNETIC MAP

IN-PHASE COMPONENT

CONTOURS IN PPM

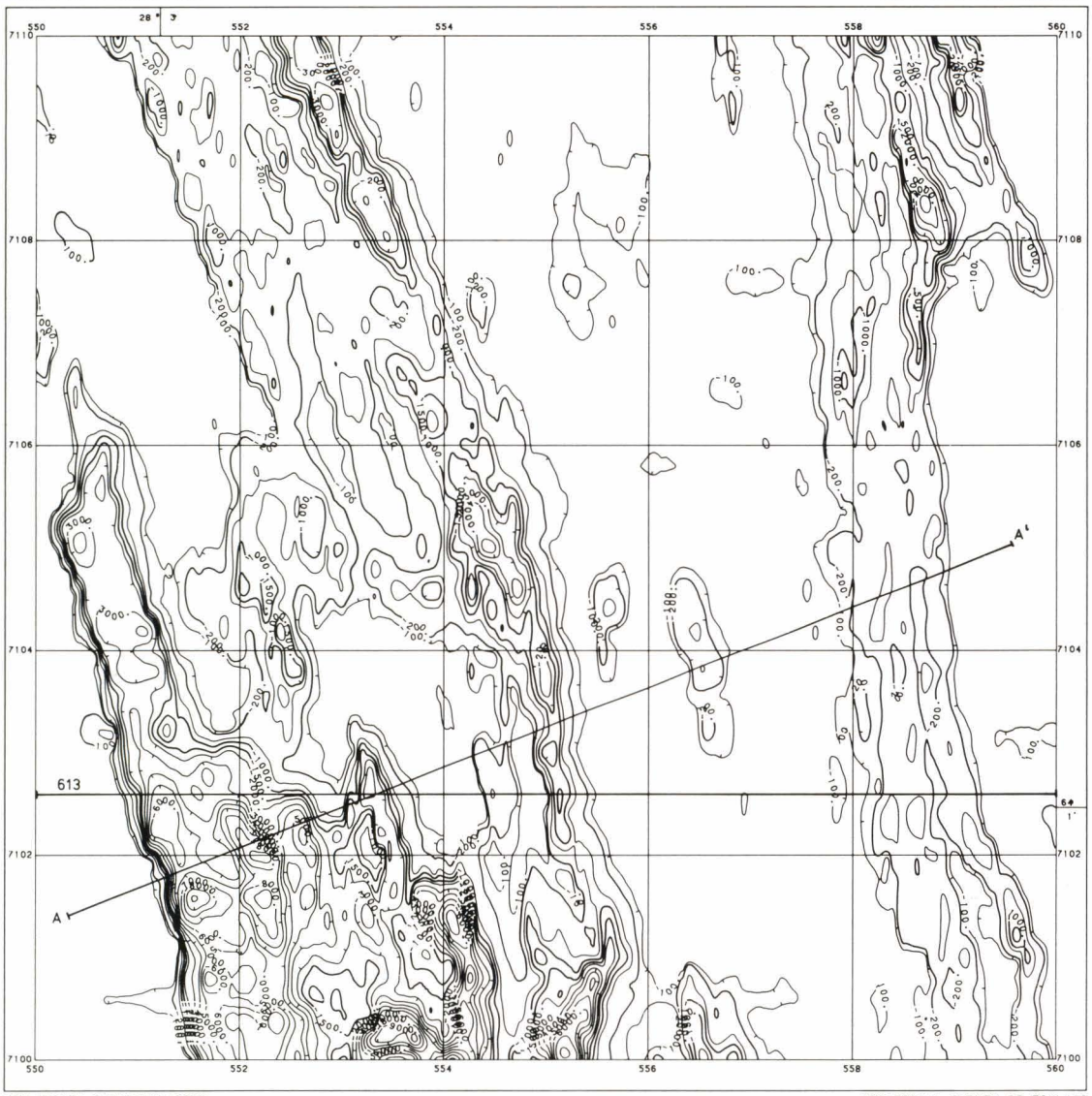

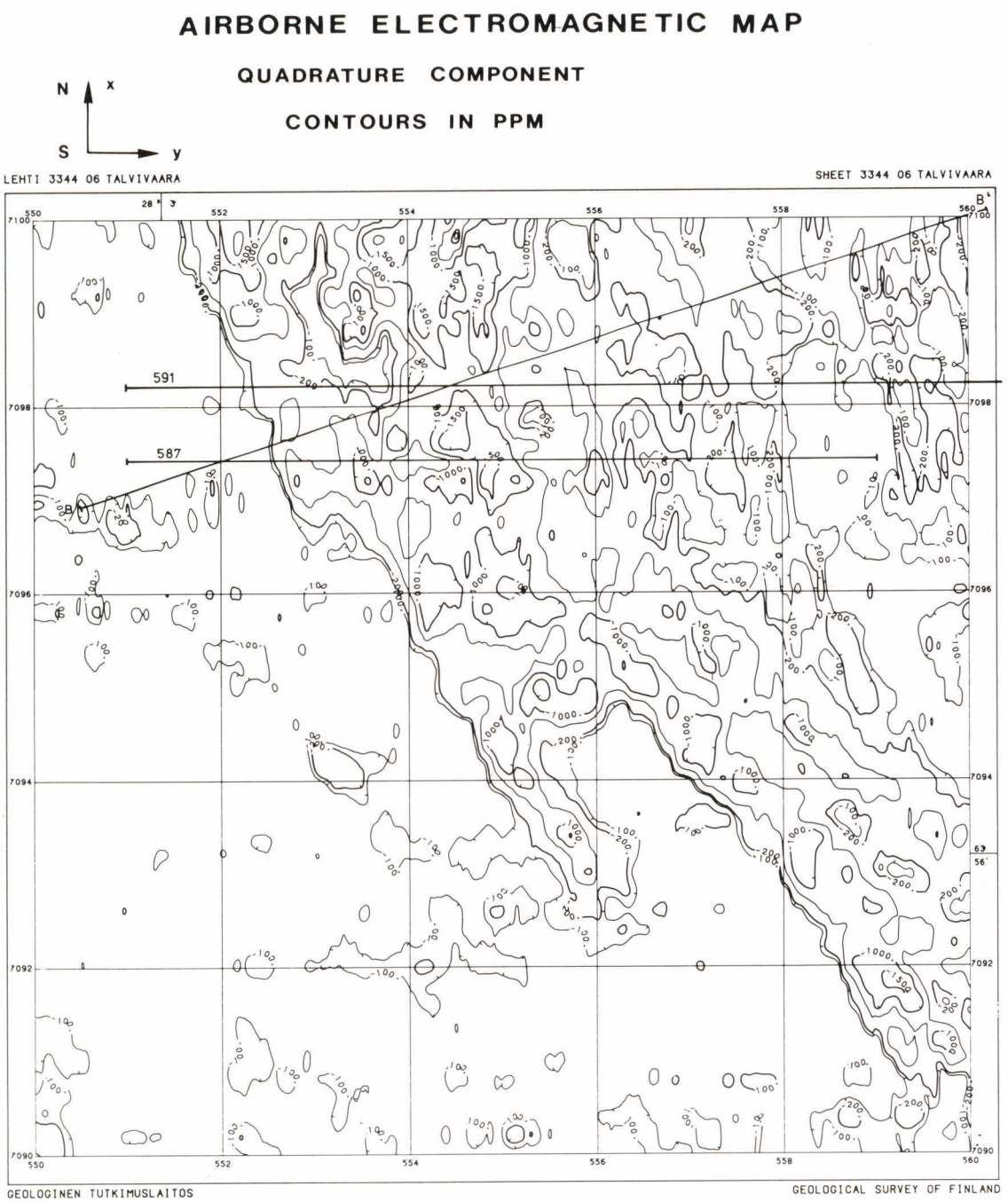
AIRBORNE ELECTROMAGNETIC MAP
QUADRATURE COMPONENT
CONTOURS IN PPM
N
S
x
y
LEHTI 3344 06 TALVIVAARA
SHEET 3344 06 TALVIVAARA
591
587
550
552
554
556
558
560
7100
7098
7096
7094
7092
7090
GEOLOGINEN TUTKIMUSLAITOS
GEOLOGICAL SURVEY OF FINLAND

Fig. 81 b)

AIRBORNE ELECTROMAGNETIC MAP

QUADRATURE COMPONENT

CONTOURS IN PPM

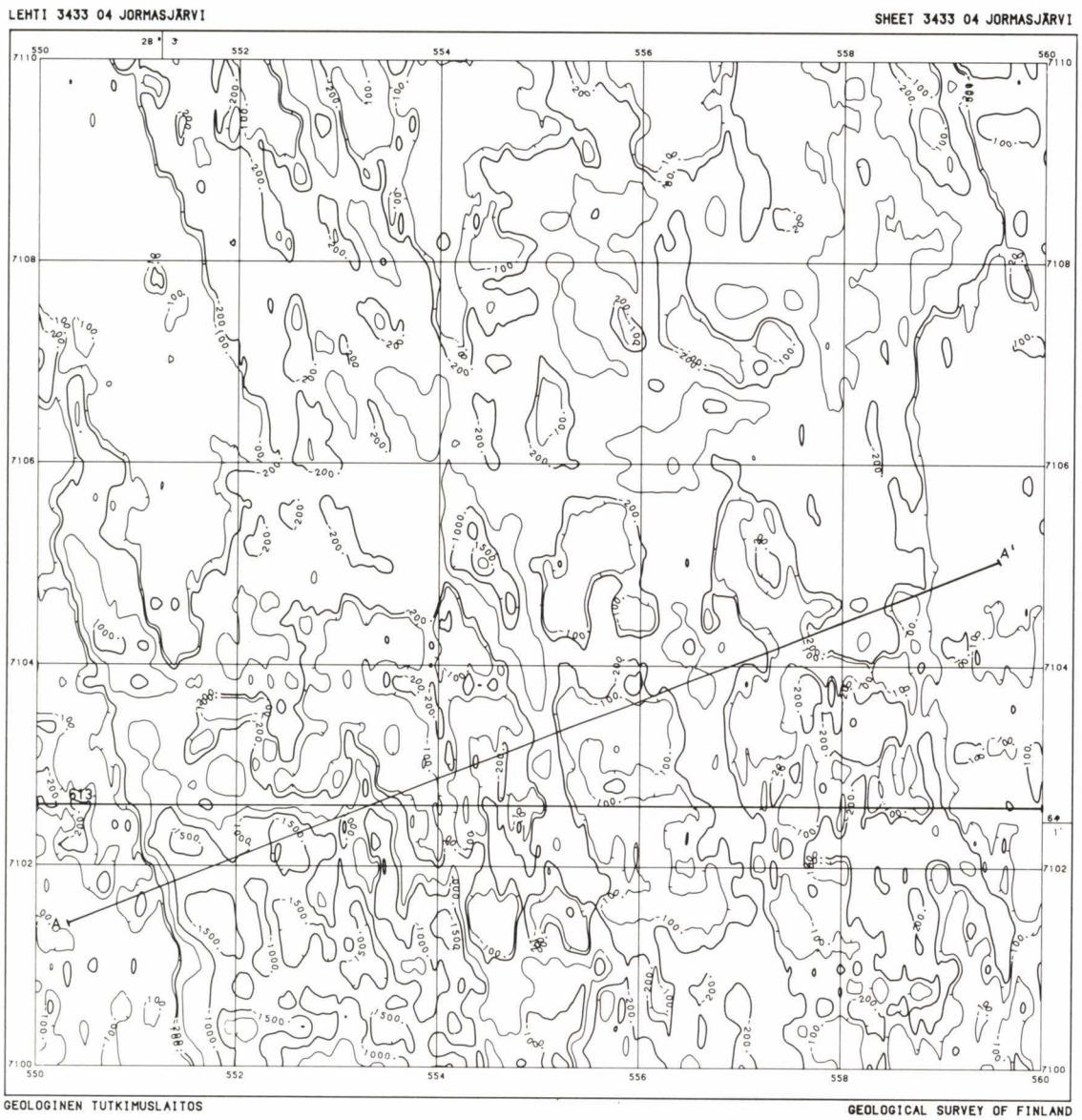

Fig. 81 b)

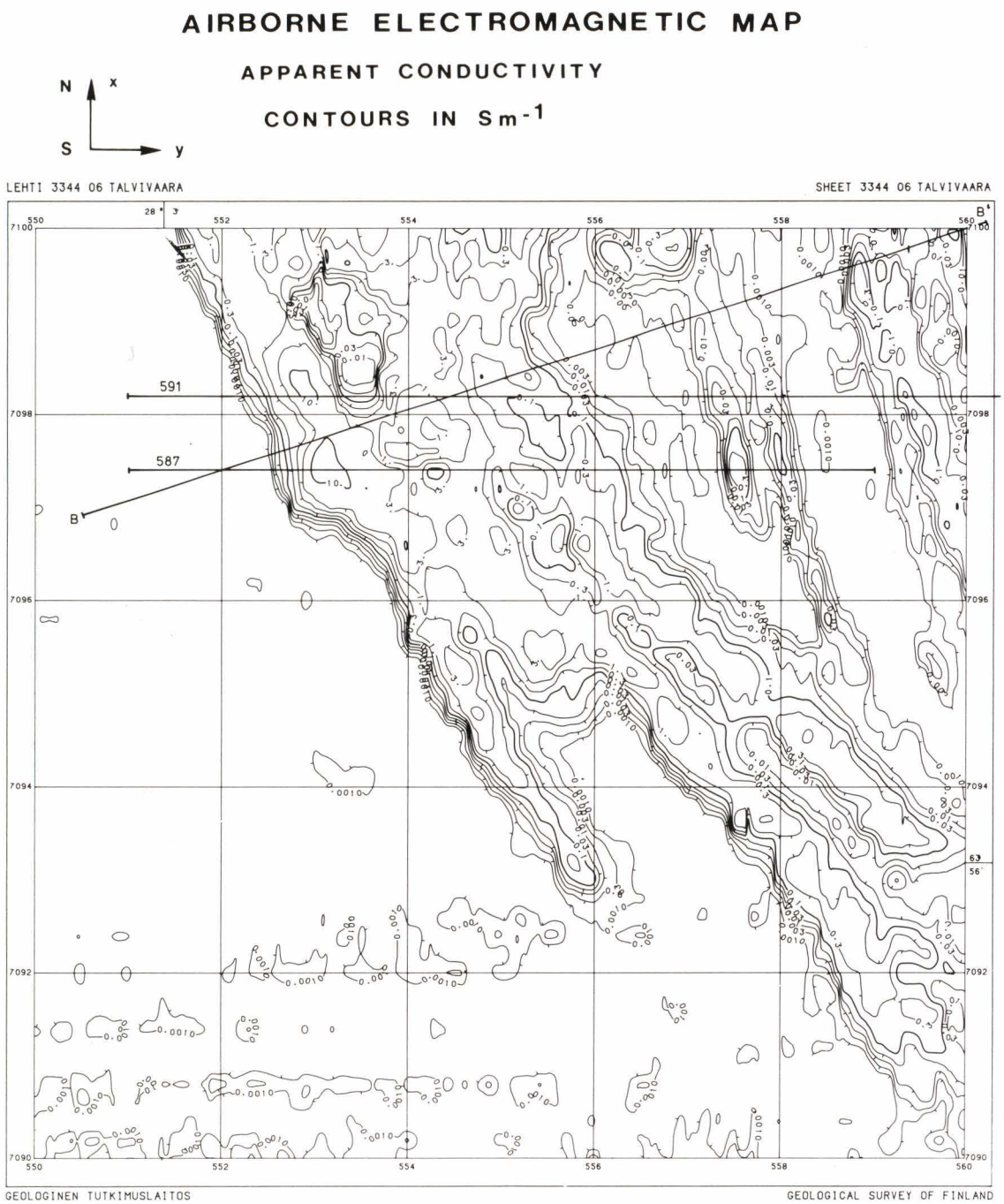

Fig. 82. The values of apparent conductivity σ_a of map sheets 3344 06 and 3433 04 (Sotkamo area) calculated from the AEM data in Fig. 81 with a conductive half-space model. Test lines 587, 591, 613 and geological profiles A-A', B-B' are marked on the maps (see pages 160–161).

AIRBORNE ELECTROMAGNETIC MAP

APPARENT CONDUCTIVITY

CONTOURS IN Sm^{-1}

LEHTI 3433 04 JORMASJÄRVI

SHEET 3433 04 JORMASJÄRVI

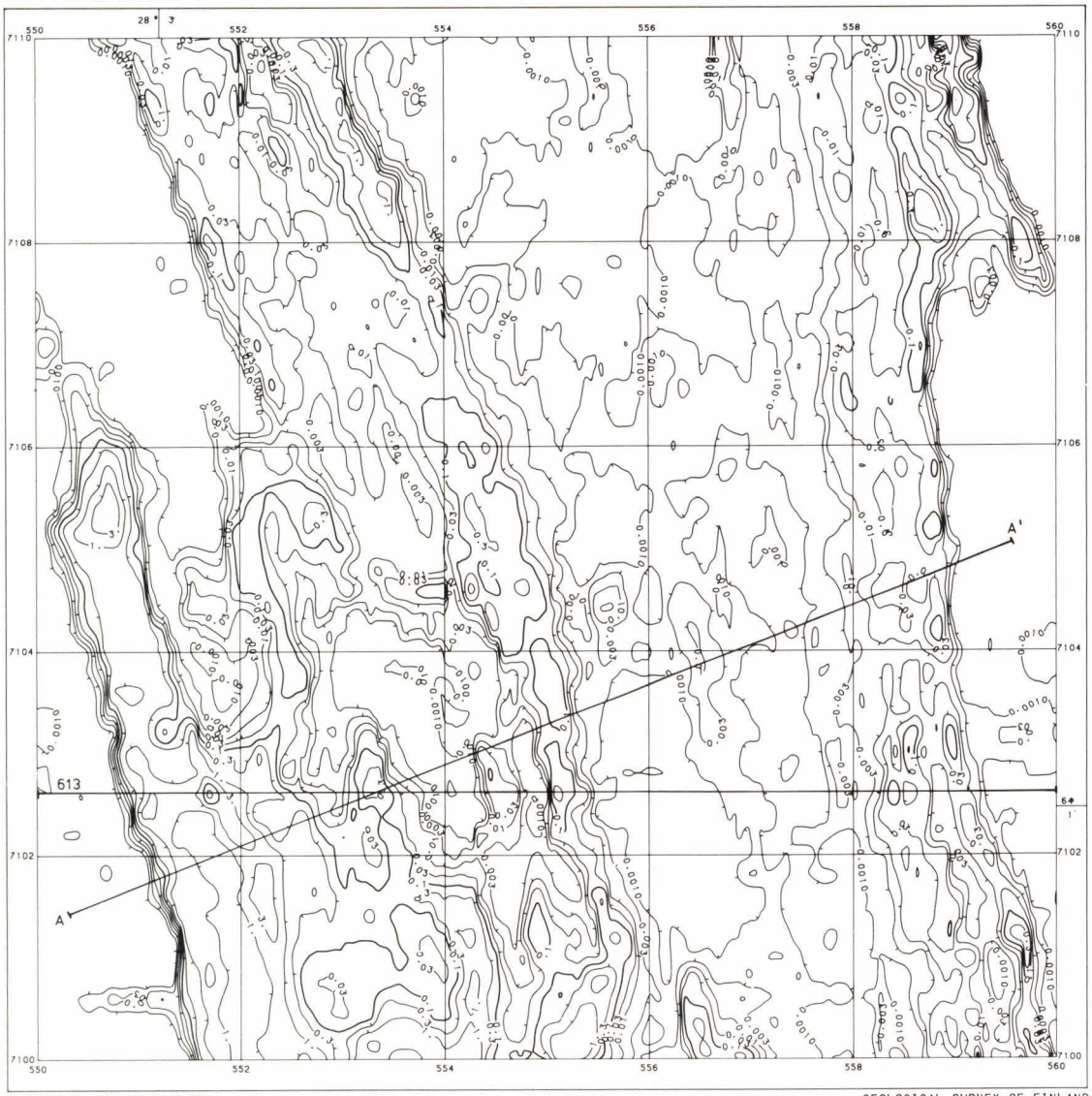

GEOLOGINEN TUTKIMUSLAITOS

GEOLOGICAL SURVEY OF FINLAND

AIRBORNE ELECTROMAGNETIC MAP

APPARENT CONDUCTIVITY

CONTOURS IN Sm^{-1}

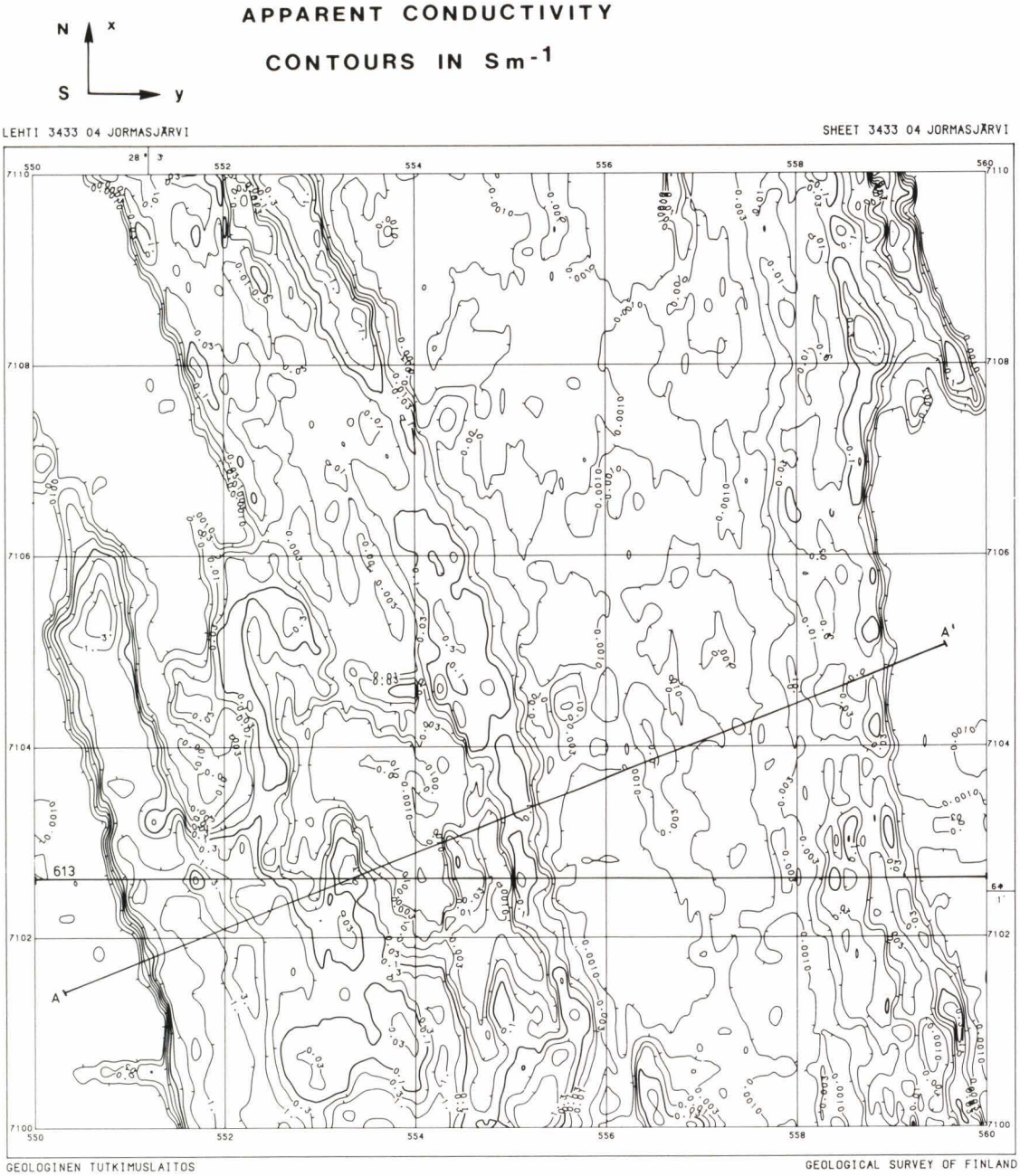

zone is extensive and consists of separate parts. The maximum of the anomaly values is reached at point y = 553.260, at which in-phase = −12 840 ppm, quadrature = −480 ppm. Hence, the AEM response parameter, although already close to the inductive limit, is still within the conductivity aperture. The westernmost narrow black schist layer (marked by 2) is so close to the main zone (marked by 3) that the in-phase anomalies of the zones are completely summed up. In contrast, the effects of zones 2 and 3 on the quadrature component data are separate. Closer examination shows that the in-phase/quadrature ratio is highest in zones 3a and 3b but already distinctly lower in zone 3c. Above a mica schist outcrop, a high AEM anomaly with in-phase = −2 200 ppm, quadrature = −240 ppm was recorded in the spot denoted by symbol 4. The result indicates the depth to the gently dipping black schist bed at this point. On the basis of Fig. 27, the interpretation gives $\sigma_a = 2$ Sm^{-1}, $da_1 = 40$ m from the ground surface for this conductor. Judged by the in-phase/quadrature ratio, the eastern black schist zone (marked by 6) is a poorer conductor than the western zone. On account of the complicated structure of black schist beds 2–6 it is not possible to estimate their dip from the AEM data; the dip of the separate narrow black schist layers (marked by 7a and 7b) is, however, suggested to be eastwards.

Fig. 83 also shows results of the multifrequency slingram survey. The survey direction was perpendicular to the strike of the

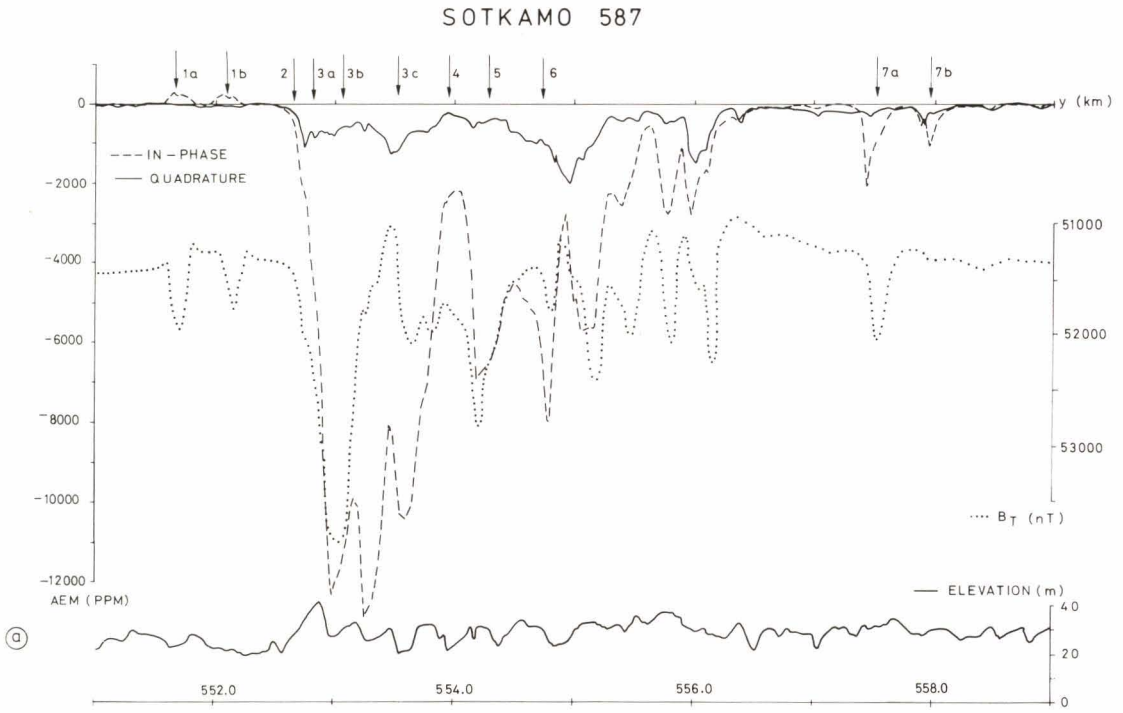

Fig. 83. Test line Sotkamo 587, results of various geophysical methods. See text for explanation of symbols 1a–7b. (a) DC-3 aerogeophysical survey, AEM, aeromagnetic and flight elevation data, point spacing $\Delta y = 29$ m. (b) Slingram survey in-phase and quadrature data with frequency f = 3 555 Hz, coil separation $l = 60$ m, $\Delta y = 20$ m. (c) Slingram data, f = 888 Hz, $l = 60$ m, $\Delta y = 20$ m. (d) Slingram data, f = 222 Hz, $l = 60$ m, $\Delta y = 20$ m (see page 163).

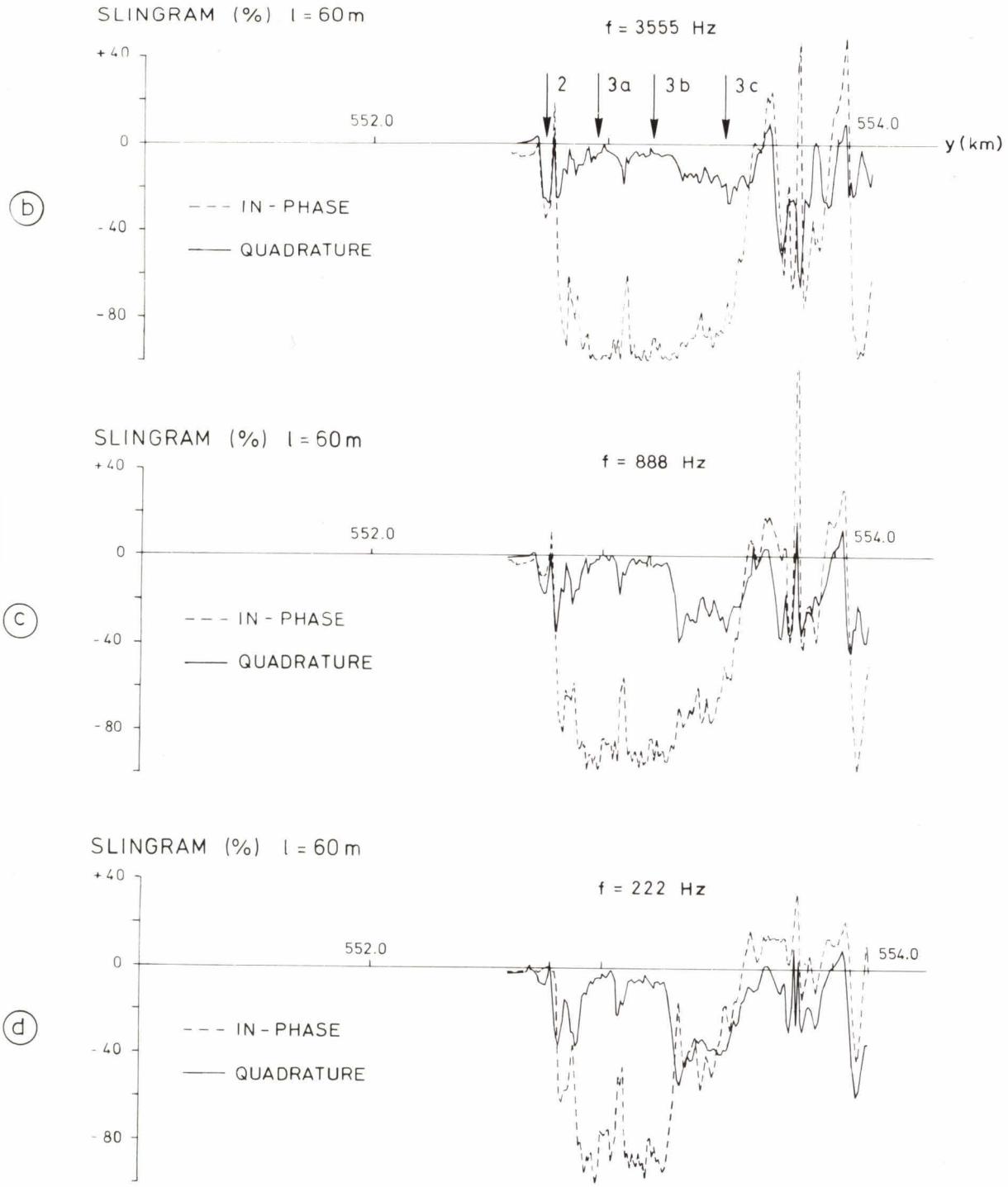
SLINGRAM (%) l = 60 m
f = 3555 Hz
+40
0
-40
-80
552.0
554.0
y (km)
2
3a
3b
3c
IN - PHASE
QUADRATURE
b
SLINGRAM (%) l = 60 m
f = 888 Hz
+40
0
-40
-80
552.0
554.0
IN - PHASE
QUADRATURE
c
SLINGRAM (%) l = 60 m
f = 222 Hz
+40
0
-40
-80
552.0
554.0
IN - PHASE
QUADRATURE
d

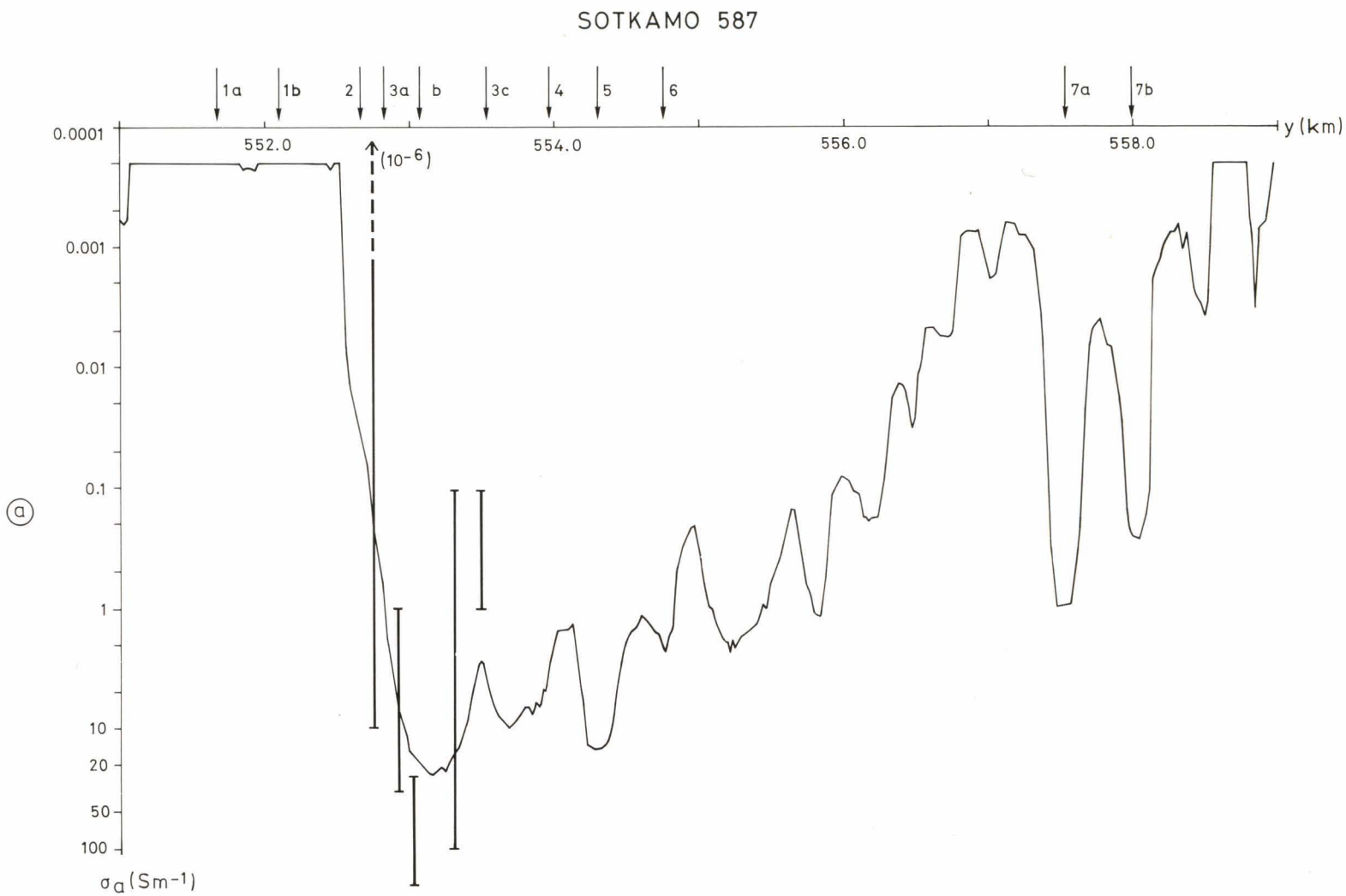

Fig. 84. Test line Sotkamo 587, results of various geophysical methods. (a) The values of apparent conductivity σ_a calculated from AEM survey data. Conductivities measured from the samples (Tervo 1980) are marked as vertical bars on the figure. (b) Geological profile B-B' of the test line (Heino & Havola 1980) (see page 165).

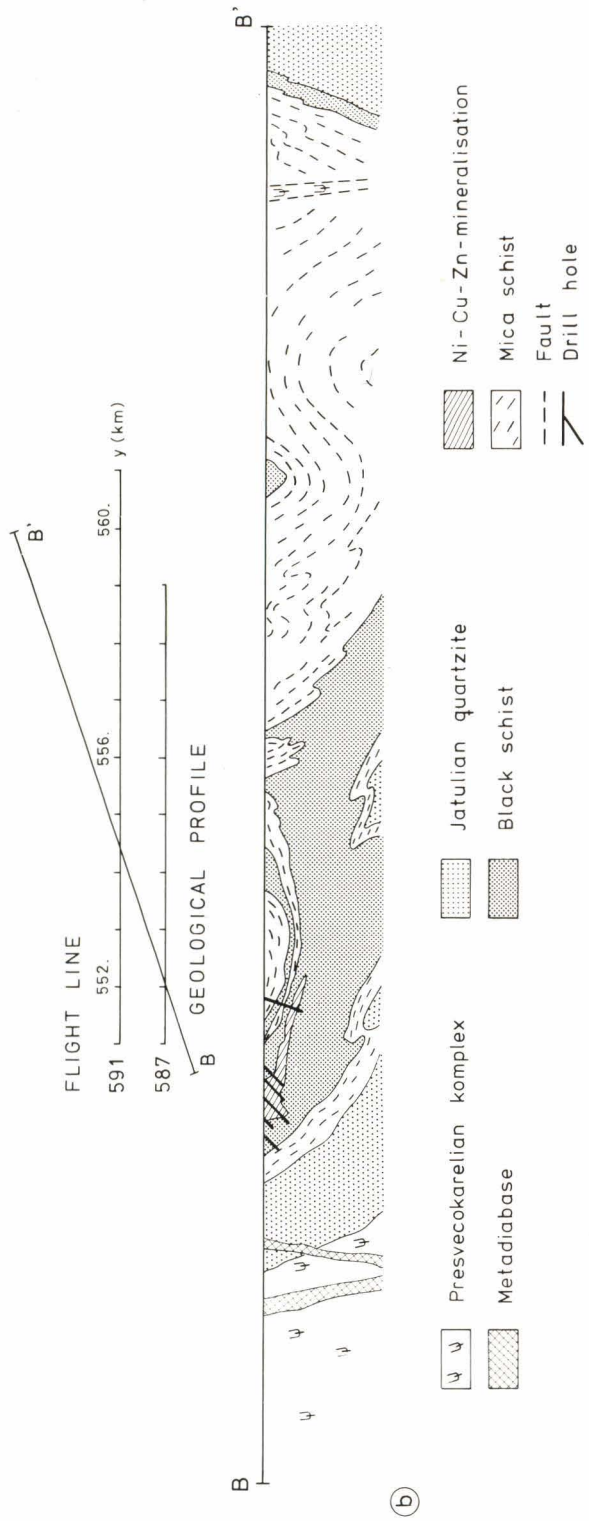

formation, i.e. the airborne and ground survey lines make an angle of 20° with each other. The coil separation was $l = 60$ m but the frequency varied. The data given in the figure were recorded at f = 3 555 Hz, 888 Hz and 222 Hz. At higher frequencies the slingram responses are very close to the inductive limit. The difference in conductivity between zones 3a, b and c is hardly discernible in the quadrature component data. At frequencies f = 888 Hz and 222 Hz the difference in the in-phase/quadrature ratio between various zones is already distinct.

The σ_a and da_1 values of the survey line calculated with the transformation program are shown in Fig. 84a. They corroborate the concept of the difference in conductivity between various parts of the black schist formation suggested by the visual interpretation. The highest σ_a values are over the mineralised black schist in area 3b, where $\sigma_a = 30$ Sm^{-1}, $da_1 = 5$ m. The eastern zone 5, which dips below the mica schist, is only slightly less conductive, $\sigma_a = 10$ Sm^{-1}, $da_1 = 15$ m, than area 3b. This is not easy to see by visual examination. The graph of apparent conductivity also shows the conductivities of samples taken across the formation and reported by Tervo (1980). It is seen that the σ_a values from the AEM interpretation are systematically lower than but satisfactorily compatible with the measured petrophysical data.

Theoretical slingram responses were calculated for various frequencies and thicknesses of overburden by means of the ADP modelling program of multilayer earth. On the basis of the model results, Tervo (1980, Fig. 16) interpreted the slingram data from the line; the values are also in good agreement with the results shown in Fig. 84a.

Finally, Fig. 84b shows the geological profile over the whole study area compiled by Heino and Havola (1980, p. 9) from geological observations and geophysical results.

Line 591

The various geophysical results on the line are shown in Fig. 85. Line 591 is less favourable in terms of AEM data than is line 587, because the western black schist zone is located in a topographic low and the flight elevation at this site was 30 m higher than in the environment. Consequently, the peak amplitudes of the whole anomaly zone, in-phase = −3 000 ppm, quadrature = −80 ppm, were much lower than those of line 587. Over the black schist zone (marked by 6) east of the mica schist area the peak anomalies are in-phase = −7 800 ppm and quadrature = −1 000 ppm. The transformation results show that the σ_a map and profile are now distinctly more useful than are the original anomaly values. The maximum value, σ_a = 50 Sm^{-1}, da_1 = 6 m, is over zone 3b, and the effect of the large variation in flight elevation on the in-phase, quadrature data has thus been eliminated. Correspondingly, values σ_a = 3 Sm^{-1}, da_1 = 11 m are obtained for the eastern anomaly zone 6.

The interpretation of the mica schist area (marked by symbols 4 and 5 in Fig. 85) gives the following outcome. In area 4 the anomaly values are in-phase = −500 ppm, quadrature ≈ 0 ppm; hence, the conductor is deep-buried and highly conductive. With a minimum value of $\sigma_a \geq 5$ Sm^{-1} for the conductor, we obtain da_1 = 95 m. In area 5 the depth to the conductor is already smaller, and from the anomaly values of in-phase = −4 000 ppm, quadrature = −1 240 ppm, values σ_a = 0.5 Sm^{-1}, da_1 = 20 m are obtained. Diamond drill hole R340, which is located 300 m south of line 591 in the western margin of the mica schist area, intersected 75 m of mica schist before penetrating the uppermost black schist bed. In the slingram data (l = 60 m, f = 3 600 Hz) the conductor overlain by the mica schist in areas 4 and 5 produces a weak posi-

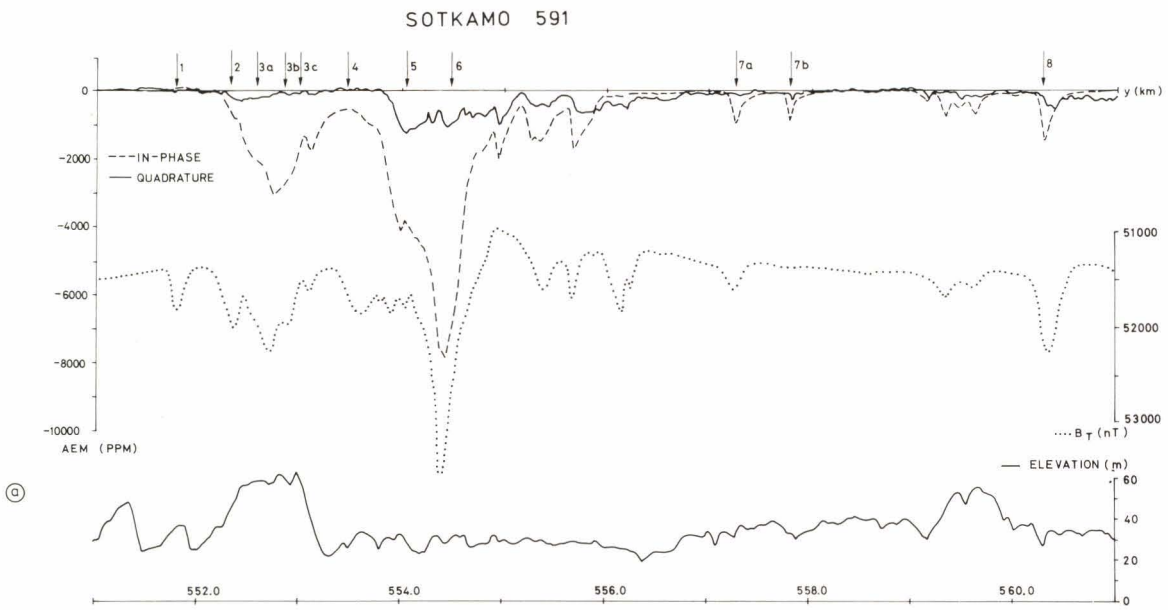

Fig. 85. Test line Sotkamo 591, results of various geophysical methods. See text for explanation of symbols 1–8. (a) DC-3 aerogeophysical survey, AEM, aeromagnetic and flight elevation data, point spacing Δy = 29 m. (b) The values of apparent conductivity σ_a calculated from AEM survey data. (c) Slingram survey in-phase and quadrature data with coil separation l 60 m, frequency f = 3 600 Hz, Δy = 20 m
(see page 167).

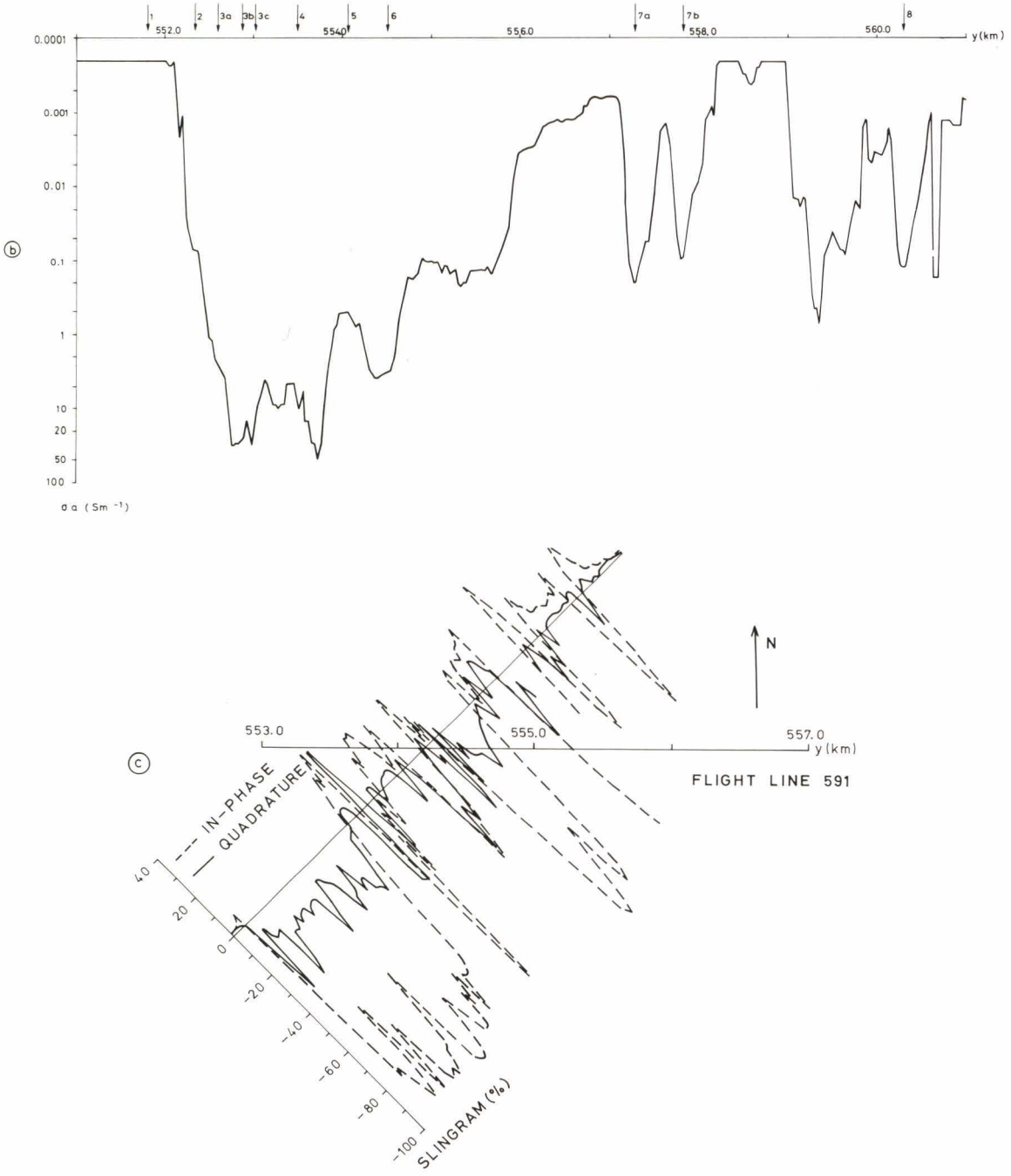

tive anomaly zone, in-phase = +4.5 %, quadrature = +1.0 %. For the slingram results the data in the characteristic diagram (Fig. 51a) give $\sigma_a = 0.3$ Sm^{-1}, $da_1 = 90$ m, which are in satisfactory agreement with the other results.

As suggested by the AEM data, zones 7a and 7b dip eastwards. On the basis of Fig. 36b

(a thin half-plane, dip 30°), $\sigma d = 8$ S, $da_3 = 28$ m are obtained for interpreted values of conductor 7b. Conductive zone 8 shows a good example of an anomaly produced by a thick half-plane with an intervening minimum in quadrature component values. Interpretation based on Fig. 39b ($h = l$, $d/l = 1.0$, $\sigma f = 10^3$) gives approximately $\sigma_a = 0.3$ Sm^{-1}, $d = 25$ m.

Line 613

The survey and transformation data on the line are shown in Fig. 86. The variations in topography and flight elevation caused by the quartzite formations along the line are higher still than on the previous line. The test line cuts the northern end of the black schist formation that is partly under the lake Kolmisoppi. The measured AEM in-phase and quadrature anomalies are higher on the western shore than on the eastern shore of the lake (zones 1a and 1b). The transformation results, however, demonstrate that the eastern black schist zone 1b has markedly better conductivity; the $\sigma_a = 100$ Sm^{-1} is the highest value recorded in the whole Sotkamo area. The outcome is not entirely compatible with the petrophysical data, according to which the sulphides occur in this portion of the formation as dissemination and farther south as breccia with higher conductivity. Even so, it can be concluded that the effect of the relatively large variations in flight elevation was satisfactorily reduced by means of transformation. Thus the transformation results are more easily applied to exploration than are the original in-phase and quadrature anomaly values.

The extensive quartzite zone is poor in outcrops. Symbol 3 denotes a poorly conductive swarm of dykes that includes mafic and ultramafic rocks. Zone 4 is a black schist bed that dips eastwards. Some of the narrow black schist beds, e.g. number 7b in Fig. 85 and number 2 in Fig. 86, were not recognised in the earlier mapping for lack of outcrops.

Summary of the Sotkamo results

The AEM results for the target area can be summarised as follows:

- On account of the shorter coil separation and the smaller value of the response parameter than in the standard slingram method, the DC-3 AEM data on the Sotkamo black schist formation are not yet on the inductive limit. Hence, the discrimination ability of the AEM method extends up to values of $\sigma_a = 100$ Sm^{-1}.

- The AEM results obtained from test line 591 demonstrate that the system has as good penetration for an extensive conductor as predicted by the modelling results.

- The merit of transformation is clear when the flight elevation and/or the depth to the conductor outcrop vary: use can be made of all interpretational information contained in the original data, including that of the in-phase/quadrature ratio. The true σ_a maxima can be recognised regardless of the anomaly amplitudes. Hence, the applicability of the AEM data to exploration can be improved if the transformation results are also available.

- The σ_a values calculated from the large AEM anomalies compare favourably with the conductivity data measured from samples. In situ variation in con-

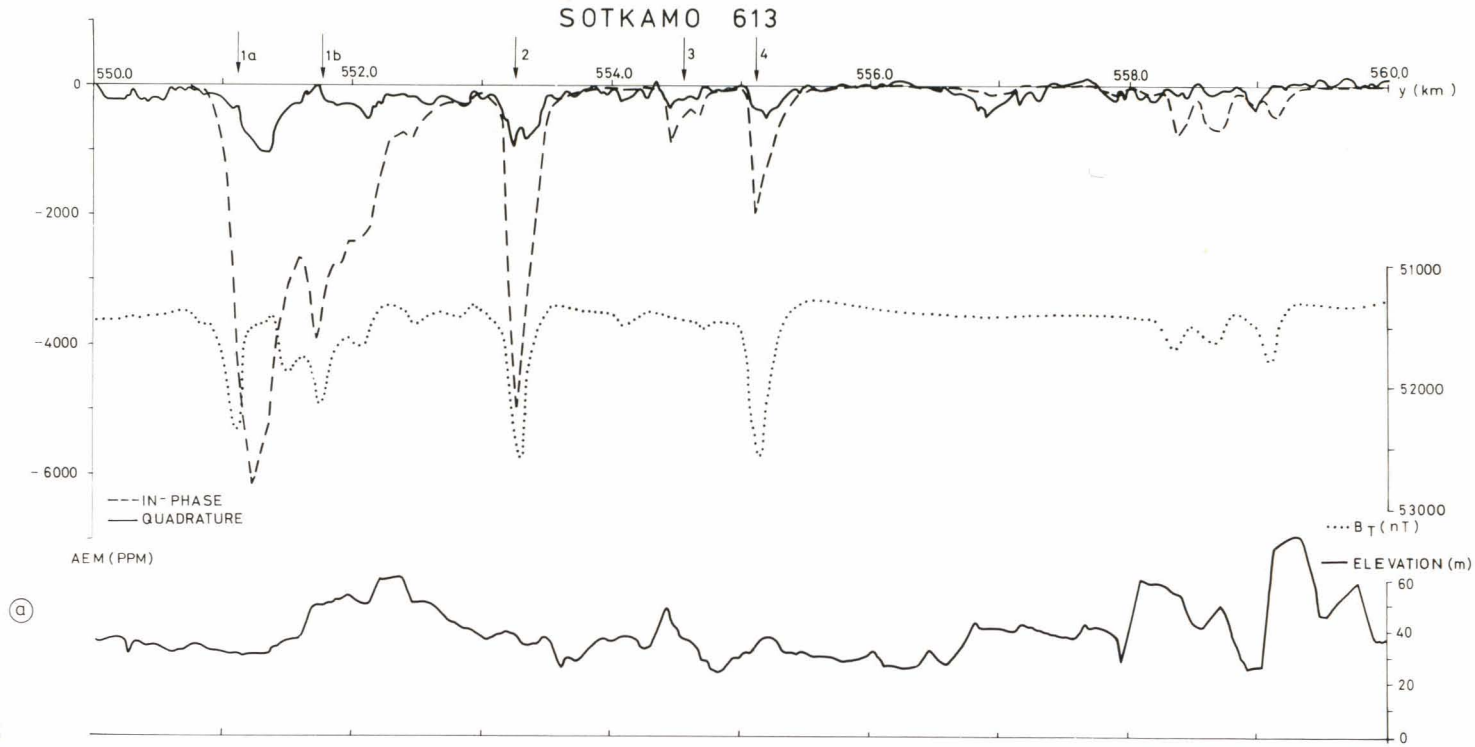

Fig. 86. Test line Sotkamo 613, results of various geophysical methods. See text for explanation of symbols 1–4. (a) DC-3 aerogeophysical survey, AEM, aeromagnetic and flight elevation data, point spacing $\Delta y = 29$ m. (b) The values of apparent conductivity σ_a calculated from AEM survey data. (c) Geological profile A-A' of the test line (Heino & Havola 1980) (see pages 170–171).

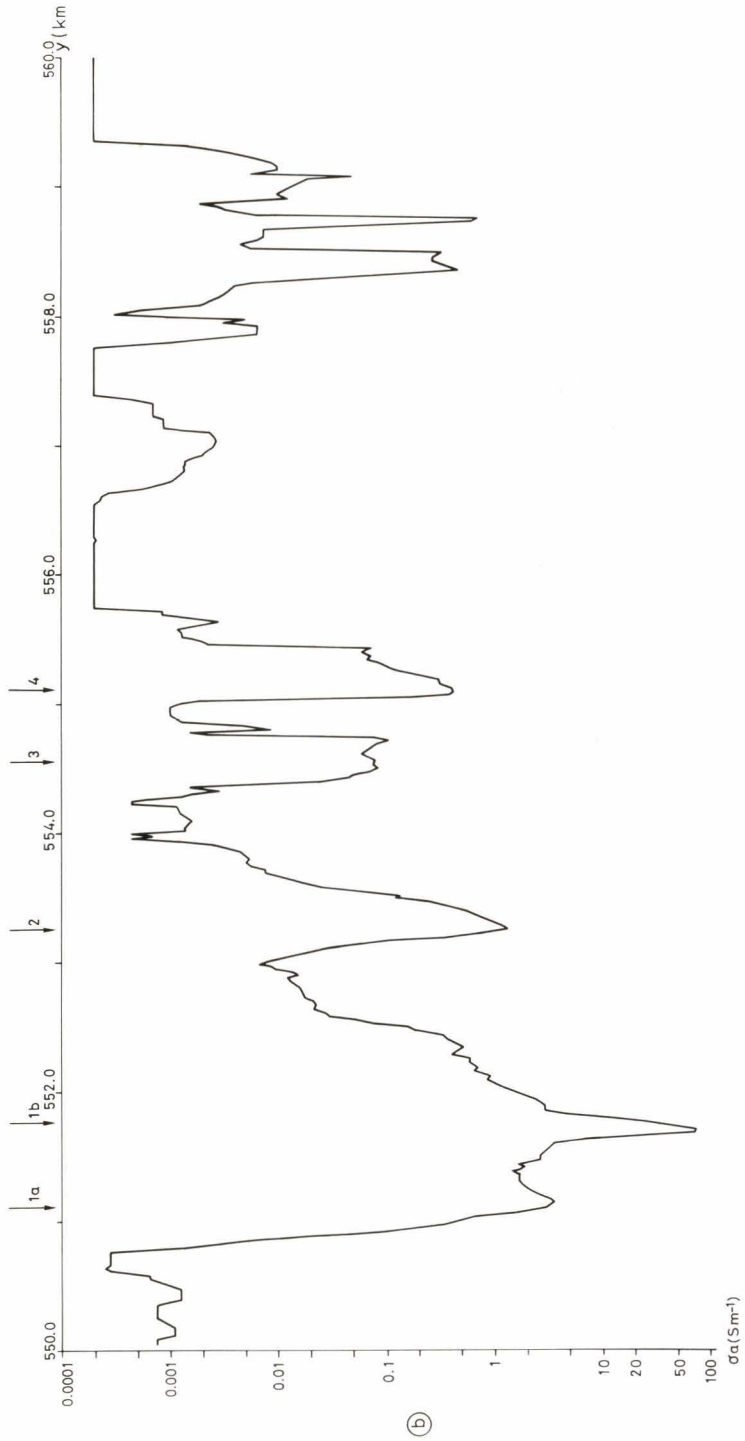
y (km
560.0
558.0
556.0
554.0
552.0
550.0
1a
1b
2
3
4
0.0001
0.001
0.01
0.1
1
10
20
50
100
σa(Sm⁻¹)
(b)

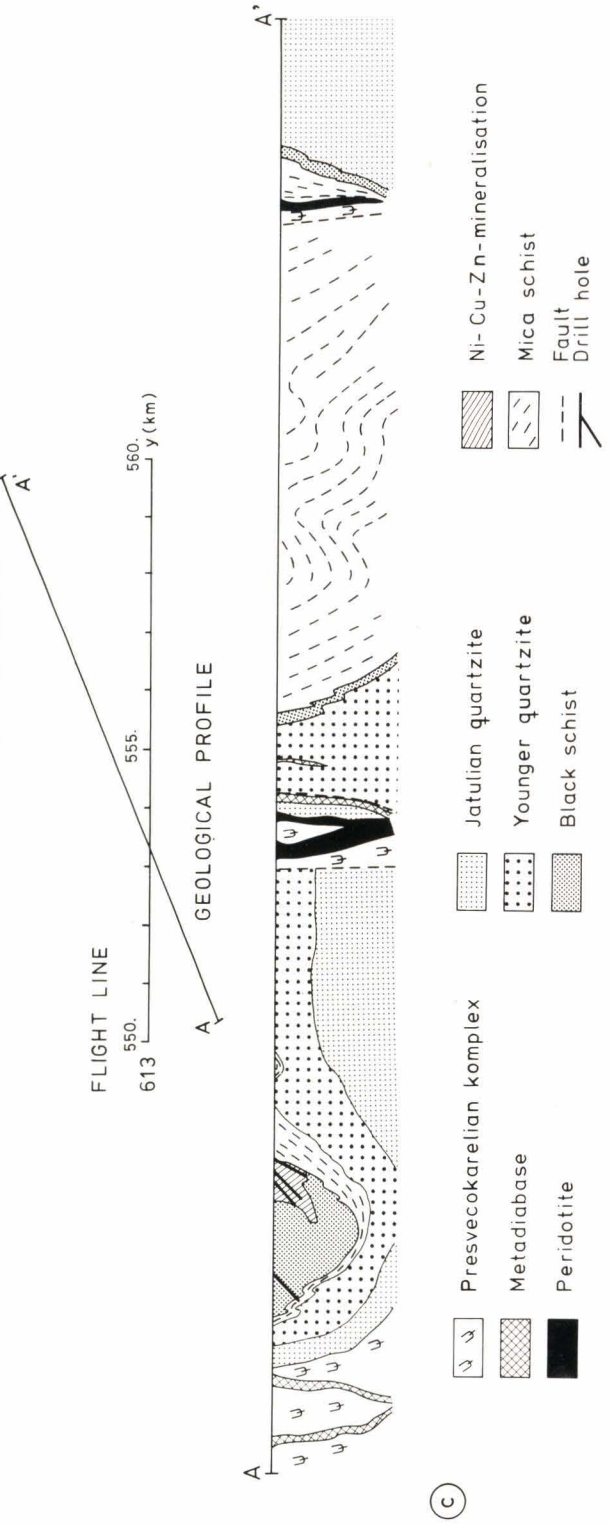

ductivity being so high, perfect compatibility is, in practice, beyond expectation.

- In the most favourable cases, the influence of the dip is also visible in the in-phase and quadrature anomaly curves, as predicted by the scale model data.
- Some of the ground measurements could have been replaced by AEM transformation results had these been available in the early stages of exploration.

Pielavesi Säviä: Conductive vertical half-plane overlain by weakly conductive overburden

The target exemplifies the AEM and EM responses to a vertical half-plane conductor. With this example the penetration and discrimination ability of various methods are compared when the conductivity of the overburden is low but significant.

The chalcopyrite–sphalerite–pyrite occurrence at Säviä was discovered in 1966 by the Geological Survey. The history of the discovery and the geological studies on the deposit have been described by Laitakari (1968) and the geophysical surveys by Siikarla (1968). The results of the slingram survey and their interpretation (Ketola 1968) are still one of the most detailed case histories of the method and constitute excellent comparative material for the AEM data of the present study.

The Säviä ore deposit, whose geological map is shown in Fig. 87, is located in the middle of a roughly 500-m-wide schist zone that strikes in an almost N–S direction. The schist zone is composed of hornblende–cummingtonite gneisses, cordierite–anthophyllite gneisses, quartz–feldspar gneisses and amphibolites. Quartz diorite rocks are encountered west and east of the schist zone. At its northern and southern ends the orebody is subvertical, dipping 70°–85°E; in the middle it has a shallower dip, 40°–50°E. At the northern end it is 10–30 m thick, and in the middle less than 10 m. In the south the orebody branches into two and finally into three separate slabs.

The massive northern part of the orebody averages 1.1 % Cu and 28 % sulphur and the less regular southern part 2 % Zn and 33 % sulphur. The ore is highly conductive. Ketola (1968, pp. 29–30) has measured conductivities $\sigma = 1–300$ Sm^{-1} on the drill-core samples and deduced conductivity-thickness products $s_a = 1.6–88$ S from the slingram data interpreted with thin half-plane models. The ore deposit also exhibits a distinct density contrast with the host rock. The density of the ore varies between 4.10 and $4.20 \cdot 10^3$ kg/m^3 and that of the host rocks between 2.68 and $3.04 \cdot 10^3$ kg/m^3. The susceptibilities are $k = 0.11–0.35$ for the ore, 0.0005–0.05 for the schists and $k = 0.05$ for the quartz diorite. The magnetisation of the schists varies in accordance with the amount of accessory magnetite. Hence it is difficult to localise the deposit by magnetic surveys. The ore deposit is entirely beneath the lake Pielavesi. The depth of the water over the deposit varies from 2.0 to 4.5 m and that of the soil (gyttja and till) from 6 to 27 m. The depth of the soil means that the target is not ideal for EM methods even though the deposit itself has high conductivity and a large conductivity contrast with the country rock. Pyrrhotite and pyrite zones have also been encountered in structures that crosscut the ore deposit diagonally. These zones do not contain minerals of economic value but produce strong electrical anomalies in places.

The area was submitted to high-elevation AEM survey in 1959 and low-elevation survey in 1979. Although not large, the variation in

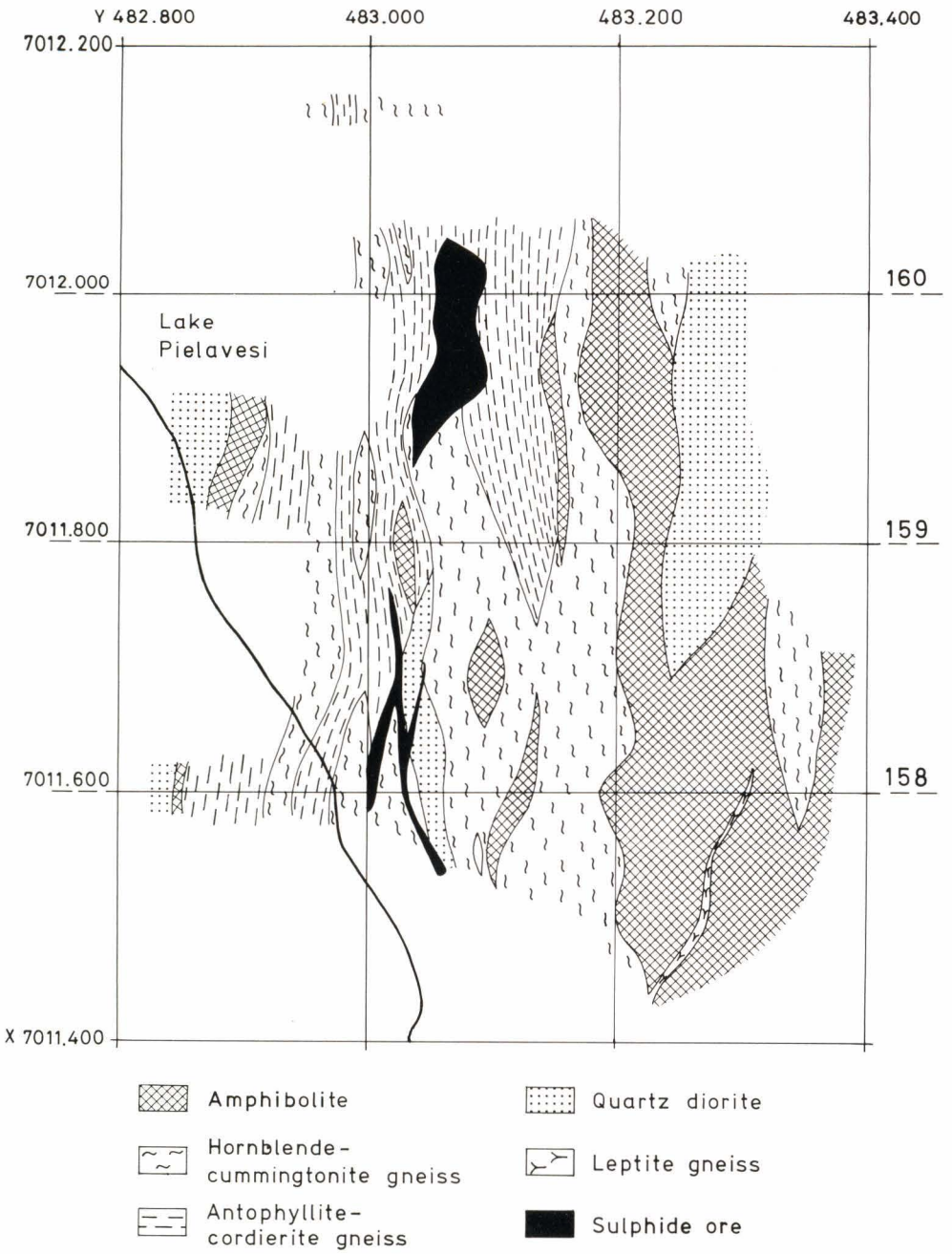

Fig. 87. Geological map of the Pielavesi Säviä area according to Laitakari (1968). Test lines 160, 159 and 158 are marked on the map.

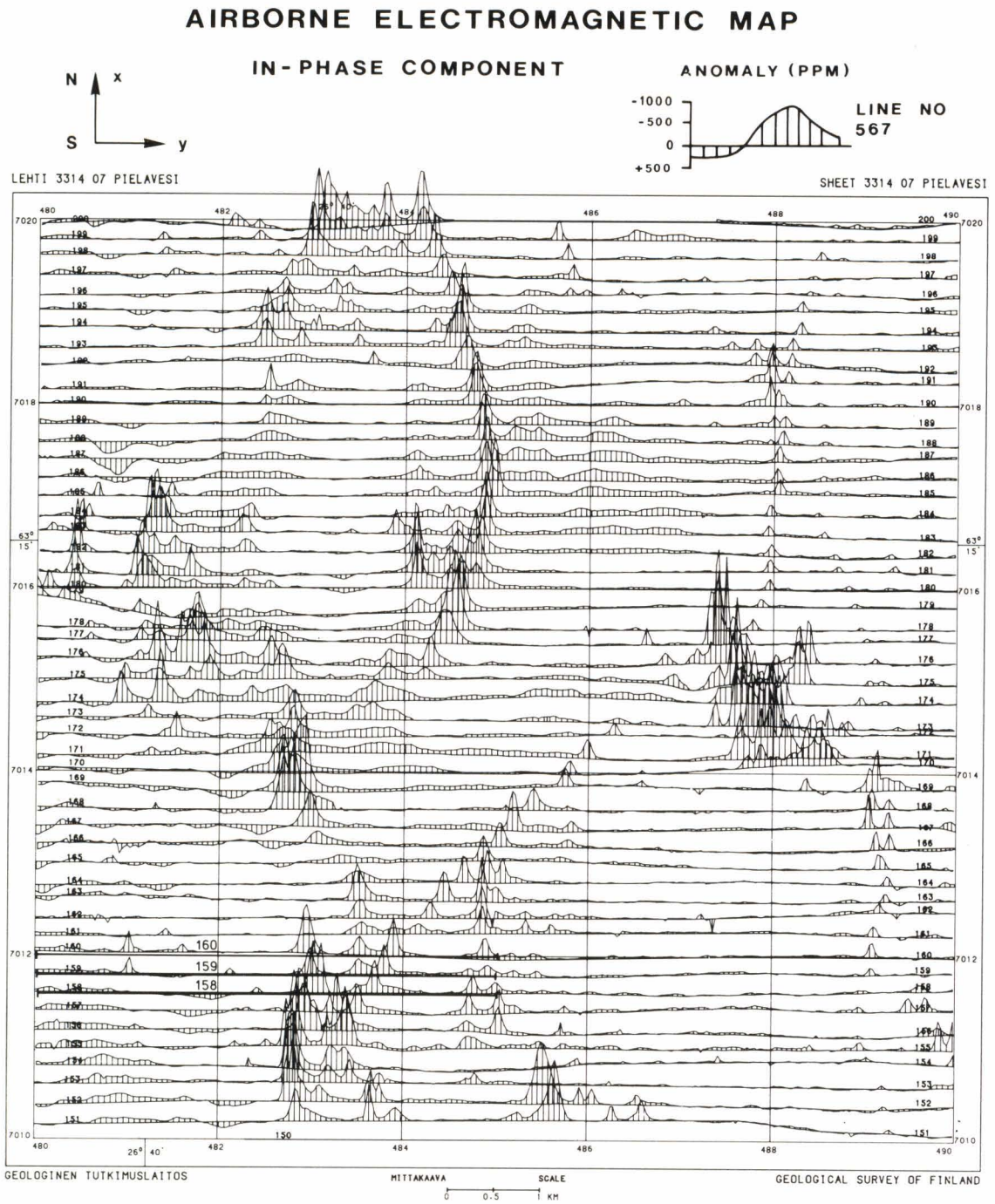

Fig. 88. DC-3 AEM survey data, map sheet 3314 07 (Pielavesi Säviä area). Test lines 160, 159 and 158 are marked on the maps. (a) In-phase component. (b) Quadrature component (see page 175).

AIRBORNE ELECTROMAGNETIC MAP

QUADRATURE COMPONENT

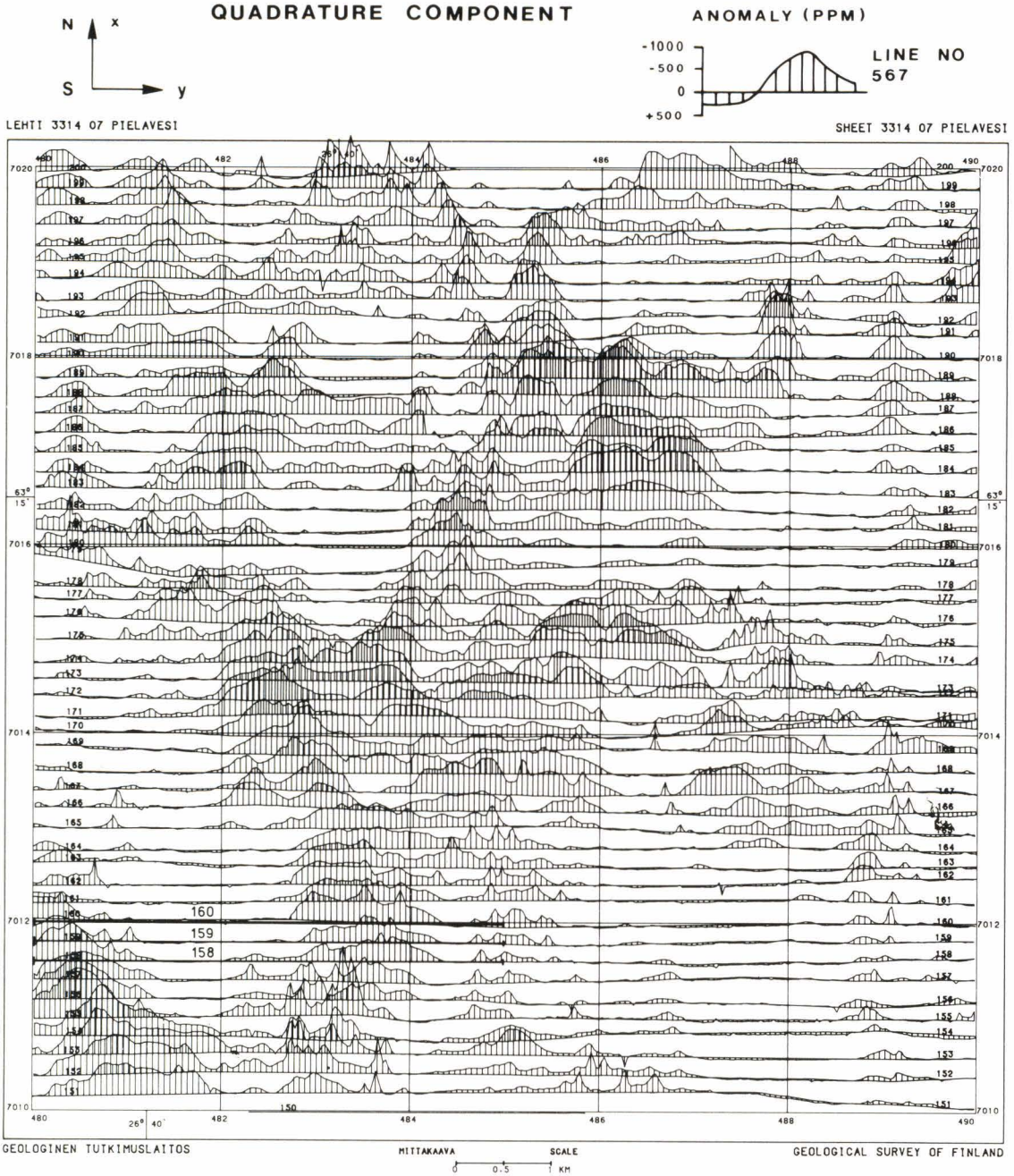

GEOLOGINEN TUTKIMUSLAITOS

MITTAKAAVA SCALE
0 0.5 1 KM

GEOLOGICAL SURVEY OF FINLAND

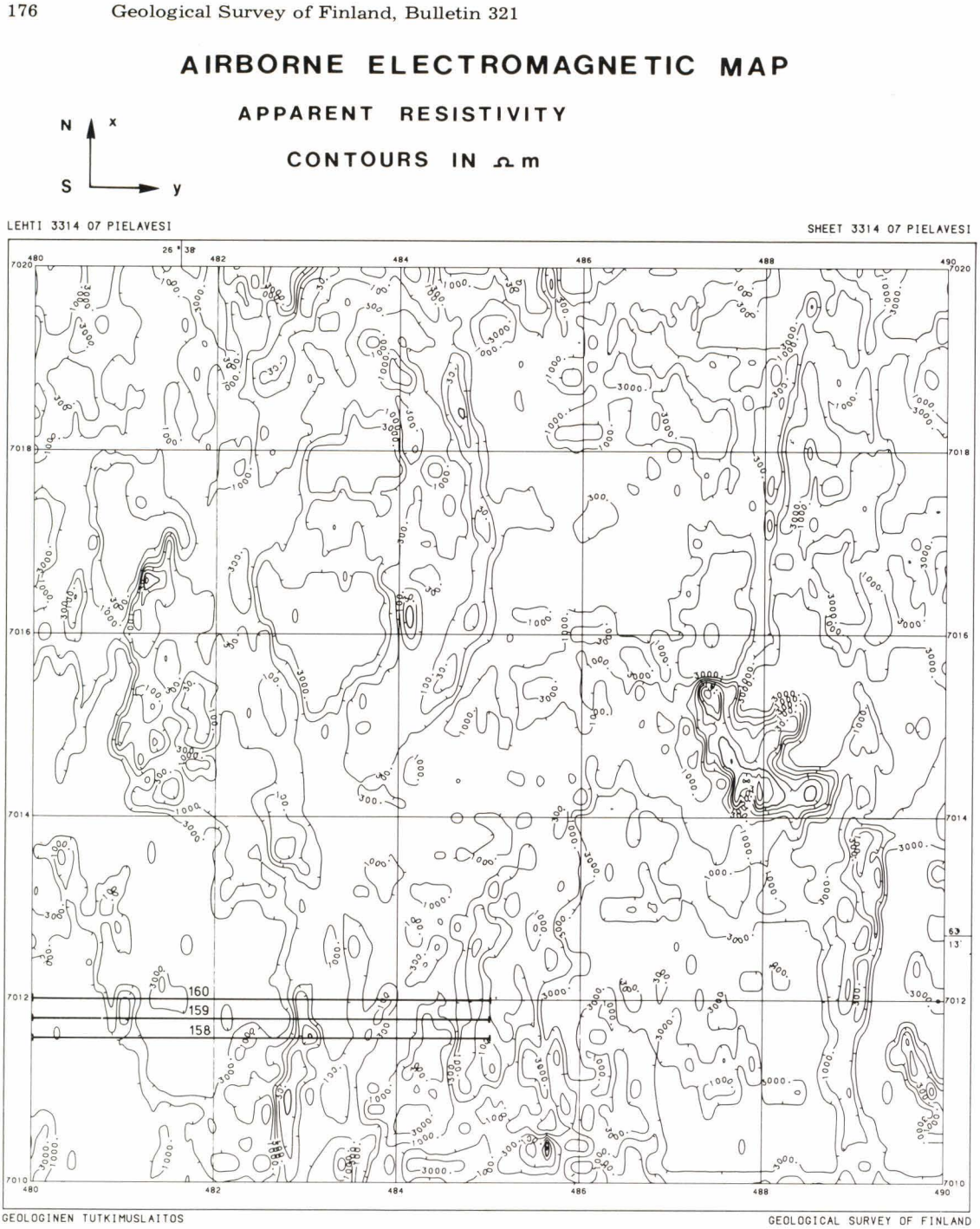

Fig. 89. Transformation results for map sheet 3314 07 (Pielavesi Säviä area) calculated from the original AEM data in Fig. 88 by means of a conductive half-space model. Test lines 160, 159 and 158 are marked on the maps. (a) The apparent resistivity values ϱ_a. (b) The apparent depths to the upper surface of the conductive half-space da_1 (see page 177).

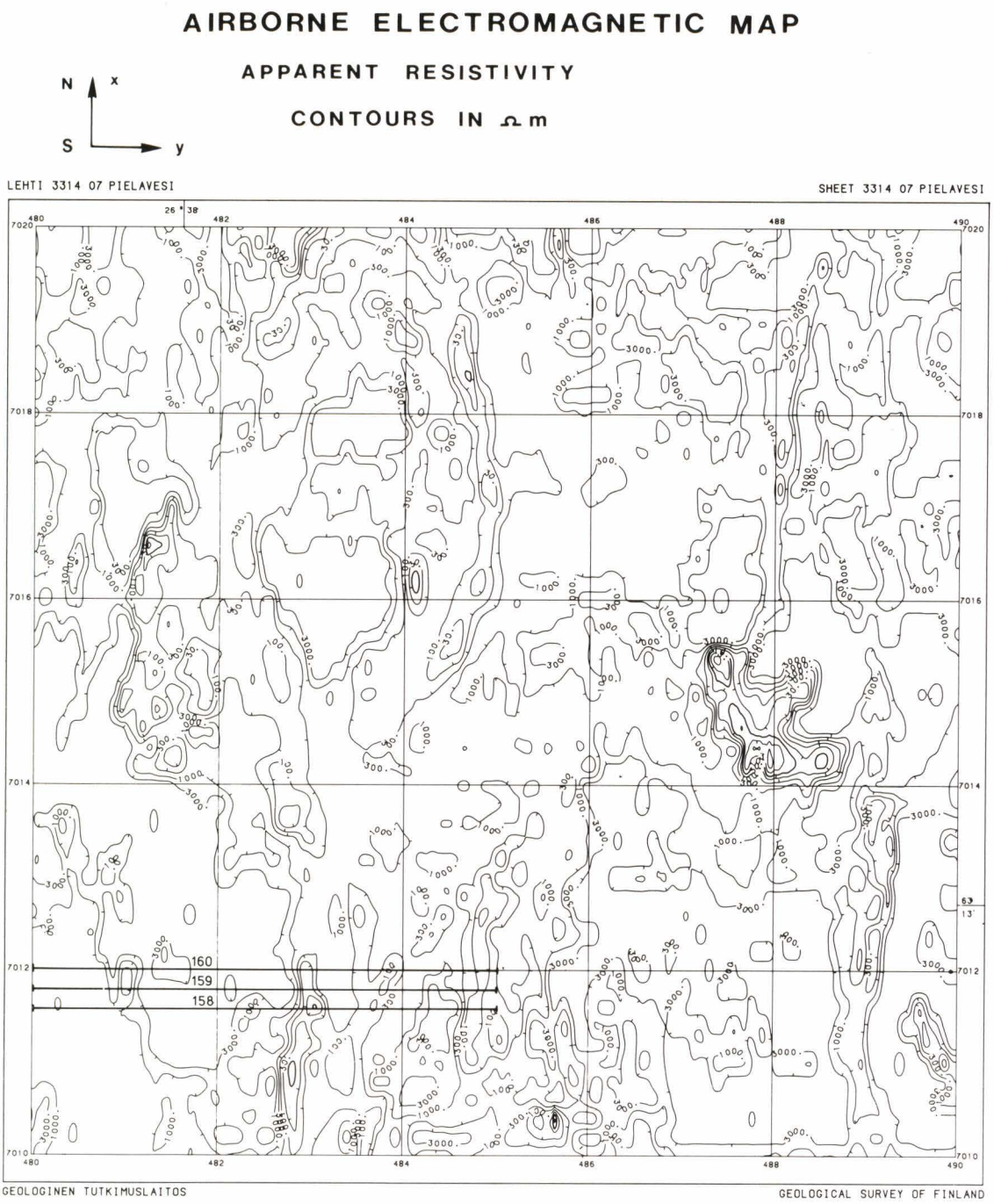

Fig. 89. Transformation results for map sheet 3314 07 (Pielavesi Säviä area) calculated from the original AEM data in Fig. 88 by means of a conductive half-space model. Test lines 160, 159 and 158 are marked on the maps. (a) The apparent resistivity values ϱ_a. (b) The apparent depths to the upper surface of the conductive half-space da_1 (see page 177).

AIRBORNE ELECTROMAGNETIC MAP

APPARENT DEPTH, 1-LAYER MODEL

CONTOURS IN m

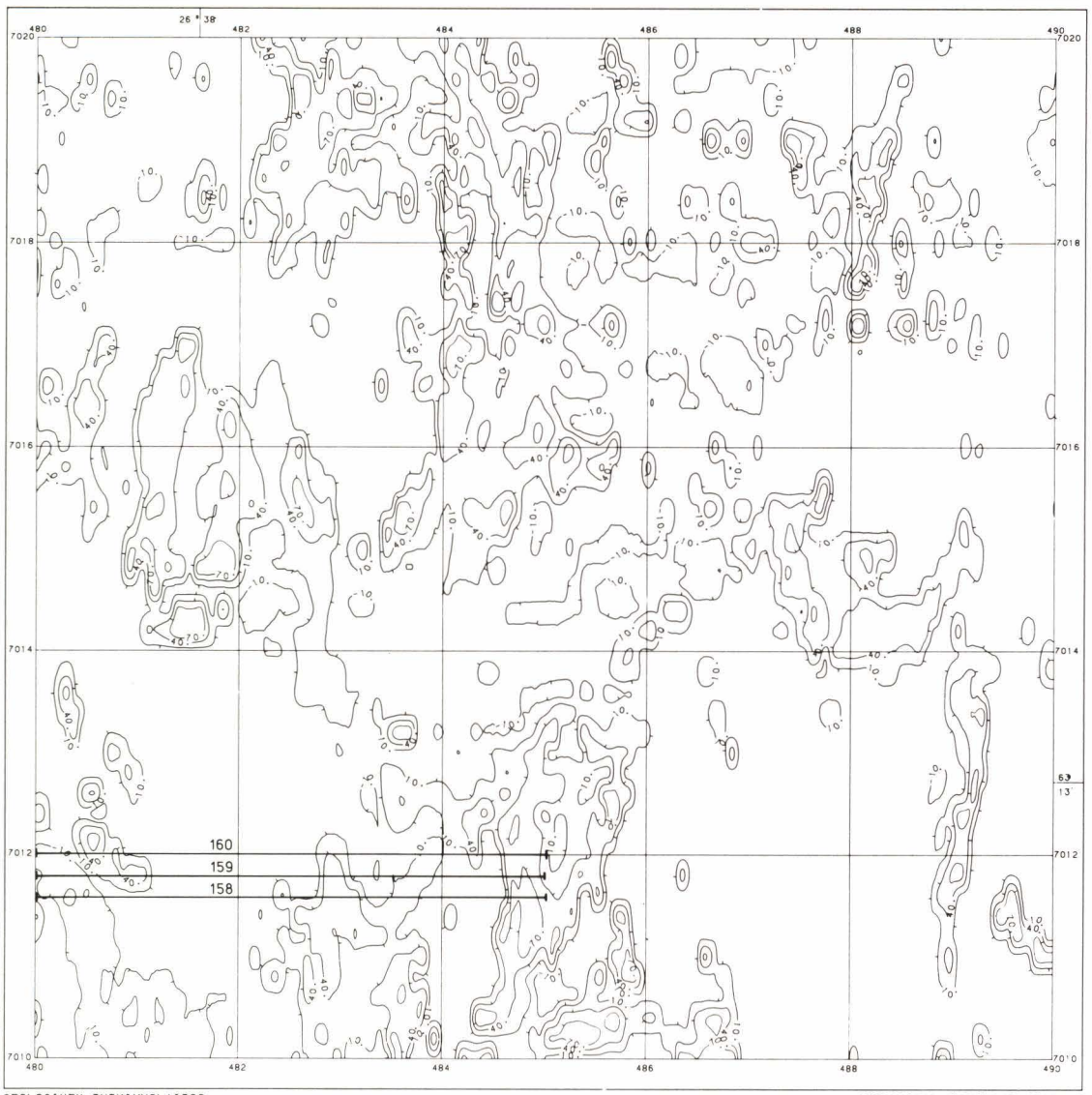

topography is sharp in some places. The average flight elevation in the area was $\bar{h}$ = 38 m and the standard deviation σ_h = 6 m. Noise anomalies due to power transmission and telegraph lines are abundant in the AEM data. The in-phase, quadrature anomaly maps of the low-elevation survey in the area (map sheet 3314 07) are shown in Fig. 88. The transformed values, apparent resistivities ϱ_a, are shown in Fig. 89. Visual examination of the AEM anomaly data shows that the quadrature component anomalies are large, although rather low in amplitude (0 ··· −600 ppm), and that they are caused by gyttja in waterways and by other poorly conductive soils. In contrast, the in-phase anomaly map exhibits anomaly zones of restricted size and fairly high amplitude, in-phase = −1 000 ··· −1 500 ppm, indicating graphite- and sulphide-bearing zones in bedrock. The strong SW-NE-trending anomaly zone on the map is caused by a power transmission cable buried in the lake bottom. One of the in-phase anomaly zones clearly indicates the Säviä ore deposit. It is seen that the quadrature component produces only such a low indication of the deposit that it is easily masked by the regional anomaly caused by the poorly conductive horizontal layer (gyttja on the lake bottom). This also explains why it was not possible to obtain clear anomalies of very good conductors, the ore deposit included, with the high-elevation airborne AEM system I that utilised merely the quadrature component.

Comparison between the original data and the transformed ϱ_a values demonstrates that transformed values equal in-phase component data in explorational applicability but that, in this case, they do not offer additional means of sorting out anomalies. This is mainly due to the quadrature anomalies of the bottom gyttja, which make the in-phase/quadrature ratios of the sum anomalies only moderate (Re/Im ≈ 2) even over good conductors in the bedrock. The ore body is outlined by a 100 Ωm-contour, but the best conductors in the study area are larger graphite- and pyrrhotite-bearing schist zones with minimum values of 0.3 Ωm around x = 7015, y = 488.

Line 160

The AEM data were analysed in more detail for three survey lines passing over the ore deposit (see Fig. 87 and Table 20). The northernmost of them, line 160 (x = 7012.0 between y = 480.000–485.000), passes over the massive and thickest portion of the deposit. Fig. 90 gives, for this line, survey data of various geophysical methods. A positioning error of 80 m along the AEM survey line is evident when the airborne and ground data are compared with each other. As pointed out earlier the difference between the in-phase component and quadrature component data is conspicuous. The outcome of the slingram survey with a coil separation of l = 40 m and a frequency of f = 3 600 Hz was negative, i.e., an indication was not produced at the deposit (Siikarla 1968). The result obtained with a coil separation of l = 60 m is, however, a good example of an anomaly produced by a thick vertical sheet-like conductor. The interpretations of the AEM and slingram data on the basis of scale model results are given in Fig. 91. In the interpretation, the regional anomaly of the horizontal conductor has been graphically subtracted from the quadrature component of the AEM survey data, because combined model results for a conductive overburden and a thick half-plane were not available. Since the depth and thickness values of the conductor in the scale model tests were only slightly varied, the AEM interpretation must be considered approximative and less effective in discrimination ability

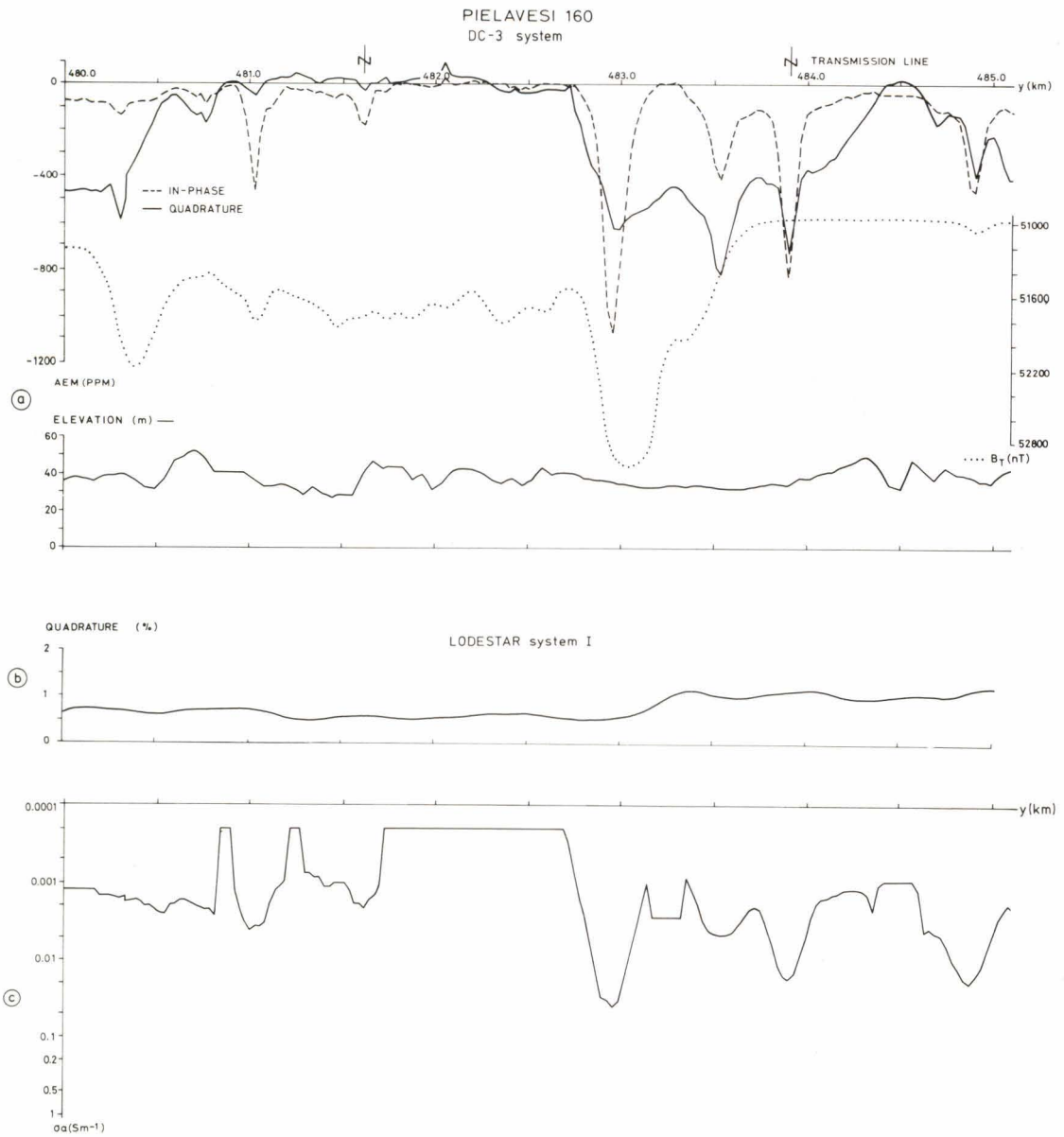

Fig. 90. Test line Pielavesi 160, results of various geophysical methods. (a) DC-3 aerogeophysical survey, AEM, aeromagnetic and flight elevation data, point spacing $\Delta y = 29$ m. (b) Lockheed Lodestar aerogeophysical survey, AEM data of high-elevation system I. (c) The values of apparent conductivity σ_a calculated from the DC-3 AEM survey data.

than the slingram data. Interpretation of AEM in-phase anomaly data (Re = −1 072 ppm, $w_{1/2}$ = 125 m) gives d = 25 m, da_3 = 43 m−36 m = 7 m from Fig. 40. The best fit was achieved with a model curve corresponding to a σd value of 116 S. In spite of its shortcomings, the AEM interpretation may be considered satisfactory.

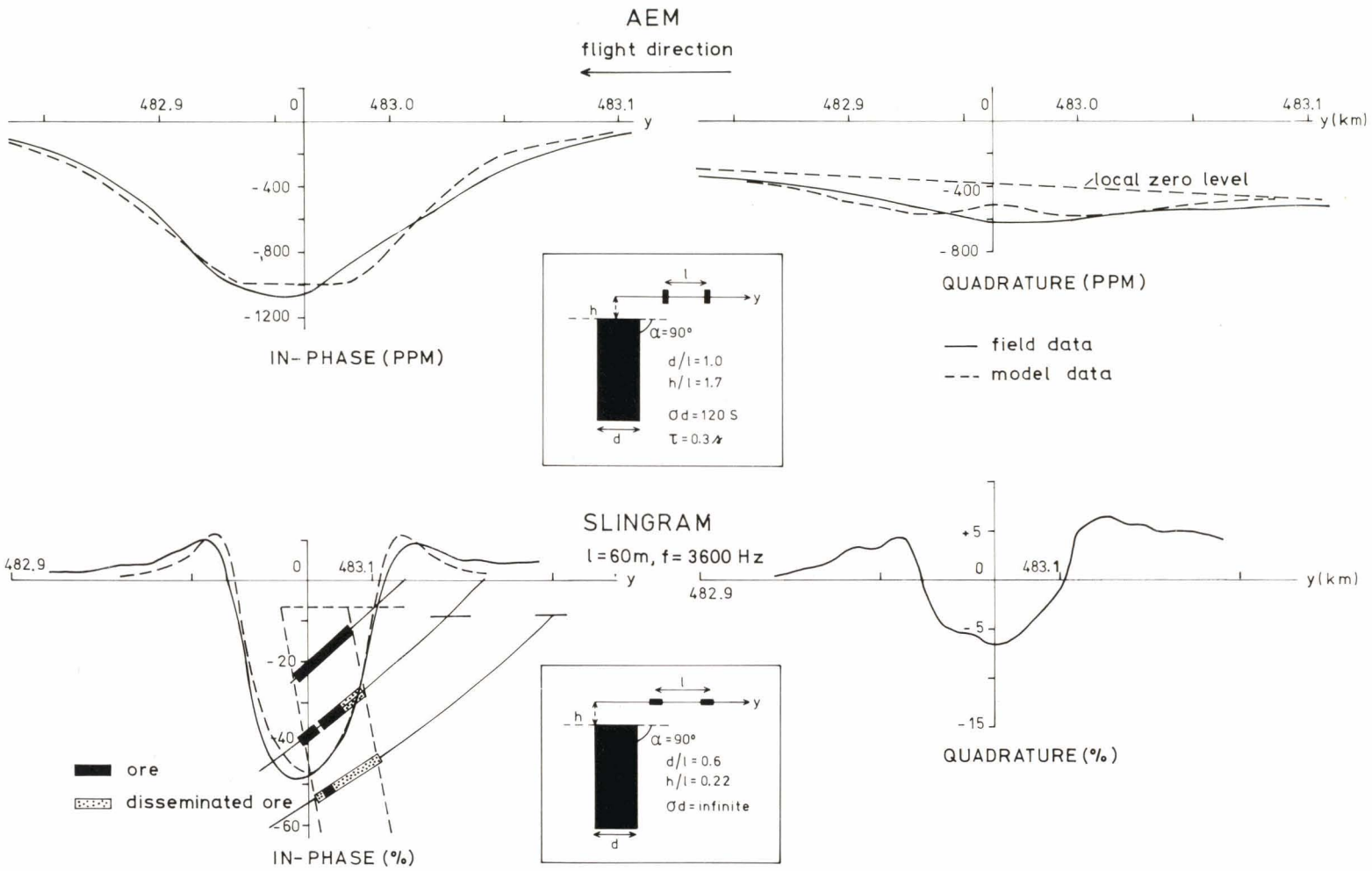

Fig. 91. Test line Pielavesi 160, comparison of AEM and slingram measurements: interpretation of AEM data with thick half-plane model. Interpretation of slingram data by Ketola (1968, Fig. 36) is shown for comparison.

Table 20

Comparison of results from Pielavesi Säviä area, test lines 160, 159 and 158.

(a) The DC-3 AEM results together with data on flight elevation and overburden thickness.

	Test line		
	160	159	158
In-phase peak anomaly (ppm)	−1072	−584	−1132
Quadrature peak anomaly (ppm)	− 620	−300	− 370
Quadrature anomaly due to overburden (ppm)	− 400	−150	− 200
Quadrature anomaly due to half-plane (ppm)	− 220	−150	− 170
Flight elevation (m)	36	46	37
Depth of water (m)	4	3	1
Thickness of soil (m)	13	13	18

(b) The results of AEM interpretation compared with the slingram interpretation results (Ketola 1968).

	Test line					
	160		159		158	
	AEM	Slingram	AEM	Slingram	AEM	Slingram
Overburden conductance (S)	0.08	0.27	0.03	0.13	0.04	0.17
Half-plane conductance (S)	120	∞	14 (81)	7.2	56	88
Depth to subsurface outcrop (m)	7	13	9 (4)	24	8	12
Half-plane dip angle (degr.)	90	90	90	60	90	90

The DC-3 AEM data in Figs. 90 and 30 give s_a = 0.08 S, da_2 = 10 m for the horizontal conductor over the ore outcrop. The slingram data in Fig. 90 also vaguely indicate the effect of the horizontal conductor as a change in the anomaly zero levels. The interpretation based on Fig. 51b and the anomaly values of in-phase = +4.0 %, quadrature = +4.5 % gives for the horizontal conductor s_a = 0.27 S, da_2 = 8 m.

Line 159

The results for line 159 (x = 7011.8, between y = 480.000–485.000) are shown in Fig. 92. The AEM anomaly is now lower in amplitude and, in spite of a 10 m increase in flight elevation, narrower than on line 160. The anomaly is symmetrical in shape, and hence, the characteristic diagrams of a vertical thin half-plane were used. The anomaly values (in-phase = −584 ppm, quadrature = −150 ppm) and Fig. 35b give σd = 14 S and da_3 = 55 m − 46 m = 9 m when the conductance of the horizontal conductor is s_a = 0. Fig. 37a, in which the horizontal conductor has a value of s_a = 0.18 S, gives correspondingly σd = 12 S and da_3 = 7 m. Hence, the field survey data give for the half-plane conductor a depth that is greater than the true one and a σd product that is higher, if the conductive overburden is not included in the scale model configuration. The phenomenon has been reported earlier in connection with AEM scale model studies, e.g. Ghosh (1972).

The AEM interpretation results above are in satisfactory agreement with those deduced

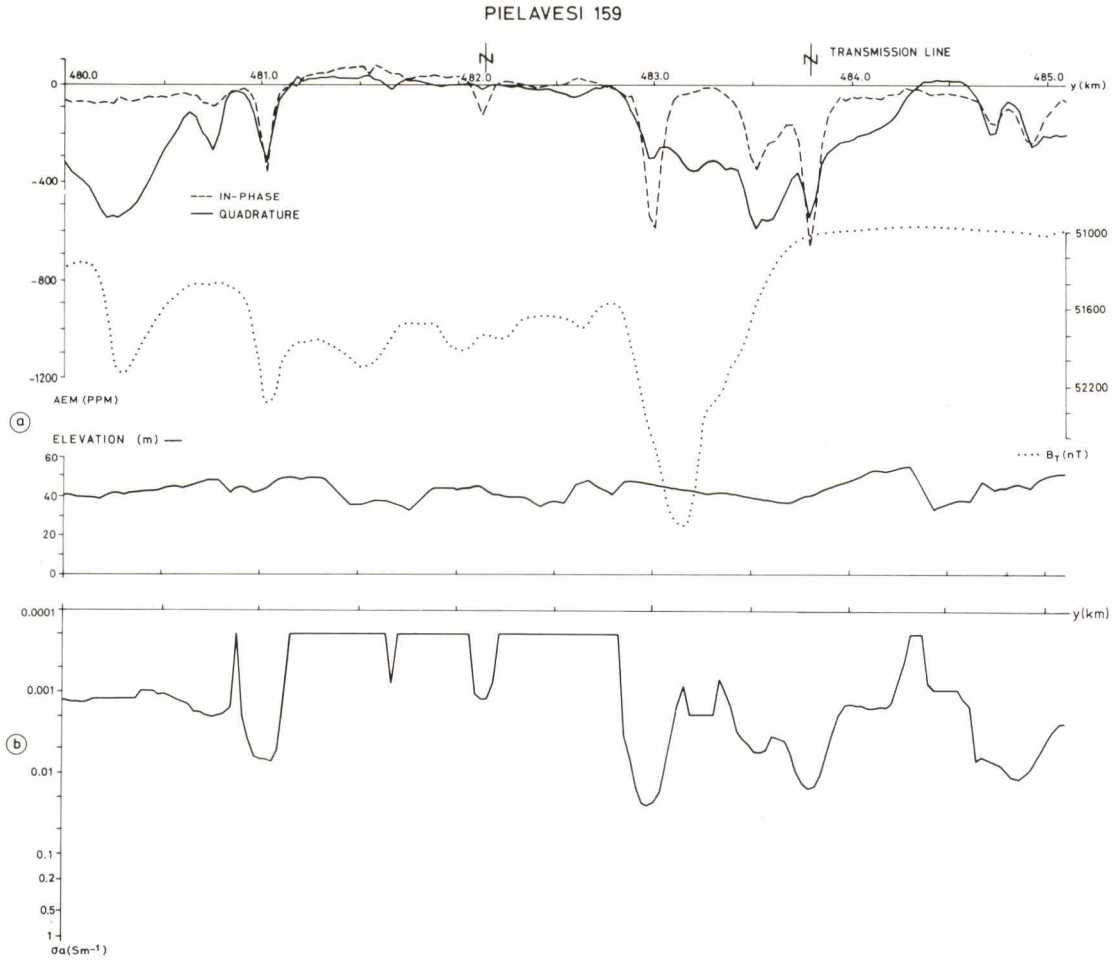

Fig. 92. Test line Pielavesi 159, results of various geophysical methods. (a) DC-3 aerogeophysical survey, AEM, aeromagnetic and flight elevation data, point spacing Δy = 29 m. (b) The values of apparent conductivity σ_a calculated from AEM survey data.

by Ketola (1968, Fig. 39) from the slingram data, σd = 7.2 S, da_3 = 24 m. A comparison of AEM field and model data as anomaly profiles, however, reveals a very poor fit: the measured anomaly is much broader than the thin half-plane model predicts. The application of the thick half-plane model gives a better fit as shown in Fig. 93. The selection of the model curve was based on measured values (in-phase = −584 ppm, $w_{1/2}$ = 90 m) and Fig. 40, which lead to d = 18 m, da_3 = 4 m. The best-fitting model curve with these parameter values corresponds to a σd value of 81 S. These results are widely different from those achieved with the thin half-plane model.

Both the AEM and the slingram interpretation results for lines 160 and 159 show that the outcrop of the conductor is deeper on line 159 than on line 160. Unlike the slingram survey, the AEM data give no indication of the change in dip.

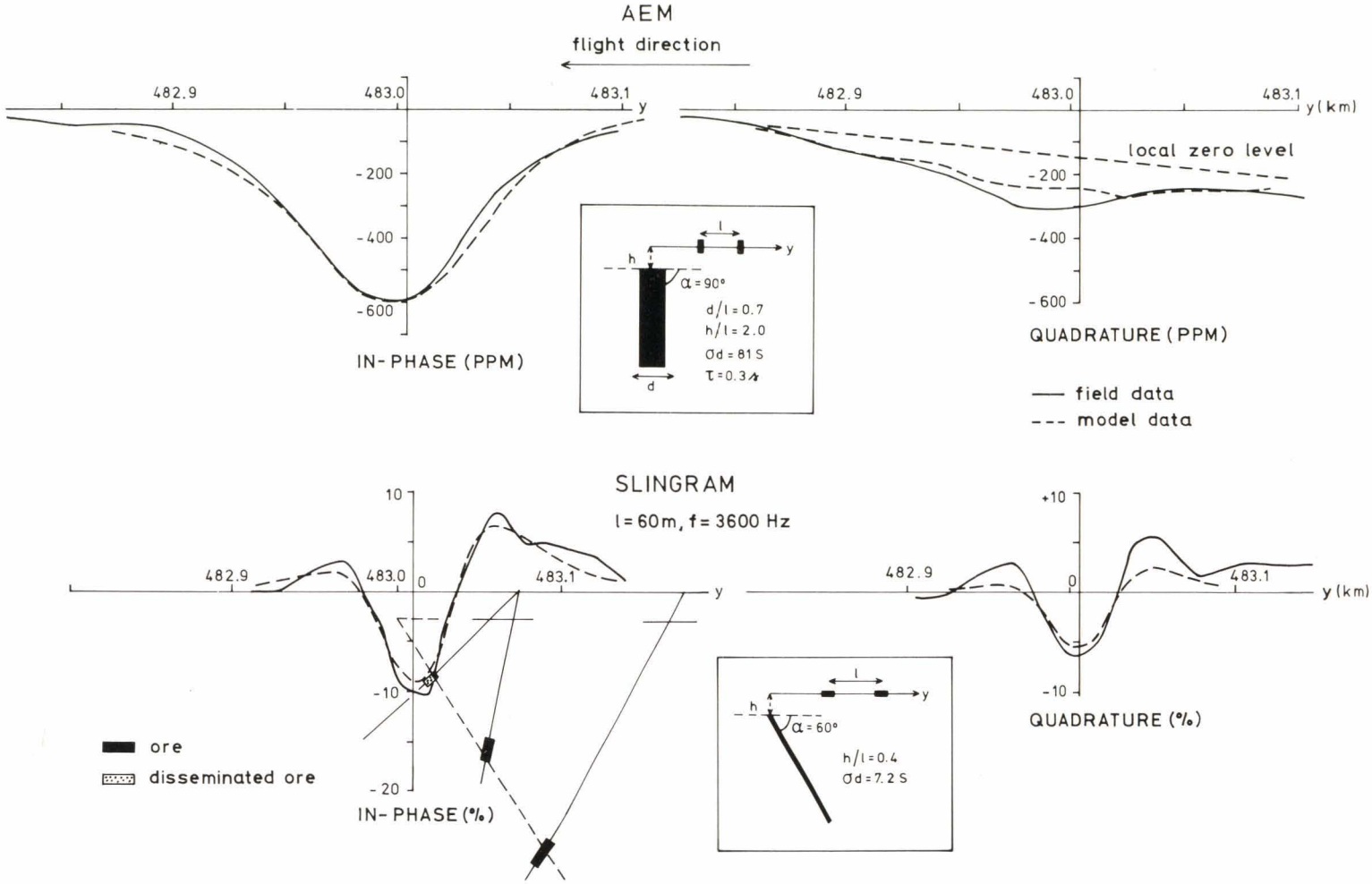

Fig. 93. Test line Pielavesi 159, interpretation of AEM data with thick half-plane model, compared with the interpretation of slingram data with thin half-plane model by Ketola (1968, Fig. 39).

Line 158

The results for line 158 (x = 7011.6, between y = 480.000–485.000) are given in Fig. 94. The AEM high-elevation results are again dominated by the response from the conductive overburden. The DC-3 in-phase anomaly has two peaks, but the quadrature anomaly only

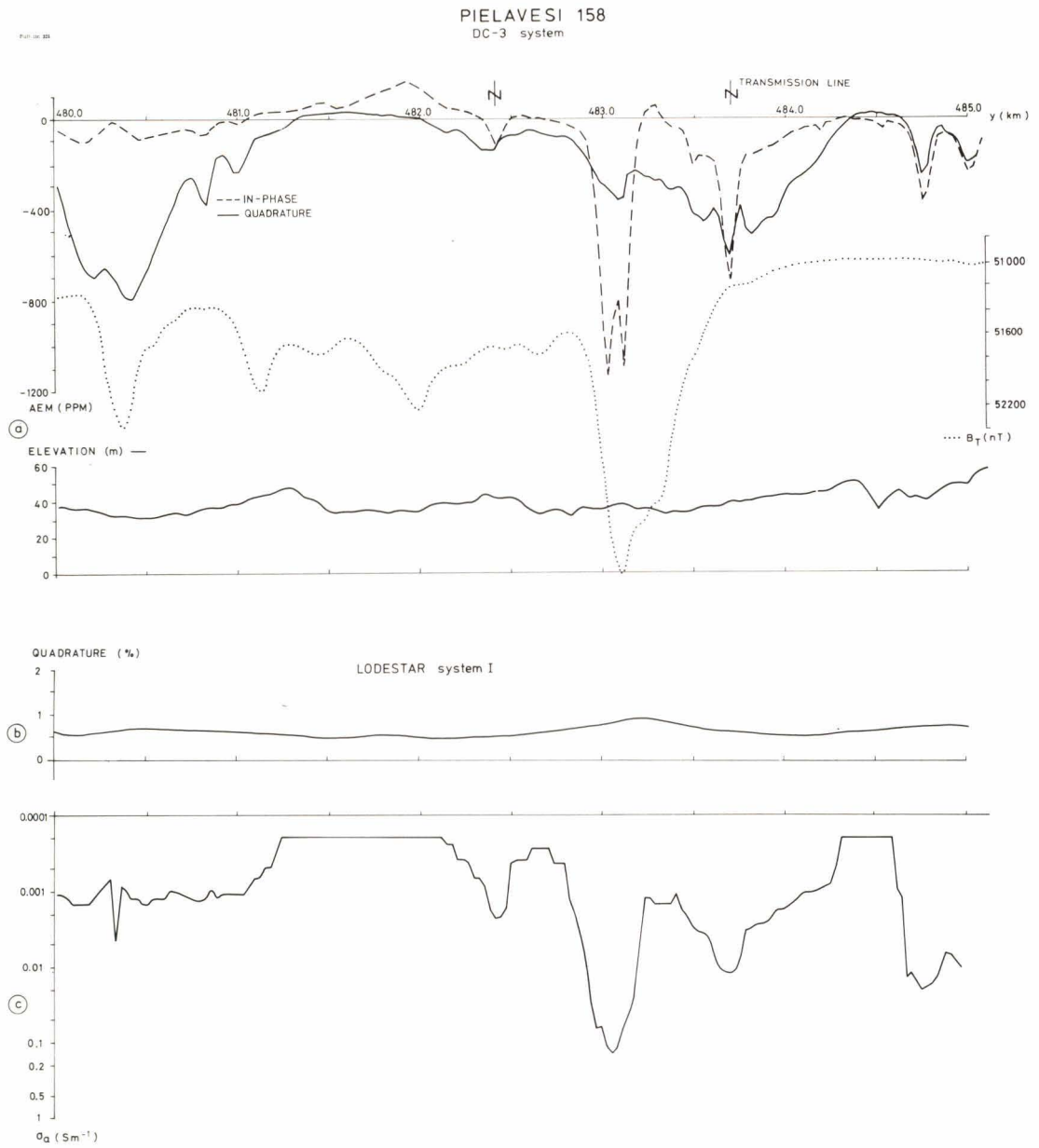

Fig. 94. Test line Pielavesi 158, results of various geophysical methods. (a) DC-3 aerogeophysical survey, AEM, aeromagnetic and flight elevation data, point spacing Δy = 29 m. (b) Lockheed Lodestar aerogeophysical survey, AEM data with high-elevation system I. (c) The values of apparent conductivity σ_a calculated from AEM survey data.

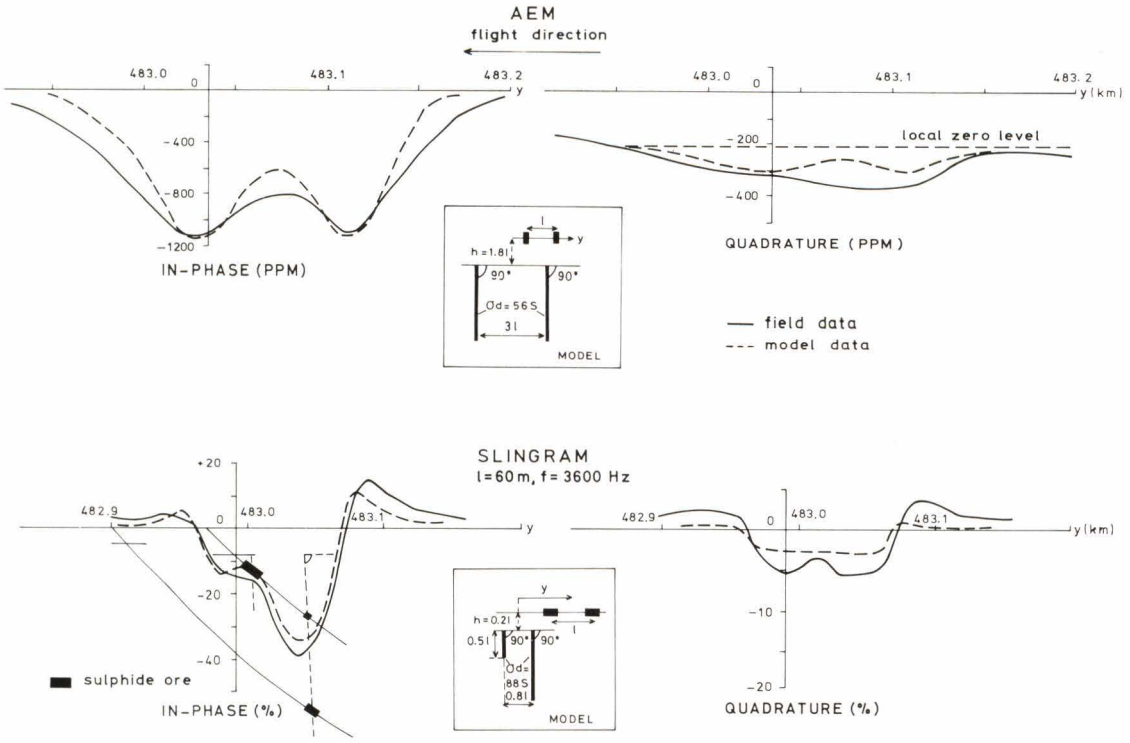

Fig. 95. Test line Pielavesi 158, interpretation of AEM data with a combination of two thin half-plane models. Interpretation of slingram data by Ketola (1968, Fig. 42, model curve 1) is given for comparison.

one; hence the type of the anomaly source is difficult to establish from the AEM data. The scale model results suggest that the anomaly may be caused by a thick conductive plate or two adjacent thin sheets. On the basis of the slingram and drilling results, the latter alternative is correct. The interpretation of the AEM data (Fig. 95) on this line remains approximative, as the model data has been obtained by adding graphically two separate thin-sheet responses. Values of $\sigma d = 56$ S, $da_3 = 8$ m are obtained for both conductors. The interpreted slingram and AEM values are of the same order of magnitude for both conductor zones. The discrimination ability of the AEM data on the western conductor, however, is markedly poorer than that of the slingram data, as no indication of the finite depth extent of the conductor is obtained.

Summary of the Säviä results

The AEM results for the Säviä deposit can be summarised as follows:

- The discrimination ability of the AEM results was found to be from satisfactory to poor in practice. The AEM response to a vertical, highly conductive half-plane could be clearly distinguished from the background anomaly caused by geological noise, and inaccurate but qualitatively correct values were obtained for the variations in the conductivity and/or depth to outcrop

of the half-plane. Although it was possible to interpret the data on the basis of the half-plane model, the discrimination ability in terms of dip angle and depth extent was distinctly poorer than in the detailed slingram survey.

- On the basis of the Säviä target and other similar examples (e.g. Sorosuo, p. 146), it can be concluded that, in practice, the penetration of the DC-3 AEM system is superior to that of the slingram survey with a coil separation of l = 40 m and at a frequency of f = 3 600 Hz. This is so at least in overburden that is even slightly conductive. In such a case, the penetration of the slingram method will be reduced to less than 0.25 l.
- There are other examples besides the Säviä deposit of explorational applications, e.g. the Pyhäsalmi ore deposit (Peltoniemi 1977, Fig. 23), which demonstrate that the conductance aperture of AEM systems operating merely on the quadrature component is closed also in practice. When applied to a highly conductive half-plane, such systems operate so close to the inductive limit of the response function that the small quadrature anomaly produced by the half-plane conductor cannot be distinguished from the geological noise generated even by weak overburden conductors.

Pielavesi Ilokangas: Small conductive ore breccia

In another context, i.e. Savukoski Miekkaoja (pp. 210–213), an example is given of AEM responses to local three-dimensional conductors. In the present example, the resolution of the AEM method is examined in relation to the minimum size of a detectable conductor. As shown by the detailed geological map in Fig. 96, the conductor is a small sulphide ore breccia in a peridotite body in the area of Ilokangas, Pielavesi (map sheet 3314 06).

The low-elevation AEM survey conducted in 1979 covered the whole Pielavesi area, including the map sheet in question. The AEM and aeromagnetic results of the target area are shown in Fig. 97. By visual inspection the target can only be localised on the aeromagnetic map. The magnetic and slingram ground survey maps of the target are given in Figs. 98a, b. The minimum of the slingram anomaly is located on profile x = 7036.950. The low-elevation airborne AEM survey was undertaken on profile x = 7037.000. According to the fixpoint and the Doppler positioning data, however, the true flight path passed between x = 7036.950 and .960 at this site, and so the AEM and ground survey profiles almost overlap. Figs. 98c, d show the AEM and aeromagnetic survey profile on the target. The AEM anomaly is very small, −70 ppm in in-phase component and −60 ppm in quadrature component. This means that within the normal detection limit of 100 ppm the anomaly would not be distinguishable from the noise. The anomaly can be recognised, however, on the basis of the in-phase component. On account of the low amplitude of the anomaly the model interpretation is not much use. The half-width (50–70 m) and the in-phase/quadrature ratio (≈1) of the anomaly, however, suggest that the conductor is small, has medium to high conductivity and is located close to the surface of the bedrock. The blanket of overburden at the site is shallow, only 1–2 m thick.

The slingram survey data on profile x =

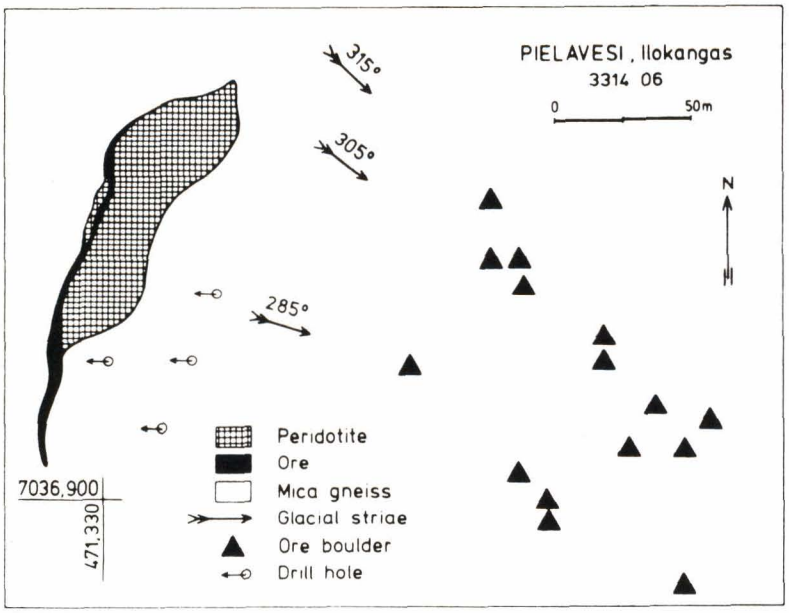

Fig. 96. Geological map of the Pielavesi Ilokangas area, according to Ekdahl (1976a).

7036.950 are so straightforward that their interpretation can be expected to give a more accurate result. With the aid of the sphere-modelling program, a set of model curves was calculated by varying the radius, depth and conductivity of the sphere and the coil separation.

The responses that best suit the slingram survey data for a coil separation of l = 100 m were computed and are shown together with the survey data in Fig. 99b. The parameters of the best-fitting model were z = 7 m, a = 5 m, σ = 100 Sm^{-1}. The compatibility between the measured and computed results is good. Figs. 99a, c give the corresponding data of the same model for coil separations of l = 60 m and l = 160 m. These results are also compatible. It became evident during the computing that the outcome of the interpretation is very sensitive to changes in the parameter values. Thus, the models z = 12 m, a = 10 m, σ = 10 Sm^{-1}, or z = 9 m, a = 7 m, σ = 30 Sm^{-1} result in a distinctly poorer fit than does the model shown in Fig. 99. Both the measured and the computed slingram responses on profiles 50 m away from the outcrop are below the reading accuracy of the instrument.

Interpretation of the slingram data with the aid of the half-plane model would not give very good results. If applied, a model with two adjacent vertical sheets should be used. In that case, however, the minima are not as sharp as in the measured data. Hence, in the slingram method as well, the anomaly of a sphere with low z/a values is diagnostic in shape and differs clearly from the anomaly of the half-plane. Consequently, the similarity pointed out by Lodha (1974) between the slingram anomalies of the half-plane and the sphere is valid only at higher values of the radius a and the depth z.

Fig. 98d shows the aeromagnetic survey results, values of the magnetic total field and its horizontal across-track difference. The latter suggest that the source is three-dimensional and occurs south of the flight line. The interpretation of the magnetic total field anomaly with the special points method gives z = 25 m, a = 5.5 m and susceptibility k = 0.01.

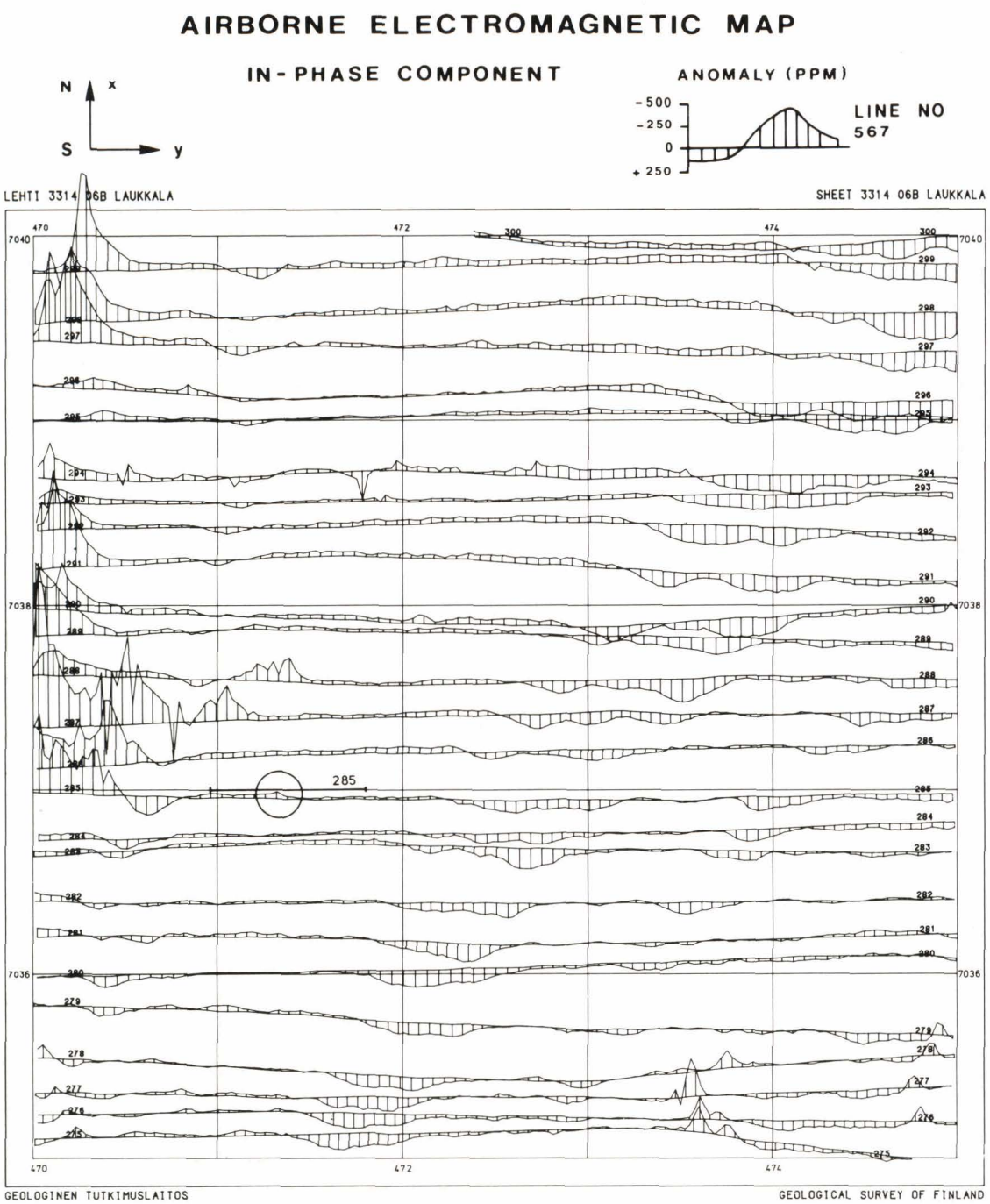

Fig. 97. DC-3 aerogeophysical survey data on the NW quarter of map sheet 3314 06 (Pielavesi Ilokangas area). Test line 285 is marked on the maps. (a) AEM in-phase component. (b) AEM quadrature component (see page 189). (c) Aeromagnetic survey data, the absolute values of the magnetic total field 1965.0 (see page 190). Horizontal transverse gradient data were employed in the interpolation of the grid for contouring (Korhonen 1979). Contour interval 50 nT.

AIRBORNE ELECTROMAGNETIC MAP

QUADRATURE COMPONENT

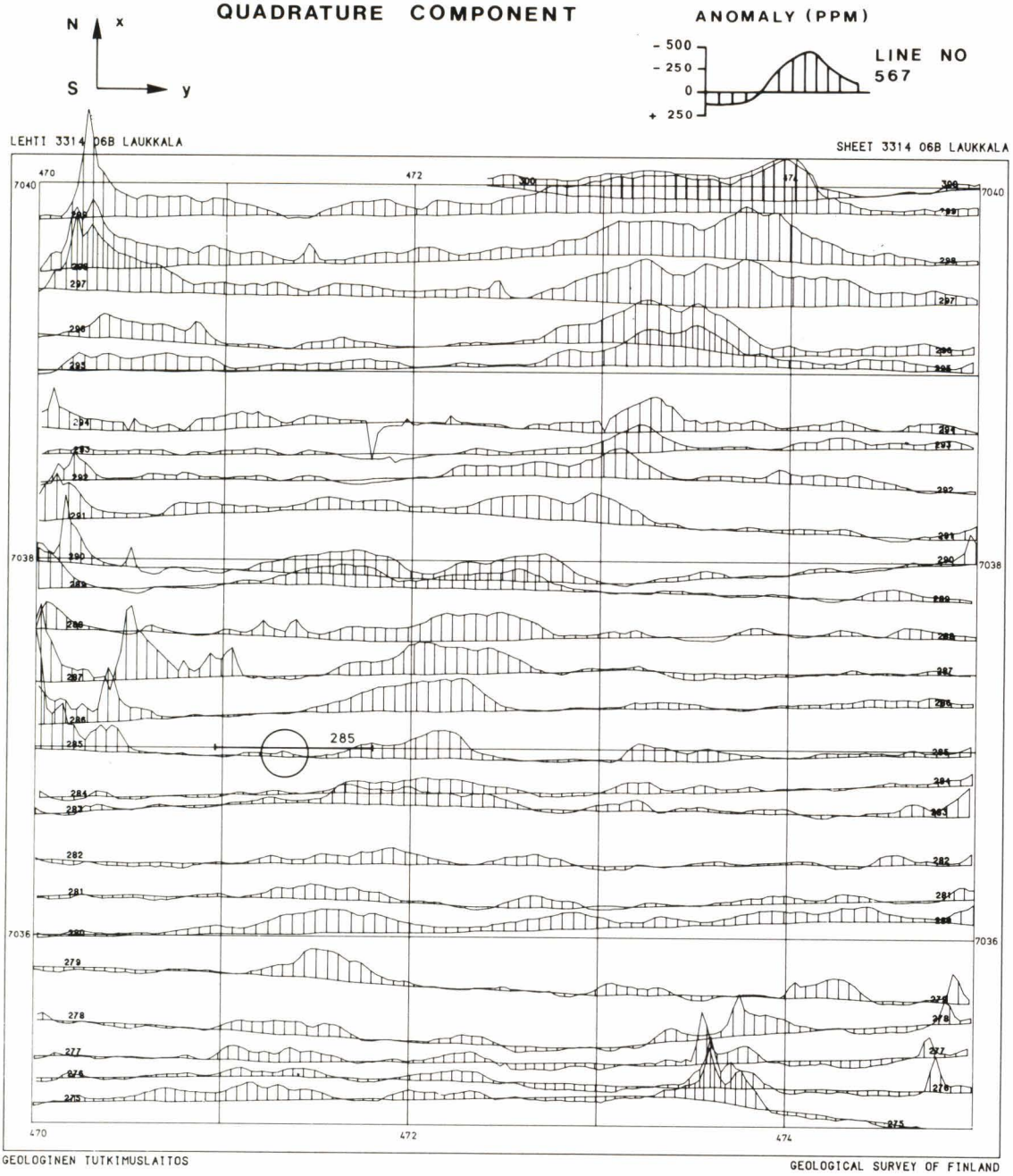

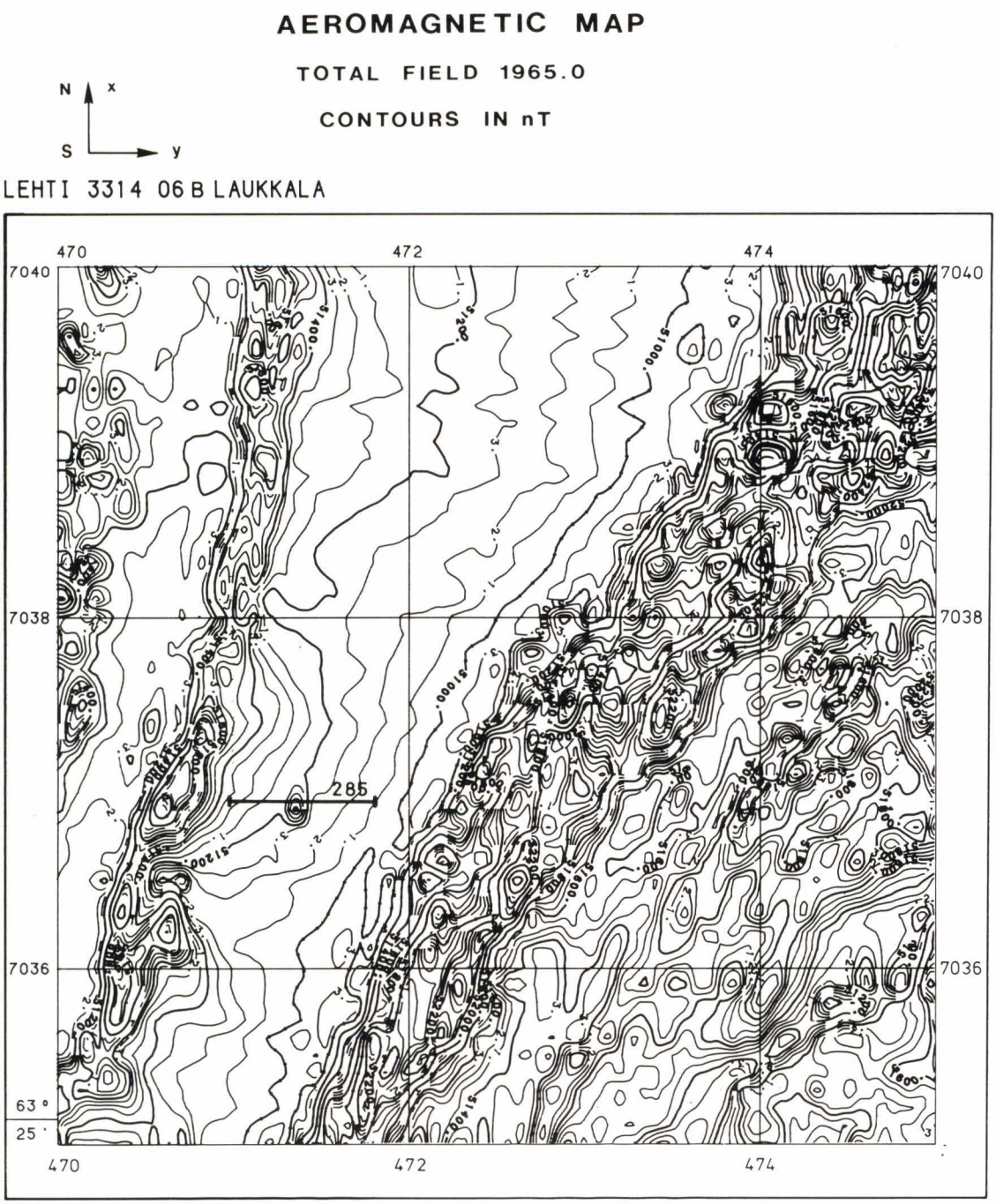
AEROMAGNETIC MAP
TOTAL FIELD 1965.0
CONTOURS IN nT
N
S
x
y
LEHTI 3314 06 B LAUKKALA
470
472
474
7040
7038
7036
63 °
25 '
285

Fig. 97 c)

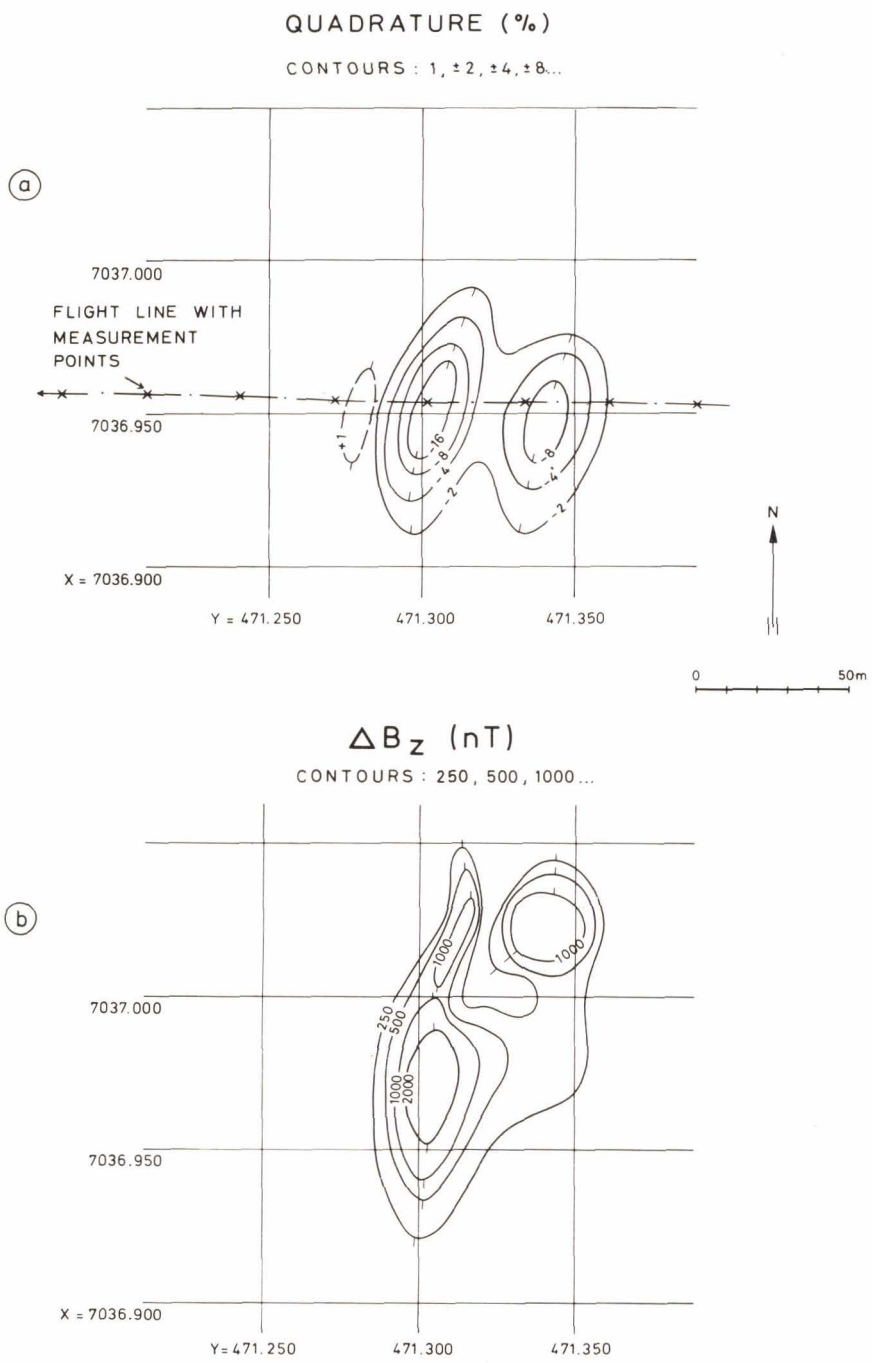

Fig. 98. Pielavesi Ilokangas area, results of various geophysical surveys. (a) Quadrature component data of slingram survey as a contour map; coil separation l = 60 m, frequency f = 3 600 Hz, point spacing Δy = 20 m. Flight survey line 285 and the exact locations of the AEM data points are also marked on the map. (b) Results of the magnetic ground survey as anomaly values of the vertical component of the magnetic total field ΔB_z (c) Test line Pielavesi 285, AEM survey in-phase, quadrature and flight elevation data. (d) Test line Pielavesi 285, aeromagnetic data: anomaly values of the magnetic total field ΔB_T (LH) and values of horizontal across-track difference B_T (RH) – B_T (LH) of the magnetic total field. Sensor distance Δx = 24.5 m (see page 192).

PIELAVESI 285

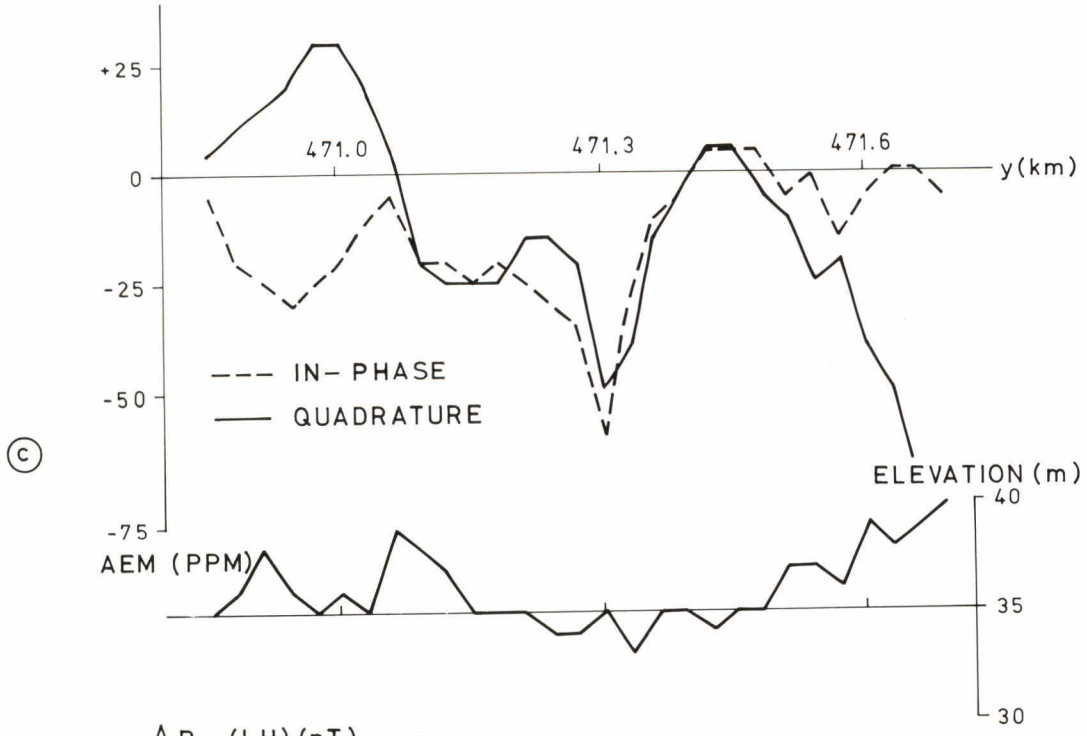

c

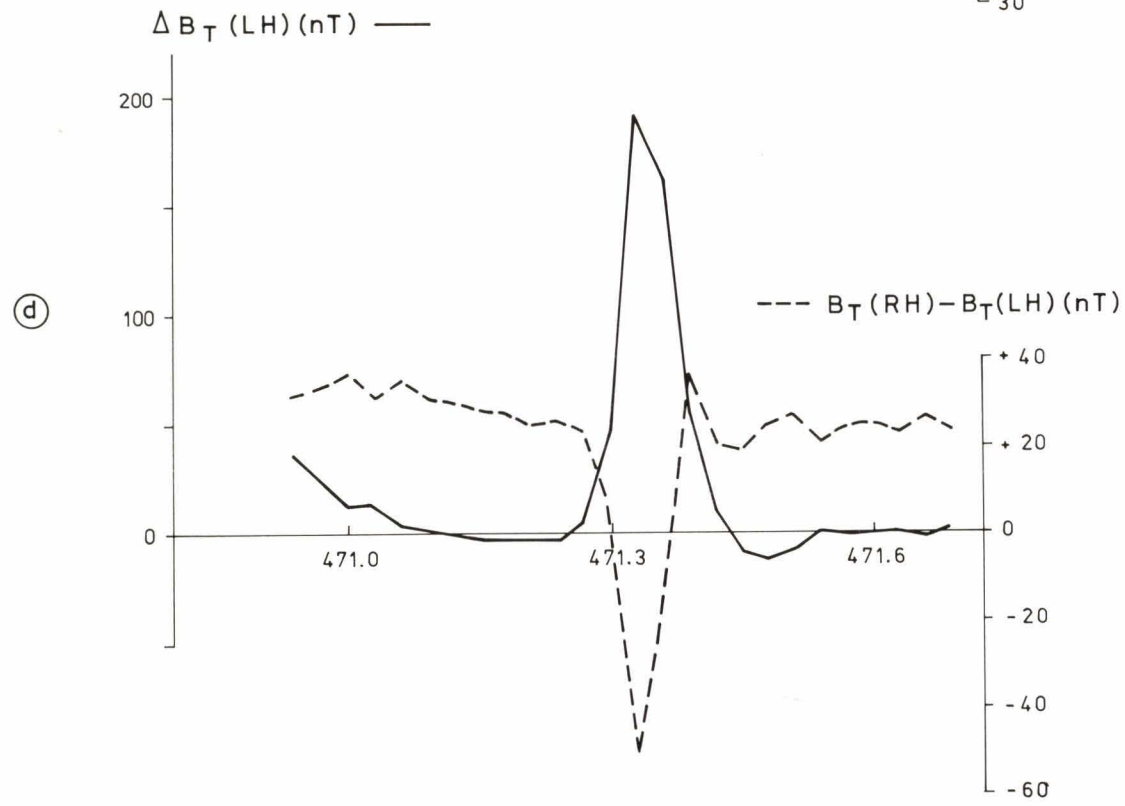

d

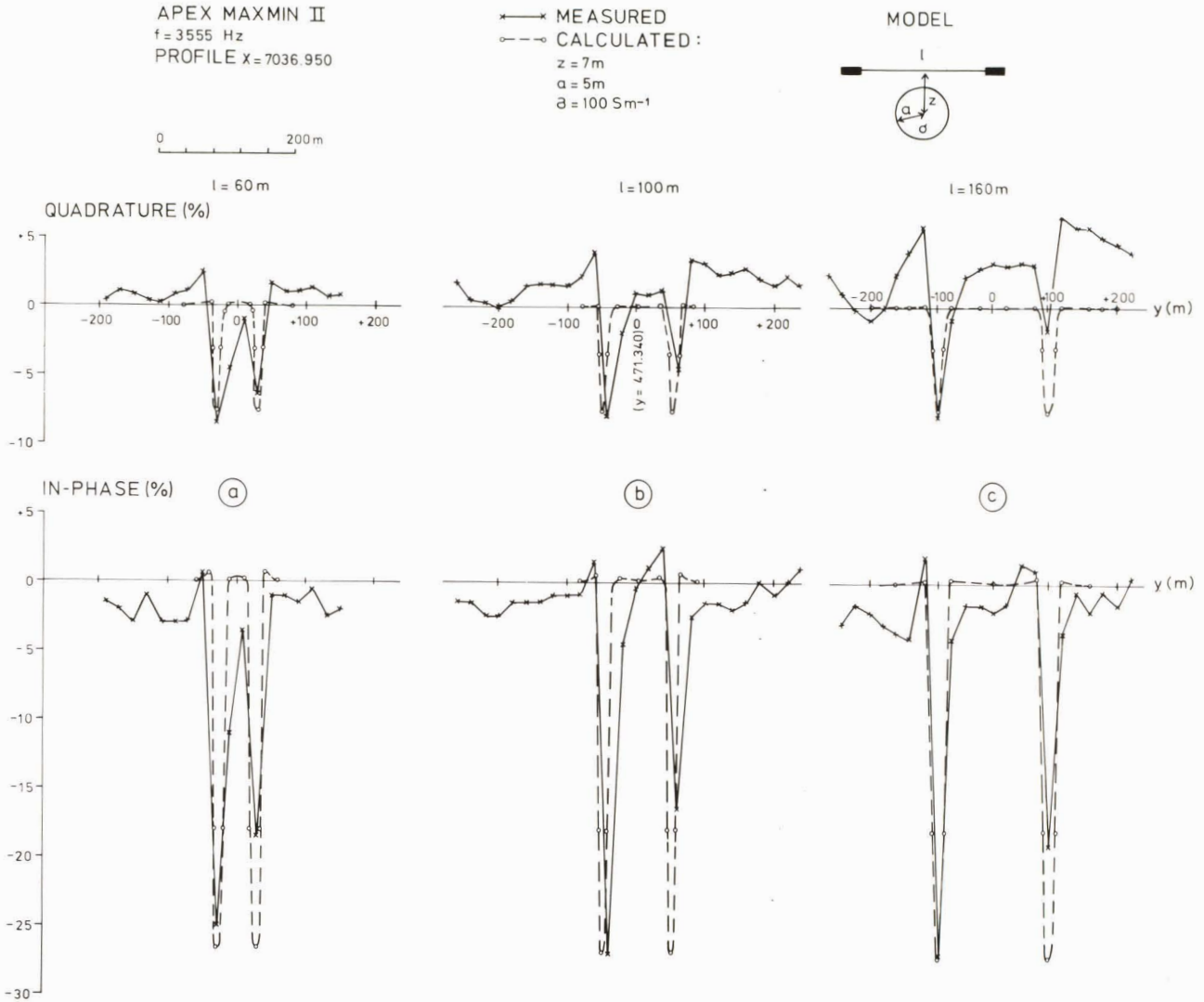

Fig. 99. Test line Pielavesi 285, slingram survey data of line x = 7036.950 with theoretical interpretation results of the sphere model. (a) Data referring to coil separation l = 60 m. (b) Data referring to coil separation l = 100 m. (c) Data referring to coil separation l = 160 m.

Since the average flight elevation on the profile was about 35 m, the interpretation of the aeromagnetic data also suggests that the source of the anomaly is a small outcropping body.

Trenching on the outcrop exposed sulphides on the surface of the bedrock. Any extensions at depth were not, however, intersected by drillholes. Hence, the drilling seems to corroborate the concept of the limited size and location of the conductor given by the interpretation.

The AEM result in Figs. 97a, b does not correspond to the normal situation, in which use can only be made of anomalies that differ more clearly from the noise. The location of the conductor directly below the flight line was also the best possible. Hence, the example must be taken as the limit of the maximum resolution of the DC-3 AEM data, and conductors smaller than the above target cannot be expected to produce anomalies distinguishable from the noise, even under the most favourable conditions. The conclusion is supported by the analysis of the theoretical results (p. 95).

Savukoski Sokli: Extensive susceptive body overlain by conductive weathered rock

The carbonatite massif of Sokli at Savukoski (map sheets 4723 01 and 4723 04) was selected as an example of an extensive, strongly magnetised formation that also produces an AEM anomaly. The example illustrates the applicability of the theoretical re-

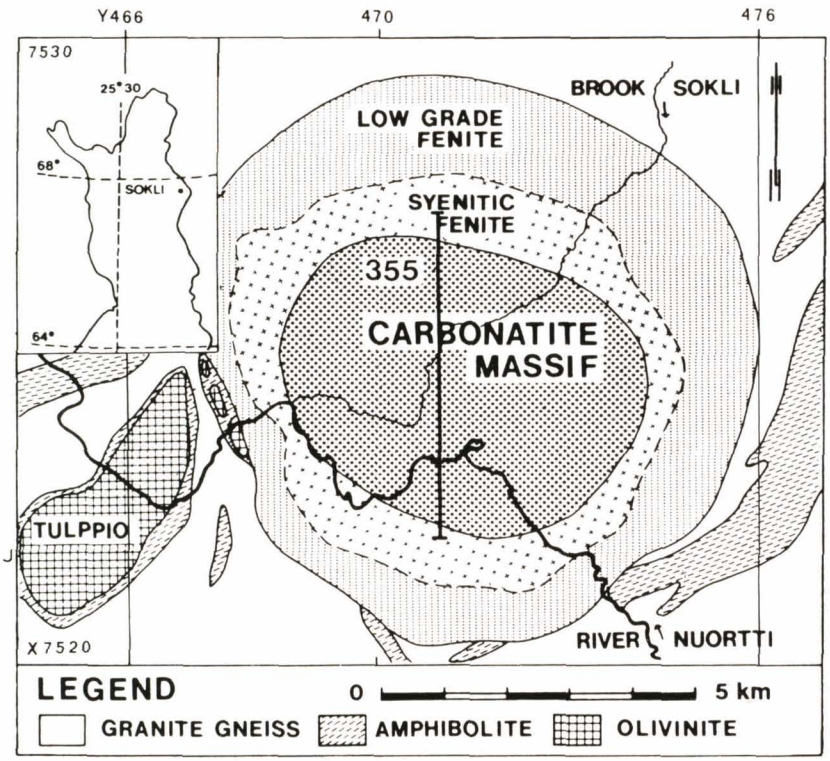

Fig. 100. Lithological map of the Savukoski Sokli area, according to Vartiainen (1980). Test line 355 is marked on the map.

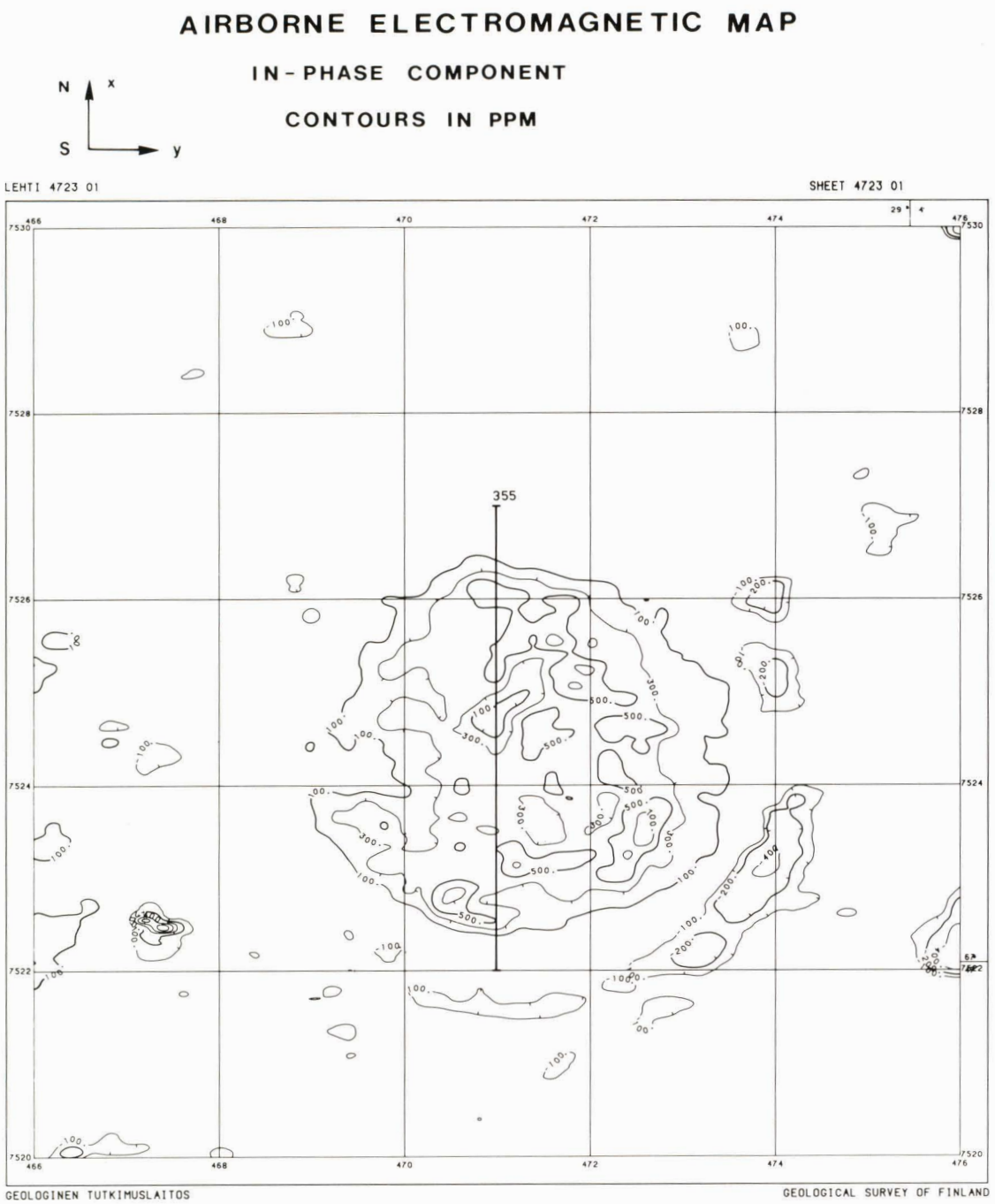

Fig. 101. DC-3 aerogeophysical survey data, parts of map sheets 4723 01 and 4723 04 (Savukoski Sokli area). Flight direction N–S, line spacing 200 m. Test line 355 is marked on the maps. (a) AEM in-phase component. (b) AEM quadrature component (see page 196). (c) Aeromagnetic survey data, the absolute values of the magnetic total field 1965.0 (see page 197). Contour interval 200 nT.

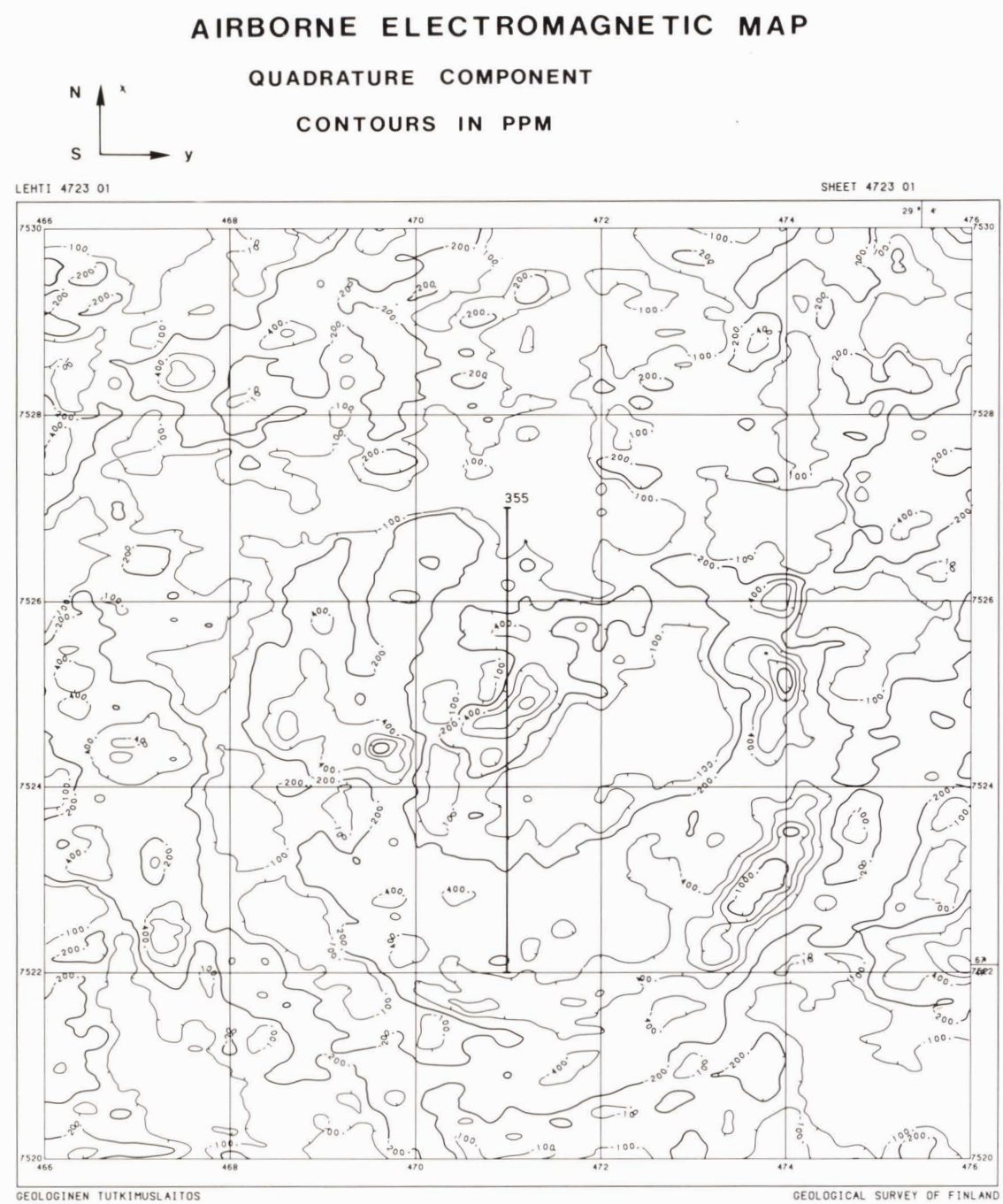
AIRBORNE ELECTROMAGNETIC MAP
QUADRATURE COMPONENT
CONTOURS IN PPM
N
S
x
y
LEHTI 4723 01
SHEET 4723 01
355
GEOLOGINEN TUTKIMUSLAITOS
GEOLOGICAL SURVEY OF FINLAND

Fig. 101 b)

AEROMAGNETIC MAP

TOTAL FIELD 1965.0

CONTOURS IN nT

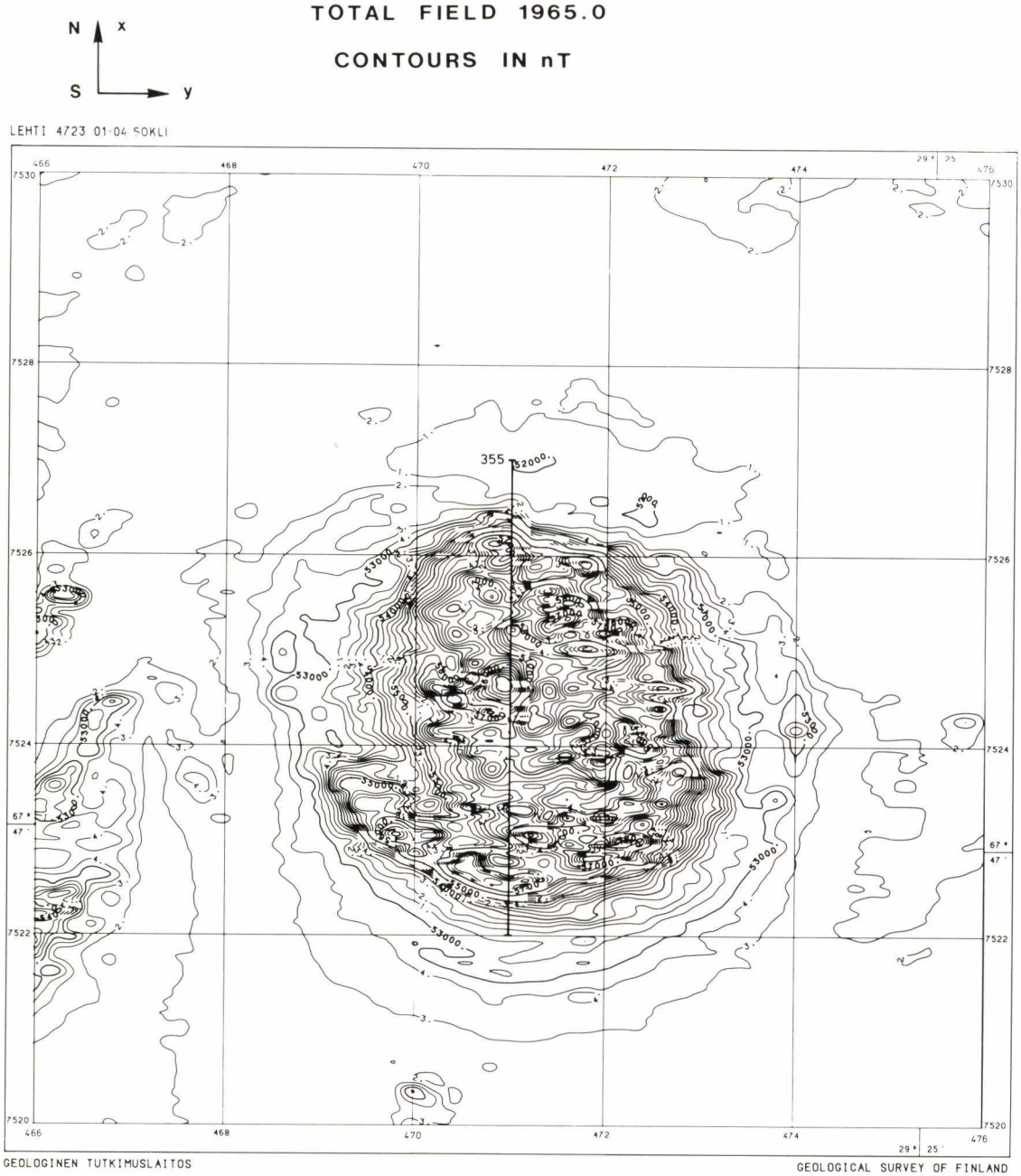

Fig. 101 c)

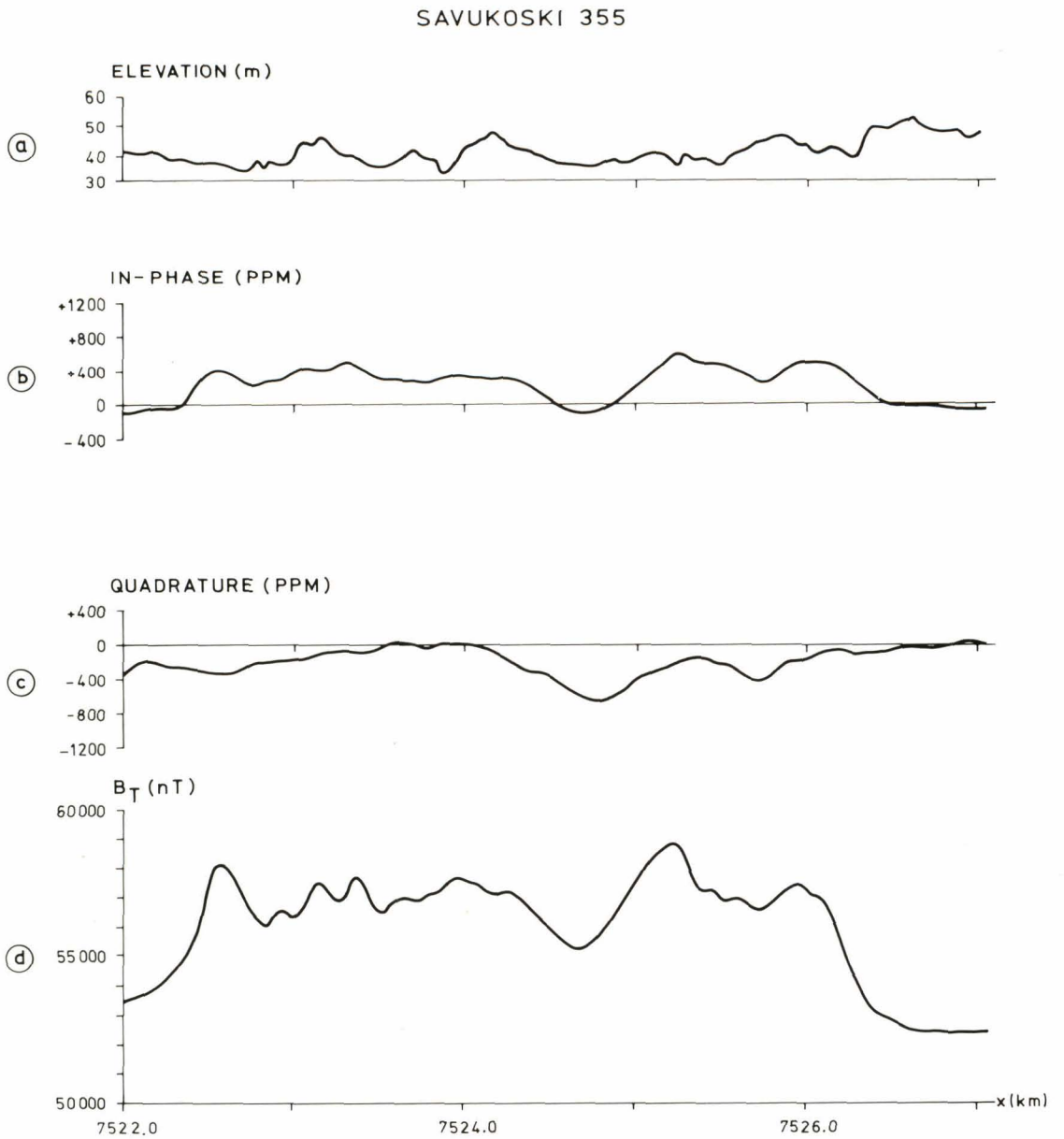

Fig. 102. Test line Savukoski 355, aerogeophysical survey data, point spacing $\Delta x = 30$ m. (a) Flight elevation. (b) AEM in-phase component. (c) AEM quadrature component. (d) Absolute values of the magnetic total field.

sults of Figs. 28–33 under favourable conditions. Comparison is also made between the susceptibility values interpreted from the AEM data and those obtained from aeromagnetic and petrophysical measurements.

The Sokli carbonatite massif was discovered in 1967 in the course of exploration by Rautaruukki Oy (Paarma 1970). The extensive work carried out in the area by the company has been summarised by Vartiainen and

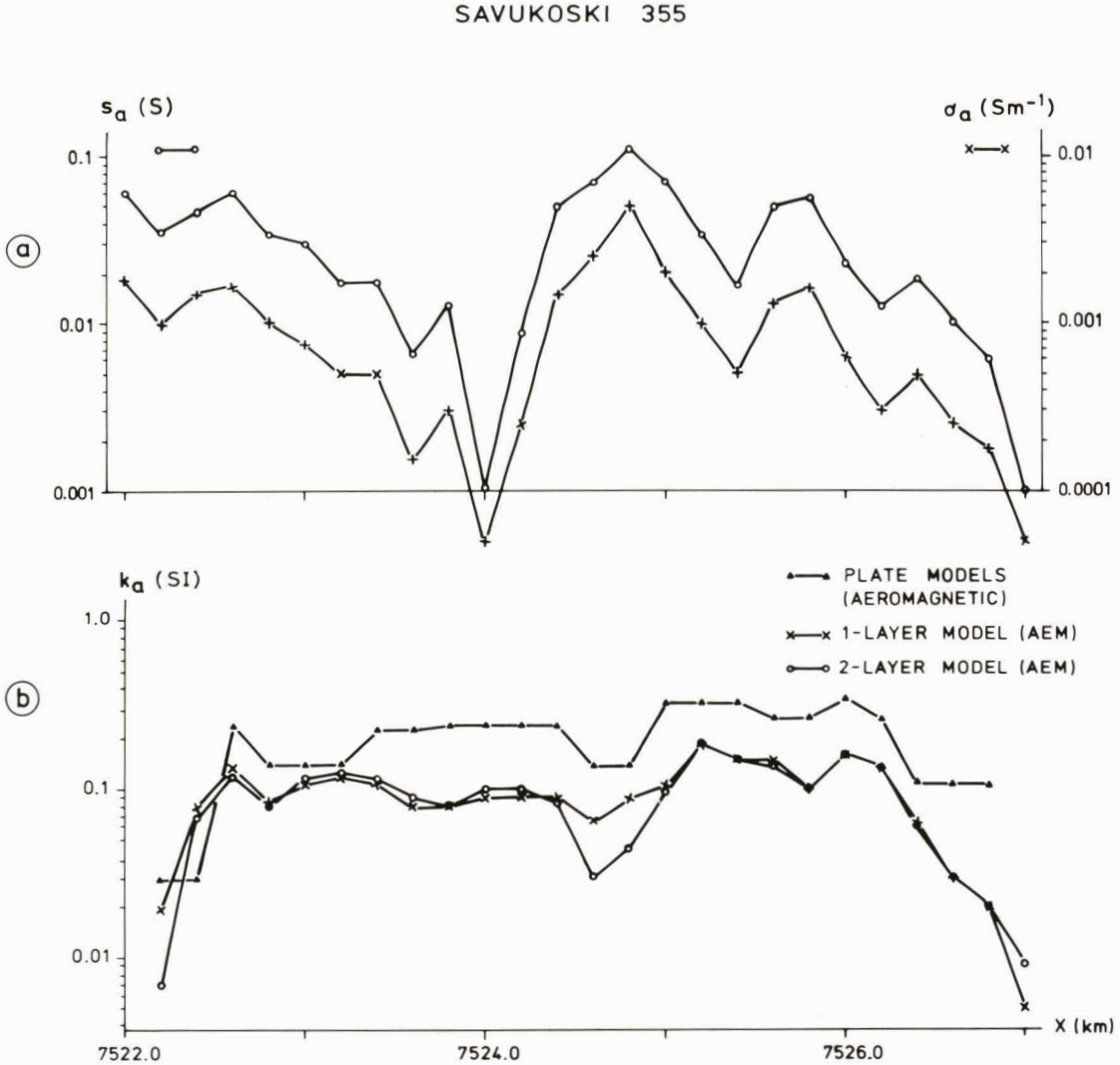

Fig. 103. Test line Savukoski 355, interpretation of various aerogeophysical data. (a) Values of apparent conductivity σ_a and apparent conductance s_a calculated from AEM data by means of one-layer and two-layer model results. (b) Values of apparent susceptibility k_a calculated from aeromagnetic data by means of plate models and from AEM data by means of one-layer and two-layer models (Figs. 29 and 32).

Paarma (1979). The geological map of the massif is shown in Fig. 100. The carbonatite core is surrounded by a fenite ring enveloped by gneisses, granites and amphibolites. West of the massif there is an ultramafic intrusion. The surface diameter of the carbonatite and fenite massif is about 6 km. The massif is covered by a layer of till, sand and, locally, peat that varies from 1 to 60 m in thickness. The surficial portions of the massif are deeply weathered, and there are extensive areas where the weathered rock is tens of metres deep.

To date, P, Nb and U mineralisations have been located in the NW portion of the Sokli massif. Both Rautaruukki Oy and the Geolog-

ical Survey have undertaken several airborne surveys over the massif; the last one was made in 1978. The massif is unusual in that it can be readily located by aeromagnetic, AEM and aeroradiometric surveys. Figs. 101a, b show the outcome of the low-elevation DC-3 AEM surveys in 1978; Fig. 101c shows the aeromagnetic results.

The massif produces a strong aeromagnetic anomaly, about 5 000 nT in intensity, and an area of positive AEM in-phase component anomalies, 100 to 1 000 ppm in intensity. The quadrature component does not allow the borders of the massif to be delineated equally well. The average flight elevation in the area was $\bar{h}$ = 40 m and the standard deviation 7.1 m. For a detailed interpretation test the low-elevation survey data on line 355 (y = 471.0, x = 7522.000–7527.000), shown in Fig. 102, were collected from the middle of the massif. The interpretation was undertaken by making use of the theoretical results given in Figs. 29 and 32 and the in-phase and quadrature anomaly values collected from the profile at every 200 m.

The outcome of the interpretation is shown in Fig. 103. The upper part of the figure illustrates the apparent conductivity σ_a (one-layer model) of the massif and the apparent conductance s_a (two-layer model) of the horizontal conductive layer. The electrical ground survey results demonstrate that the two-layer model is more realistic. The lower part of Fig. 103 shows the apparent susceptibility values of the massif interpreted with the aid of one-layer and two-layer AEM models. The figure also gives the apparent susceptibility values interpreted from the aeromagnetic survey data. The interpretation, whose outcome is shown in Fig. 104, was accomplished by assuming that the anomaly is due entirely to induced magnetisation.

The compatibility of the susceptibility values deduced from the magnetic and AEM data demonstrates the methodical feasibility of the new AEM interpretation method. Petrophysical studies have indicated that the magnetisation of the Sokli carbonatite massif is predominantly induced (Hattula, personal communication). Remanent magnetisation, with Q values between 1 and 10, has been determined in various parts of the massif. Hence, in places, the remanent magnetisation may be a significant factor contributing to the systematically lower susceptibility values interpreted from the AEM data. Another reason for the systematic difference is the thinness of the uppermost layer in the AEM model, i.e. 2 m. If the uppermost layer were in fact essentially thicker, the depth to the surface of the lower susceptive layer would then be greater than that used in the model and the interpreted k values would be too low. For instance, at point x = 7522.8, the interpreted value, k_a = 0.08, would change to k_a = 0.11 if the thickness of the overburden were 10 m instead of 2 m.

Since the two-layer model is more realistic in the light of the control data available, the values of the conductivity-thickness product of the overburden and the weathered layer obviously best describe the electrical properties. The interpreted results show that the conductance of the horizontal conductor varies between 0.001 and 0.11 S in the massif. The conductivity and thickness cannot be interpreted separately merely on the basis of AEM data. If the apparent resistivity values ϱ_a = 70–300 Ωm obtained from earth resistivity measurements are used, the AEM results suggest that the thickness of the conductive layer is 40 m at the most.

One detail that should be noted is that on the test profile at x = 7524.5 (Fig. 102) the in-phase component approaches zero, whereas the quadrature anomaly has the extreme value of –680 ppm. This is due either to the susceptibility being lower than in the environment or to the conductance being so high that it starts to dominate the AEM re-

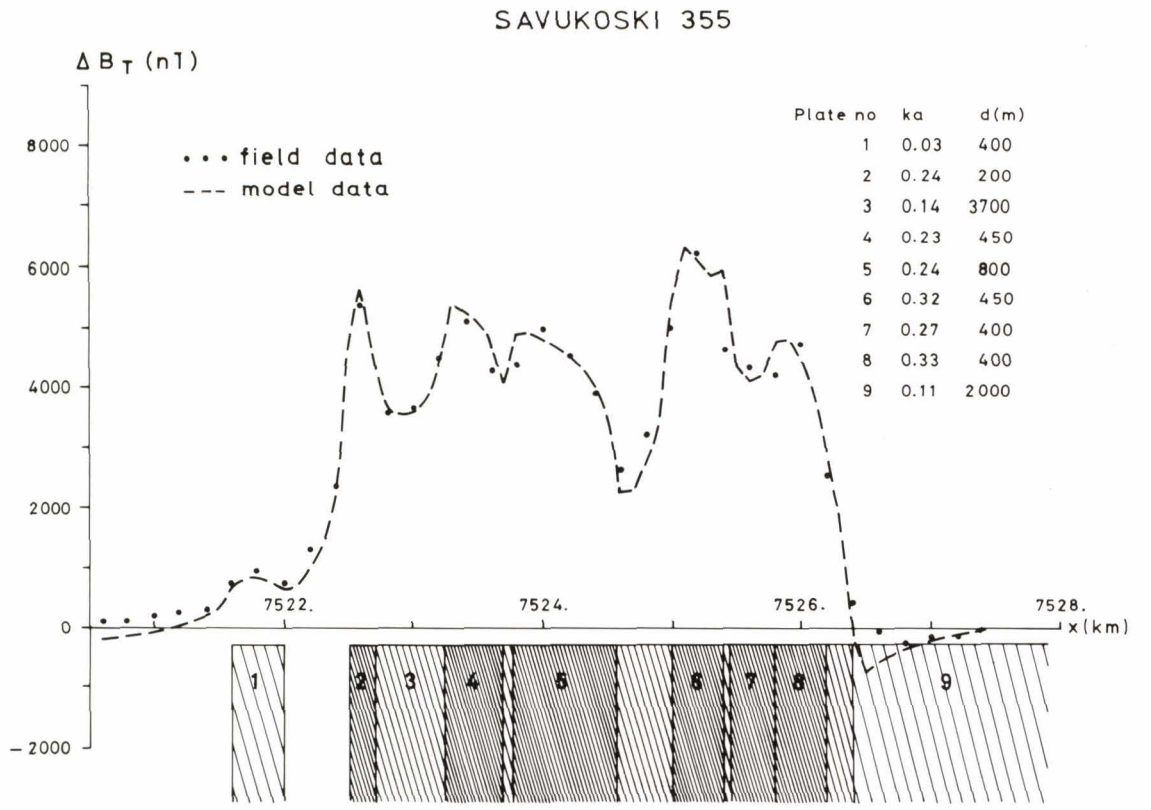

Fig. 104. Test line Savukoski 355, plate model interpretation of the aeromagnetic data. The dip angle $\alpha = 90°$ and the depth values $z_1 = 40$ m, $z_2 = 5\,000$ m are constants.

sponse. The shape of the anomaly (Fig. 101) suggests the latter alternative and that the anomaly may be due to a local two-dimensional conductive formation. If so, the conductance value s_a obtained from the layered earth model is too low, and the interpretation with a vertical thin half-plane model gives $s_a = 1.8$ S.

From the interpretation test on the AEM data for the Sokli carbonatite massif it can be concluded that, at least in this methodically favourable case, the interpretation results are compatible with the data of other methods. The agreement between the AEM and aeromagnetic interpretations also corroborates the concept that the magnetisation of the massif is largely induced.

Savukoski Kuollutvaara: Susceptive and/or conductive bodies in bedrock

The mafic Kuollutvaara formation at Savukoski (map sheets 3733 02 and 3733 05) was selected as the second example of AEM susceptibility effects. The geological setup of the area represents a more general case in which the thickness, magnetisation, conductivity and depth to the outcrop of the formations vary. The aim is to study the applicability of

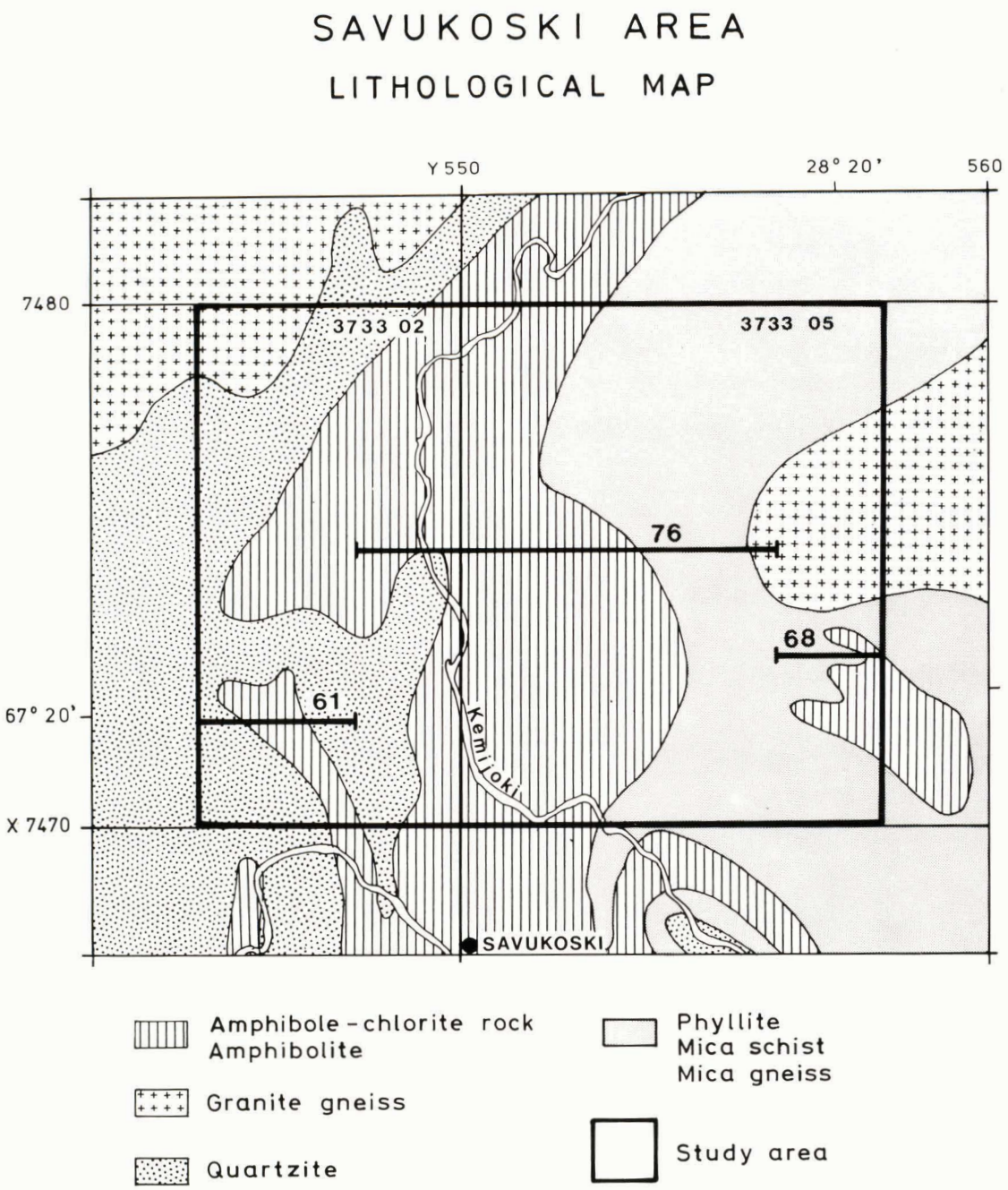

Fig. 105. Lithological map of the Savukoski Kuollutvaara area according to Mikkola (1937) and Silvennoinen *et al.* (1980). Test lines 76, 61 and 68 are marked on the map.

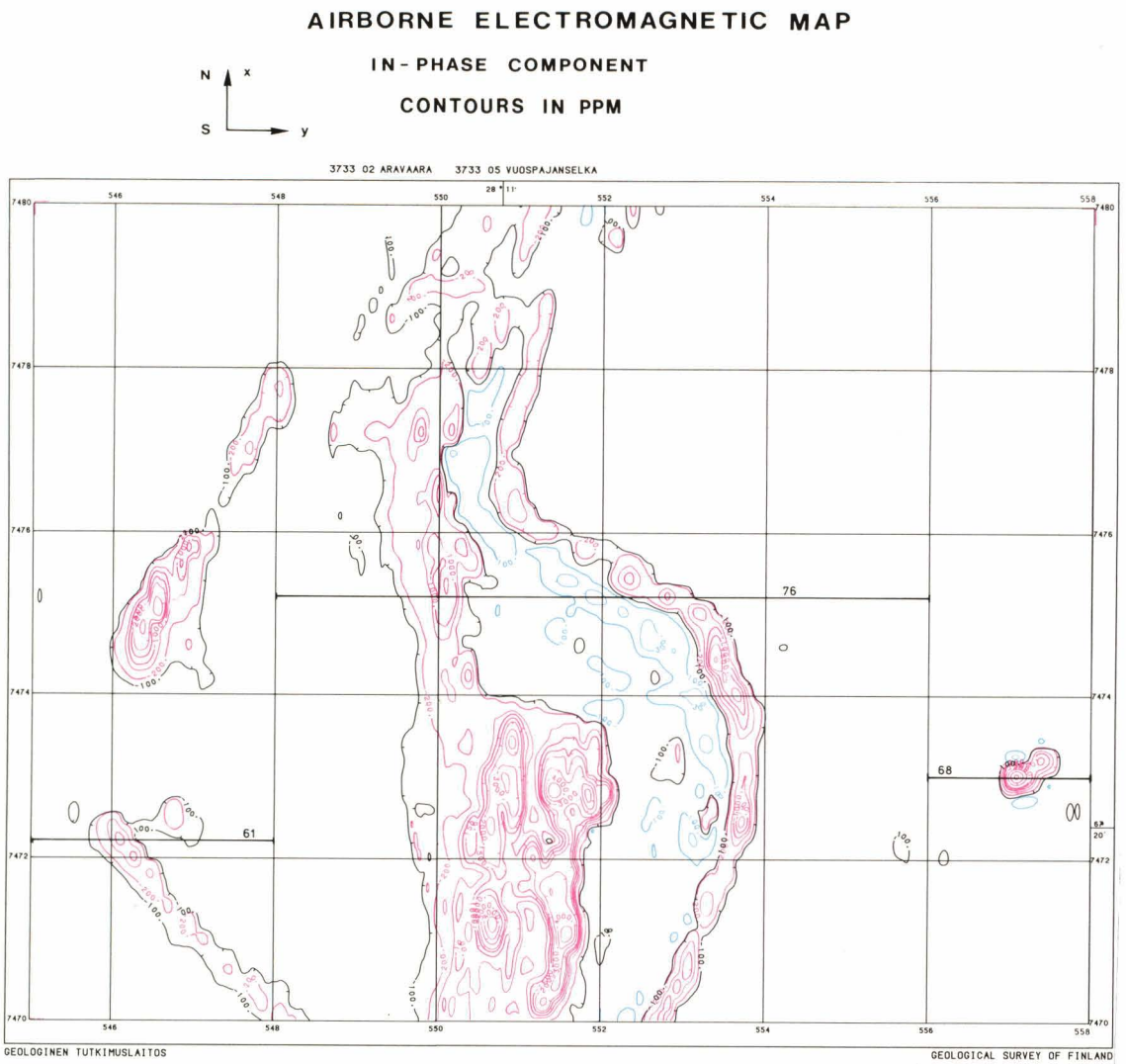

Fig. 106. DC-3 aerogeophysical survey data, parts of map sheets 3733 02 and 3733 05 (Savukoski Kuollutvaara area). Flight direction E–W, line spacing 200 m. Test lines 76, 61 and 68 are marked on the maps. (a) AEM in-phase component. (b) AEM quadrature component (see page 204). (c) Aeromagnetic survey data, the absolute values of the magnetic total field 1965.0 (see page 205). Horizontal transverse gradient data were employed in the interpolation of the grid for contouring. Contour interval 200 nT.

the theoretical AEM layered model results to two-dimensional formations under conditions normally encountered in practice. It will also be demonstrated that the AEM data may contribute to the information given by aeromagnetic interpretation, even by a visual examination of the data.

Geological mapping has shown (Mikkola 1937, Silvennoinen *et al.* 1980) that, in the Kuollutvaara–Rovaselkä area, there is an extensive volcanic sequence with black schist zones in its margins. A simplified geological map of the area is reproduced in Fig. 105. The volcanics have been metamorphosed

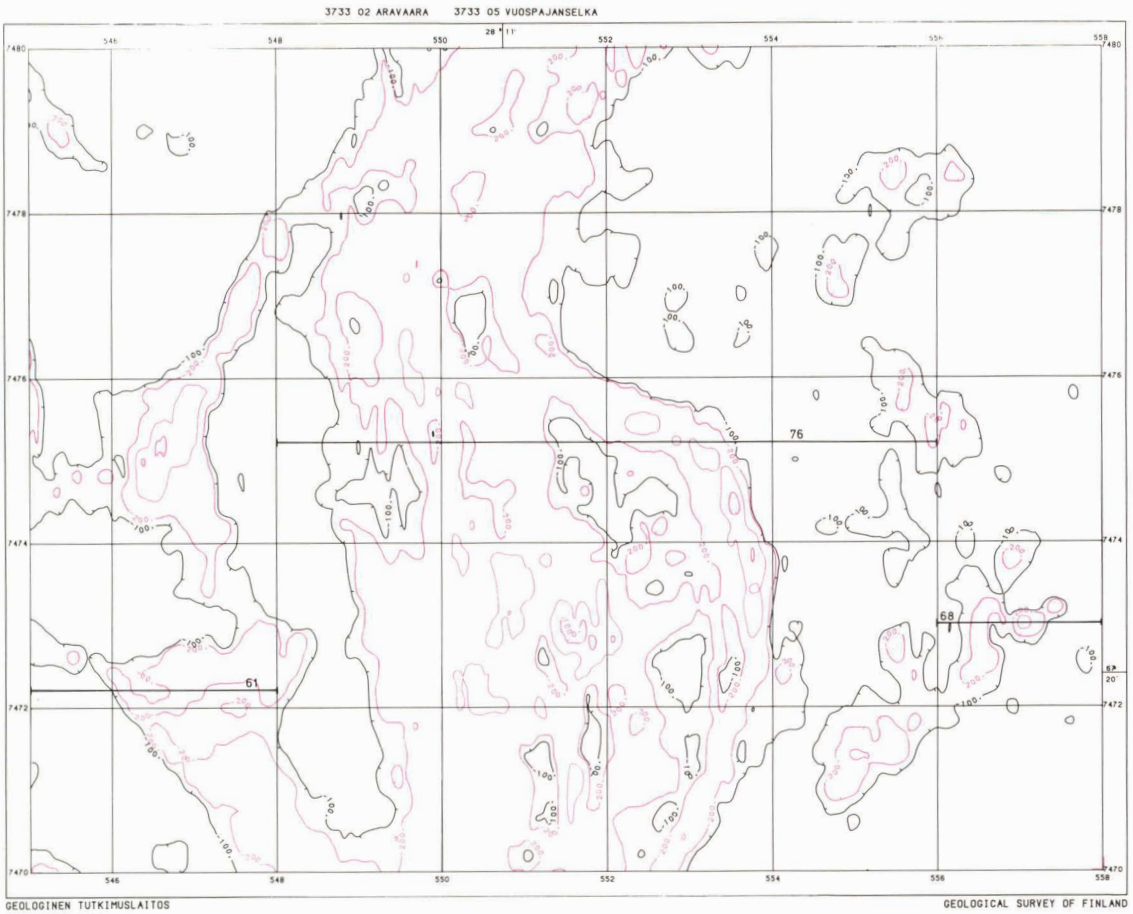

into amphibole chlorite rocks and amphibolites. The bedrock in the area is poorly exposed and the overburden is locally very thick, up to several tens of metres. The topography shows large variations in elevation, and the hill tops are 100 to 200 m above the environment. The average flight elevation in the area was $\bar{h}$ = 38 m and the standard deviation σ_h = 6.1 m.

Low-elevation airborne survey in the area was undertaken in 1979. The AEM and aeromagnetic maps are shown in Fig. 106. The in-phase component data demonstrate that there is a circular chain of AEM anomalies in the area. The circular structure consists of an outer conductive ring (black schists) and an inner susceptive ring with poorer conductivity. The western boundary and the northward extension of the circular structure are better shown by the quadrature data. The pattern of the magnetic field (Fig. 106c) is characterised by short-wavelength anomalies typical of volcanic rocks. For closer interpretation, data were collected from two test

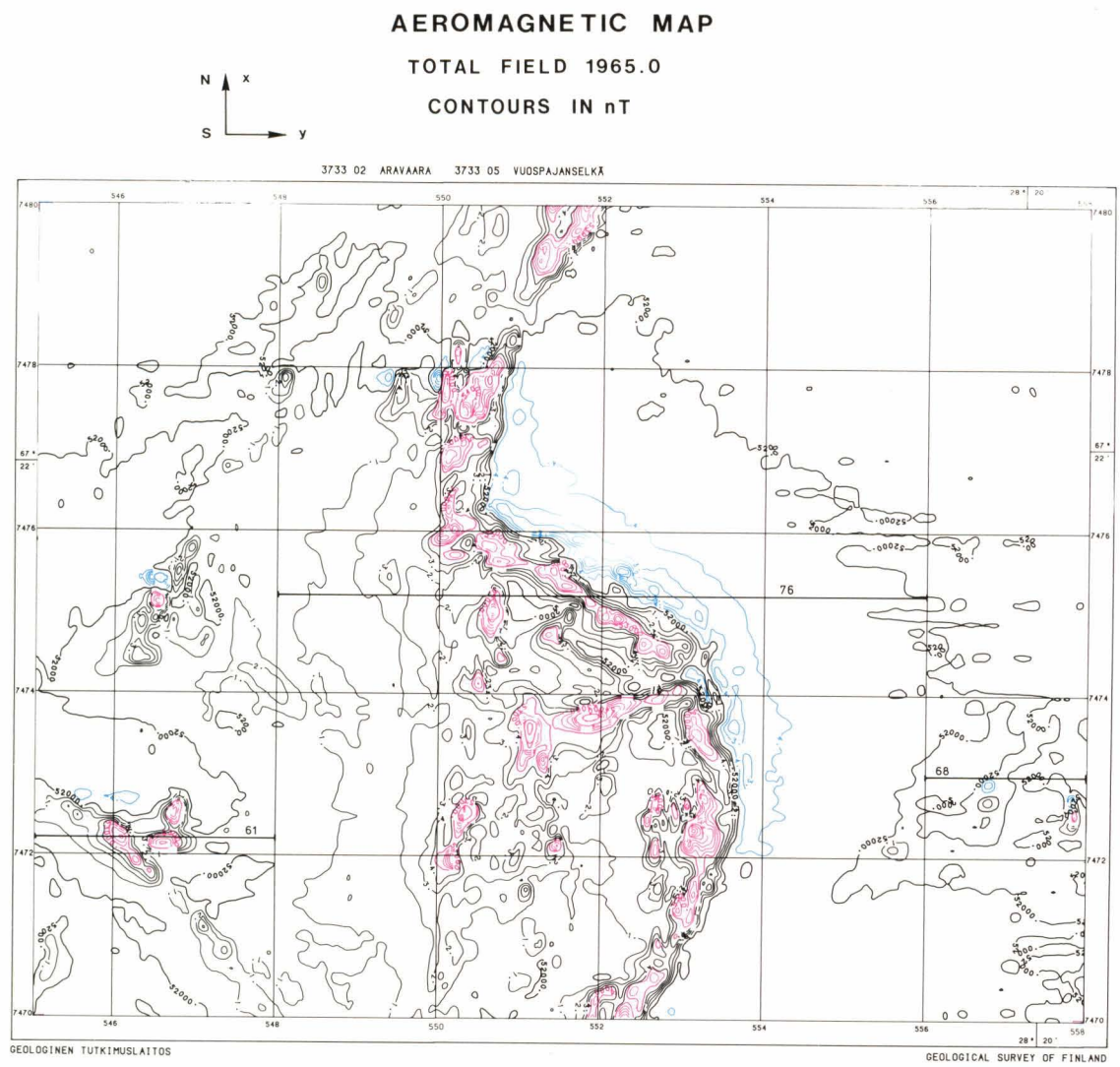

lines passing over the margins of the formation. East of the volcanic formation there is a small but strong in-phase component anomaly that was interpreted separately with the spherical conductor model.

Line 76

The results of test line 76 (x = 7475.2, between y = 548.000–556.000) are shown in Fig. 107. The magnetic minimum and the electrical anomaly »A» of a good conductor coincide, as do the magnetic maxima and the electrical anomalies »B» and »C» of the susceptive formations. The eastern area of susceptive response, anomaly »B», is about 0.5 km wide. Considering the coil separation of the DC-3 AEM system it could be assumed that the interpretation of anomaly »B» with the half-space model would still give moderately reliable results. The anomaly area »C» is so narrow and the susceptive AEM re-

sponse so low that the interpretation with the half-space model probably only gives a rough minimum estimate for susceptibility.

The AEM results in Fig. 107 were interpreted by means of a susceptive and/or conductive one-layer model, i.e. the theoretical results in Figs. 27 and 28. The outcome of the AEM interpretation is shown in Fig. 108 and that of the aeromagnetic profile in Fig. 109. The results suggest that anomaly »A» is

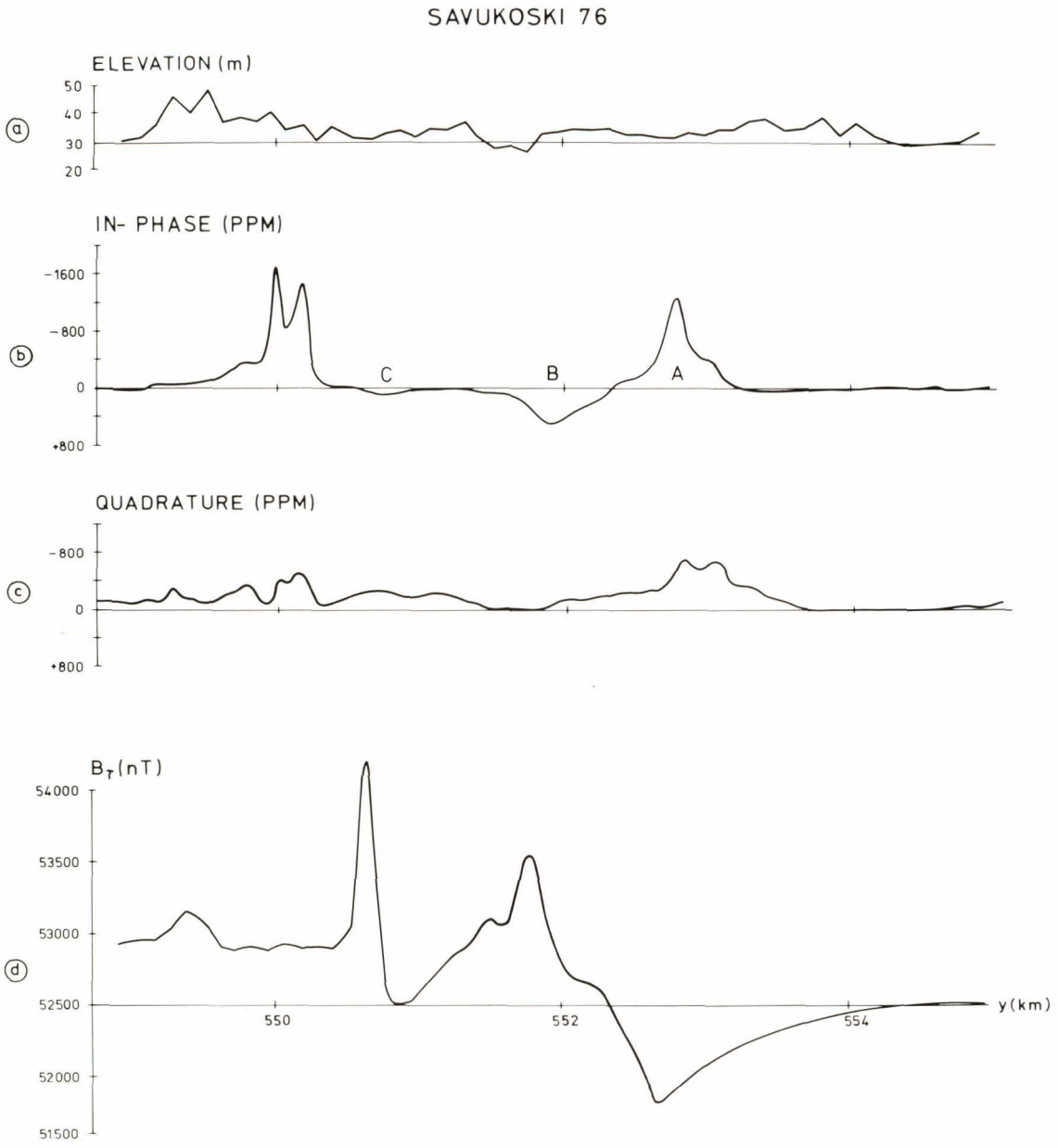

Fig. 107. Test line Savukoski 76, aerogeophysical survey data, point spacing $\Delta y = 30$ m. See text for explanation of symbols A–C. (a) Flight elevation. (b) AEM in-phase component. (c) AEM quadrature component. (d) Absolute values of the magnetic total field.

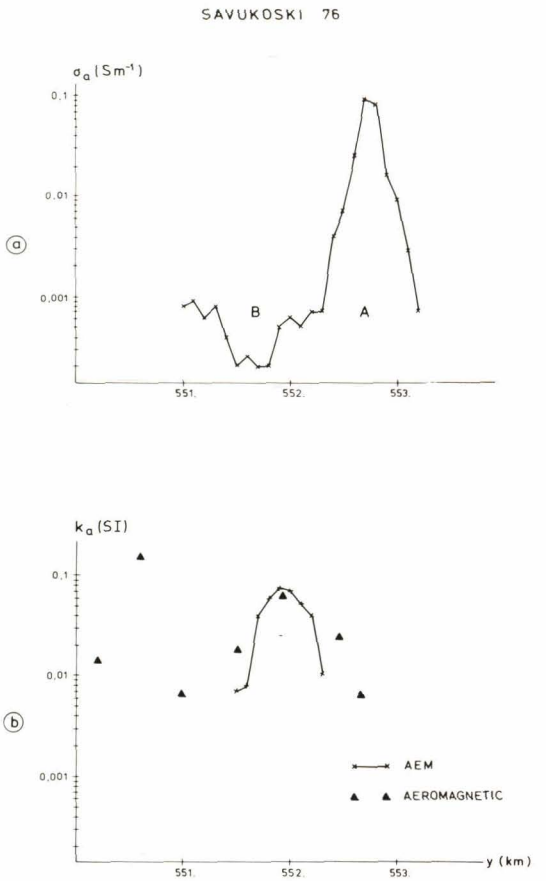

Fig. 108. Test line Savukoski 76, interpretation of AEM and aeromagnetic survey data. See text for explanation of symbols A–B. (a) Values of apparent conductivity σ_a calculated from AEM survey data by means of one-layer model results. (b) Values of apparent susceptibility k_a calculated from AEM and aeromagnetic survey data. The k_a values of AEM data were calculated with the aid of Fig. 28. The values for the aeromagnetic data were obtained by applying the plate model interpretation (Fig. 109).

due to a conductive black schist layer at the eastern margin of the formation. The coincident magnetic minimum is due to the regional anomaly of the volcanic formation dipping 70° W. Anomaly »B» is presumably due to the amphibole chlorite rock, and its susceptibility values deduced from AEM and aeromagnetic anomalies are of the same order of magnitude. Anomaly »C» is produced by a thin sheet-like body. The true location of its outcrop is shown directly by the AEM data. As expected, the k value 0.012 interpreted from the AEM data is far too low compared with the k value 0.17 interpreted from the aeromagnetic data.

Line 61

The results of test line 61 (x = 7472.0, between y = 545.000–548.000) are shown in Fig. 110. Comparison of the AEM with the aeromagnetic data reveals that the case is now more complicated than it was above. The western source of anomaly is strongly magnetised and produces a negative in-phase anomaly as good conductors normally do. Hence the anomaly could be produced by a pyrrhotite-bearing black schist horizon. Interpretation on the basis of the half-plane model data in Fig. 35b gives z = 43 m for the depth to the outcrop and σd = 20 S for the conductivity-thickness product. The extensive quadrature anomaly is partly due to poorly conductive overburden. The eastern anomaly source »E» produces a slightly larger magnetic anomaly but no AEM anomaly. As pointed out on pages 70 and 77, there are three possible reasons for this:

1. The formation that gives rise to the magnetic anomaly is at such a great depth that it is beyond the AEM penetration.
2. The conductivity of the formation is such that the values of the response function fall in the transition region in which the in-phase component passes through zero and thus has very low values (see e.g. Fig. 28).
3. The magnetisation of the formation is remanent.

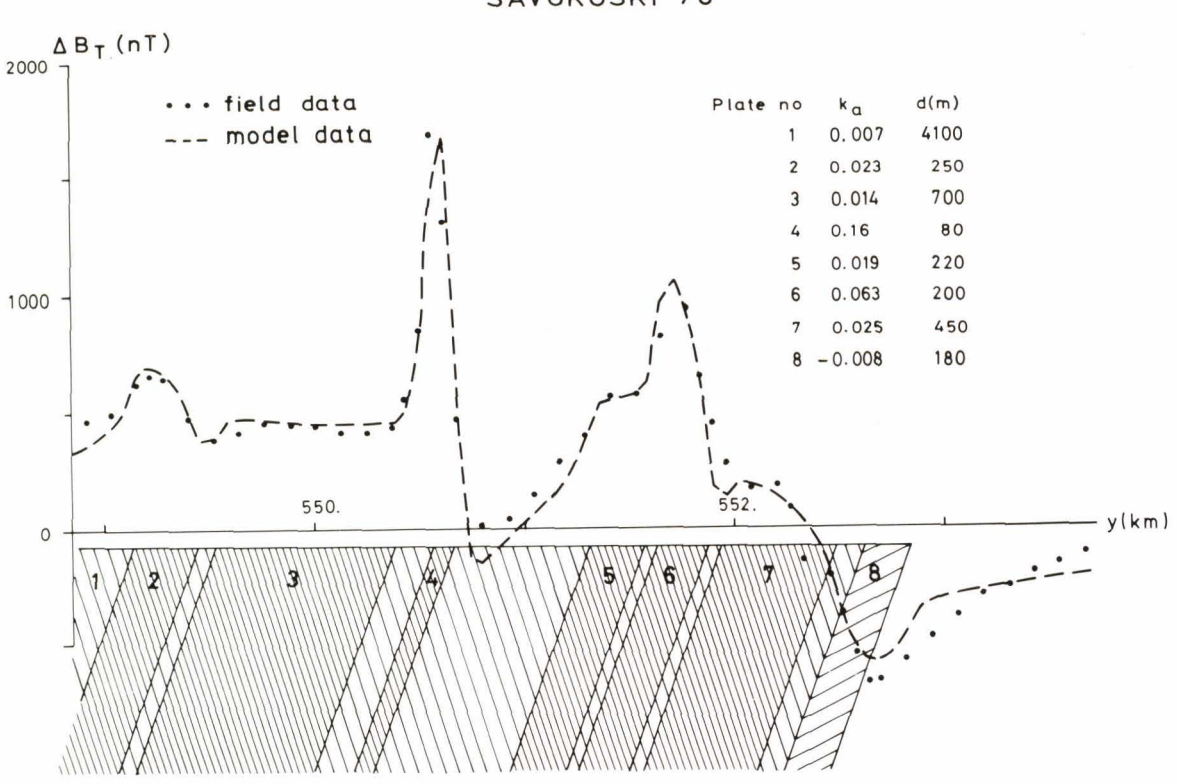

Fig. 109. Test line Savukoski 76, plate model interpretation of the aeromagnetic data. The dip angle $\alpha = 70°$ W and the depth values $z_1 = 40$ m, $z_2 = 5\,000$ m are constants.

An aeromagnetic profile interpretation was undertaken to test the first hypothesis. The outcome is shown in Fig. 111. The interpretation suggests that anomaly source »D», which is composed of several layers, has a depth of 62–65 m and a susceptibility of 0.015–0.12 SI units. The corresponding figures for anomaly source »E» are depth 110 m and k = 0.15 SI units. The results of the interpretation show that hypothesis 1 is capable of explaining the lack of in-phase anomaly, for it was demonstrated previously (page 00 and Fig. 33) that at k = 0.1 the penetration of the AEM system is only 75 m. To test the second hypothesis, the AEM data were interpreted by means of Fig. 29. The anomaly values of in-phase < +50 ppm, quadrature = −250 ppm, give $k_a = 0.02$. Since the flight elevation was 60 m instead of 40 m, the k_a value obtained is too low, and $k_a = 0.05$ is a more correct value on the basis of Figs. 29 and 33. The outcome contradicts the results of the aeromagnetic interpretation. Hence the explanation based on hypothesis 2 is very unlikely. The third hypothesis was tested by petrophysical measurements. Fourteen amphibole chlorite rock samples collected from the area during geological mapping were measured for petrophysical parameters. Three samples showed remanence values of Q exceeding 7, with the maximum value of Q = 83. Since the samples could not be collected directly from profile 61 but from farther east, from the formation that is traversed by test line

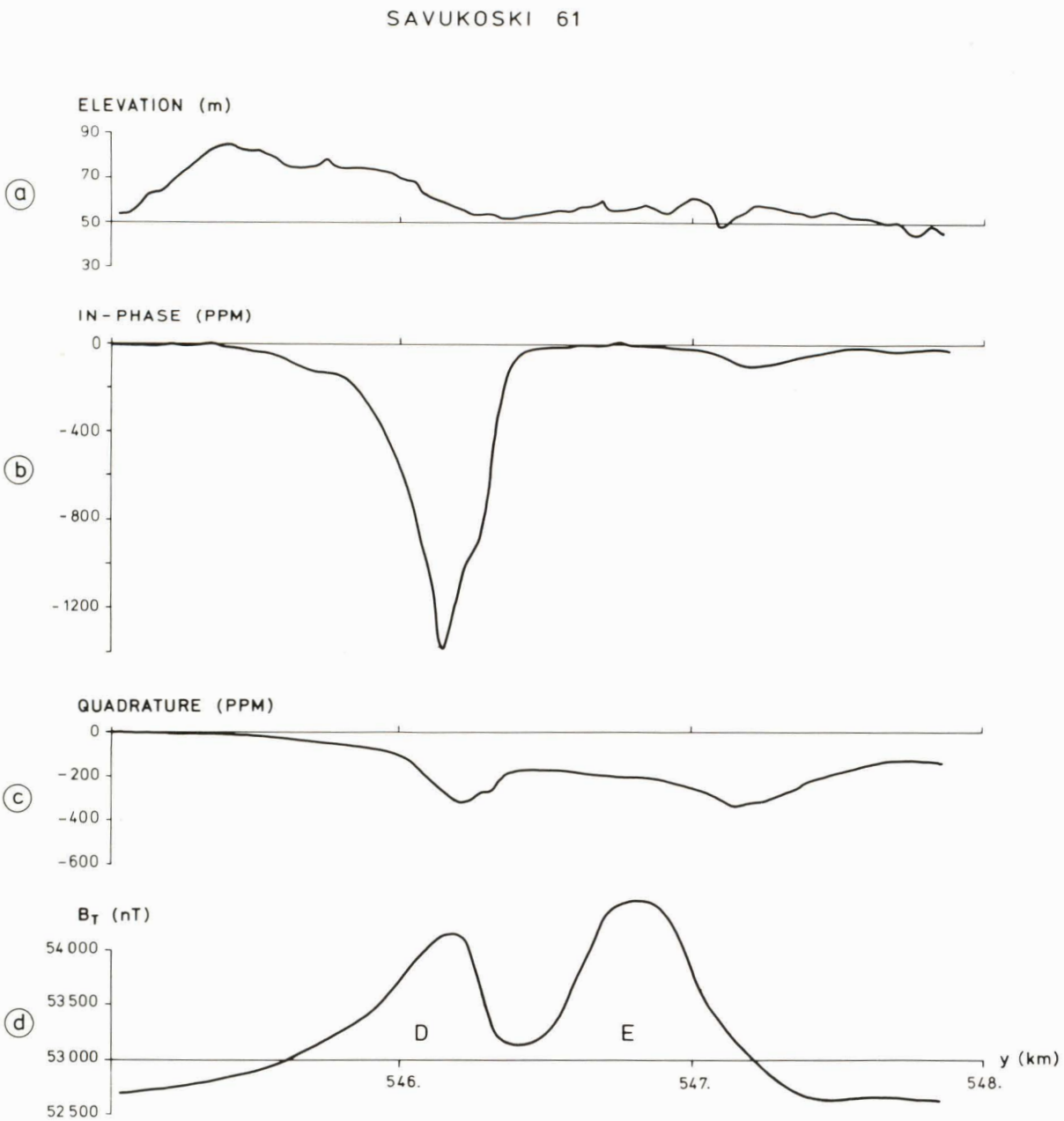

Fig. 110. Test line Savukoski 61, aerogeophysical survey data, point spacing $\Delta y = 30$ m. (a) Flight elevation. (b) AEM in-phase component. (c) AEM quadrature component. (d) Absolute values of the magnetic total field.

76, nothing definite can be said about hypothesis 3. Nevertheless, the interpretation of the aeromagnetic data suggests that the first hypothesis is most likely the correct one.

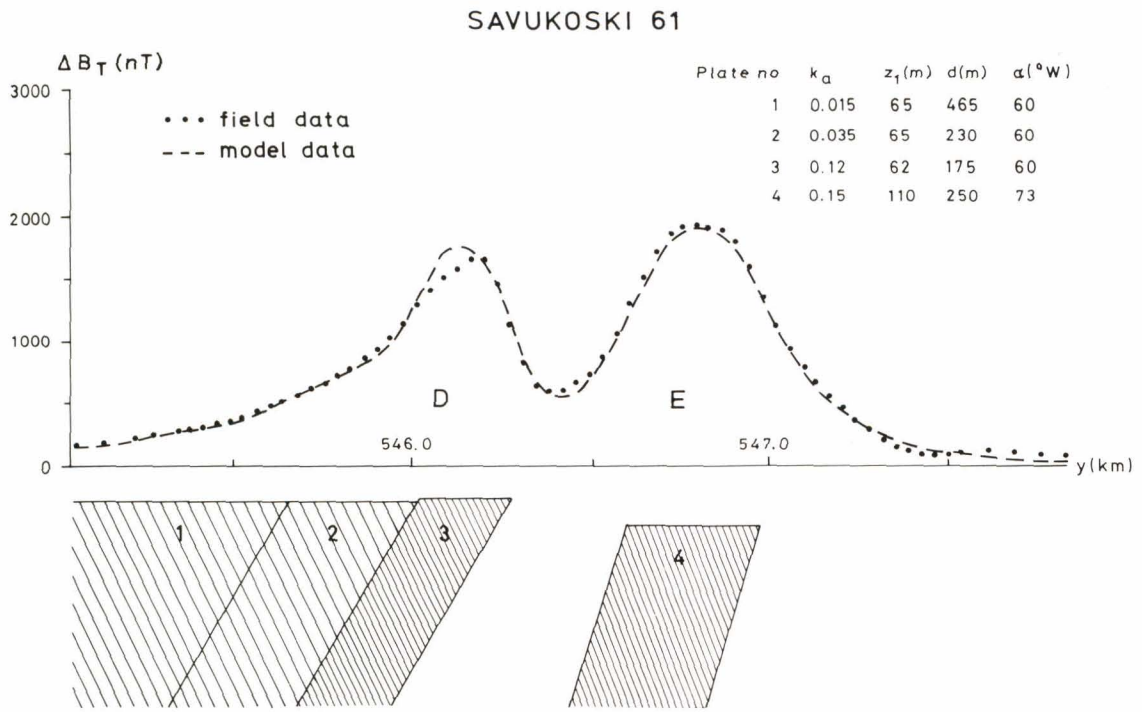

Fig. 111. Test line Savukoski 61, plate model interpretation of the aeromagnetic data. The depth value $z_2 = 5\,000$ m is constant.

Line 68

The results of a small but strong anomaly in Miekkaoja on test line 68 (x = 7473.2 between y = 556.000–558.000) are shown in Fig. 112. Owing to the 3-dimensional structure of the conductor, the high-elevation AEM data result in a distinctly lower S/N-ratio than do the DC-3 AEM data. The target was also submitted to slingram measurements, the outcome of which is given in the same figure. The AEM and slingram survey lines both pass over the conductor, but the lines cross in a 70-degree angle as shown in Fig. 112c.

The data were interpreted on the basis of one-layer and sphere models, and the results are given in Fig. 113. Transform with the conductive half-space model leads to $\sigma_a = 5$ Sm^{-1}, $da_1 = 10$ m. In contrast, the interpretation employing the sphere model gives a = 200 m for the radius, $\sigma = 2$ Sm^{-1} for the conductivity and $da_4 = 10$ m for the depth to the outcrop. A good fit could be found for both sets of data when different sphere models were used. However, a combined interpretation of AEM and slingram data with the same model (Fig. 113b) gives only a poor agreement between the measured and theoretical anomalies. One of the reasons for this phenomenon must be a more complex geometry than the spherical one of the conductive body.

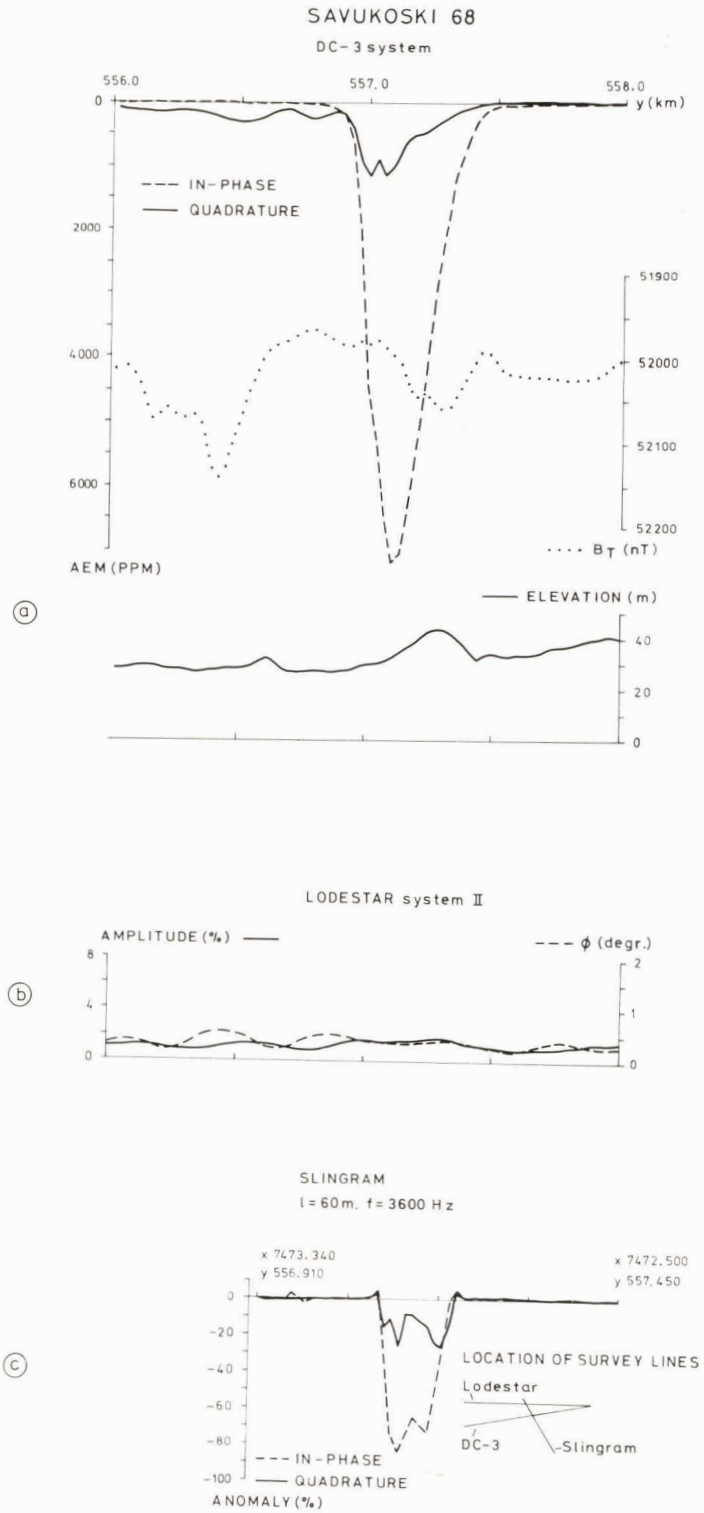

Fig. 112. Test line Savukoski 68, results of various geophysical surveys. (a) AEM, aeromagnetic and flight elevation data, DC-3 system, point spacing $\Delta y = 30$ m. (b) AEM data, Lockheed Lodestar system II. (c) Slingram survey, in-phase and quadrature components, coil separation $l = 60$ m, frequency f = 3 600 Hz, survey line direction 148°, point spacing 20 m.

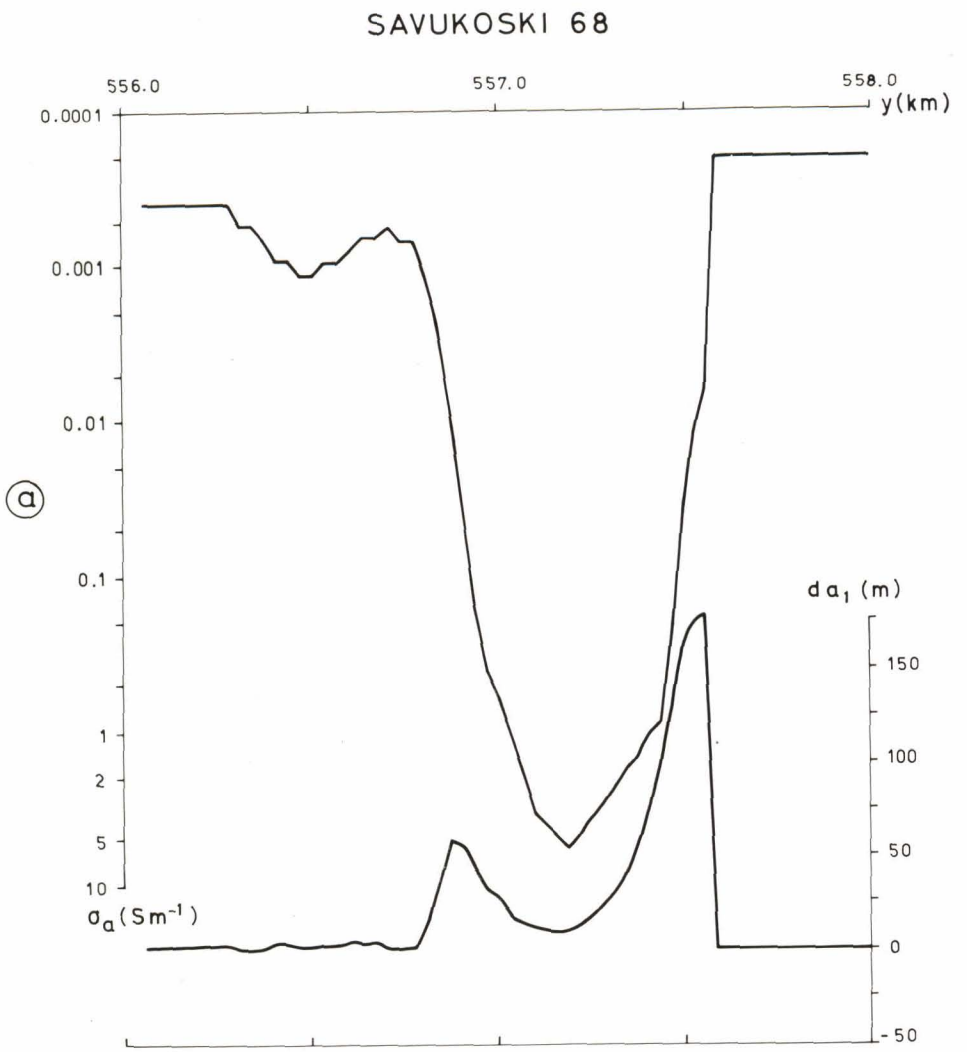

Summary of the Savukoski Kuollutvaara results

Interpretation tests on the Savukoski AEM data applying the model results of a susceptive layered earth demonstrated that:

- If the width of the outcrop of the magnetised formation is ≥ 200 m and k ≥ 0.01, the AEM interpretation can give susceptibility values of the right order of magnitude for the formation. If the width of the outcrop is shorter, the k values obtained are too low. On the other hand, the lack of AEM anomaly over a strongly magnetised formation is a diagnostic fact that can be put to use in interpreting the depth to the outcrop.
- The AEM method is naturally not the primary method of mapping susceptibility variations in the bedrock. Even so, interpretation of the susceptibility effects of the AEM data may usefully

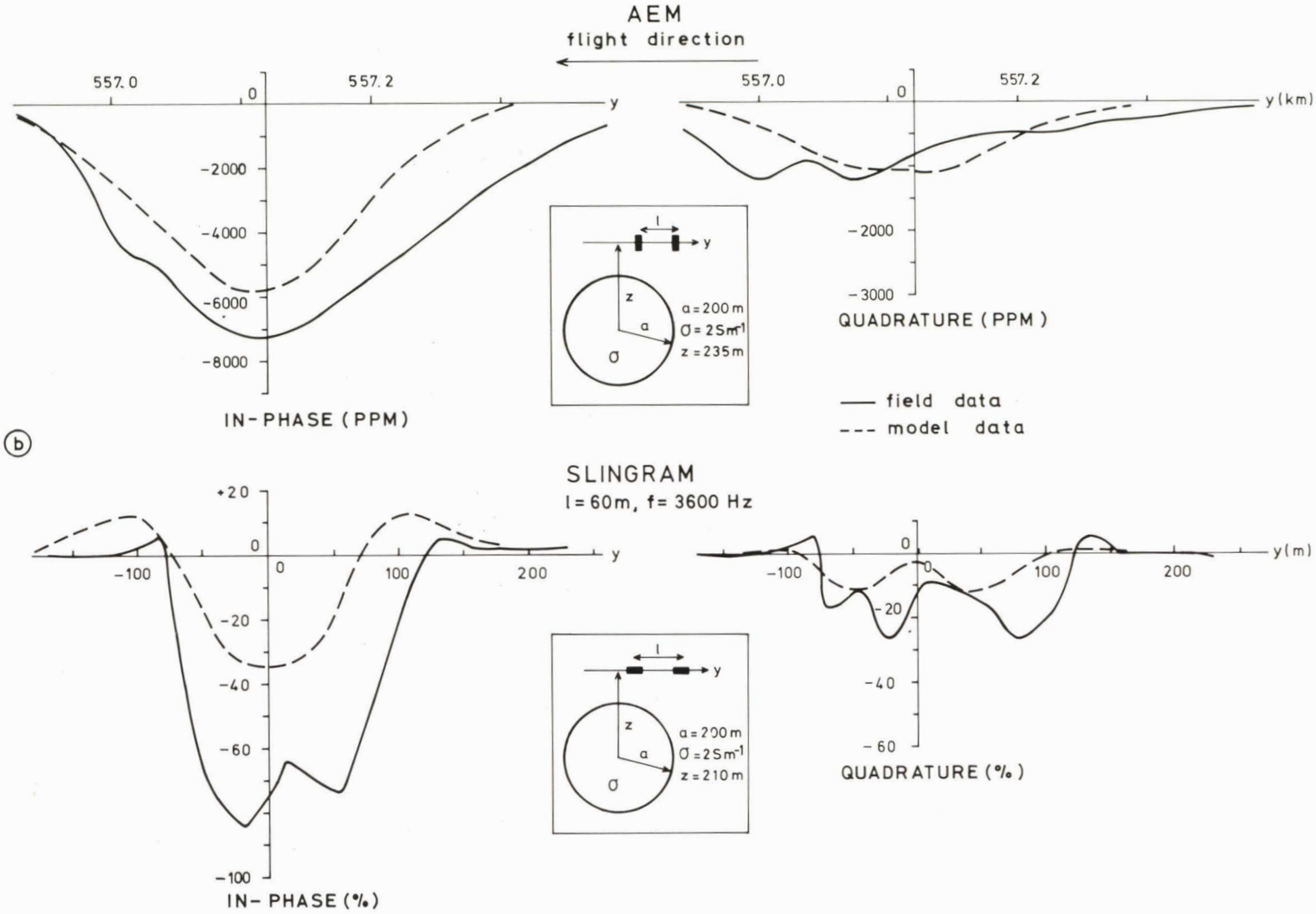

Fig. 113. Test line Savukoski 68, comparison of AEM and slingram results. (a) Values of apparent conductivity σ_a and apparent depth da_1 calculated from AEM survey data by means of one-layer model results (see page 212). (b) Interpretation of DC-3 AEM and slingram data on the basis of the spherical conductor model (radius a = 200 m, depth of subsurface outcrop da_4 = 10 m, conductivity $\sigma = 2\ Sm^{-1}$).

contribute to combined interpretation. Since AEM and aeromagnetic anomalies differ radically in their mode of origin, the results of different methods are independent in terms of interpretation. Thus, the reliability of the combined interpretation can be improved, particularly if petrophysical data are not available. The combined interpretation, however, does not make the determination of petrophysical parameters obsolete; on the contrary, the combined interpretation may give inconsistent results, indicating that petrophysical data are indispensable to a reliable outcome.

Ylivieska: In situ distinction between induced and remanent magnetisation of a mafic intrusive rock

The Ylivieska gabbro massif (map sheet 2431 07) has been subjected to intense geological and geophysical studies. The geological map of the area is reproduced in Fig. 114. The massif is composed of olivine pyroxene gabbro, but more rare variants, such as troctolite and harrisite, are also encountered. The country rocks include granodiorite, mica schist and conglomerate (Salli 1955). The petrophysical and paleomagnetic properties of the massif have been studied by Pesonen and Stigzelius (1972) and the electrical deep

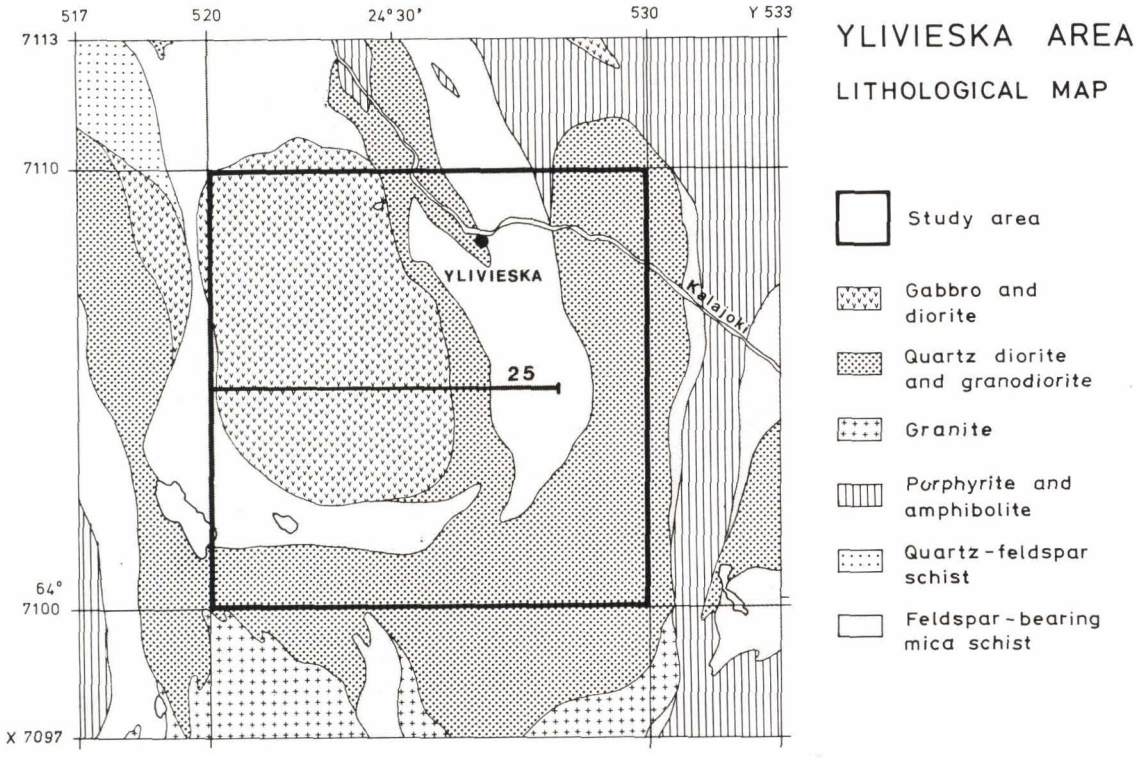

Fig. 114. Lithological map of the Ylivieska area according to Salli (1955). Test line 25 is marked on the map.

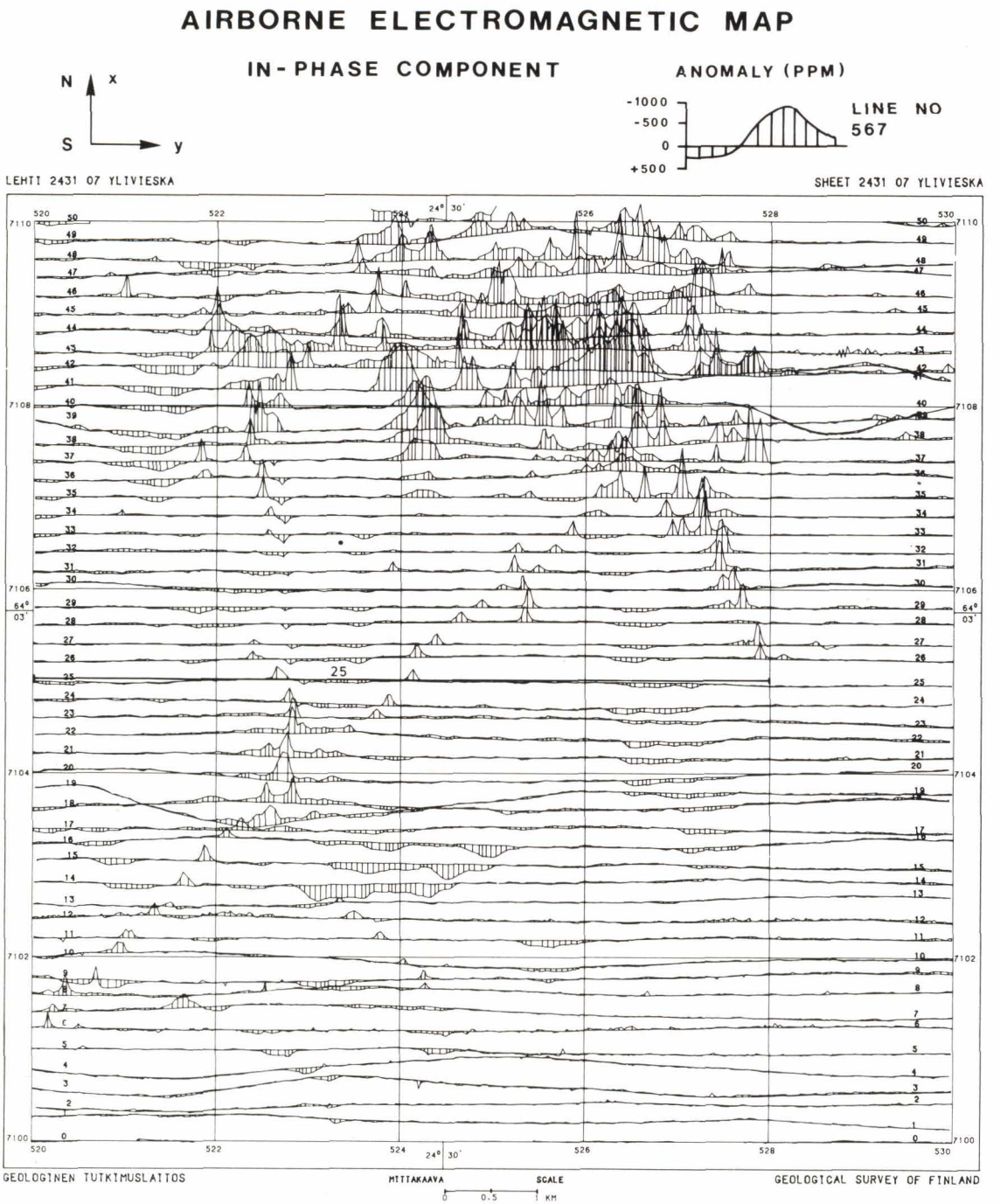

Fig. 115. DC-3 aerogeophysical survey data, map sheet 2431 07 (Ylivieska area). Test line 25 is marked on the maps. (a) AEM in-phase component. (b) AEM quadrature component (see page 216). (c) Aeromagnetic survey data, the absolute values of the magnetic total field 1965.0 (see page 217). Contour interval 200 nT.

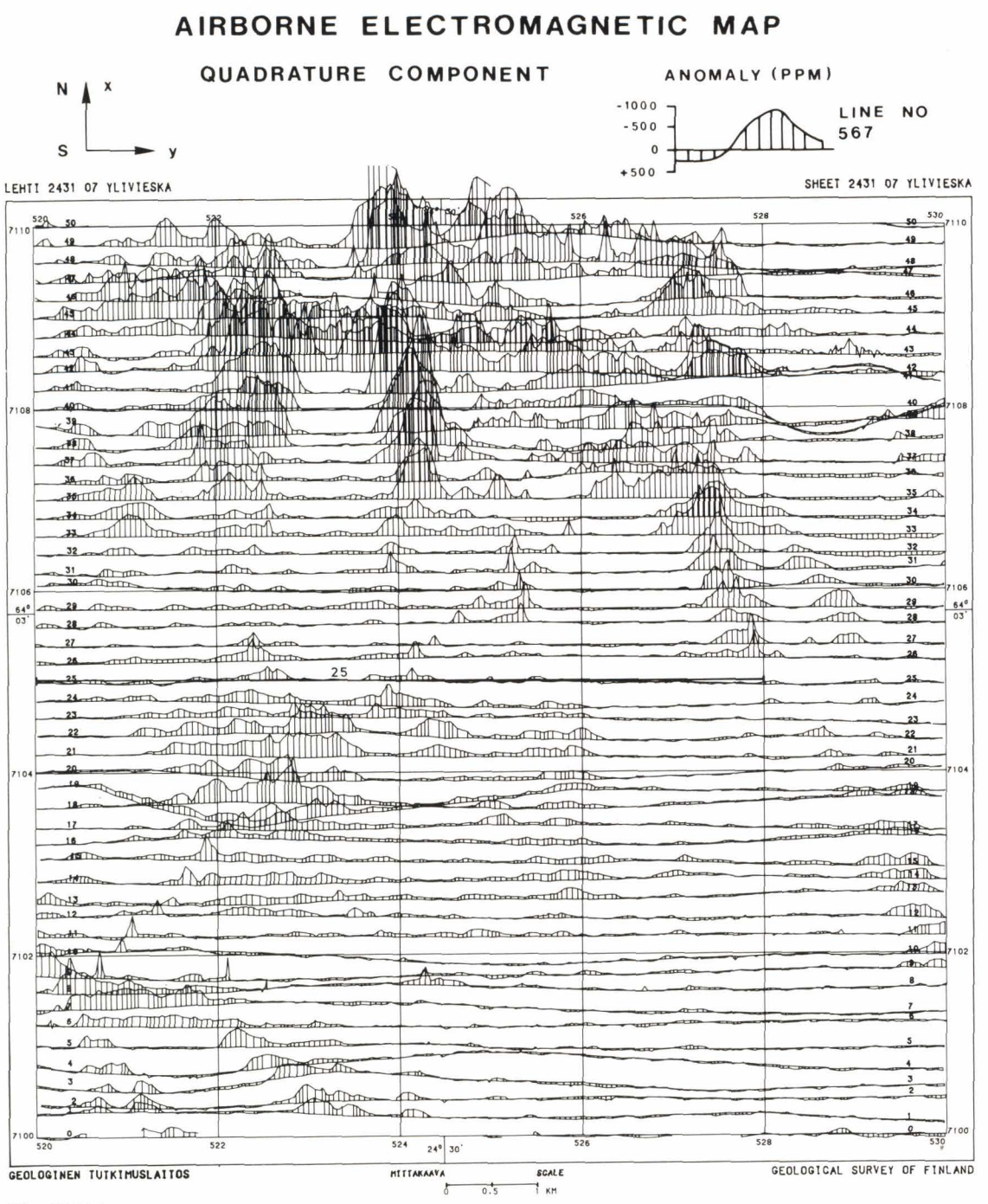
AIRBORNE ELECTROMAGNETIC MAP
QUADRATURE COMPONENT
ANOMALY (PPM)
N
S
x
y
-1000
-500
0
+500
LINE NO
567
LEHTI 2431 07 YLIVIESKA
SHEET 2431 07 YLIVIESKA
520
522
524
526
528
530
7110
7108
7106
7104
7102
7100
64° 03'
24° 30'
25
GEOLOGINEN TUTKIMUSLAITOS
MITTAKAAVA
SCALE
0
0.5
1 KM
GEOLOGICAL SURVEY OF FINLAND

Fig. 115 b)

AEROMAGNETIC MAP

TOTAL FIELD 1965.0

CONTOURS IN nT

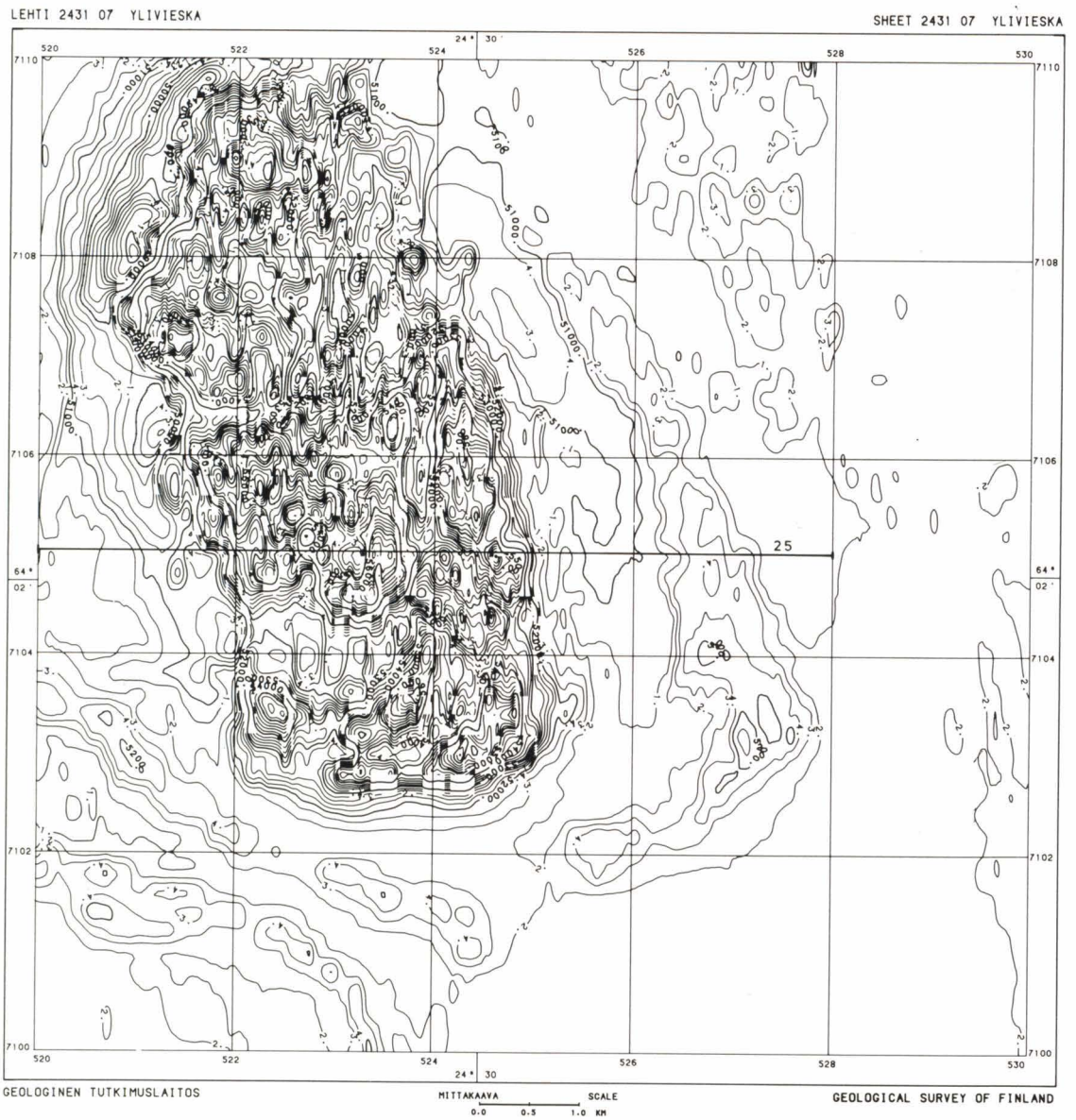

Fig. 115 c)

structure by Pietilä (1979). The topography of the area is flat and the variation in elevation less than 20 m. The average flight elevation of the low-elevation airborne surveys conducted in 1979 was $\bar{h}$ = 32 m and the standard deviation σ_h = 5.5 m. The overburden, which is composed of till, sand, silt and peat, usually varies between 0 and 5 m in thickness. In the valley of the river Kalajoki, in the northern part of the area, the maximum thickness of the overburden encountered so far is 16 m, of which clay accounts for 11 m.

The outcome of the low-elevation AEM and aeromagnetic survey in the map sheet area is shown in Fig. 115. The most outstanding features of the AEM results are the conductivity anomalies caused by clay in the valley of the river Kalajoki and those resulting from human activity (the town of Ylivieska, railway, power transmission lines). Small positive AEM in-phase anomalies, 50–300 ppm, are associated with the southern end of the gabbro body and the mica schist formations northwest and east of the gabbro. The gabbro massif is strongly magnetised, and the aeromagnetic survey map offers a beautiful example of short-wavelength anomaly patterns typical of volcanics. The anomaly maxima over the gabbro formation are about 6 000 nT. Distinct anomalies, although lower in intensity, of about 1 000 nT, are encountered over mica schists.

The results of survey line 25, which passes through the centre of the gabbro massif (x = 7105.0, between y = 520.000–528.000), were compared more closely on the basis of the survey data shown in Fig. 116. The aeromagnetic data were interpreted with prism models by assuming the magnetisation to be entirely induced. The outcome is shown in Fig.

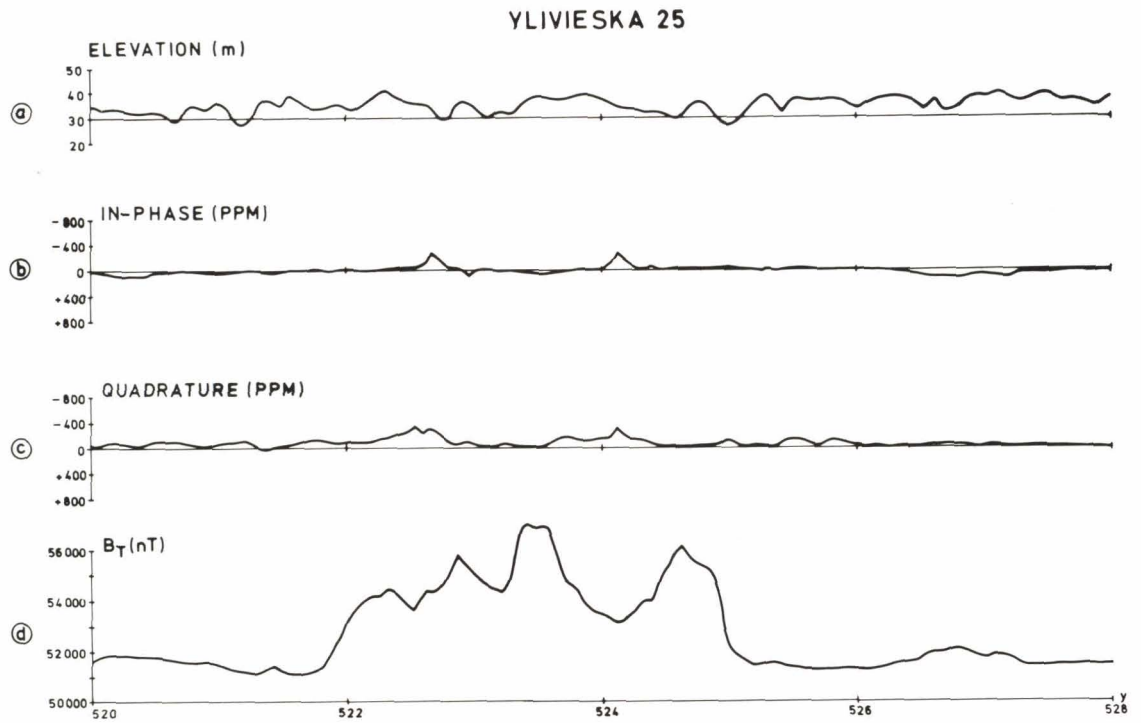

Fig. 116. Test line Ylivieska 25, data of various aerogeophysical methods, point spacing Δy = 29 m. (a) Flight elevation. (b) AEM in-phase component. (c) AEM quadrature component. (d) Absolute values of the magnetic total field.

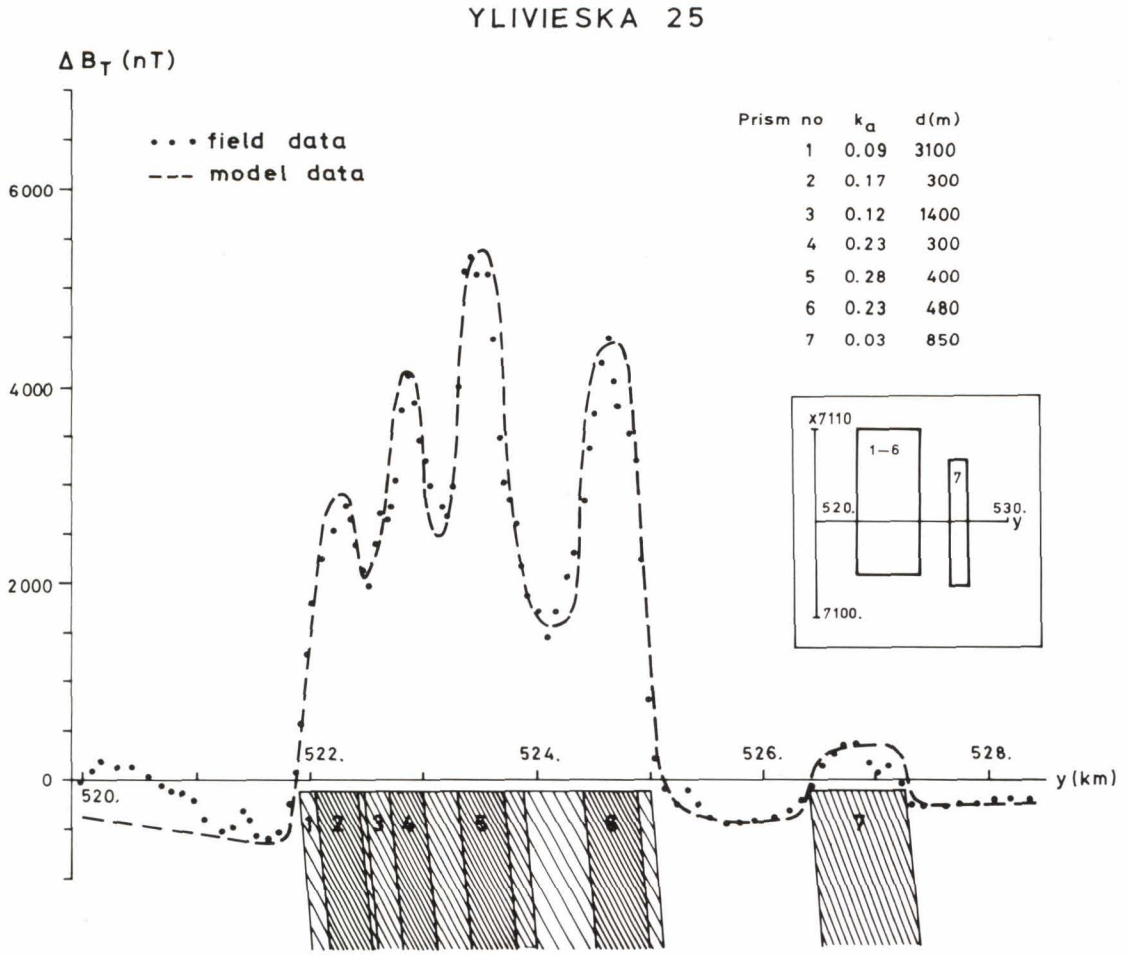

Fig. 117. Test line Ylivieska 25, the aeromagnetic data interpreted by means of prism models. The dip angle $\alpha = 85°$ E and the depth values $z_1 = 40$ m, $z_2 = 4\,000$ m are constants.

117. The interpreted values of susceptibility for gabbro are $k_a = 0.17-0.28$ and for mica schists $k_a = 0.01-0.03$. The interpretation of the AEM data on the basis of Fig. 28, however, gives $k_a = 0.01-0.02$ (maximum values) for gabbro and $k_a = 0.02$ for mica schists. The interpreted values for the mica schists are compatible. In contrast, the values for gabbro differ by an order of magnitude. Again there are three possible reasons for this difference:

1. The depth to the outcrop is > 100 m.
2. The AEM in-phase data fall into the transition region of the response function.
3. The magnetisation is remanent.

Hypothesis 1 is not compatible with the magnetic interpretation. On the basis of Fig. 26, hypothesis 2 would require the conductivity of the gabbro to be 0.005–0.01 Sm^{-1}. In that case, however, the quadrature anomalies would be much higher than those observed, at least −1 000 to −1 500 ppm. In fact, they measure only −100 to −300 ppm, which makes hypothesis 2 very unlikely. Hence,

remanent magnetisation remains the most probable explanation of the difference between the AEM and aeromagnetic interpretations. The petrophysical parameters measured on the gabbro samples average k = 0.02, Q = 13, inclination 40° and declination −30° (Pesonen & Stigzelius 1972). Pietilä (1979 p. 63) has interpreted the high-elevation aeromagnetic data applying the prism model and taking into account the remanent magnetisation as the average value. He ended up with k = 0.018 for the gabbro.

The methodic example of the Ylivieska gabbro demonstrates that, under favourable conditions, the presence of strong remanent magnetisation can be recognised by combined interpretation of aeromagnetic and AEM data. In such a case, the AEM method gives susceptibility values that are closer to the true ones.

SUMMARY

The development and application of AEM methods have been described and the underlying principles outlined. The AEM measurements and the relevant methods applied in Finland by the Geological Survey and other exploration organizations have been reviewed. The vertical coaxial fixed-coil system fitted in a DC-3 aircraft has been described in detail with special reference to technical performance, results and auxiliary measurements. The coil separation of the system was 25.0 m, the transmitter frequency 3 220 Hz and the detector time constant 0.3 s. The digital recording of data took place at an interval of 0.5 s with a resolution of 5 parts per million (ppm) of the primary field. The survey flights were undertaken at a line spacing of 200 m, at a speed of 200 km/h and at a nominal elevation of 30 m. In 1973–1979 the Geological Survey of Finland applied the system to exploration and bedrock mapping studies over a total of 295 000 line kilometres.

A set of computer programs has been developed to process the AEM digital data into anomaly profile and contour maps. The main stages of the data processing have been described and the principles underlying the methodic reductions were given. As a result of the data processing, the Geological Survey has compiled and released the AEM survey data as in-phase and quadrature anomaly maps on a scale of 1 : 20 000.

The physical properties of the Finnish rocks and soils, the methods of interpretation of the survey data and the models used in the interpretation have been discussed as factors related to the application of the AEM results. The characteristic response diagrams have been deduced by numerical modelling for the following anomaly sources: a conductive and/or susceptive half-space, a conductive horizontal layer overlying a resistive and/or susceptive half-space, and a conductive sphere in a resistive medium. Results relevant to a thin conductive half-plane have been elaborated by means of scale modelling. Preliminary measurements have also been undertaken on a thick conductive half-plane model, and the effect of the detector time constant on the responses of the thin half-plane and sphere have been studied.

Based on the modelling results of the conductive half-space and the thin conductive horizontal layer, computer programs have been developed that permit the anomaly data produced by the system to be transformed into apparent conductivity, conductance and depth values. The principles underlying the transformation are given, and the accuracy

and properties of the transformed data are discussed.

The AEM responses produced by different geological formations have been interpreted by applying the modelling results. The examples include 8 case histories. Anomalies due to conductive overburden and sheet-like and local conductors in the bedrock have been examined and compared with results obtained by other electrical and electromagnetic methods. Similarly, the qualitative interpretation of the susceptibility and remanence effects has been studied with the aid of combined AEM and aeromagnetic survey data. The AEM anomaly data have been transformed by means of computer programs, and the apparent conductivity values thus obtained were compared with those produced by earth resistivity survey methods. It has been demonstrated that, under favourable conditions, the apparent conductivity and conductance values deduced from the original AEM anomaly data can be used directly to guide follow-up studies and to establish potential targets even in explorationally difficult, e.g. black schist, areas.

The characteristics of the DC-3 AEM system can be summarised as follows:

1. The system coil separation l and the frequency f were dimensioned so that the conductivity and conductance apertures of the results are large (Table 14).
2. As demonstrated by the low noise in relation to the coil separation and the linearity and slow rate of drift, the technical realisation of the system was good. This means that the penetration is good in both theoretical approaches (Table 15) and field survey data (page 166). Owing to the low flight elevation and the low time constant, the resolution and the sensitivity of the data are good.
3. Analysis of the field survey data established 25 ppm as the average noise level and 100 ppm as the detection limit of an anomaly. At the nominal flight elevation, this limit value and the model tests performed give 0.0003 -300 Sm^{-1} for the conductivity aperture of a half-space, 0.01–400 S for the conductance aperture of a horizontal conductor, 0.2–100 S for the conductance aperture of a vertical thin half-plane, and 0.01–100 Sm^{-1} for the conductivity aperture of a sphere with a diameter of 50 m. The upper limits refer to the inductive saturation limit of the anomaly values. For the same conductor models the penetration of the system, flight elevation included, is correspondingly 210 m, 210 m, 125 m and 85 m. The detection limit of the system is 0.01 SI units for the susceptibility of a resistive and susceptive half-space, and the penetration 75 m at a susceptibility of 0.10 SI units. When the conductivity σ of a half-space is less than 0.001 Sm^{-1}, susceptibility is the predominant property affecting the AEM response; within the range of $\sigma = 0.001$ to 0.05 Sm^{-1} both properties are significant and when σ exceeds 0.05 Sm^{-1} conductivity is the predominant property.
4. The penetration values of the DC-3 AEM system from field examples compare favourably with ground EM slingram results. The penetration was found (p. 147 and p. 178) to exceed that of the slingram method with a coil separation of $l = 40$ m and a frequency of f = 3 600 Hz, and to be equal or better than with $l = 60$ m. These results are from test areas in which the overburden conductance varies between 0.01–0.1 S.
5. The digital recording and the computer processing of the survey data

combined with the high quality of the original data made possible the systematic production of profile and contour maps. To maintain resolution, the former were not submitted to any smoothing at all, and the contour maps only to the minimum amount. The lowermost contour on the contour maps equals a detection limit of $S_d = 4$ N, i.e. 100 ppm.

6. Owing to the large conductivity and conductance apertures, the DC-3 AEM survey data contain abundant anomalies produced by various conductors. Visual and manual interpretation of the survey maps is feasible but cumbersome. The interpretation can be developed and facilitated by means of computer-based transformation of data (σ_a, s_a, da_i maps). The production of transformation maps was shown to be technically feasible and often useful for the utilisation of the results. The transformation results were found to agree well with the apparent resistivity values measured with earth resistivity methods.
7. The high quality of the results (items 1–4) and the use of computer data processing methods (items 5–6) would have made it possible to partly replace slingram surveys by AEM data in regional exploration. In practice, the substitution was rarely achieved owing to the time lag in data processing. The results can be directly applied to bedrock mapping as well as to exploration.
8. Although theoretical modelling data on the responses to the system have been obtained earlier as well as in the course of the present work, these data are not sufficient. Particularly the results of the thick half-plane conductor and the responses to the combined effect of poorly conductive country rock and overburden should be further studied. Existing scale-model data could be put to more effective use if more computing capacity for interactive graphic interpretation software were available.
9. In Finland the total conductance of the overburden, saline clays excluded, is usually rather low, 0.01 to 0.1 S. Hence, the influence of the overburden can usually be interpreted from AEM data only with the aid of an electrically thin sheet model. Even in favourable cases, only approximate values of conductivities and thicknesses can be separately interpreted for the electrically thick horizontal conductor.
10. The interpretation capability of the AEM data can be somewhat improved with multifrequency or multicomponent systems. These systems, though, inevitably cause additional problems with regard to technical realisation, cost and the maintenance of high quality results. The above examples of field survey results indicate that, under the geological conditions in Finland, these systems would have no decisive advantages over the DC-3 AEM system. In terms of methodology and total costs, a better way of enlarging the field of application of the AEM method would be to supplement a dipolar AEM system with a plane-wave method.

ACKNOWLEDGEMENTS

The present study was undertaken in 1975–1981 at the Geological Survey of Finland using the AEM data of the DC-3 aerogeophysical system of the Survey as starting material. The system was designed, manufactured and installed by Professor Maunu Puranen, Mr. Keijo Westerlund, Mr. Uljas Hämäläinen, Mr. Tapani Ista, Mr. Simo Lehtinen, Mr. Kalevi Sulkanen, Mr. Veikko Mäkinen and Mr. Kari Kuusa. The digital recording subsystem was developed by Mr. Eero Hiltunen, Mr. Kalevi Sulkanen and Mr. Veli Leinonen. The success of the flying operations was due to the pilots and the technical staff of Kar-Air Oy. The aerogeophysical maps were produced in cooperation with the airborne geophysics group of the Geophysics Department and the ADP group of the Geological Survey. The figures were drawn by Mrs. Kirsti Blomster, Mrs. Anja Leskinen, Mrs. Leena Mäkilä and Mrs. Sisko Sulkanen and the manuscript typed by Mrs. Marjatta Niemi and Miss Ulla Kuokkanen.

I thank my colleagues at the Geological Survey and in the Laboratory of Economic Geology of the Helsinki University of Technology for all the help and advice I received during the study.

I express my gratitude to Shell Canada Resources Ltd. for the ADP program of the sphere model, and to Dr. Ajit K. Sinha of the Geological Survey of Canada for the original version of the published layered-earth program. The Exploration Departments of Outokumpu Oy and Rautaruukki Oy kindly permitted me to use information relevant to their airborne surveys.

I thank my superiors, Professor Maunu Puranen, Professor Toivo Siikarla and Professor Lauri Eskola, and the former Director of the Geological Survey, Professor Herman Stigzelius, for the interest they showed in my work. I also thank Professor Aimo K. Mikkola of Helsinki University of Technology for his help and encouragement.

I am grateful to Professor Maunu Puranen and Dr. Gabor Gaál for their constructive criticism and to Mrs. Gillian Häkli for the translation of the manuscript.

Finally, I thank the Outokumpu Oy Foundation, the Finnish Natural Research Council and my parents for their financial support.

Accepted for publication 18th February 1982

REFERENCES

Arcone, S. A., 1979. Investigation of a VLF airborne resistivity survey conducted in northern Maine. Geophysics 43, 1399–1417.

Bärlund, H., 1966. En jämförelse mellan tolkningen av olika geofysikaliska mätningar över Pyhäsalmi, Raajärvi och Leveäselkä malmfyndigheter och dennas överensstämmelse med geologin. Manuscript, Tek. korkeakoulu, Vuoriteollisuusosasto, Espoo. 117 p + append.

Barringer, A. R., 1971. Airborne exploration. Min. Mag. 124, 182–189.

Becker, A., 1979. Airborne electromagnetic methods. 33–43 *In* Geophysics and Geochemistry in the Search for Metallic Ores, ed. by Hood, Geol. Surv. Canada, Econ. Geol. Rep. 31.

Best, M. E. & Shammas, B. R., 1979. A general solution for a spherical conductor in a magnetic dipole field. Geophysics 44, 781–800.

Boie, D. C., 1970. Untersuchungen zur Doppler-Navigation und -Ortung von geophysikalischen und photogrammetrischen Messflugen. Diss. 39, Tech. Univ., Hannover. 137 p.

Boniwell, J. B., 1967. Some recent results with the INPUT airborne EM system. CIM Bull. 60 (659), 325–332.

Brant, A. A.; Dolan, W. M. & Elliot, C. L., 1966. Coplanar and coaxial EM tests in Bathurst area, New Brunswick, Canada, 1956. 130–141 *In* Society of Exploration Geophysicists' Mining Geophysics I, Case Histories, ed. by Hansen, Heinrichs, Holmer, MacDougall, Rogers, Summer and Ward, Soc. Explor. Geophys., Tulsa, Okla.

California Computer Products Inc., 1972. GPCP-II, A general purpose contouring program, User's manual. 138 p.

Ekdahl, E., 1976a. Paljastumakartta, Pielavesi Ilokangas. Geol. tutkimusl., Malmiosasto, M 11.1/3314 06B/76/2.

–, **1976b.** Raportti Tervon alueella vuosina 1973–1974 suoritetuista malmitutkimuksista. Geol. tutkimusl., Malmiosasto, rap. M 19/3313/76/1/10. 30 p + append.

Ervamaa, P. & Heino, T., 1980. Väliraportti Kainuun–Ylä-Savon mustaliuske–serpentiniittijakson malmitutkimuksista v. 1977–1979. Geol. tutkimusl., Malmiosasto, rap. M 19/3344/-80/1/10. 26 p + append.

Fraser, D. C., 1973. Magnetite ore tonnage estimates from an aerial electromagnetic survey. Geoexploration 11, 97–106.

–, **1978.** Resistivity mapping with an airborne multicoil electromagnetic system. Geophysics 43, 144–172.

–, **1979.** The multicoil II airborne electromagnetic system. Geophysics 44, 1367–1394.

–, **1981.** Magnetite mapping with a multicoil airborne electromagnetic system. Geophysics 46, 1579–1593.

Frischknecht, F. C., 1967. Fields about an oscillating magnetic dipole over a two-layer earth, and application to ground and airborne electromagnetic surveys. Colo. Sch. Mines Quart. 62 (1). 326 p.

Gaur, V. K. & Verma, O. P., 1973. Enhancement of electromagnetic anomalies by a conducting overburden II. Geophys. Prospect. 21, 159–184.

Gaur, V. K.; Verma, O. P. & Gupta, C. P., 1972. Enhancement of electromagnetic anomalies by a conducting overburden. Geophys. Prospect. 20, 580–604.

Geological Survey of Finland, 1951. Ann. rep. act. year 1950. 28 p.

–, **1952.** Ann. rep. act. year 1951. 34 p.

–, **1955.** Ann. rep. act. year 1954. 38 p.

–, **1957.** Ann. rep. act. year 1956. 30 p.

Geonics Limited, 1975. EM16R (Radiohm) two-layer interpretation curves. Techn. Note TN-1. 8 p + append.

Ghosh, M. K., 1972. Interpretation of airborne EM measurements based on thin sheet models. Unpublished Ph. D. Thesis, Univ. Toronto. 195 p.

Ghosh, M. K. & West, G. F., 1971. AEM analogue model studies. Norman Paterson and Assos. Toronto. 12 p + append.

Goldstein, N. E. & Wards, S. H., 1966. The separation of remanent from inducent magnetism in situ. Geophysics 31, 779–796.

Grant, F. S., & West, G. F., 1965. Interpretation Theory in Applied Geophysics. McGraw-Hill, New York. 583 p.

Grasty, R. L., 1972. Airborne gamma-ray spectrometry data processing manual. Geol. Surv. Canada, Open File 109. 83 p.

Grip, E., 1978. Fjärranalys för prospektering i Sverige. STU-information nr 87-1978. Styr. tek. utveckling, Stockholm. 44 p.

Hämäläinen, T., 1977. Aerosähköisiin matalalentomittauksiin liittyviä pienoismallitutkimuksia. Manuscript, Tek. korkeakoulu, Vuoriteollisuusosasto, Espoo. 60 p + append.

Hartimo, I., 1981. Näytteenotto ja A/D-muunnos. II/1–II/13 *In* Digitaalinen signaalinkäsittely. Insinöörijärjestöjen koulutuskeskus, kurssimoniste 53–81.

Hattula, A., 1970. Geofysikaalisten anomalioiden alueellisesta tulkinnasta. Manuscript, Tek. korkeakoulu, Vuoriteollisuusosasto, Espoo. 72 p + append.

Heino, T. & Havola, M., 1980. Jormasjärven-Talvivaaran alueen geologiasta. Geol. tutkimusl., Malmiosasto, rap. M 19/3344/-80/2/10. 10 p + append.

Hirvas, H. & Nenonen, K., 1978. Raportti malminetsintää palvelevista maaperätutkimuksista Tervon Utrianlahden Zn-lohkaretihentymäellä. Geol. tutkimusl., Maaperäosasto, projekti 905. 7 p + append.

Hjelt., S-E., 1964. Erään induktiivisen malminetsintämenetelmän mahdollisuuksista. Manuscript, Tek. korkeakoulu. Tek. fysiikan osasto, Espoo. 50 p + append.

–, 1972. Magnetostatic anomalies of dipping prisms. Geoexploration 10, 239–254.

–, 1973. Experiences with automatic magnetic interpretation using the thick plate model. Geophys. Prospect. 21, 243–265.

Hoekstra, P., Sellmann, P. V. & Delanay, A., 1975. Ground and airborne resistivity surveys of permafrost near Fairbanks, Alaska. Geophysics 40, 641–656.

Jain, S. C., 1973. Inline and broadside EM dipole dipole profiling over a thin vertical infinitely conducting vein. Geophys. Prospect. 21, 648–659.

Järvimäki, P., 1977. Seisminen luotaus, Nurmo L198. Geol. tutkimusl., Geofysiikan osasto, rap. Q 23/2222 06. 1 p.

Jensen, O. G. & Becker, A., 1979. Phase-compensating deconvolution to reduce distortion caused by in-aircraft reactive integrators. Geophysics 44, 1531–1540.

Jokinen, T., 1979. Malminetsinnän geofysikaaliset tutkimukset. 37–42 *In* Geofysiikan osaston vuosikertomus 1979. Manuscript, Geol. tutkimusl. 97 p.

Kaila, I., 1976. Sama-arvokäyränpiirto-ohjelman GPCP II siirtäminen HP 3000 tietokoneelle. Manuscript, Tek. korkeakoulu, Tek. fysiikan osasto, Espoo. 37 p + append.

Keller, G. V. & Frischknecht, F. C., 1966. Electrical Methods in Geophysical Prospecting. Pergamon, Oxford. 519 p.

Ketola, M., 1968. The interpretation of slingram (horizontal loop) anomalies by small-scale model measurements. Geol. Surv. Finland, Rep. Invest. 2. 35 p + append.

–, 1972. Eräitä näkökohtia magneettisten ja elektromagneettisten anomalioiden tulkinnasta. III/1–III/21 *In* Geofysiikan päivät 11–12. 11. 1971 Helsinki, ed. by Peltoniemi, Tek. korkeakoulu, Vuoriteollisuusosasto, rap. HTKK-V-GF-2.

–, 1979. On the application of geophysics in the indirect exploration for copper sulphide ores in Finland. 665–684 *In* Geophysics and Geochemistry in the Search for Metallic Ores, ed. by Hood, Geol. Surv. Canada, Econ. Geol. Rep. 31.

Ketola, M.; Laurila, M. & Suokonautio, V., 1971. On a digital two-plane rotary field airborne system and its use in conjunction with the magnetic method in Finland. Geoexploration 10, 203–220.

Ketola, M. & Puranen, M., 1967. Type curves for the interpretation of slingram (horizontal loop) anomalies over tabular bodies. Geol. Surv. Finland, Rep. Invest. 1. 19 p + append.

Korhonen, J., 1974. Aeromagneettinen tuloskäsittely. 60–61 *In* Atk-sovellutukset geologiassa. Geologiliitto, koulutusmoniste 1.

–, 1979. Computer processing of aeromagnetic data in Geological Survey of Finland. 12th NOFTIG Meeting, 8–10. 1. 1979, Oslo.

Kujansuu, R., 1972. On landslides in Finnish Lapland. Geol. Surv. Finland, Bull. 256. 22 p.

Kurimo-Salminen, M., 1979. Loivakaateisen puolitason ja homogeenisen irtomaakerroksen slingramanomalioista. Manuscript, Tek. korkeakoulu, Vuoriteollisuusosasto, Espoo. 52 p + append.

Laiho, J., 1975. Maaperän efektiivisen johtokyvyn määrääminen radiotaajuisia kentänvoimakkuuksia mittaamalla. Manuscript, Tek. korkeakoulu, Sähköteknillinen osasto, Espoo. 90 p + append.

Laitakari, A. J., 1968. Säviän kupariesiintymän geologiasta. Geol. tutkimusl., Malmiosasto, rap. M 17/Plv -68/2. 71 p + append.

Lanne, E., 1980a. Aerogeofysikaalisten korkealentomittausten yleispiirteiden kuvausmenetelmä. Summary: A descriptive method for the general features of high altitude airborne maps. Univ. Oulu, Inst. Geophys., Contrib. 110. 14 p.

–, 1980b. Sähkömagneettisten korkealentohavaintojen tulkinta johtavaa puoliavaruusmallia käyttäen. Summary: Interpretation of electromagnetic high altitude airborne data using the conductive half space model. Univ. Oulu, Inst. Geophys., Contrib. 111. 31 p.

Lee, T., 1981. Transient electromagnetic response of a polarizable ground. Geophysics 46, 1037–1041.

Lehtimäki, J., 1981. IP-mittaus dipoli-dipoli elektrodijärjestelmällä FP-laitteistolla ja saatujen tulosten vertailu gradienttimittauksiin Tervon ja Perhon alueilla. Geol. tutkimusl., Geofysiikan osasto, rap. Q 16.1/28.3/81/1. 19 p + append.

Liljestrand, B., 1972. Pienoismallimittauksia aerosähköisten anomalioiden tulkintaa varten. Manuscript, Tek. korkeakoulu, Vuoriteollisuusosasto, Espoo. 47 p + append.

Lodha, G. S., 1974. Quantitative interpretation of AEM response for a sphere model. Unpublished M.Sc. thesis, Univ. Toronto. 59 p + append.

Lodha, G. S. & West, G. F., 1976. Practical airborne E.M. (AEM) interpretation using a sphere model. Geophysics 41, 1157–1169.

Malmqvist, D., 1965. A numerical calculation of the electromagnetic field from a vertical and a horizontal magnetic dipole above a homogeneous earth. Geoexploration 3, 175–227.

March, H. W., 1953. The field of a magnetic dipole in the presence of a conducting sphere. Geophysics 18, 671–684.

Marmo, V., 1960. On the sulphide and sulphide-graphite schists of Finland. Bull. Comm. Géol. Finlande 190. 80 p.

–, 1964. Aerogeofysikaalisten karttojen geologisesta tulkinnasta. Summary: On the geological interpretation of the aerogeophysical maps. Terra 76, 105–119.

Marmo, V. & Puranen, M., 1966. Aerogeofysikaalisten karttojen käytöstä geologisen tutkimuksen apuna. Geol. tutkimusl., Opas N:o 3, 33 p + append.

Mikkola, E., 1937. Kivilajikartta – Pre-Quaternary rocks, Sheet–C7 Sodankylä. Suomen geologinen yleiskartta – General geological map of Finland, 1 : 400 000.

Mizyuk, L. Ya., 1960. Methods and apparatus for airborne prospecting. Bull. Acad. Sci. U.S.S.R., Ser. Geophys. 6, 789–797.

Morrison, H. F.; Phillips, R. J. & O'Brien, D. P., 1969. Quantitative interpretation of transient electromagnetic fields over a layered half space. Geophys. Prospect. 17, 82–101.

Neuvonen, K. J., 1961. Kallioperäkartta – Pre-Quaternary rocks, Sheet–2222 Seinäjoki. Suomen geologinen kartta – Geological map of Finland, 1 : 100 000.

Noukka, P., 1979. Uudistuva ilmakuvakartta. Maanmittaus 54 (4), 55–70.

Okko, V., 1964. Maaperä. 239–332 *In* Suomen geologia, ed. by Rankama. Kirjayhtymä, Helsinki.

Ovaskainen, E., 1976. Pienoismallimittauksia slingrammenetelmällä. Manuscript, Tek. korkeakoulu, Vuoriteollisuusosasto, Espoo. 55 p + append.

Ovaskainen, E. & Peltoniemi, M., 1979. Geologisen tutkimuslaitoksen käyttämille aerosähköisille mittauslaitteistoille suoritettuja pienoismallimittauksia. Geol. tutkimusl., Geofysiikan osasto, rap. Q 16.2./24.8/79/2. 11 p + append.

Paarma, H., 1969. Aerometodisista tutkimuksista. 359–366 *In* »Pohjola 2000»-seminaari 5.–8. 8. 1968, esitelmät ja alustukset, ed. by Varjo, Oulun yliopisto, Oulu.

–, 1970. A new find of carbonatite in North Finland, the Sokli plug in Savukoski. Lithos 3, 129–133.

–, 1971. Aerometodisista tutkimuksista. Pioneeriupseeri 29 (2), 10–13.

Palacky, G. J., 1972. Computer assisted interpretation of multichannel airborne electromagnetic measurements. Unpublished Ph.D. Thesis, Univ. Toronto. 152 p.

–, 1976. Use of decay patterns for the classification of anomalies in time-domain AEM measurements. Geophysics 41, 1031–1041.

–, 1981. The airborne electromagnetic method as a tool of geological mapping. Geophys. Prospect. 29, 60–88.

Parasnis, D. S., 1971. Analysis of some multi-

frequency, multiseparation electromagnetic surveys. Geophys. Prospect. 19, 163–179.

Paterson, N. R., 1961. Experimental and field data for the dual-frequency phase-shift method of airborne electromagnetic prospecting. Geophysics 26, 601–617.

–, **1971.** Airborne electromagnetic methods as applied to the search for sulphide deposits. CIM Bull. 64 (1), 29–38.

Peltoniemi, M., 1975. Esiraportti aerogeofysikaalisista matalalentotutkimuksista sekä aeroradiometristen mittaustulosten ATK-käsittelystä vuosina 1972–1974. Geol. tutkimusl. 38 p + append.

–, **1977.** Conductive bedrock and overburden effects on airborne electromagnetic methods used by the Geological Survey of Finland. 89–103 *In* Prospecting in areas of glaciated terrain 1977, ed. by Jones, Inst. Min. and Metall., London.

–, **1978a.** About computer processing and interpretation of airborne electromagnetic (AEM) data. Geoexploration 16, 321.

–, **1978b.** Karakteristisia käyrästöjä aerosähköisten mittaustulosten tulkintaa varten. Geol. tutkimusl., Geofysiikan osasto, rap. Q 16.2/24.9/78/1. 8 p + append.

–, **1979a.** Aerogeofysikaalisista matalalentomittauksista ja tulosten hyväksikäytöstä. Geologi 31, 17–21.

–, **1979b.** Aeroradiometristen gammasäteilymittausten käytöstä uraaninetsintään Suomessa. 99–119 *In* Uraaniraaka-ainesymposiumi, sarja B, No 27, ed. by Parkkinen, Vuorimiesyhdistys-Bergsmannaföreningen, Helsinki.

–, **1980a.** Johtavan, magneettisen kerrosrakenteen aiheuttamista aerosähköisistä anomalioista. Geol. tutkimusl., Geofysiikan osasto, rap. Q 16.2/24.8/80/1. 57 p.

–, **1980b.** Johtavan pallon vasteita geologisen tutkimuslaitoksen aerosähköisille matalalentojärjestelmille. Geol. tutkimusl., Geofysiikan osasto, rap. Q 16.2/24.8/80/2. 48 p.

–, **1981a.** Tulkintadiagrammeja sekä tulosesimerkkejä APEX MK I- ja MH/GTL-malmiharaville. Geol. tutkimusl., Geofysiikan osasto, rap. Q 16.2/24.1/81/1. 55 p.

–, **1981b.** Airborne electromagnetic anomalies of permeable, conducting earth. 13th NOFTIG Meeting, 12–14. 1. 1981, Luleå.

Peltoniemi, M. & Kuittinen, R., 1978. Lumen vesiarvon mittaus luonnon gammasäteilyn avulla. Vesitalous 19 (1), 17–26.

Peltoniemi, M. & Vironmäki, J., 1977. Dopplerpaikannusmenetelmän käytöstä aerogeofysikaalisissa matalalentotutkimuksissa. 207–216 *In* Geofysiikan päivät Helsingissä 10.–11. 3. 1977, ed. by Helminen, Geofysiikan seura, Helsinki.

Pemberton, R. H., 1962. Airborne electromagnetics in review. Geophysics 27, 691–713.

Pernu, T., 1979. Maa- ja kallioperän tutkiminen tasavirtavastusmittauksilla, erityisesti Suomen oloissa. Manuscript, Oulun yliopisto, Geofysiikan laitos, 99 p.

Pesonen, L. J. & Stigzelius, E., 1972. On petrophysical and paleomagnetic investigations of the gabbros of the Pohjanmaa region, Middle-West Finland. Geol. Surv. Finland, Bull. 260. 27 p.

Pietilä, R., 1979. Ylivieskan gabron sähköinen rakennetutkimus. Manuscript, Oulun yliopisto, Geofysiikan laitos. 71 p.

Pitcher, D. H.; Barlow, R. B. & Lewis, M., 1980. Tridem airborne conductivity mapping as a lignite exploration method. CIM Bull. 73 (5), 53–63.

Podolsky, G., 1966. An evaluation of an airborne electromagnetic anomaly in northwestern Quebec. 197–205 *In* Society of Exploration Geophysicists' Mining Geophysics I, Case Histories, ed. by Hansen, Heinrichs, Holmer, MacDougall, Rogers, Sumner and Ward, Soc. Explor. Geophys., Tulsa, Okla.

Puranen, M., 1959. Aerosähköisistä mittausmenetelmistä. Manuscript, Helsingin Yliopisto, Matemaattis-luonnontieteellinen tiedekunta, 71 p + append.

–, **1963.** Aerogeofysikaalisista tutkimuksista. Geologi 15, 67–69.

Puranen, M. & Kahma, A., 1947. Malminetsintätapa. Patentti 24629. 5 p.

–, **1949.** Geofysikaaliset mittaukset lentokoneista käsin, uusi tehokas apuneuvo malminetsijälle. Vuoriteollisuus 7 (1), 1–19.

–, **1956.** U.S.Patent 2 741 736. 5 p.

Romu, M., 1980. Etelä-Pohjanmaan savikerrostumista ja niiden tiiliteknisistä ominaisuuksista. Manuscript, Turun yliopisto, Maaperägeologian laitos. 177 p + append.

Rönkä, V., 1958. U.S.Patent 2 839 751. 3 p.

Ruotoistenmäki, T., 1979. FOURPACK-digitalisoidun datan Fourieranalyysiin perustuva analysointi- ja muokkausohjelmisto. Geol. tutkimusl., Geofysiikan osasto, rap. Q 17/17.4/1979/1. 67 p.

–, **1980.** Aerosähköisten mittaustulosten riippuvuus vertikaalikiihtyvyydestä ja lentokorkeudesta Suomenlahden ja Sotkamon alueilta valitussa datassa. Geol. tutkimusl., Geofysiikan osasto, rap. Q 24.9/80/2. 26 p.

Salli, I., 1955. Kallioperäkartta – Pre-Quaternary rocks, Sheet –2431 Ylivieska. Suomen geologinen kartta – Geological map of Finland, 1 : 100 000.

Savolainen, H., 1979. Aerosähkömagneettisen VLF-mittauksen käyttömahdollisuuksista. Manuscript, Tek. korkeakoulu, Vuoriteollisuusosasto, Espoo. 38 p + append.

Seguin, M. K., 1975. Quantitative interpretation of a combined electromagnetic and magnetic heliported survey for the search of economic magnetic taconite. Geophys. Prospect. 23, 471–491.

Seigel, H. O. & Pitcher, D. H., 1978. Mapping earth conductivities using a multifrequency airborne electromagnetic system. Geophysics 43, 563–575.

Sellmann, P. V.; Arcone, S. A. & Delaney, A. J., 1976. Airborne resistivity and magnetometer survey in northern Maine for obtaining information on bedrock geology. CRREL Rep. 76–37. 24 p.

Siikarla, T., 1968. Selostus geofysikaalisista tutkimuksista Säviän alueella Pielavedellä 1965–1968. Geol. tutkimusl., Malmiosasto, rap. M 17/P1v-68/4. 12 p + append.

Silvennoinen, A; Honkamo, M.; Juopperi, H.; Lehtonen, M.; Mielikäinen, P.; Perttunen, V.; Rastas, P.; Räsänen, J. & Väänänen, J., 1980. Main features of the stratigraphy of north Finland. 153–162 *In* Jatulian geology in the eastern part of the Baltic shield. Proceedings of a Finnish-Soviet symposium held in Finland 21st–26th August 1979, ed. by Silvennoinen, Rovaniemi. Finland.

Sinha, A. K., 1977a. Influence of altitude and displacement currents on plane-wave EM fields. Geophysics 42, 77–91.

–, **1977b.** Dipole electromagnetic mapping of permafrost terrains: theoretical developments and computer programs. Geol. Surv. Canada, Pap. 77–13. 27 p.

Sinha, A. K. & Collett. L. S., 1973. Electromagnetic fields of oscillating magnetic dipoles placed over a multilayer conducting earth. Geol. Surv. Canada, Pap. 73–25. 48 p.

Tammenmaa, J.; Grasty, R. L. & Peltoniemi, M., 1976. The reduction of statistical noise in airborne radiometric data. Can. J. Earth Sci. 13, 1351–1357.

Tammenmaa, J. & Peltoniemi, M., 1979. Menetelmä ukkoshäiriöiden poistamiseksi aerosähköisistä mittaustuloksista. Geol. tutkimusl., Geofysiikan osasto, rap. Q 16.2/24.8/79/1. 11 p + append.

Tenhola, M., 1979. Karttalehti 3313 Vesanto. Geol. tutkimusl., Geokemian osasto, esitutkimusrap. 18 p + append.

Tervo, T., 1980. Sotkamon Talvivaaran geofysikaaliset tutkimukset vuosina 1977–1979. Geol. tutkimusl., Geofysiikan osasto, rap. Q 19/3344/-80/1. 27 p + append.

Thomas, L., 1977. Electromagnetic sounding with susceptibility among the model parameters. Geophysics 42, 92–96.

Törnqvist, G., 1958. Some practical results of airborne electromagnetic prospecting in Sweden. Geophys. Prospect. 6, 112–126.

Valkeila, T., 1978. Slingrammenetelmän tietokonetulkinnan kehittäminen. Manuscript, Tek. korkeakoulu, Vuoriteollisuusosasto, Espoo. 67 p + append.

Vartiainen, H., 1980. The petrography, mineralogy and petrochemistry of the Sokli carbonatite massif, northern Finland. Geol. Surv. Finland, Bull. 313. 126 p.

Vartiainen, H. & Paarma, H., 1979. Geological characteristics of the Sokli carbonatite complex, Finland. Econ. Geol. 74, 1296–1306.

Västi, K., 1978. Selostus Pielaveden Paloniemen-Tervon Utrianlahden välisellä vyöhykkeellä suoritetuista malmitutkimuksista kesällä ja syksyllä 1978. Geol. tutkimusl., Malmiosasto, rap. M/19/3313/-78/1/10. 13 p + append.

Vironmäki, J., 1977. FORTRAN V kielisiä anomalioiden laskentaohjelmia eräille sovelletussa geofysiikassa yleisesti käytetyille malleille. Tek. korkeakoulu, Vuoriteollisuusosasto, Espoo. 64 p.

Vironmäki, J. & Multala, J., 1981. Geologisen tutkimuslaitoksen uusi aerogeofysikaalinen mittausjärjestelmä. 157–162 *In* X Geofysiikan päivät Helsingissä 23.–24. 4. 1981, ed. by Leppäranta, Geofysiikan seura, Helsinki.

Wait, J. R., 1953. A conducting permeable sphere in the presence of a coil carrying an oscillating current. Can. J. Phys. 31, 670–678.

–, **1955.** Mutual electromagnetic coupling of loops over a homogeneous ground. Geophysics 20, 630–637.

–, **1958.** Induction by an oscillating magnetic

dipole over a two layer ground. Appl. Sci. Res., Sect. B, 7 (1), 73–80.

–, **1962.** Electromagnetic waves in stratified media. Pergamon, Oxford. 372 p.

Ward, S. H., 1953. A method for measuring the electrical conductivity of diamond drill core specimens. Geophysics 18, 434–447.

–, **1959.** Unique determination of conductivity, susceptibility, size and depth in multi-frequency electromagnetic exploration. Geophysics 24, 531–546.

–, **1967a.** Electromagnetic theory for geophysical applications. 10–196 *In* Society of Exploration Geophysicists' Mining Geophysics II, Theory, ed. by Hansen, Heinrichs, Holmer, MacDougall, Rogers, Sumner and Ward, Soc. Explor, Geophys., Tulsa, Okla.

–, **1967b.** The electromagnetic method. 224–372 *In* Society of Exploration Geophysicists' Mining Geophysics II, Theory, ed. by Hansen, Heinrichs, Holmer, MacDougall, Rogers, Sumner and Ward, Society Explor. Geophys., Tulsa, Okla.

–, **1970.** Airborne electromagnetic methods. 81–108 *In* Mining and Groundwater Geophysics/1967, ed. by Morley, Geol. Surv. Canada, Econ. Geol. Rep. 26.

Ward, S. H. & Hood, P., 1969. Low-frequency airborne electromagnetic methods. 41–88 *In* Advances in Geophysics 13, ed. by Landsberg and Mieghem, Academic Press, New York.

Westerlund, K., 1973. Ohjelmaselosteet LUE, CHK ja DGNST. Geol. tutkimusl., Geofysiikan osasto, rap. Q 17.2/20.8/73/1. 59 p.

Wieduwilt, W. G., 1962. Interpretation techniques for a single frequency airborne electromagnetic device. Geophysics 27, 493–506.

Tätä julkaisua myy

VALTION PAINATUSKESKUS
MARKKINOINTIOSASTO

Postimyynti
PL 516
00101 HELSINKI 10
Puh. 90-539 011

Kirjakauppa
Annankatu 44
00100 HELSINKI 10
Puh. 90-17341

Denna publikation säljes av

STATENS TRYCKERICENTRAL
MARKNADSFÖRINGSAVDELNINGEN

Postförsäljning
PB 516
00101 HELSINGFORS 10
Tel. 90-539 011

Bokhandel
Annegatan 44
00100 HELSINGFORS 10
Tel. 90-17341

This publication can be obtained from

GOVERNMENT PRINTING CENTRE
MARKETING DEPARTMENT

Bookshop
Annankatu 44
00100 HELSINKI 10
Phone 90-17341

Orders from abroad:
AKATEEMINEN KIRJAKAUPPA
Keskuskatu 1
SF-00100 Helsinki 10

ISBN 951-690-162-X
ISSN 0367-522X